Università degli Studi di Salerno

Dipartimento di Chimica e Biologia "A. Zambelli"

PhD Thesis in Chemistry

XXXV cycle

Sustainable approaches for the synthesis and the chemical degradation of polyesters

Tutors:

Prof. Marina Lamberti

Prof. Mina Mazzeo

Coordinator:

Prof. Claudio Pellecchia

PhD Student:

Federica Santulli

Academic Year 2022-2023

INDEX

List of abbreviations

LIST OF ABBREVIATIONS

°C	Celsius degree
AMM	Activated Monomer Mechanism
BHET	Bis(2-hydroxyethyl)terephthalate
BnOH	Benzyl alcohol
Đ	Dispersity index
DBU	1,8-diazabicyclo(5.4.0)undec-7-ene
DCM	Dichloromethane
DMAP	4-(N,N-dimethylamino)pyridine
EG	Ethylene glycol
Et-La	Ethyl lactate
GHG	GreenHouse Gas
GPC	Gel Permeation Chromatography
HMTA	hexamethylenetetramine
^{i}PrOH	Isopropanol
LA	Lactide
LCA	Life Cycle Assessment
MALDI-ToF-MS	Matrix assisted laser desorption/ionization-Time of Flight Mass
Me-La	Methyl lactate
$Mg(n\text{-}Bu)_2$	Di-n-butylmagnesium
$Mg[N(SiMe_3)_2]_2$	Magnesium bis(hexamethyldisilazide)
M_n	Number average molecular weight
NMR	Nuclear Magnetic Resonance
PCW	Plastic packaging waste
PET	Poly(ethylene terephthalate)
PLA	Polylactide
P_r	Probability of heterotactic enchainment
P_s	Probability of syndiotactic enchainment
ROP	Ring-Opening Polymerization
S_{BHET}	Selectivity of BHET
$Sn(Oct)_2$	Sn (2-ethylhexanoate)2
$S_{R\text{-}La}$	Selectivity of alkyl-lactate
T_g	Glass transition temperature
THF	Tetrahydrofuran
T_m	Melting temperature
TOF	Turnover frequency
X_{Int}	Conversion of PLA degraded
Y_{BHET}	Yield of BHET
$Y_{R\text{-}La}$	Yield of alkyl-lactate
$ZnEt_2$	Diethylzinc
$Zn[N(SiMe_3)_2]_2$	Zinc bis[bis(trimethylsilyl)amide]

CHAPTER 1

General Introduction

Plastics are an indispensable material with numerous advantages compared to traditional ones, such as glass and paper. The consumption of plastic worldwide is increasing day by day since its introduction in the market during the first half of the last century. According to Plastics Europe, 367 million tons of plastic materials were produced worldwide in 2020, of which 55 million tons in Europe, and used for several market sectors, such as packaging (40.5 %), building and construction (20.4 %), automotive (8.8 %) and others.[1]

Most of plastics comes from petroleum-based resources, with only a fraction currently derived from renewable feedstocks. This is of particular concern as the use of petroleum resources is associated with global pollution and climate change, as well as being a limited resource.[2] To mitigate these issues, a transition towards bio-based plastics is needed, especially considering the growing demand for such materials. Another problem currently associated with plastic usage is the pollution that is caused by end-of-life mismanagement, of particular concern for marine environments, where it tends to accumulate and persist.[3]

Nowadays, 40 % of post-consumer plastic packaging waste (PCW) is destined for landfills, where they lose almost all their intrinsic value. About 14 % of PCW plastic packaging is incinerated for energy recovery, a process that releases GreenHouse Gas (GHG) and carries a substantial risk of generating and releasing toxic combustion products.[4] The same percentage is collected for recycling (14 % in total) and of this amount mostly is redirected to lower value applications (secondary recycling, 8 %) or lost in processing (4 %). Only 2 % of all recovered plastic packaging waste is returned to applications of the same or similar kind (primary recycling). The remaining 32 % of plastic packaging waste escapes the collection system, spreading into the environment during transport and/or use (**Figure 1.1**).[5]

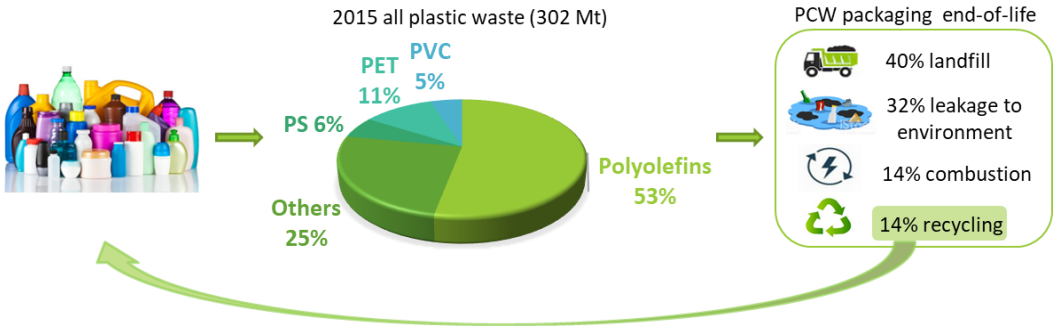

Figure 1.1 A scheme explaining plastic waste composition and faith.

To counter the problem of plastic pollution, the solutions may be the shift towards bio-based materials for which end-of-life treatments have been designed and / or the upcycling of traditional plastics, difficult to replace in the market. The current use of plastics follows a linear pattern, whereby plastics are prepared, used, and disposed, and this is particularly problematic for single-use materials.[6] The future of plastic use must be based on a circular system, whereby the value of the material is maintained after its useful life (**Figure 1.2**).[3c,7]

Figure 1.2 A graphical summary of circular economy.

A very interesting class of polymers that offers a wide range of characteristics and properties are polyesters, polymers containing ester groups in the main chain that can be classified as aliphatic, semi-aromatic and aromatic based on the structure of the repeating unit. Aromatic moieties improve the hardness, and heat resistance of the polymeric material, while aliphatic portions increase the flexibility, lower the melting temperature (T_m) and the tendency to biodegradation.

The most important commercial polyester is poly(ethylene terephthalate) (PET), a semi-aromatic polyester, easily moldable to obtain films and fibers. Due to its good mechanical properties, it is widely used in everyday life. On the other hand, polylactide (PLA) is among the most important aliphatic polyesters, bio-based, biodegradable, and biocompatible. The interesting characteristics of this polymer have been detailed in the following paragraphs.

Within this framework, in this thesis project, metal-based catalytic system for the synthesis and chemical degradation of PLA have been explored, while as regards PET, already widespread on the market, attention has been focused on its chemical recycling.

1.1 Polylactide

Polylactide (PLA) is considered the most commercially promising material because it combines good mechanical properties, improved biodegradability, and biocompatibility, a series of features that make this material suitable for a wide range of applications and economic disposal procedures. Furthermore, PLA is derived from annually renewable resources, and its Life Cycle Assessment (LCA) suggests a reduction of up to 40 % in GHG emissions and 25 % in the use of non-renewable energy compared to traditional polyolefins.[8]

The major PLA application is packaging (nearly 70 %) as this polymer offers a new combination of attributes including stiffness, clarity, dead-fold, and twist retention, as well as an interesting combination of barrier properties, including flavor and aroma barrier characteristics. PLA is also used in biomedical applications, such as internal body components, surgical sutures, implants, and drug delivery systems (**Figure 1.3**).[9]

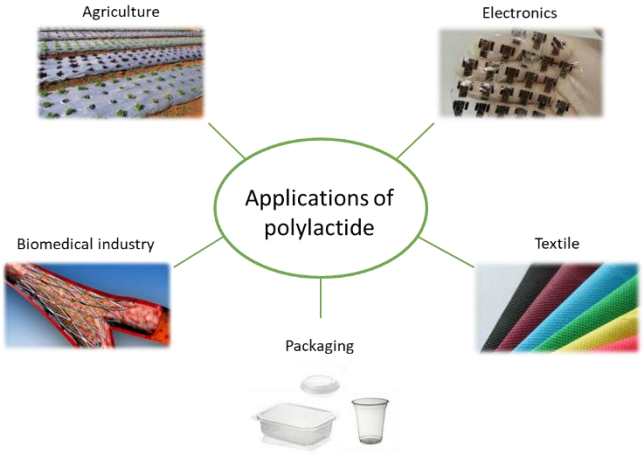

Figure 1.3 Some of the most common applications of the PLA.

Despite being a commercially available polymer, its widespread use has been limited by a high manufacturing cost compared to traditional synthetic plastics. This can be attributed to the complexity associated with fermentation and lactic acid purification, which accounts for approximately 50 % of total production costs.[10] Since global awareness about the necessity for bioplastic material utilization, together with legislation and high petroleum prices, a high demand is spreading among customers. Therefore, a huge effort is being put through toward designing of new affordable synthetic procedures in recent years.

1.2 Microstructures and properties

PLA derives from lactic acid (2-hydroxypropionic acid), obtained from the microbial fermentation of starch-rich raw materials, such as corn and sugar.[11] From this substrate, through a polycondensation reaction, oligomers are obtained. By subsequent heat treatment, the lactic acid oligomers are transformed into the corresponding cyclic diester of lactic acid, called lactide (LA) (**Figure 1.4**).[12]

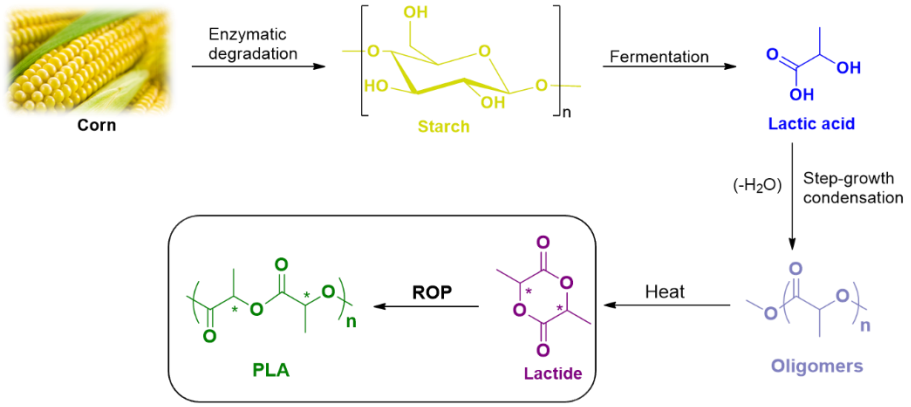

Figure 1.4 Synthesis of polylactide (PLA).

Since lactic acid has a chiral carbon atom, the lactide obtained can have different stereochemistry. L- and D-lactide derive from two molecules of L- and D-lactic acid, respectively; *meso*-lactide consists of both L- and D-lactid acids; and the *rac*-lactide is the result of an equimolar mixture of the two enantiomers of lactic acid (**Figure 1.5**).

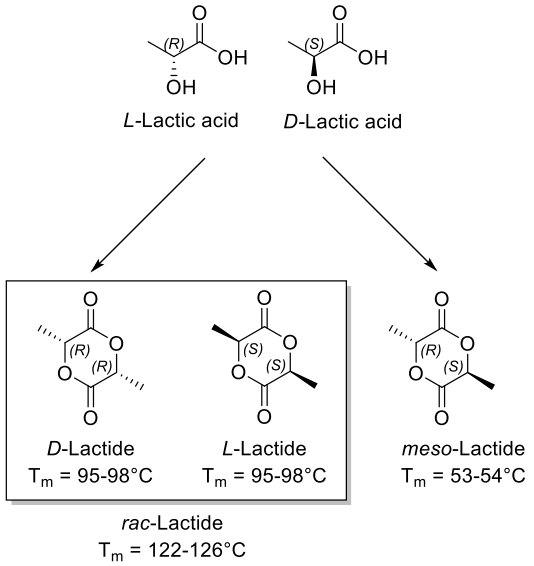

Figure 1.5 Stereoisomers of lactide and their thermal properties.

The availability of different stereoisomers allows to obtain different PLA microstructures (**Figure 1.6**) that significantly influence the physical, mechanical and degradation properties of the polymer.[13] The isotactic poly (L-lactide) (PLLA) or poly (D-lactide) (PDLA) are generally obtained by kinetic resolution of the racemic mixture or by using enantiopure L-LA or D-LA. The polymers contain stereogenic centers which have the same configuration. Heterotactic PLAs have a regular alternation of pairs of stereogenic centers with the same configuration and are generally synthesized by stereocontrolled polymerization of *meso*-LA or *rac*-LA based on the catalyst used. Syndiotactic PLAs contain sequential stereocenters with opposite configuration and can

be synthesized by stereocontrolled *meso*-LA. Finally, atactic PLAs are characterized by stereo-irregular sequences and obtained by non-stereocontrolled reaction of *rac*-LA or *meso*-LA.[14]

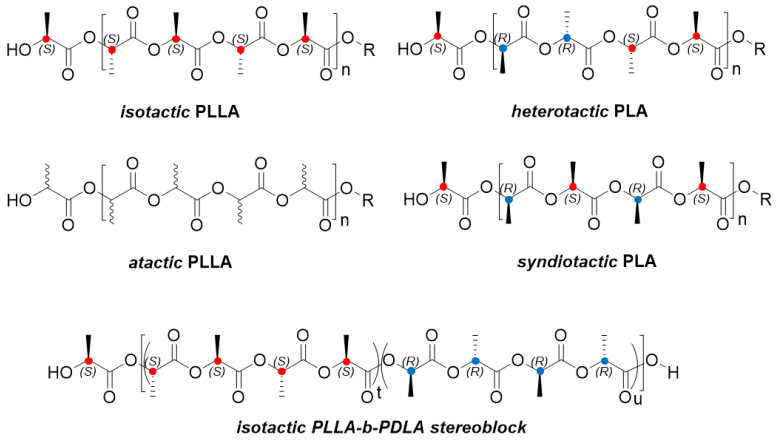

Figure 1.6 Stereoregular microstructures of PLA.

Isotactic polymers exhibit high glass transition temperature (T_g), melting temperature (T_m) and thermal stability (**Table 1.1**). The formation of stereocomplexes between two homochiral polymers or in a stereoblock involves a further increase in T_g and T_m, which could lead to new materials with modified properties.[15] On the other hand, heterotactic and atactic polymers are amorphous and have just T_g.[14b,16]

Table 1.1 Thermal proprieties of PLAs with different microstructures.

PLA's tacticity	T_g (°C)	T_m (°C)
Isotactic	55-60	180
Syndiotactic	34	151
Stereocomplex	65-72	220-230
Heterotactic	<45	-
Atactic	44-55	-

1.3 Ring-Opening Polymerization (ROP)

PLA can basically be obtained through two reactions: the direct polycondensation of lactic acid or the ring-opening polymerization (ROP) of the lactide. During the first reaction an equilibrium is established with the elimination of water molecules. To obtain polymers with a high molecular weight, it is necessary to remove water from the reaction environment using hard conditions. On the other hand, the ROP of lactide uses mild reaction conditions as the driving force is the release of the ring tension during polymerization. The process can proceed through different mechanisms depending on the type of initiator used.[17]

The most effective synthetic methods are certainly the ROP promoted by metal complexes through the "coordination-insertion" mechanism or through the activated monomer mechanism (AMM) by a cationic initiator. Both mechanisms are described below.[18]

1.3.1 "Coordination-insertion" Mechanism

Industrially, PLA is produced from the ring opening polymerization (ROP) of cyclic lactide diesters under solvent free conditions. This method exploits an inexpensive catalyst such as $Sn(Oct)_2$ (Oct=2-ethylhexanoate) which operates via a coordination-insertion mechanism.[19] The toxicity problems associated with the industry standard $Sn(Oct)_2$ have stimulated considerable research into sustainable and biocompatible alternatives.

The mechanism proceeds *via* the coordination of the monomer to a Lewis acid metal complex, which activates and attaches the monomer to the carbonyl carbon (**Figure 1.7**). The ester bond is subsequently broken, and the metal-alkoxide propagation species is formed. The reaction ends when the metal-alkoxide bond is cleaved by the termination reactions or by the consumption of the monomer.[20]

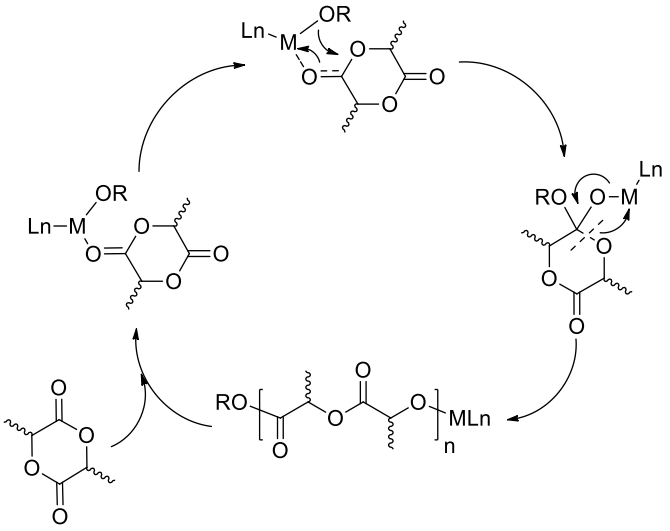

Figure 1.7 Coordination-insertion mechanism for lactide promoted by an alkoxide metal complex.

It allows to operate under mild reaction conditions, this involves a very effective control on the microstructure and on the distribution of the molecular weights of the polumer. Through the choice of suitable initiators, it is possible to effectively control the nature of the chain-end groups of the polymer and the stereoregularity of the chain.

1.3.2 Activated Monomer Mechanism (AMM)

In addition to the coordination-insertion mechanism, another frequently proposed pathway for lactide polymerization reactions is the activated monomer mechanism (AMM) (**Figure 1.8**). This process begins with the electrophilic activation of the lactide using either a Bronsted acid initiator or a Lewis acid catalyst. In both cases, an oxo-carbenium ion intermediate 1 is formed, which acts as an activated monomer ready for nucleophilic attack. Therefore, either the initiator or the growing polymer chain attacks this oxo-carbenium ion, forming the tetrahedral intermediate 2. After the proton transfer, collapsing of the intermediate causes the ring opening and the incorporation of a lactide unit into the growing polymer chain.[21]

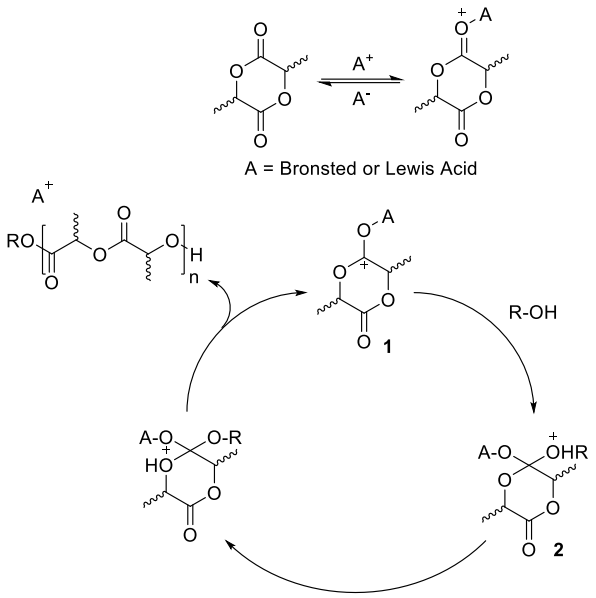

Figure 1.8 Activation monomer mechanism for lactide promoted by a Bronsted or Lewis acid.

1.4 Representative catalyst systems for the ROP of lactide

The toxicity associated with tin residues in the polymer is a cause of concern, especially for biomedical and food packaging applications. On this basis, catalysts based on non-toxic metals, such as zinc, magnesium, or aluminum, with alkoxide auxiliary ligands, β-diketiminates, bis (phenolates), Schiff bases, phenoxyimines and so on have been extensively explored over the last two decades.[22] In this paragraph some representative examples are described for the ROP of lactide carried out both in solution and in industrial conditions. The complexes described are mainly zinc complexes in which the ancillary ligands are of the NO, NN, and NNO type, which constitute the most representative class. They have numerous advantages such as ease of synthesis, the ability to coordinate with a wide range of metal ions, the ability to easily functionalize by varying the type of steric encumbrance and the electronic effect.

In 2001, the first Schiff-based zinc complex was developed by Chisholm et al. for the polymerization of *rac*-LA (**Figure 1.9**).[23] The reaction proceeded slowly with a conversion of 90 % of PLA after 3 hours at room temperature. Furthermore, the obtained polymer was atactic.

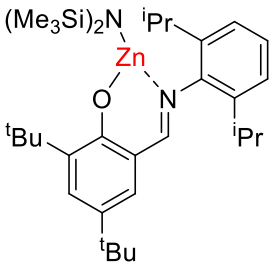

Figure 1.9 Chisholm complex.

Subsequently, Chen et al. modified Schiff-based ligands from bidentate to tridentate and observed different activities in lactide polymerization (**Figure 1.10**).[24] Several NNO-tridentate type Schiff base ligands were prepared with different substituents on the phenyl group to study the electronic and steric effect. Reaction of the LH ligand with $ZnEt_2$ produced a dimeric zinc complex **2a-e** with pentacoordination around the zinc center. Further reaction with benzyl alcohol (BnOH) led to the formation of **3a-e** which also revealed a dimeric behavior with two pentacoordinated symmetrical zinc centers. All zinc alkoxide complexes **3a-e** showed high

activity and reactivity increased with the help of the electron donor group on the phenyl ring. At room temperature, catalyst **3a** achieved 91 % conversion of PLA in just 30 minutes.

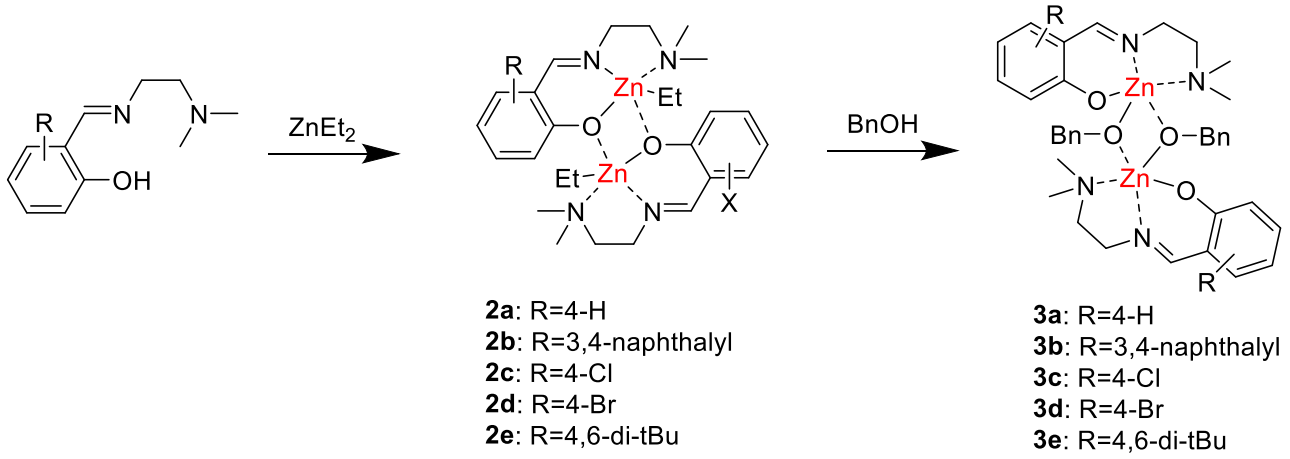

Figure 1.10 Chen complexes **2-3**.

Tolman et al. reported zinc complexes with phenoxide-type tridentate ligands bearing two neutral amino-type donors (**Figure 1.11**).[25] The X-ray crystal structure revealed that the alkoxide complexes **5a-b** were dimeric in the solid state, while nuclear magnetic resonance and mass spectrometry showed that the monomer predominates in solution (80 %). Dimeric alkoxide complex **5a** showed high activity (96 % conversion in 5 min), whereas the monomeric analogue **4a**, without an alkoxide initiating/propagating group, was inactive toward *rac*-LA polymerization, demonstrating that the alkyl group is not a good nucleophile. These alkoxide catalysts **5a-b** displayed good control of the molecular weights for lactide polymerization even with catalysts loadings < 0.1 %.

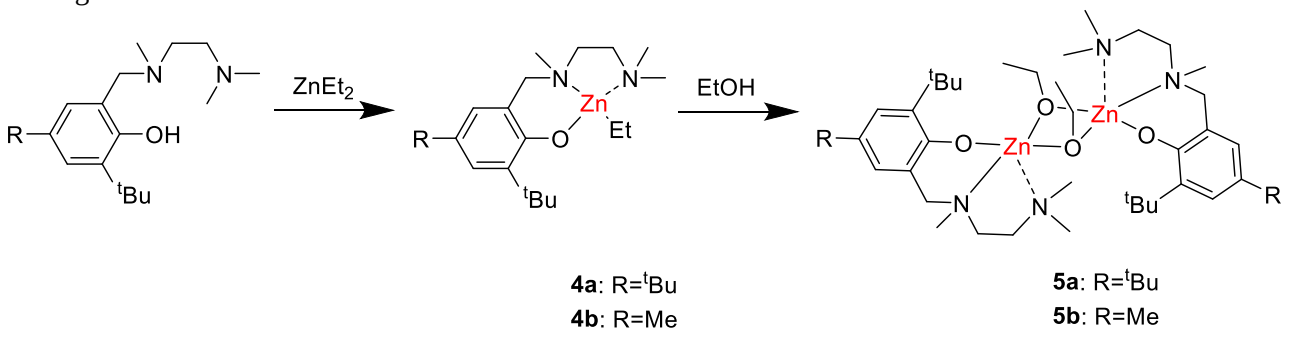

Figure 1.11 Tolman complexes **4-5**.

Among the most important Zn complexes active for the ROP of lactide, the complexes of Coates et al. were able to combine good activity with high stereoselectivity (**Figure 1.12**).[26] They synthesized a series of zinc alkoxides **7** based on a β-diiminate ligand which in the polymerization of *rac*-LA obtained heterotactic PLA (P_r = 0.94 at 0 °C) and with *meso*-LA synthesized syndiotactic PLA (P_s = 0.76 at 0 °C). Kinetic studies with **7a** indicated that the polymerizations were of the first order with respect to the monomer (*rac*-LA) and of the order of 1.56 for the catalyst, assuming a dimeric structure. Polymerization experiments with **7a** revealed that this complex was extremely fast for the polymerization of *rac*-LA, polymerizing 200 equiv. in 20 min at 20 °C. Under the same conditions, the analogous magnesium complex managed to achieve the same conversion in just 2 min, but the polymer had a higher molecular weight than the theoretical one, probably due to a low initiation constant and / or the presence of transesterification phenomena.

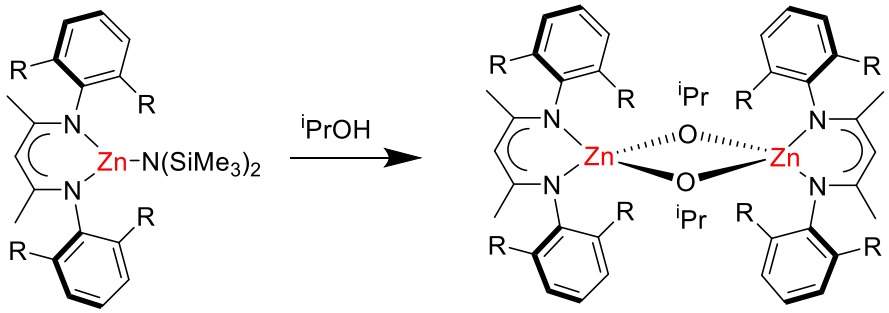

6a: R=^{i}Pr
6b: R=Et
6c: R=^{n}Pr

7a: R=^{i}Pr
7b: R=Et
7c: R=^{n}Pr

Figure 1.12 Coates complexes **6-7**.

The most active catalyst reported to date for the polymerization of LA in solution is the bimetallic Zn complex published by Williams in 2016. The authors showed mono- and bi- metallic zinc complexes supported by bis(imino)diphenylamide ligands, which revealed remarkable activities (**Figure 1.13**).[27] The bimetallic complex with propyl bridge **8b** was twice as active as the bimetallic complex with ethyl bridge **8a** and three times more active than the monometallic complex **9a**. These results confirmed the importance of the cooperativity of the two metal centers, which also depends on the distance between the two metals. The authors also observed that depending on the nature of the labile ligand coordinated with the zinc, the macrocyclic ligand could assume two different conformations: folded and planar. When the labile ligand was an amide group, in complex **8b**, the macrocyclic ligand assumed a "folded" conformation and the metal catalyst showed a TOF with values up to 60000 h^{-1} (0.1 % catalyst loading, 298 K, [LA] = 1 M). On the other hand, when the labile ligand was an alkoxide group (complex **8d**) the conformation was “planar” and the corresponding catalyst was much slower under similar conditions (TOF = 30 h^{-1}).

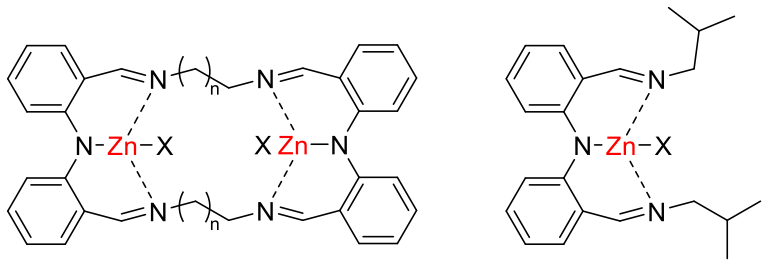

8a: X=N(SiMe$_3$)$_2$ n=1
8b: X=N(SiMe$_3$)$_2$ n=2
8c: X=O^{i}Pr n=1
8d: X=O^{i}Pr n=2

9a: X=N(SiMe$_3$)$_2$
9b: X=O^{i}Pr

Figure 1.13 Williams complexes **8-9**.

Although the catalysts described above have shown the highest activities even reported for the ROP of the lactide in solution and at room temperature, they are not stable under industrially relevant conditions and could not be applied on a large scale. More recently some examples of catalysts that preserve their activity also under industrially relevant reaction conditions have been reported.

In 2020, Herres-Pawlis et al. presented novel zinc guanidine complexes able of polymerizing unpurified technical *rac*-LA at 150 °C, producing colorless PLA with high molecular weight and narrow dispersity (**Figure 1.14**).[28] Complex **10a** was the most active, polymerizing 52 % lactide after 90 min.

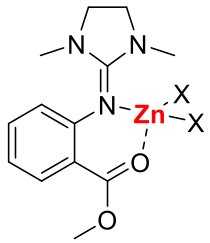

10a: X=Cl
10b: X=Br

Figure 1.14 Herres-Pawlis complexes **10**.

Jones et al. reported simple ethylenediamine based Mg(II) and Zn(II) complexes for the ROP of lactide under industrially relevant conditions (**Figure 1.15**).[29] Incredibly high activities were achieved with the Zn complex **11a** using low catalyst loading and high temperatures (180 °C), reaching TOF values of 180000 h^{-1}. Using a tertiary amine as an additional donor group, the complex **11b** was found to be three times less active, keeping the substituents on the phenoxy portion unchanged. The Mg complex **12a** analogs showed lower activity with TOF = 14000 h^{-1}, under the same reaction conditions. However, reasonable molecular weight control was maintained and MALDI-ToF analysis of these polymers confirmed the terminal benzyl alcohol groups.

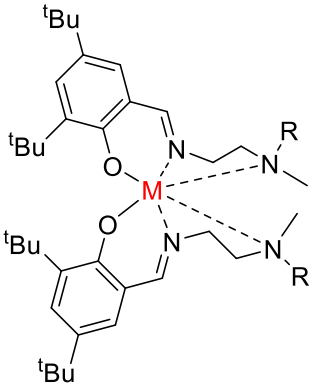

11a: M=Zn R=H **12a**:M=Mg R=H
11b: M=Zn R=Me

Figure 1.15 Jones complexes **11-12**.

Further work by the same research group demonstrated that by modifying the length of the pendant arm bearing the additional donor with a propylamine group, this resulted in increased L-LA polymerization activity.[30] With complex **13a** (**Figure 1.16**), high conversion was observed after just 1 min using low initiator loading and at 180 °C (TOF = 590000 h^{-1}). Also in this case, the increase of steric hindrance on the amine led to a decrease in activity of the complex **13b** reaching the same conversion after 3 min (TOF = 180000 h^{-1}). In the opposite case, in which the additional donor is not present, high conversions were achieved after 12 min (TOF = 45000 h^{-1}) with complex **13c**. The reduced activity had suggested that the presence of the pendant amino groups is important, as the reaction proceeded by activation of the monomer. The pendant amino groups participated in the reaction, potentially assisting in the proton transfer steps, leading to an activated monomer.

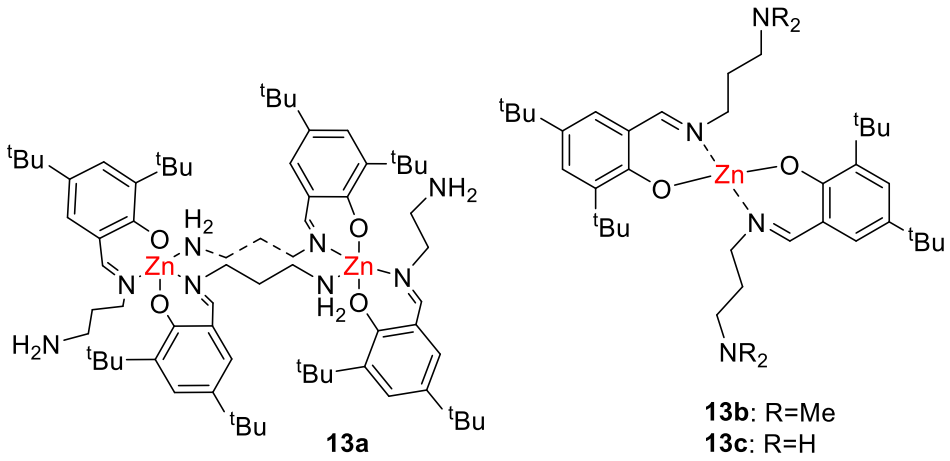

Figure 1.16 Jones complexes **13**.

1.5 Recycling of PLA

Since PLA is a biodegradable polymer, it is mistakenly thought that this material degrades easily in the natural environment. In soil or domestic composters, degradation can take up to a year at 20 °C, or 12 weeks at temperature above 25 °C.[31] The most worrying fact is that the polymer persists in the marine environment. Indeed, recent studies have not observed any degradation within one year under laboratory conditions simulating static seawater, although weight loss was detected under dynamic conditions via mechanical processes.[32]

Therefore, it is imperative to design efficient PLA waste management for the development of environmentally friendly materials, which do not contribute to plastic pollution. The first step is the identification and separation of PLA from other plastics. A common problem is the contamination of PET and PLA waste streams as these plastics are difficult to distinguish. For PET, the presence of PLA during the recycling process can severely reduce the properties of the reformed PET.[33]

Once identified and collected, there are several end-of-life scenarios for PLA, schematized in **Figure 1.17**.[3c] Under industrial conditions, PLA is efficiently composted at a temperature around the one of the polymer's glass transition temperature T_g (60 °C) and high relative humidity. In this case, the time required for complete degradation is up to 30 days.[34] The composting products are CO_2 and water, thus losing the precious value associated with the polymer.

A different strategy can be mechanical recycling, where generally the polymer is thermally treated, and this can compromise the properties of the next generation of the material.[35] Indeed, the molecular weight of the polymer is often reduced, preventing the use of the material in the same application, and therefore downgrading it to a less demanding use.

A particularly interesting option is the chemical recycling of PLA which makes it possible to obtain low-molecular-weight molecules of industrial interest that would otherwise be lost in composting products. Furthermore, the quality of the recycled plastic can be adjusted in the polymerization or in the plastic formation stage and is independent of the quality of the plastic waste. Among the most investigated chemical recycling reactions are pyrolysis, hydrolysis and alcoholysis.

The pyrolysis reaction consists of a thermal degradation based on a transesterification process initiated from the hydroxy end by backbiting. This reaction occurs in the presence of metals, such as Sn, and the major product is lactide.[36] However, this process requires high temperatures, and can lead to racemization/epimerization and side reactions with products other than lactide.

The chemical recycling by hydrolysis depends on the interaction of the water molecules with the ester bonds of the chain. Based on the solubility of the polymer in aqueous systems, the reaction can proceed through a homogeneous bulk erosion, when the water diffusivity is high, or through a heterogeneous surface erosion when the water diffusivity is low. The final product, lactic acid, is a platform chemical that can be made into a variety of other valuable raw materials or a starting monomer for PLA production.[37] As in the pyrolysis reaction, hydrolysis can require high temperatures and/or strongly acidic/basic conditions.

In the presence of alcohols, chemical recycling occurs through transesterification reactions, producing value-added molecules such as alkyl lactates. These can be useful on their own or used to reform lactic acid, and thus PLA, to facilitate a circular economy approach.[3c] This process seems to be the most economical and environmentally sustainable process on an industrial scale. For this reason, most of the scientific community effort is being dedicated to the optimization of this process, by developing new catalysts showing outstanding performance and stability under milder conditions. That is why this topic is worth for a detailed explanation, which will be accomplished in the following paragraphs, with particular attention to catalysts and conditions used in the literature up to now.

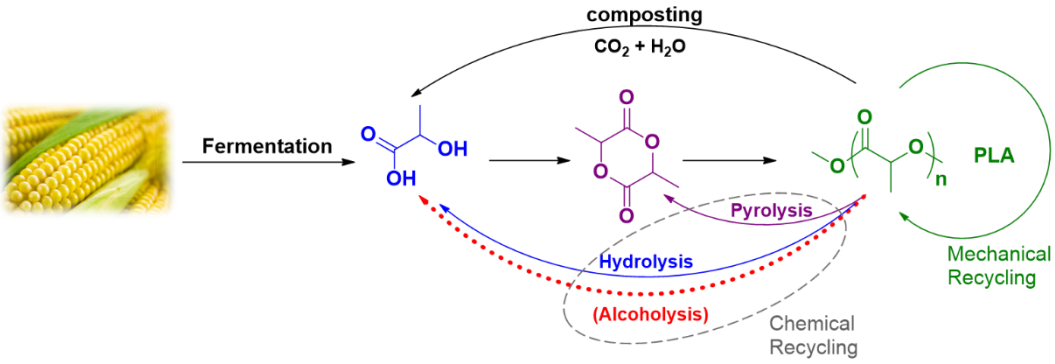

Figure 1.17 Polylactide formation and potential end-of-life scenarios.

1.6 Alcoholysis of PLA

The alcoholysis of PLA is most commonly performed with the support of a sustainable catalyst and in the presence of an excess of alcohol. Alkyl lactate is formed as the major low-molecular weight product, and the released alcohol can be reused/recycled for subsequent degradation processes. Consequently, small amounts of waste are generated and the whole process is made highly atomically efficient.

The growing interest in this reaction depends not only on being a sustainable option for recycling end-of-life PLA, but also on the enormous economic value associated with the reaction product, the alkyl lactates (**Figure 1.18**).

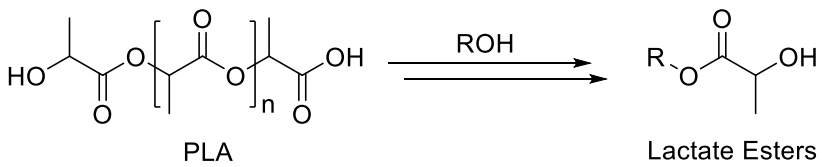

Figure 1.18 Alcoholysis reaction of PLA.

Alkyl lactates are classified as green solvents and are considered potential renewable substitutes for petroleum-derived solvents due to their inherent biodegradability and low toxicity.[38] In addition, their low vapor pressure ensures that they are safer and easier to handle than conventional solvents. Alkyl lactates are already employed in several sectors such as the pharmaceutical, food, agriculture, polymer, and their use is expected to increase

further in the future. The market value of ethyl lactate (Et-La) is estimated to reach $ 92 million by 2024 and currently trades at £2.54-3.49 per kg relative to £1.69 per kg for virgin PLA.[39]

1.6.1 Representative catalyst systems for the alcoholysis of PLA

Several systems able of degrading PLA into alkyl lactates have been reported in the literature. The first example was developed as early as 1945 where a range of acid catalysts and $ZnCl_2$ were used with temperatures up to 150 °C.

Such studies have been resumed more recently by Collins et al. in 2011, in which $Zn(OAc)_2$ was used for both methanolysis and ethanolysis of PLA at the boiling temperature of the respective alcohols.[40] Me-La formation was easier, with a yield of 70 % after 16 h. In the presence of a 1:1 mixture of PLA and PET, the degradation of PLA proceeded at a similar yield (65 %) with the PET remaining unreacted and could be separated by post-reaction filtration.

Other metals have been also explored by Sobota et al. such as magnesium- and calcium-based catalysts for the solvothermal alcoholysis of PLA (M_n = 64200–115700 $gmol^{-1}$).[41] Using *Mg* or $Mg(^nBu)_2$, efficient alcoholysis was achieved at 200 °C within 1 h using a wide range of linear and branched alcohols. High reaction temperatures were preferred to avoid the use of excess alcohol, obtaining high yields of Et-La (71–88 %) at 100 °C in the presence of 4–10 equiv. of ethanol.

The application of *ionic liquids* was also investigated for this type of reaction, as reported by Song et al. for the methanolysis of PLA (M_w = 400000 $gmol^{-1}$).[42] [Bmim] [OAc] (**Figure 1.19**) was identified as the exceptional candidate reaching a Me-La yield of up to 93 % within 3 hours at 115 °C and it could be reused up to 6 times without a reduction in activity. The used of ionic liquid in combination with simple metal salts [e.g., $Zn(OAc)_2$ and $FeCl_3$] has also been shown to facilitate the degradation of PLA under milder conditions.[43] $2[Bmim][OAc]\text{-}Zn(OAc)_2$ achieved a Me-La yield of 92 % within 2 hours at 110 °C. This improvement in synergistic reactivity could probably be attributed to greater activation of the carbonyl group in the presence of Lewis acid. Although the ionic liquid exhibited high activity, their scalability was limited by their high cost and intrinsic viscosity.

Organocatalysts have also been tested for the alcoholysis reaction of PLA.[44] Recently, Enthaler at al. demonstrated the use of *DMAP* (**Figure 1.19**) for the methanolysis of PLA under microwave irradiation, achieving a high Me-La yield within 10 minutes at 180 °C.[45] The use of excess MeOH (23 equiv.) allowed the reaction to proceed under neat conditions, avoiding solvent, which are potentially harmful and a source of waste for the industry. A higher Me-La yield was observed by replacing *DMAP* with *1,8-diazabicyclo(5.4.0)undec-7-ene (DBU)* (**Figure 1.19**) under the same reaction conditions.

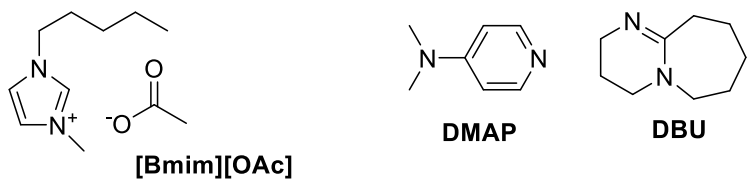

Figure 1.19 Ionic liquid and organocatalysts examples.

Perhaps, the least studied area of PLA alcoholysis reaction is from discrete metal complexes, although a wide range of complexes are reported for the ROP of lactide in the literature. These systems allow to modulate the degradation activities easily, by varying the type of metal center or the ligand used, possibly employing milder reaction conditions.

For the first time, Whitelaw et al. reported a series of zirconium and hafnium (IV)-salalen complexes for the polymerization and degradation of PLA (**Figure 1.20**).[46] The Hf-salalen complex (R = Me) was able to degrade PLA samples of various tacticity and different molecular weights (atactic and isotactic; M_n = 10000–200000 $gmol^{-1}$), achieving a 75 % conversion to Me-La within 24 hours at room temperature starting from commercial PLLA (M_n = 200000 $gmol^{-1}$). However, the complexity of the ligand limited the scalability of these systems, highlighting the need for easy ligand preparation.

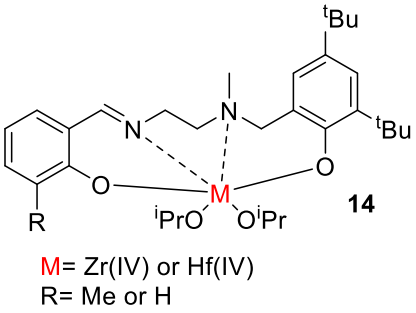

Figure 1.20 Whitelaw complexes.

Of all potentially usable metals, zinc-based complexes are the most attractive as they are highly active for lactide polymerization, in addition to the biocompatibility and cheapness of the metal. In recent years, various zinc-based complexes have been investigated in this type of reaction and are described below.

Fliedel et al. reported the first example of a zinc-carbene (NHC) alkoxide complexes for the controlled degradation of PLA (**Figure 1.21**).[47] After quenching the PLA polymerization with methanol, ^{1}H NMR spectrum of the sample contained signals corresponding to PLA along with the traces of Me-La and associated oligomers. This observation was confirmed by GPC analyses of MeOH quenched sample in which two peaks at lower molecular weight was observed, corresponding of smaller oligomers and methyl lactate. Based on these preliminary results, the authors managed a controlled degradation of a commercial PLLA (M_n = 18410 $gmol^{-1}$). In presence of methanol, only oligomeric PLA (M_n = 2000 $gmol^{-1}$) and Me-La (30 %) were present in the solution after 24 hours at room temperature.

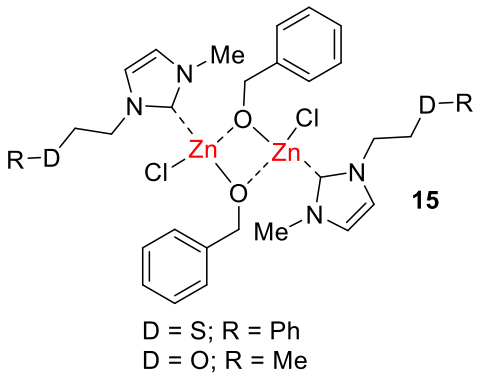

Figure 1.21 Fliedel complexes.

Recently, Payne et al. reported a series of homoleptic and heteroleptic dimeric Zn(II)-Schiff-base complexes for the methanolysis of PLA (**Figure 1.22**).[48] Schiff-based ligands are traditionally easy to prepare, and therefore are ideal candidates for ligand scale-up. Furthermore, their functional versatility offers considerable possibilities for catalyst tuning. Interestingly, while the dimers showed a greater activity than the monomeric analogue in the polymerization of *rac*-LA, an inversion of activity in the methanolysis of PLA was generally observed (M_n = 45150 $gmol^{-1}$). The homoleptic complexes achieved 100 % Me-LA yield within 8 hours at 80 °C in THF. The difference in activity between the two complexes could be attributed to lower stability of the dimeric catalyst, highlighting the importance of robustness for this kind of reaction.

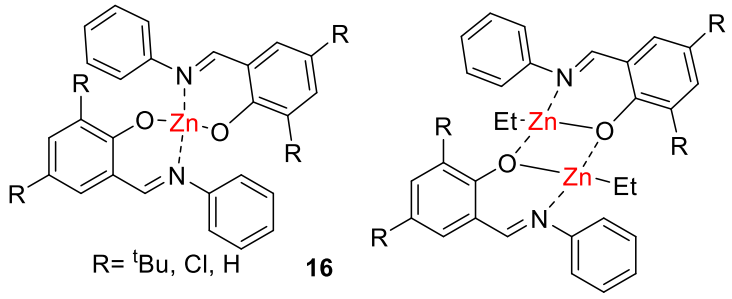

Figure 1.22 Payne complexes.

Following these results, McKeown et al. developed other homoleptic Zn(II)-Schiff base complexes bearing a simple ethyleneamine moieties (**Figure 1.23**).[49] Different commercial samples of PLA (M_n = 44350–71900gmol^{-1}) have been degraded, achieving conversions of up to 100 % of Me-LA within 1 h at 90 °C in THF solution. PLA degradation proceeded with a pseudo-first order kinetic profile, while the production of Me-La was shown to proceed through a two-step process through the intermediate formation of oligomers.

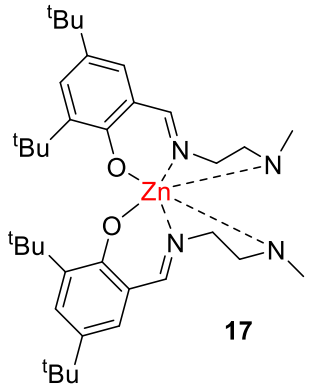

Figure 1.23 McKeown ethylamine complexes.

Subsequently, McKeown et al. demonstrated that switching from ethyleneamine to propyleneamine moieties had a significant impact on the activity (**Figure 1.24**).[30] Indeed, the degradation of a PLA cup (M_n = 45150 gmol^{-1}), occurred within 30 min at 50 °C in THF with a Me-La yield of 81 %. The corresponding analog with ethyleneamine moieties showed significantly reduced activity (Me-La yield 12 % in 6 h) under similar conditions, highlighting the importance of structure-activity relationships. Substitution of the propyleneamine substituent (R = NMe_2) resulted in lower activity, although it remained high, observing Me-La yield 84 % within 1 h. Finally, the removal of the amino group (R = H) drastically reduced the activity of the complex under the same conditions. This might suggest the presence of the pendant amine groups to be important, perhaps assisting in the degradation mechanism through hydrogen-bonding interactions to the alcohol, with a double activation mechanism.

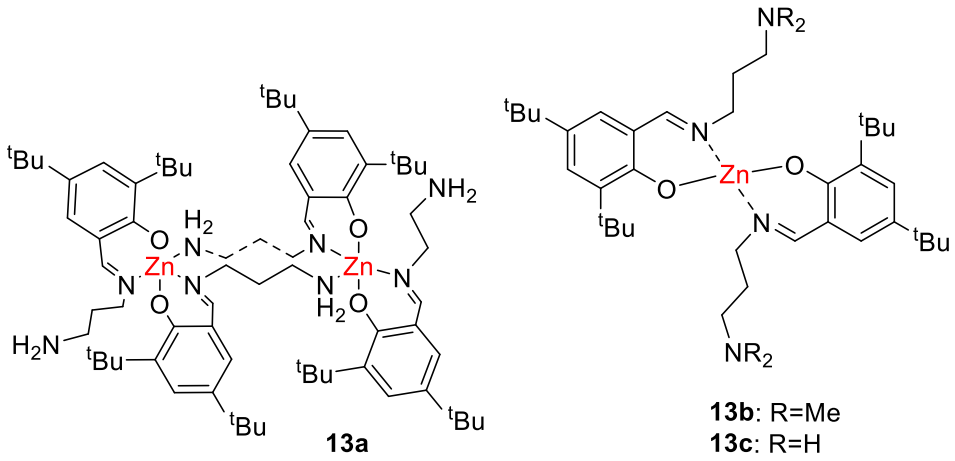

Figure 1.24 McKeown propylamine complexes.

1.7 Recycling of PET

While the development of recycling technologies for emerging bioplastics is crucial, there is also an urgent need to address the waste problems associated with current products. Indeed, bio-based plastics accounted for only 1 % of all processed plastics in 2019.[50] Polyethylene terephthalate (PET) is a commercially important polyester, exhibiting excellent chemical and physical properties for many implementations, such as high mechanical strength, good barrier properties and clearness.[51] Accordingly, PET has been widely exploited in the packaging industry and has also found use in construction, transport, and textiles industry. On the other hand, PET waste is becoming a problem for humans and the environment. Each year, approximately millions of metric tons of PET waste is transferred into the ocean and landfills. Currently, the methods of handling plastics are landfill, incineration, and plastics recycling. The first two methods involve the release of hazardous substances released into the environment; therefore, PET recycling seems to be the most interesting method. It offers opportunities to reduce the use of petrochemical-based products, minimize carbon dioxide emissions and reduce landfill space.[52]

The mechanical recycling of PET is a well-established process, but it causes the degradation of the properties of the plastic. This means that recycled PET is reused for lower value products, such as fibers in carpeting, which can no longer be recycled. Furthermore, this process requires transparent and not contaminated raw materials by other polymers such as PLA and polyvinyl chloride (PVC). A possible solution is chemical recycling which allows to preserve the value of the material in the long term. In addition, it is possible to access to product which a higher economic value than the polymer itself and use it for other applications.[53] Chemical recycling typically provides various degradation products depending on the method used, including hydrolysis, ammonolysis, methanolysis, and glycolysis (**Figure 1.25**).

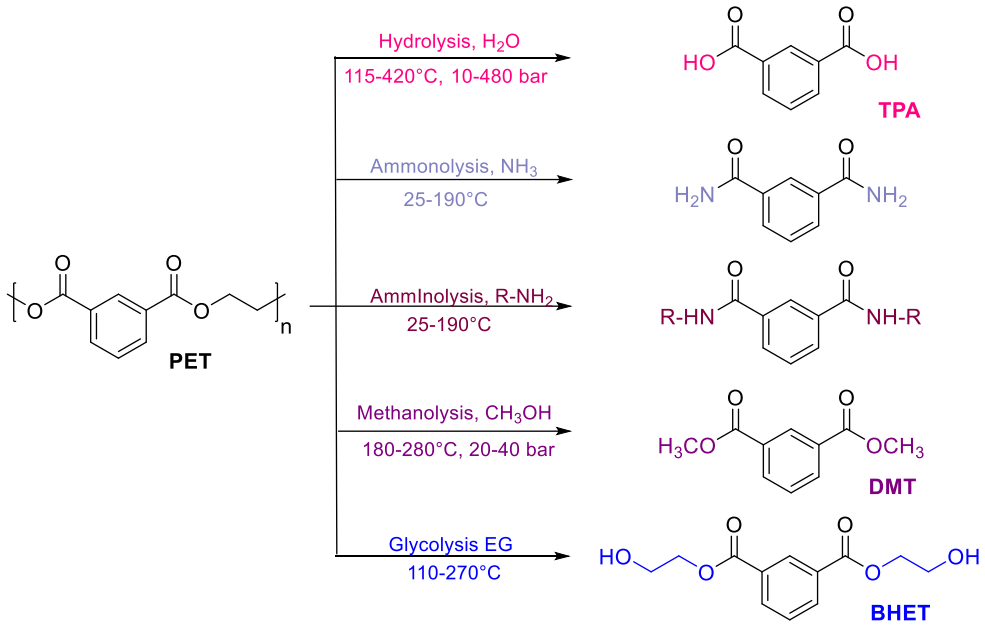

Figure 1.25 Examples of chemical degradation reactions of PET.

1.8 Glycolysis of PET

Among the various chemical recycling processes of PET, glycolysis is one of the most promising ways for polymer degradation due to its mild reaction conditions and the less volatile alcoholysis reagent, ethylene glycol (EG). Indeed, the glycolysis of PET is an industrially consolidated process managed by numerous leading companies worldwide such as DuPont, Shell and Eastman Kodak.[54]

Usually, the process was conducted with a temperatures range of 180–250 °C, extended reaction times (0.5–8 h) and in the presence of a catalyst. The insertion of glycol in the PET chain leads to the formation of dimers, oligomers or bis(2-hydroxyethyl) terephthalate (BHET). Often a large excess of EG (EG / PET > 5: 1) is used to mediate the formation of long-chain oligomers, thus promoting the formation of BHET.[39]

The reaction products can be easily separated and purified by water extraction and crystallization.[55] Despite these outstanding advantages of the glycolysis reaction, the relatively long reaction time and low BHET yield pose great challenges to large-scale commercial application. Hence the development of new high-efficiency catalysts is an important topic for PET glycolysis.[56] An ideal catalyst for PET degradation should be abundant, sustainable, inexpensive, and highly reactive in solvent-free scenarios. Some examples of literature are listed below.

1.8.1 Representative catalyst systems for the glycolysis of PET

Organocatalysts have been extensively investigated as efficient catalysts for PET glycolysis. Wang et al. used *urea* (10 % by weight) as a cheap and reusable catalyst, obtaining 100 % PET degradation and a BHET yield of about 80 % after 3 h at 180 °C.[57] Fukushima et al. employed the use of a commercially available guanidine, namely *TBD* (**Figure 1.26**).[58] After 3.5 h at 190 °C, BHET was isolated after crystallization in a yield of 78 %. Although traditional organocatalysts generally exhibit high activity for PET glycolysis, they remain limited by the loss of activity experienced during repeated use due to of oxodegredative reactions or concurrent side reactions.

Figure 1.26 Organocatalyst examples.

Recent advances in this area have involved the development of amidine and guanidine-type eutectic salts, which showed higher stability and efficiency. Jehanno et al. developed a TBD/methanesulfonic acid complex (TBD / MSA, 1/ 1), the first industrially relevant organocatalyst (**Figure 1.27**).[59] This combined the high catalytic activity of the free base with excellent thermal stability (> 400 °C), resulting in a 91 % BHET yield within 2 h at 180 °C. Furthermore, the catalyst could be recycled at least 5 times. The reaction products were easily separated from the ionic liquid by addition of water followed by filtration, allowing for easy recovery and reuse of the catalyst.

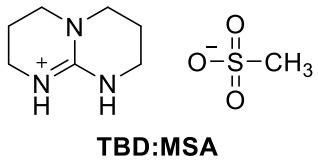

Figure 1.27 Jehanno example.

Metal-based catalysts for PET glycolysis have also been developed. Pingale et al. investigated several metal chlorides (e.g., Zn, Li, Mg and Fe) for the catalytic degradation of waste PET bottles.[60] Zinc chloride was the most active, achieving a BHET yield of 73 % within 8 h under reflux. A reactivity scale of Zn> Pr / Nd> Mg> Li> Fe was defined, even though the optimal PET/EG molar ratio varied with the type of metal. Although such salts are inexpensive and readily available, they were relatively slow, and it was difficult to recover the catalyst.

Despite the plethora of catalysts reported in the literature, the use of metal-based discrete systems for PET glycolysis remains rare. In particular, Troev et al. reported a very efficient catalyst, Ti(IV)-phoshate (**Figure 1.28**), obtaining a 98 % BHET conversion within 150 min in a temperature range between 190-200 °C.[61]

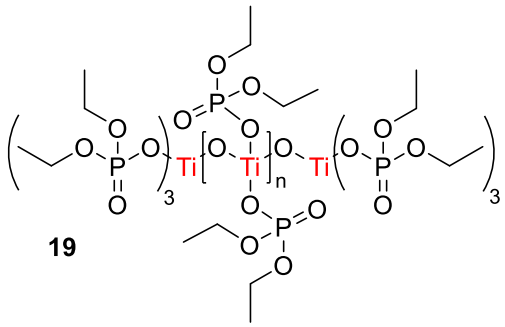

Figure 1.28 Troev complex.

The first example of Zn-based complex used for the PET glycolysis was reported by Jones et al. in 2021 (**Figure 1.29**).[62] Its application in the PLA methanolysis under mild conditions had already been demonstrated. For PET degradation, the Zn complex was able to degrade the PET with a BHET conversion of 61 % within 1 h at 180 °C, exceeding the yield obtained using $Zn(OAc)_2$ (% BHET conversion = 48 %) under the same reaction conditions.

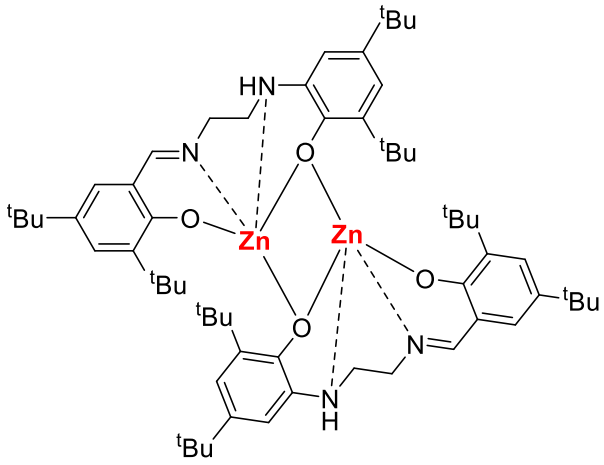

Figure 1.29 Jones complex.

1.9 Aim of the thesis

In recent years, scientists around the world have been wondering about possible solutions to tackle the problem of plastic pollution. The shift towards bio-based materials could eliminate the use of petroleum-based material, but it is necessary to define *a priori* end-of-life treatments. There are applications in which biopolymers still fail to meet these characteristics, thus a chemical recycling of traditional plastics would reduce accumulation and help the reuse of the raw material. The future of the plastic must be based on a circular economy in which the material retains its value even after its use.

Polylactide (PLA) is the most attractive eco-friendly biopolymer deriving from renewable resources, biodegradable and biocompatible. Industrially, it is obtained by polymerization of lactide promoted by highly toxic tin-based complex.

Therefore, purpose of this Ph.D. thesis was the development of new catalytic systems able of synthesizing PLA using non-toxic and sufficiently robust metals able to withstand even industrially relevant reaction conditions. To fulfill the principles of circular economy, designed metal complexes were tested into the chemical degradation reactions too, both of PLA and of widely used traditional polymers, such as poly(ethylene) terephthalate (PET), the most important commercial polyester used to produce disposable products mainly.

In *Chapter 2*, the work focused on the functional design of catalytic species in terms of ancillary ligand structure, nature of the metal center and coordination geometry. Indeed, heteroleptic and homoleptic complexes of zinc and magnesium supported by pyridyl phenoxy-imine ligands were synthesized and used to promote both the synthesis and the degradation of PLA.

The exciting results obtained with zinc heteroleptic complexes prompted us, in *Chapter 3*, to investigate the effect of different substituents on the ligand. Excellent activities were observed for the polymerization of lactide both in solution and in melt conditions. The same complexes were used for the PLA alcoholysis reaction too. Mechanistic studies were carried out for the latter reaction, showing two different pathways depending on the conditions employed (in solution or solvent-free).

As a matter of fact, the chemical degradation reaction of PLA promoted by metal complexes is still little investigated in literature and the identification of easy-to-obtain and inexpensive catalytic systems is one of the challenges to be faced in this field. *Chapter 4* reports the catalysis behavior of commercially available amides of non-toxic and low-cost metals in the degradation reactions of PLA. Furthermore, these studies have been extended to the chemical degradation (by glycolysis) of PET.

Recent literature studies have shown that bimetallic complexes, both dimeric and dinucleating, can show a peculiar catalytic behavior compared to monometallic analogues due to cooperative effects that can be established between two reactive centers.[63] In *Chapter 5*, the pyridyl phenoxy-imine ligand, described in the previous chapters, was introduced with a binaphthol backbone, in order to obtain hexacoordinate ligands. These were tailored to have a coordinated pocket that promoted the formation of bimetallic complexes. Both the enantiomerically pure complex and the racemic form were synthesized and used in the polymerization of lactide under different reaction conditions. Mechanistic studies were conducted to obtain information on active species.

During the last year of Ph.D., I spent six-month period as a visiting student at the School of Chemistry in Tel Aviv University (TAU) under the supervision of prof. Moshe Kol. Here, the synthesis of new zirconium complexes supported by tris(phenolate) amino ligands and their use as catalysts for the polymerization of *rac*-lactide and *meso*-lactide, were performed. Related details are, thus, described in *Chapter 6*.

References

[1] Plastics-the Facts 2021. An analysis of European plastics production, demand and waste data. *Plastics Europe* (2021). https://plasticseurope.org/knowledge-hub/plastics-the-facts-2021/

[2] Shafiee, S., Topal, E. When will fossil fuel reserves be diminished? *Energy Policy* **37**, 181–189 (2009).

[3] [a]Bonanno, G., Orlando-Bonaca, M. Ten inconvenient questions about plastics in the sea. *Environmental Science & Policy* **85**, 146–154 (2018).
[b]Lebreton, L., Slat, B., Ferrari, F., Sainte-Rose, B., Aitken, J., Marthouse, R., Hajbane, S., Cunsolo, S., Schwarz, A., Levivier, A., Noble, K., Debeljak, P., Maral, H., Schoeneich-Argent, R. Brambini R., Reisser, J. Evidence that the Great Pacific Garbage Patch is rapidly accumulating plastic. *Scientific Report* **8**, 4666-4681 (2018).
[c]McKeown, P., Jones, M. D. The Chemical Recycling of PLA: A Review. *Sustainable Chemistry* **1**, 1-22 (2020).

[4] The new plastics economy: rethinking the future of plastics & catalysing action. *Ellen Macarthur Foundation* (2017). https://ellenmacarthurfoundation.org/the-new-plastics-economy-rethinking-the-future-of-plastics-and-catalysing

[5] Coates, G. W., Getzler, Y. D. Y. L. Chemical recycling to monomer for an ideal, circular polymer economy. *Nature Reviews Materials* **5**, 501–516 (2020).

[6] Payne, J., McKeown, P., Jones, M. D. A circular economy approach to plastic waste. *Polymer Degradation and Stability* **165**, 170–181 (2019).

[7] Kaur, G., Uisan, K., Ong, K. L., Ki Lin, C. S. Recent Trends in Green and Sustainable Chemistry & Waste Valorisation: Rethinking Plastics in a circular economy. *Current Opinion in Green and Sustainable Chemistry* **9**, 30–39 (2018).

[8] Cosate de Andrade, M. F., Souza, P. M. S., Cavalett, O., Morales, A. R. Life Cycle Assessment of Poly(Lactic Acid) (PLA): Comparison Between Chemical Recycling, Mechanical Recycling and Composting. *Journal of Polymers and the Environment* **24**, 372–384 (2016).

[9] [a]Jamshidian, M., Tehrany, E. A., Imran, M., Jacquot, M., Desobry, S. Poly-Lactic Acid: Production, applications, nanocomposites, and release studies. *Comprehensive Reviews in Food Science and Food Safety* **9**, 552–571 (2010).
[b]Balla, E., Daniilidis, V., Karlioti, G., Kalamas, T., Stefanidou, M., Bikiaris, N. D., Vlachopoulos, A., Koumentakou, I., Bikiaris, D. N. Poly(lactic acid): A versatile biobased polymer for the future with multifunctional properties-from monomer synthesis, polymerization techniques and molecular weight increase to PLA applications. *Polymers* **13**, 1822-1872 (2021).

[10] Van Wouwe, P., Dusselier, M., Vanleeuw, E., Sels, B. Lactide Synthesis and Chirality Control for Polylactic acid Production. *ChemSusChem* **9**, 907-921 (2016).

[11] [a]Abdel-Rahman, M. A., Tashiro, Y., Sonomoto, K. Recent advances in lactic acid production by microbial fermentation processes. *Biotechnology Advances* **31**, 877–902 (2013).
[b]Luo, F., Fortenberry, A., Ren, J., Qiang, Z. Recent Progress in Enhancing Poly(Lactic Acid) Stereocomplex Formation for Material Property Improvement. *Frontiers in Chemistry* **8**, 688-696 (2020).
[c]Jem, K. J., Tan, B. The development and challenges of poly (lactic acid) and poly (glycolic acid). *Advanced Industrial and Engineering Polymer Research* **3**, 60–70 (2020).

[12] Auras, R., Harte, B., Selke, S. An overview of polylactides as packaging materials. *Macromolecular Bioscience* **4**, 835–864 (2004).

[13] [a]Worch, J. C., Prydderch, H., Jimaja, S., Bexis, P., Becker, M. L., Dove, A. P. Stereochemical enhancement of polymer properties. *Nature Reviews Chemistry* **3**, 514–535 (2019).
[b]Pang, X., Zhuang, X., Tang, Z., Chen, X. Polylactic acid (PLA): Research, development, and industrialization. *Biotechnology Journal* **5**, 1125–1136 (2010).

[14] [a]Thomas, C. M. Stereocontrolled ring-opening polymerization of cyclic esters: Synthesis of new polyester microstructures. *Chemical Society Reviews* **39**, 165–173 (2010).
[b]Tschan, M. J. L., Gauvin, R. M., Thomas, C. M. Controlling polymer stereochemistry in ring-opening polymerization: A decade of advances shaping the future of biodegradable polyesters. *Chemical Society Reviews* **50**, 13587–13608 (2021).

[15] Bai, H., Deng, S., Bai, D., Zhang, Q., Fu, Q. Recent Advances in Processing of Stereocomplex-Type Polylactide. *Macromolecular Rapid Communications* **38**, 1700454-1700466 (2017).

[16] Chile, L. E., Mehrkhodavandi, P., Hatzikiriakos, S. G. A Comparison of the Rheological and Mechanical Properties of Isotactic, Syndiotactic, and Heterotactic Poly(lactide). *Macromolecules* **49**, 909–919 (2016).

[17] Masutani, K., Kimura, Y. Chapter 1. PLA Synthesis. From the Monomer to the Polymer. In book: *Poly(lactic acid) Science and Technology* 1–36 (2014).

[18] Platel, R. H., Hodgson, L. M., Williams, C. K. Biocompatible initiators for lactide polymerization. *Polymer Reviews* **48**, 11–63 (2008).

[19] Williams, C. K. Synthesis of functionalized biodegradable polyesters. *Chemical Society Reviews* **36**, 1573–1580 (2007).

[20] Zhang, X., Fevre, M., Jones, G. O., Waymouth, R. M. Catalysis as an Enabling Science for Sustainable Polymers. *Chemical Reviews* **118**, 839–885 (2018).

[21] [a]Kiesewetter, M. K., Shin, E. J., Hedrick, J. L., Waymouth, R. M. Organocatalysis: Opportunities and challenges for polymer synthesis. *Macromolecules* **43**, 2093–2107 (2010).
[b]Fazekas, E., Lowy, P. A., Rahman, M. A., Lykkeberg, A., Zhou, Y., Chambenahallia R., Garden, J. A. Main group metal polymerisation catalysts. *Chemical Society Reviews* **51**, 8793-8814 (2022).
[c]Ottou, W. N., Sardon, H., Mecerreyes, D., Vignolle, J., Taton, D. Update and challenges in organo-mediated polymerization reactions. *Progress in Polymer Science* **56**, 64–115 (2016).

[22] [a]Kremer, A. B., Mehrkhodavandi, P. Dinuclear catalysts for the ring opening polymerization of lactide. *Coordination Chemistry Reviews* **380**, 35–57 (2019).
[b]Gao, J., Zhu, D., Zhang, W., Solan, G. A., Ma, Y., Sun, W.-H. Recent progress in the application of group 1, 2 & 13 metal complexes as catalysts for the ring opening polymerization of cyclic esters. *Inorganic Chemistry Frontiers* **6**, 2619–2652 (2019).
[c]Dong, X., Robinson, J. R. The versatile roles of neutral donor ligands in tuning catalyst performance for the ring-opening polymerization of cyclic esters. *New Journal of Chemistry* **46**, 444–453 (2022).
[d]Roy, S. S., Sarkar, S., Chakraborty, D. Macrocycles in dual role: ancillary ligands in metal complexes and organocatalysts for the ring-opening polymerization of lactide. *Journal of Inclusion Phenomena and Macrocyclic Chemistry* **100**, 1-36 (2021).
[e]Santoro, O., Zhang, X., Redshaw, C. Synthesis of biodegradable polymers: A review on the use of schiff-base metal complexes as catalysts for the ring opening polymerization (ROP) of cyclic esters. *Catalysts* **10**, 1–49 (2020).

[23] Chisholm, M. H., Galluci, J. C., Zhen, H., Huffman, J. C. Three-coordinate zinc amide and phenoxide complexes supported by a schiff base ligand. *Inorganic Chemistry* **40**, 5051–5054 (2001).

[24] Chen, H. Y., Tang, H. Y., Lin, C. C. Ring-opening polymerization of lactides initiated by zinc alkoxides derived from NNO-tridentate ligands. *Macromolecules* **39**, 3745–3752 (2006).

[25] Williams, C. K., Breyfogle, L. E., Choi, S. K., Nam, W., Young, V. G., Hillmyer, M. A., Tolman, W. B. A highly active zinc catalyst for the controlled polymerization of lactide. *Journal of the American Chemical Society* **125**, 11350–11359 (2003).

[26] Chamberlain, B. M., Cheng, M., Moore, D. R., Ovitt, T. M., Lobkovsky, E. B., Coates, G. W. Polymerization of lactide with zinc and magnesium β-diiminate complexes: Stereocontrol and mechanism. *Journal of the American Chemical Society* **123**, 3229–3238 (2001).

[27] Thevenon, A., Romain, C., Bennington, M. S., White, A. J. P., Davidson, H. J., Brooker, S., Williams, C. K. Dizinc Lactide Polymerization Catalysts: Hyperactivity by Control of Ligand Conformation and Metallic Cooperativity. *Angewandte Chemie* **128**, 8822–8827 (2016).

[28] Schäfer, P. M., Fuchs, M., Ohligschläger, A., Rittinghaus, R., McKeown, P., Akin, E., Schmidt, M., Hoffmann, A., Liauw, M. A., Jones, M. D., Herres-Pawlis, S. Highly Active N,O Zinc Guanidine Catalysts for the Ring-Opening Polymerization of Lactide. *ChemSusChem* **10**, 3547–3556 (2017).

[29] McKeown, P., McCormick, S. N., Mahon, M. F., Jones, M. D. Highly active Mg(II) and Zn(II) complexes for the ring opening polymerization of lactide. *Polymer Chemistry* **9**, 5339–5347 (2018).

[30] McKeown, P., Román-Ramírez, L. A., Bates, S., Wood, J., Jones, M. D. Zinc Complexes for PLA Formation and Chemical Recycling: Towards a Circular Economy. *ChemSusChem* **12**, 5233–5238 (2019).

[31] Ho, K.-L. G., Pometto, A. L., Gadea-Rivas, A., Briceno, J. A., Rojas, A. Degradation of Polylactic Acid (PLA) Plastic in Costa Rican Soil and Iowa State University Compost Rows. *Journal of Environmental Polymer Degradation* **7**, 173-177(1999).

[32] [a]Payne, J., Jones, M. D. The Chemical Recycling of Polyesters for a Circular Plastics Economy: Challenges and Emerging Opportunities. *ChemSusChem* **14**, 4041–4070 (2021).
[b]Bagheri, A. R., Laforsch, C., Greiner, A., Agarwal, S. Fate of So-Called Biodegradable Polymers in Seawater and Freshwater. *Global Challenges* **1**, 1700048 (2017).

[33] [a]La Mantia, F. P., Botta, L., Morreale, M., Scaffaro, R. Effect of small amounts of poly(lactic acid) on the recycling of poly(ethylene terephthalate) bottles. *Polymer Degradation and Stability* **97**, 21–24 (2012).
[b]Alaerts, L., Augustinus, M. & van Acker, K. Impact of bio-based plastics on current recycling of plastics. *Sustainability* **10**, 1487-1493 (2018).

[34] [a]Kale, G., Kijchavengkul, T., Auras, R., Rubino, M., Selke, S. E., Singh, S. P. Compostability of bioplastic packaging materials: An overview. *Macromolecular Bioscience* **7**, 255–277 (2007).
[b]Emadian, S. M., Onay, T. T., Demirel, B. Biodegradation of bioplastics in natural environments. *Waste Management* **59**, 526–536 (2017).

[35] Beltrán, F. R., Lorenzo, V., Acosta, J., De la Orden, M. U. & Martínez Urreaga, J. Effect of simulated mechanical recycling processes on the structure and properties of poly(lactic acid). *Journal of Environmental Management* **216**, 25–31 (2018).

[36] [a]Feng, L., Feng, S., Bian, X., Li, G., Chen, X. Pyrolysis mechanism of Poly(lactic acid) for giving lactide under the catalysis of tin. *Polymer Degradation and Stability* **157**, 212-223 (2018).
[b]McNeill, I. C., Leiper, H. A. Degradation under isothermal conditions, thermal degradation mechanism and photolysis of the polymer. *Polymer Degradation and Stability* **11**, 309-326 (1985).

[37] Dusselier, M., Van Wouwe, P., Dewaele, A., Makshina, E., Sels, B.F. Lactic acid as a platform chemical in the biobased economy: The role of chemocatalysis. *Energy & Environmental Science* **6**, 1415–1442 (2013).

[38] [a]Calvo-Flores, F. G., Monteagudo-Arrebola, M. J., Dobado, J. A., Isac-García, J. Green and Bio-Based Solvents. *Topics in Current Chemistry* **376**, 18-58 (2018).

[b]Lamberti, F. M., Román-Ramírez, L. A., Mckeown, P., Jones, M. D., Wood, J. Kinetics of alkyl lactate formation from the alcoholysis of poly(lactic acid). *Processes* **8**, 738-751 (2020).

[39] Lamberti, F. M., Román-Ramírez, L. A., Wood, J. Recycling of Bioplastics: Routes and Benefits. *Journal of Polymers and the Environment* **28**, 2551–2571 (2020).

[40] Carné Sánchez, A., Collinson, S. R. The selective recycling of mixed plastic waste of polylactic acid and polyethylene terephthalate by control of process conditions. *European Polymer Journal* **47**, 1970–1976 (2011).

[41] Petrus, R., Bykowski, D., Sobota, P. Solvothermal Alcoholysis Routes for Recycling Polylactide Waste as Lactic Acid Esters. *ACS Catalysis* **6**, 5222–5235 (2016).

[42] Song, X., Zhang, X., Wang, H., Liu, F., Yu, S., Liu, S. Methanolysis of poly(lactic acid) (PLA) catalyzed by ionic liquids. *Polymer Degradation and Stability* **98**, 2760–2764 (2013).

[43] Song, X., Bian, Z., Hui, Y., Wang, H., Liu, F., Yu, S. Zn-Acetate-Containing ionic liquid as highly active catalyst for fast and mild methanolysis of Poly(lactic acid). *Polymer Degradation and Stability* **168**, 108937 (2019).

[44] Jehanno, C., Pérez-Madrigal, M. M., Demarteau, J., Sardon, H., Dove, A. P. Organocatalysis for depolymerisation. *Polymer Chemistry* **10**, 172–186 (2019).

[45] Alberti, C., Damps, N., Meißner, R. R. R., Enthaler, S. Depolymerization of End-of-Life Poly(lactide) via 4-Dimethylaminopyridine-Catalyzed Methanolysis. *ChemistrySelect* **4**, 6845–6848 (2019).

[46] Whitelaw, E. L., Davidson, M. G., Jones, M. D. Group 4 salalen complexes for the production and degradation of polylactide. *Chemical Communications* **47**, 10004–10006 (2011).

[47] Fliedel, C., Vila-Viçosa, D., Calhorda, M. J., Dagorne, S., Avilés, T. Dinuclear zinc-N-heterocyclic carbene complexes for either the controlled ring-opening polymerization of lactide or the controlled degradation of polylactide under mild conditions. *ChemCatChem* **6**, 1357–1367 (2014).

[48] Payne, J., McKeown, P., Mahon, M. F., Emanuelsson, E. A. C., Jones, M. D. Mono-and dimeric zinc(II) complexes for PLA production and degradation into methyl lactate-a chemical recycling method. *Polymer Chemistry* **11**, 2381–2389 (2020).

[49] Román-Ramírez, L. A., McKeown, P., Jones, M. D., Wood, J. Poly(lactic acid) Degradation into Methyl Lactate Catalyzed by a Well-Defined Zn(II) Complex. *ACS Catalysis* **9**, 409–416 (2019).

[50] European Bioplastics, Facts and Figures. (2020)
https://docs.european-bioplastics.org/publications/EUBP_Facts_and_figures.pdf

[51] [a]Dhaka, V., Singh, S., Anil, A.G., Kumar Naik, T. S. S., Garg, S., Samuel, J., Kumar, M., Ramamurthy, P. C., Singh, J. Occurrence, toxicity and remediation of polyethylene terephthalate plastics. A review. *Environmental Chemistry Letters* **20**, 1777–1800 (2022).
[b]Ghasemi, M. H., Neekzad, N., Ajdari, F. B., Kowsari, E., Ramakrishna, S. Mechanistic aspects of poly(ethylene terephthalate) recycling-toward enabling high quality sustainability decisions in waste management. *Environmental Science and Pollution Research* **28**, 43074-43101 (2021).

[52] Damayanti, Wu, H. S. Strategic possibility routes of recycled PET. *Polymers* **13,** 1475-1512 (2021).

[53] Chu, M., Liu, Y., Lou, X., Zhang, Q., Chen, J. Rational Design of Chemical Catalysis for Plastic Recycling. *ACS Catalysis* **12**, 4659–4679 (2022).

[54] [a]Kojima, Y., Takahara, M., Matsuoka, T. & Takahashi, H. Studies of glycolysis of poly(ethylene terephthalate) recycled from postconsumer soft-drink bottles. I. Influences of glycolysis conditions. *Journal of Applied Polymer Science* **80**, 943–948 (2001).
[b]Xi, G., Lu, M., Sun, C. Study on depolymerization of waste polyethylene terephthalate into monomer of bis(2-hydroxyethyl terephthalate). *Polymer Degradation and Stability* **87**, 117–120 (2005).
[c]Chen, C. H. Study of glycolysis of poly(ethylene terephthalate) recycled from postconsumer soft-drink bottles. III. Further investigation. *Journal of Applied Polymer Science* **87**, 2004–2010 (2003).

[55] Duque-Ingunza, I., López-Fonseca, R., de Rivas, B., Gutiérrez-Ortiz, J. I. Process optimization for catalytic glycolysis of post-consumer PET wastes. *Journal of Chemical Technology and Biotechnology* **89**, 97–103 (2014).

[56] Xin, J., Zhang, Q., Huang, J., Huang, R., Jaffery, Q. Z., Yan, D., Zhou, Q., Xu, J., Lu, X. Progress in the catalytic glycolysis of polyethylene terephthalate. *Journal of Environmental Management* **296**, 113267 (2021).

[57] Wang, Q., Yao, X., Tang, S., Lu, X., Zhanga, X., Zhang, S. Urea as an efficient and reusable catalyst for the glycolysis of poly(ethylene terephthalate) wastes and the role of hydrogen bond in this process. *Green Chemistry* **14**, 2559–2566 (2012).

[58] Fukushima, K., Coulembier, O., Lecuyer, J. M., Almegren, H. A., Alabdulrahman, A. M., Alsewailem, F. D., Mcneil, M. A., Dubois, P., Waymouth, R. M., Horn, H. W., Rice, J. E., Hedrick, J. L. Organocatalytic depolymerization of poly(ethylene terephthalate). *Journal of Polymer Science Part A: Polymer Chemistry* **49**, 1273–1281 (2011).

[59] Jehanno, C., Flores, I., Dove, A. P., Müller, A. J., Ruipérez, F., Sardon, H. Organocatalysed depolymerisation of PET in a fully sustainable cycle using thermally stable protic ionic salt. *Green Chemistry* **20**, 1205–1212 (2018).

[60] Pingale, N. D., Palekar, V. S., Shukla, S. R. Glycolysis of postconsumer polyethylene terephthalate waste. *Journal of Applied Polymer Science* **115**, 249–254 (2010).

[61] Troev, K., Grancharov, G., Tsevi, R., Gitsov, I. Erratum: A Novel Catalyst for the Glycolysis of Poly(ethylene terephthalate). *Journal of Applied Polymer Science* **90**, 1148-1152 (2003).

[62] Payne, J., McKeown, P., Driscoll, O., Kociok-Köhn, G., Emanuelsson, E. A. C., Jones, M. D. Make or break: Mg(II)-and Zn(II)-catalen complexes for PLA production and recycling of commodity polyesters. *Polymer Chemistry* **12**, 1086–1096 (2021).

[63] Kremer, A. B., Mehrkhodavandi, P. Dinuclear catalysts for the ring opening polymerization of lactide. *Coordination Chemistry Reviews* **380**, 35–57 (2019).

CHAPTER 2

Differences between homoleptic and heteroleptic zinc and magnesium complexes for the synthesis and chemical degradation of PLA

The results described in this Chapter have been published in:

Santulli, F., Gravina, G.; Lamberti, M.; Tedesco, C.; Mazzeo, M. Zinc and magnesium catalysts for the synthesis for PLA and its degradation: Clues for catalyst design. *Molecular Catalysis* **528**, 112480-112488 (2022).

2.1 Introduction

Although polylactide (PLA) is considered a sustainable polymer, its current synthetic and waste management strategies show some challenges.[1] Currently, $Sn(Oct)_2$ is the catalyst used industrially to produce PLA by ring opening polymerization (ROP) of lactide, which is classified as a toxic compound. In recent years, lower toxic complexes of zinc[2] and magnesium[3] have been introduced as alternative catalysts offering high activity and control on the polymerization process.[4] Some of these examples reported in the literature are extremely active in solution and at room temperature[5] concurrently they often show a certain instability at high temperatures which causes a drop in performance under industrially relevant conditions (solvent-free conditions and temperature above the T_f of the polymer, generally 180 °C).[5a] Only few some exceptions are reported in the literature for Zn complexes.[6]

Ideally, implementing an efficient and environmentally friendly synthetic PLA procedure is not enough, but it must be accompanied by adequate waste management strategies in order to fit into a circular economic model. Currently, recycling of PLA is not yet effectively planned, and end-of-life items are incinerated or accumulated in landfills.

In this context, the chemical recycling of PLA by conversion into other useful chemicals is a particularly interesting route.[7] Several methods have been reported in the literature, including the alcoholysis of PLA to obtain alkyl lactates.[8] This is a very promising strategies as the products of the reaction can be used as green solvents[9] or, alternatively, can represent fruitful chemical platforms to produce lactic acid which can be reintroduced into the production cycle of PLA or for conversion to other chemicals.[10] Therefore, this approach would offer the added benefit of reducing PLA production costs and its impact on the food supply chain. Discrete metal complexes[11] have been successfully applied in this field. Recently, Jones and McKeown have described several families of homoleptic Zn (II) and Mg (II) complexes bearing tridentate NNO ligands for the transesterification of PLA.[12] In these studies, the authors highlighted the importance of structure of the ancillary ligand and the role of the additional amine donor.

Motivated by these results, we extended these studies to homoleptic and heteroleptic magnesium and zinc complexes stabilized by phenoxy-imine ligands bearing an additional pyridine moiety that is a weaker base than amine and moreover it may behave as a hemilabile donor, offering the chance of a flexible coordination geometry, with the aim to elucidate the role of the structural parameter advantageous for the catalytic activity.

2.2 Results and discussion

2.2.1 Synthesis and characterization

The ligand LH was obtained by simple condensation of the 2-(2-pyridyl) ethylamine with the 3,5-di-tert-butyl-2-hydroxybenzaldehyde in high yield (**Scheme 2.1**). The ligand was characterized by ^{1}H NMR spectroscopy (**Figures 2.9**).

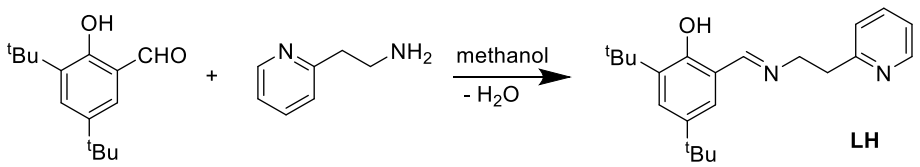

Scheme 2.1 Synthesis of ligand LH.

The homoleptic Zn (II) and Mg (II) complexes were synthetized by direct reaction of 2 equiv. of ligand LH with 1 equiv. of the alkyl metal precursors $Zn(Et)_2$ and $Mg(^nBu)_2$ in benzene at room temperature (**Scheme 2.2**).

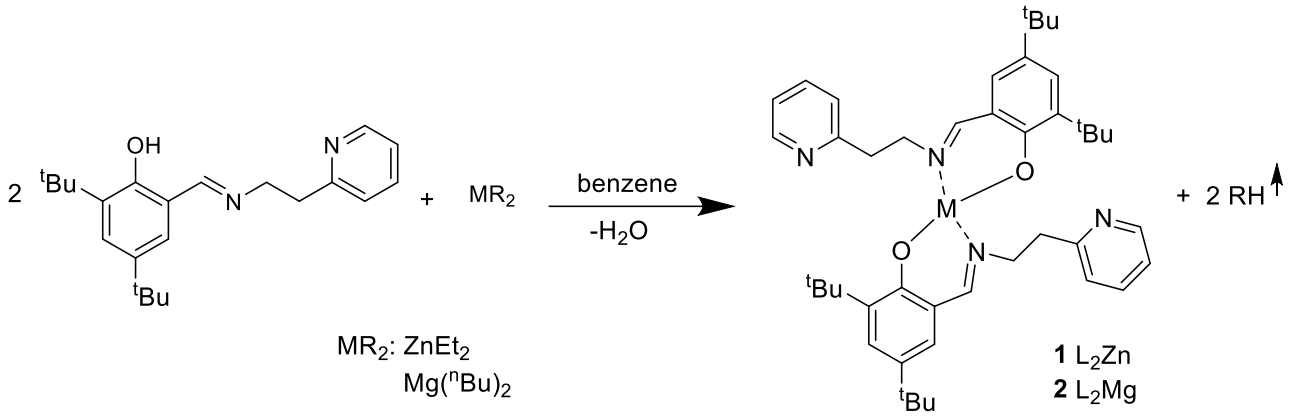

Scheme 2.2 Synthesis of homoleptic Zn (II) and Mg (II) complexes **1-2**.

The corresponding heteroleptic complexes were obtained by using the ligand LH and 1 equiv. of the opportune trimethylsilylamide metal precursor $M[N(SiMe_3)_2]_2$ in benzene at room temperature (**Scheme 2.3**).

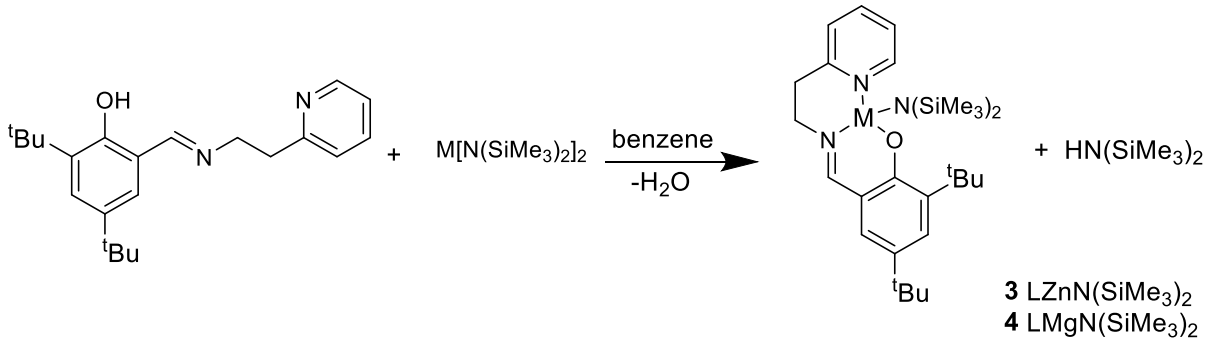

Scheme 2.3 Synthesis of heteroleptic Zn (II) and Mg (II) complexes **3-4**.

The analogous bis(phenoxy-imine) zinc complex bearing ^{t}Bu substituents (complex **5)** was also synthetized (**Scheme 2.4**) to understand the role of the additional neutral donor on the imine fragment. This complex was previously delineated by Jones in recent studies.[12a]

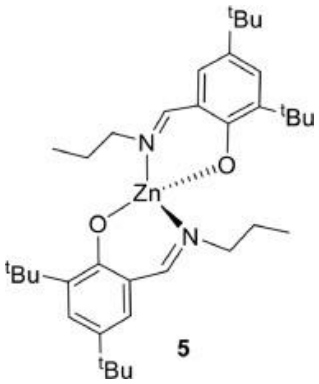

Scheme 2.4 Homoleptic Zn (II) complex **5**.

Complexes **1**–**5** were characterized by mono- and bi-dimensional NMR spectroscopy (**Figures 2.10 – 2.23**)

In the ^{1}H NMR spectrum of complex **1**, the disappearance of the -OH signal at δ =14.2 ppm of the ligand demonstrated the complete formation of the complex. The proton imine signal changed the chemical shift from

the ligand to the complex (from δ = 7.75 ppm for the ligand to δ = 7.67 ppm for the complex **1**) indicative of the coordination to the metal center. Two triplets were observed at δ = 3.77 ppm and δ = 3.01 ppm for the methylene protons of the pyridine pendant arms whose multiplicity was indicative of a high conformational freedom of the moieties. Moreover, the absence of correlations between the protons of the pyridyl rings and other fragments of the ligand skeleton in the NOESY spectrum suggested that pyridine nitrogen atoms were not coordinated at metal center (**Figure 2.13**).

The symmetrical structure observed for complex **1** in solution was similar to that observed by Jones for the homoleptic amine phenoxy-imine complexes in which the metal centers were tetracoordinated to the imine nitrogen and oxygen atoms.[13] This is entirely consistent with that observed in the solid state of a homoleptic zinc analog in which the pyridine pendant arms were far from the metal center.[14]

A different coordination geometry was observed for the homoleptic magnesium complex **2**, established by single-crystal X-ray diffraction studies (**Figure 2.1**, CCDC: 2,152,705). The crystals were obtained by slow diffusion of pentane into a benzene solution of complex **2** at room temperature. Selected bond lengths and angles are listed in **Table 2.3** of the Experimental Part.

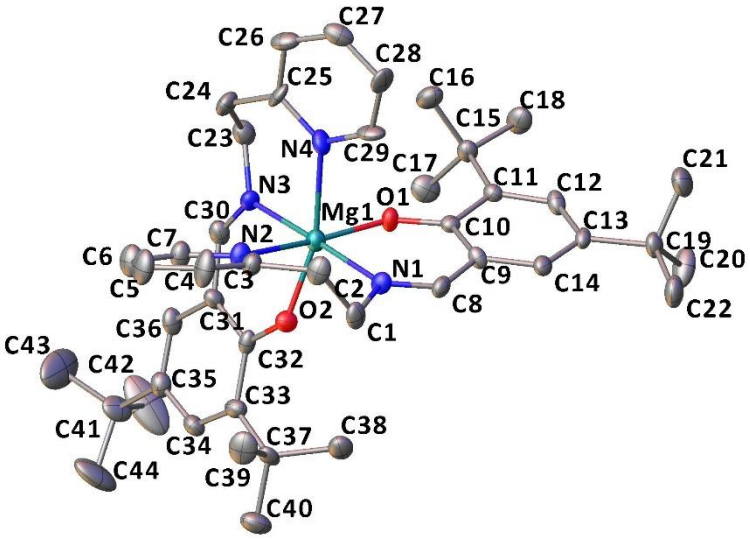

Figure 2.1 ORTEP representation of the crystallographic structure of complex **2** obtained by single crystal X-ray diffraction. Ellipsoids were drawn at 20 % probability level. Hydrogen atoms were omitted for clarity.

A distorted octahedral geometry was observed with the ligands wrapped around the magnesium in a mer–mer manner (**Figure 2.1**). The imine groups of both ligands are in the equatorial plane, while the pyridine nitrogen atoms and the phnoxy groups are opposite to each other; the imine N1 and N3 atoms are at a shorter distance from the Mg atom (2.145(7) Å and 2.159(7) Å) than the pyridine N2 and N4 atoms (2.366(8) Å and 2.274(8) Å).

The different coordination geometries of complexes **1** and **2** determined in the solid-state structures were also observed in solution in the NMR spectra. In the ^{1}H NMR spectrum of complex **2** performed at 25 °C, four broad resonances were observed at δ = 2.41, 2.68, 3.38, 4.28 ppm, each attributable to the four diasterotopic protons of the methylene groups present in the complex. Spectra obtained at higher temperatures showed only two triplet peaks (**Figure 2.2**), such as those observed for the complex **1** in which the pyridine is dissociated. Therefore, at higher temperatures, a fluxional phenomenon is plausible in which a tetracoordinate complex is formed by reversible detachment of the pyridine pendants.

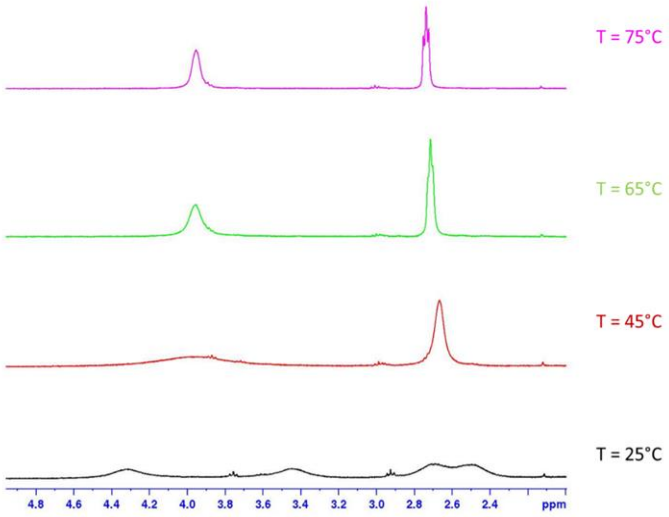

Figure 2.2 ^{1}H NMR spectra of methylene groups of complex **2** at variable-temperature.

The ^{1}H spectra of the heteroleptic complexes **3** and **4** (**Figures 2.18–2.21**) showed sharp and well resolved resonances for the pyridyl imino-phenolate ligand and the bis-(trimethylsilyl)amide group.

For zinc complex **3**, a light high-field ^{1}H NMR shift of the proton in the *ortho*- position of the pyridyl ring (δ = 8.35 ppm) in comparison to the same resonance for the free ligand (δ = 8.45 ppm) and broad signals for the methylene protons at δ = 3.19 ppm and δ = 2.95 ppm were observed. Differently, for the magnesium complex the same proton showed a low-field ^{1}H NMR shift (δ = 8.56 ppm). This difference could be a consequence of the different hard-soft character of the metals: for zinc complex a metal-to-ligand charge-transfer from its d^{10} closed shell to the π system of the pyridine ring could be responsible of observed high-field shift, while for magnesium a ligand-to-metal charge-transfer is a plausible explanation for the deshielding of the cited proton.

Strong evidence of coordination of the pyridine fragment to the two metal centres in heteroleptic complexes **3** and **4** was the NOESY correlations of the bis-(trimethylsilyl)amide groups with the α-protons of the pyridyl moiety, the imine protons and the methylene protons of the ligand (**Figure 2.19**).

2.2.2 Polymerization studies

Initially, all complexes were used for the polymerization of L-LA under solution conditions (in dichloromethane at room temperature and in toluene at 80 °C), and in the presence of 1 equiv. of alcohol (iPrOH or BnOH, respectively) as a co-initiator. Selected polymerization results are reported in **Table 2.1**. In all polymerization experiments, lactide purified by a single recrystallization from dry toluene was used.

Table 2.1
Polymerization Data of L-LA with complexes **1-5**.

Entry[a]	cat	time (min)	T (°C)	Solvent	Conv (%)	TOF (h^{-1})	M_{nGPC}[b] (KDa)	Đ[b]	M_{nth}[c] (KDa)
1	**1**	10	25	CH_2Cl_2	64	384	9.6	1.3	9.2
2	**2**	360	25	CH_2Cl_2	66	11	7.3	1.3	9.5
3	**3**	2	25	CH_2Cl_2	56	1700	8.7	1.2	8.1
4	**4**	360	25	CH_2Cl_2	33	5	5.3	1.3	4.7
5	**5**	1200	25	CH_2Cl_2	0	-	-	-	-
6	**1**	4	80	toluene	96	1400	10.3	1.8	13.8
7	**2**	4	80	toluene	60	900	11.1	1.2	8.6
8	**3**	2	80	toluene	100	3000	2.2	1.8	14.4
9	**4**	2	80	toluene	64	1920	2.1	1.2	9.2
10	**5**	2	80	toluene	0	-	-	-	-

11[d]	**1**	1	130	-	73	21900	23.4	1.1	52.6
12[d]	**3**	1	130	-	81	24300	21.5	1.5	58.4
13[e]	**1**	180	150	-	31	1033	3.8	n.d.	4.5

[a]All polymerizations were carried out by using 5 µmol of catalyst in 2 mL of solvent, with 1 equiv. of ROH (iPrOH for polymerizations at 25 °C and BnOH for polymerizations at 80 °C) and 100 equiv. of L-LA. [b]Experimental Mn and Đ values of the polymers were determined by gel-permeation chromatography (GPC) in THF relative to polystyrene standards and multiplied by a correction factor of 0.58. [c]Calculated according to the monomer conversion: M_{nth} (KDa) = 144.14 gmol^{-1} × ([LA]/[ROH]) × conversion of LA. [d]10µmol of catalyst and not purified LA (Sigma Aldrich) L-LA:BnOH = 500:1 [e]10 µmol of catalyst and technical grade L-LA:BnOH = 10 000:100.

From the polymerization reactions conducted in CH_2Cl_2 at room temperature, a drastic difference in terms of activity emerged between zinc and magnesium complexes. With the homoleptic complex **1**, the conversion of 60 equiv. of L-LA was achieved after 10 min (entry 1, **Table 2.1**), while with the homoleptic magnesium complex **2** the same conversion was achieved only after 6 h (entry 2, **Table 2.1**). The heteroleptic zinc complex **3** showed the highest activity reaching a TOF of 1700 h^{-1} (entry 3, **Table 2.1**); this value is among the highest reported in the literature for polymerization of LA performed at room temperature, although it is significantly lower than that reported for bimetallic zinc catalysts developed by Williams and co-workers (TOF up to 60000 h^{-1} in THF).[5a] The heteroleptic magnesium complex **4** showed low activity, about half that of the magnesium homoleptic complex **2** (compare entries 2 and 4, **Table 2.1**). No activity was observed with complex **5** even after prolonged reaction times (entry 5, **Table 2.1**).

A similar trend of activities was observed for polymerization reactions in toluene at 80 °C (entries 6–10, **Table 2.1**) and the best performance was achieved with the heteroleptic zinc complex **3**. Even at a higher temperature, complex **1** revealed to be more efficient than complex **5** confirming the pivotal role of the neutral donor of the pendant arm in the catalytic process.[11c]

Subsequently, Zn (II) complexes were tested at a higher temperature (130 °C) under melt conditions (entries 11 and 12, **Table 2.1**). These conditions offer the advantage of avoiding the use of solvents that are a significant source of waste, to date very few metal catalysts can withstand these harsh conditions.[15] Instead, in this case very high TOF were reached with both zinc complexes. Furthermore, polymerization experiment was conducted with catalyst **1** under conditions relevant to the industrial process, using a large amount of L-LA of technical grade purity with benzyl alcohol as the chain transfer agent for molecular weight control (L-LA: Zn: BnOH = 10 000: 1: 100) at 150 °C and in the absence of solvent. Also under these conditions, the catalyst preserved its high activity and the conversion of 3000 equiv. of monomer was achieved after 3 h (entry 13, **Table 2.1**).

Kinetic studies for the zinc complexes were performed by NMR experiments in CD_2Cl_2 solution at 25 °C. It was observed that the polymerization rate follows a pseudo-first order reactions with respect to lactide consumption over time with k_{obs} = 0.028 min^{-1} for complex **1** (**Figure 2.24**) and k_{obs} = 0.975 min^{-1} for complex **3** (**Figure 2.25**).

The observed molecular weights for the polymerizations performed at room temperature (entries 1–4, **Table 2.1**), were in moderate agreement with the values theoretically expected (difference less than 23 %) and the disperisities were always lower than 1.3.

To evaluate the control degree of the different catalysts over the polymerization processes, the Matrix-Assisted Laser Desorption Ionization-Fourier Transform Ion Cyclotron Resonance (MALDI-FT-ICR) analysis of low molecular weight PLAs purposely prepared were performed. MALDI-FT-ICR spectra of PLA samples obtained from zinc catalysts **1** and **3** revealed a family of peaks separated by 144 mass units bearing the BnO/OH end groups demonstrating the absence of undesired transesterification reactions (**Figure 2.3**).

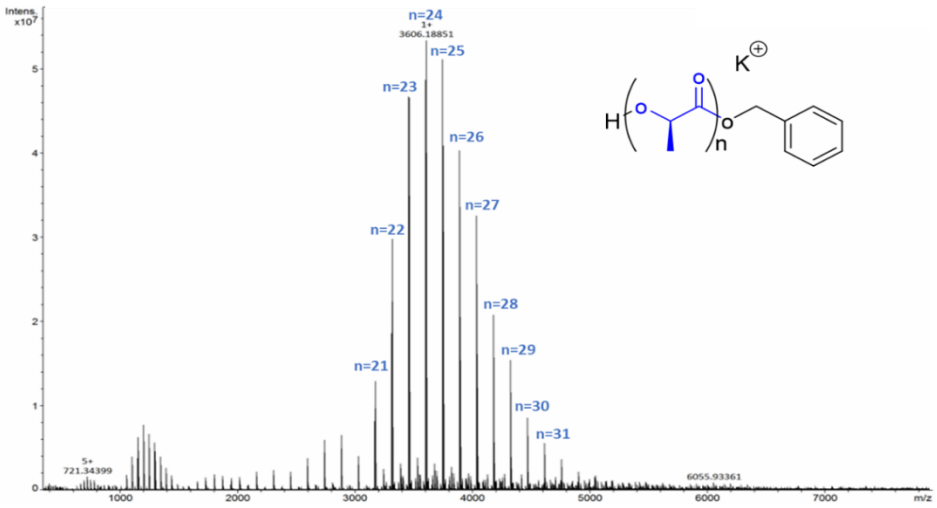

Figure 2.3 MALDI-FT-ICR MS spectrum of PLA synthesized by **1**.

However, when the reaction time was extended beyond the complete conversion of the monomer without quenching (entry 8, **Table 2.1**), transesterification reactions occur causing a lowering of the molecular weights of the polymers and an increase in dispersity (**Figure 2.26**). When unpurified or technical grade monomer was used, molecular masses of the polymers were significantly lower than the calculated values as a consequence of the presence of protic impurities acting as chain transfer agents and the increase in viscosity due to the absence of solvent (entries 11–12, **Table 2.1**), however, by increasing the equiv. of alcohol the control over molecular weights was restored (entry 13, **Table 2.1**).

On the other hand, the control degree on the molecular weights by the magnesium catalyst **4** was very low. In the MALDI-FT-ICR MS spectra of a PLAs obtained with **4** (**Figure 2.4**) multiple distributions were evident with a peak separation of 144 mass units, this could be a consequence of the presence of several active species in the polymerization medium.

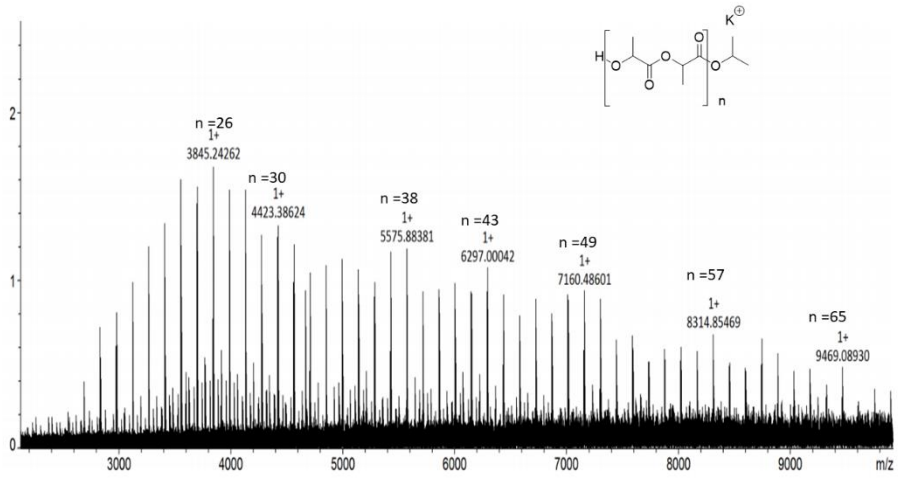

Figure 2.4 MALDI-FT-ICR MS spectrum of PLA synthesized by **4**.

For all polymers, the homonuclear decoupled ^{1}H NMR spectra demonstrated the absence of racemization phenomena, even at high temperature.

2.2.3 Mechanistic studies

Some mechanistic studies have been carried out by NMR analysis to clarify the different behavior of the complexes studied in the ROP of lactide. The reaction between complex **1** and 1 equiv. of isopropanol was performed at room temperature, in benzene-d6 solution and was monitored by ^{1}H NMR analysis. All signals of the metal complex **1** and the alcohol remained unchanged (**Figure 2.5**), and no interaction was shown between the two species.

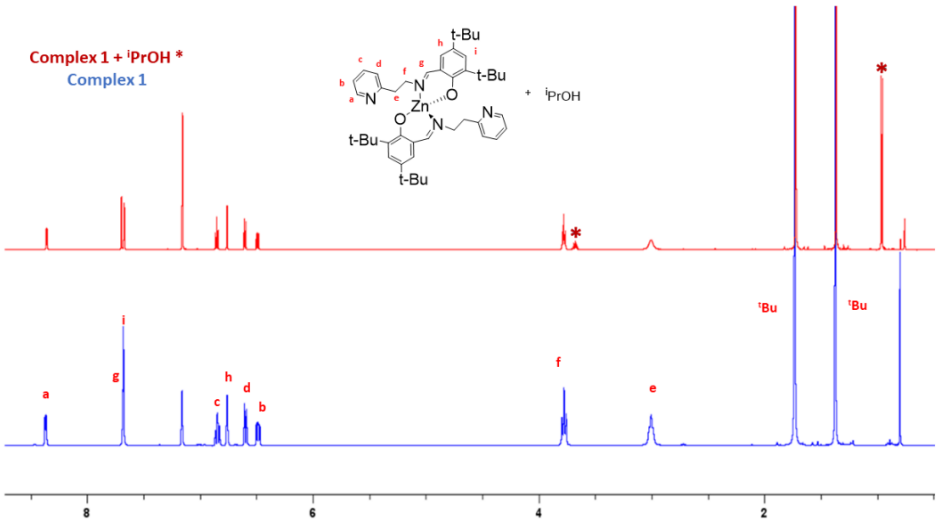

Figure 2.5 ^{1}H NMR spectrum (600 MHz, C_6D_6, 298 K) of complex **1** with 1 equiv. of ^{i}PrOH.

5 equiv. of lactide were then added and left for 10 min at room temperature. This did not change the resonances of metal complex signals while a weak upfield shift of methine resonances of lactide was evident as a consequence of its coordination at the metal center. At the same time, the resonances of the free isopropyl alcohol disappeared and additional resonances corresponding to the formation of PLA sequences were observed (**Figure 2.6**).

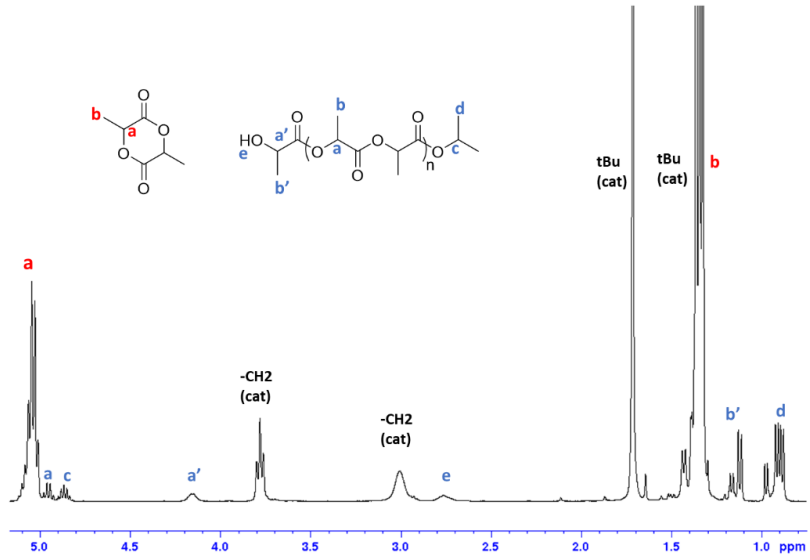

Figure 2.6 ^{1}H NMR spectrum (600 MHz, C_6D_6, 298 K) of complex **1** with iPrOH and 5 equiv. of L-LA.

All these observations were consistent with the hypothesis that an activated monomer mechanism is operative for the homoleptic complex **1** (**Scheme 2.4**) in which the metal center acts as a Lewis acid toward the monomer activating the carbonyl carbon and favoring the opening of the ring. The pyridine moieties do not compete significantly for the coordination at the metal center.

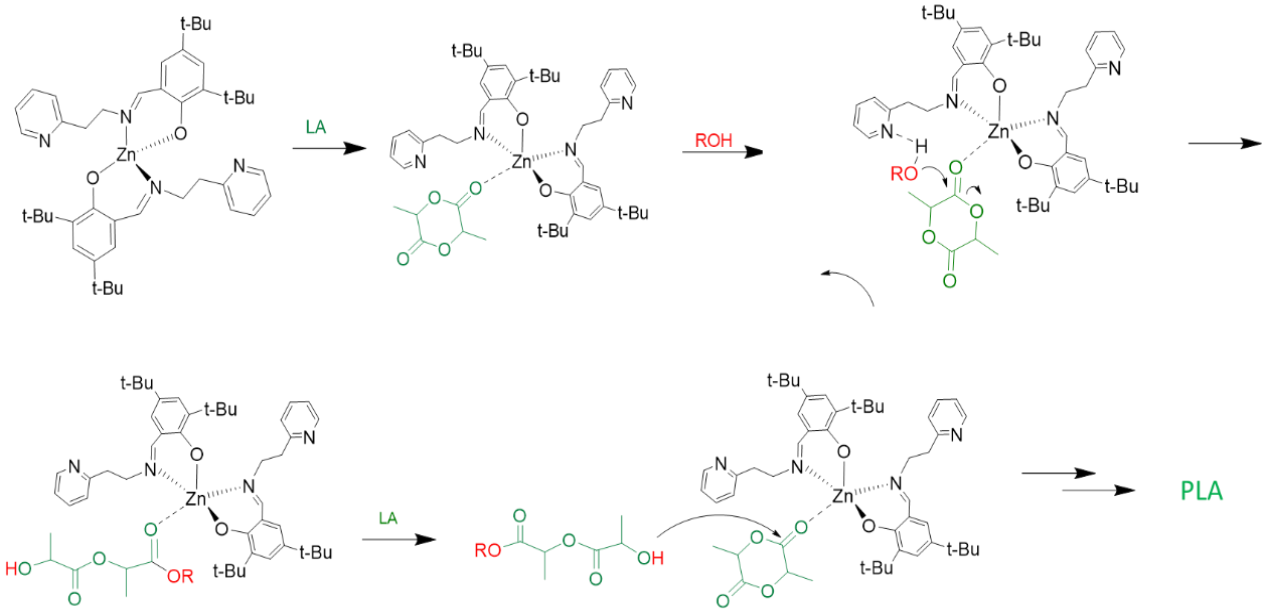

Scheme 2.4 Possible mechanism of polymerization of lactide with complex **1**.

As previously reported by Jones, the presence of an additional N donor in the ancillary ligands could have an active role during the polymerization process potentially supporting in the proton-transfer steps by activating the external nucleophile.[16] This could explain the great difference in activity between complex **1** and complex **5**, lacking an additional donor.

Conversely, when an equiv. of iPrOH was added to a benzene-d6 solution of the corresponding heteroleptic complex **3**, the formation of a related alkoxide derivative (82 %) and a small percentage of the homoleptic complex **1** (18 %) was observed (**Figure 2.7**). The ratio between these two species did not change by increasing the temperature up to 65 °C. After the addition of 5 equiv. of lactide, the signals of the homoleptic species did not change while the resonances related to the alkoxide derivative changed significantly and the simultaneous formation of lactide oligomers were detected.

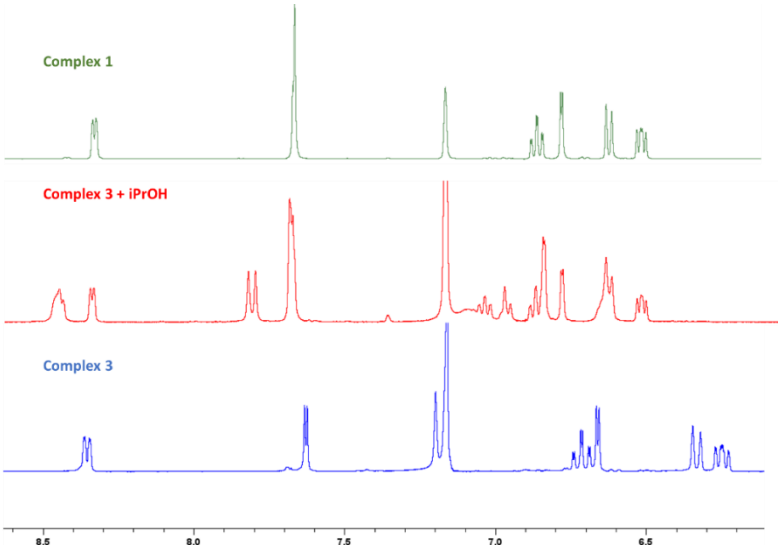

Figure 2.7 ^{1}H NMR spectrum (400 MHz, C_6D_6, 298 K) complex **3** with 1 equiv. of ^{i}PrOH.

The PLA oligomer was studied from the MALDI-FT-ICR MS mass spectra, indicating that the sequence was capped with isopropyl ester group and hydroxyl group. Therefore, we can conclude that the alkoxide zinc derivative was responsible for the polymerization and a coordination-insertion mechanism was operative.

Subsequently the same experiments were performed with the magnesium complexes **2** and **4**. When 1 equiv. of ^{i}PrOH was added to a benzene-d6 solution of complex **2**, the resonances of the methylene protons of the pyridine pendants resolved into two broad signals which suggest fluxional coordination of the pyridine nitrogen atoms due to the competitive coordination of alcohol to the magnesium center or to the pyridine moiety (**Figure 2.25**). No significative differences were observed in other regions of the NMR spectrum.

After the addition of 5 equiv. of lactide, the formation of the alkoxide derivative of the heteroleptic complex and 1 equiv. of free ligand were observed. This process could be favored by the coordination of the monomer to the metal center. At the same time, additional resonances for PLA sequences bearing isopropyl ester chain-end group were observed (**Figure 2.26**).

All these observations suggest that the active species is the alkoxide derived from the heteroleptic complex for which a coordination insertion mechanism can be hypothesized, considering the lesser coordination of the magnesium and the presence of the labile group of isopropoxide (**Scheme 2.5**).

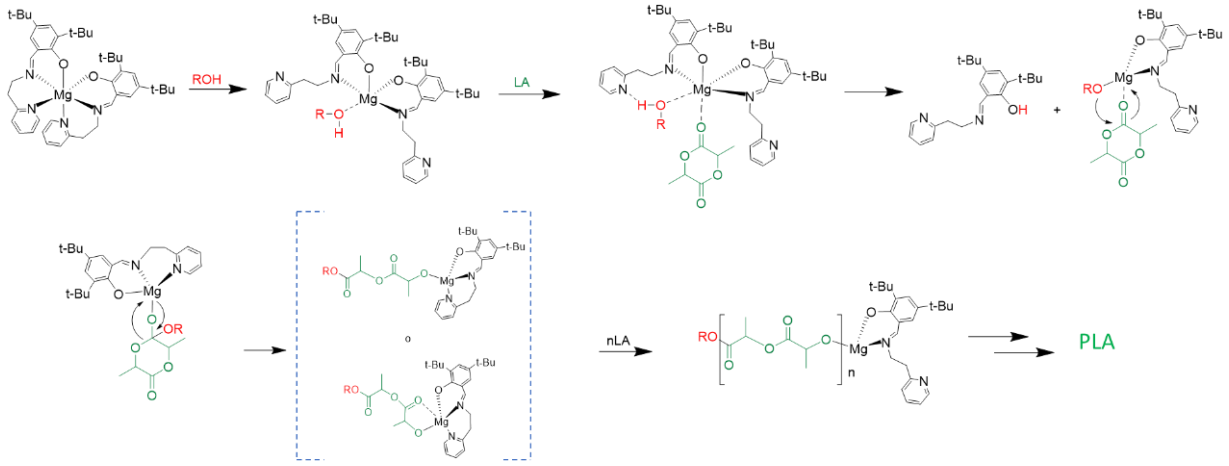

Scheme 2.5 Possible mechanism of polymerization of lactide with complex **2**.

Finally, when 1 equiv. of ^{i}PrOH was added to complex **4**, the homoleptic complex **2** was produced quantitatively, reasonably by a Schlenk equilibrium (**Figure 2.8**). After the addition of lactide, a mixture of species was formed probably due to the coordinating capacity of the monomer which stabilizes the heteroleptic species.

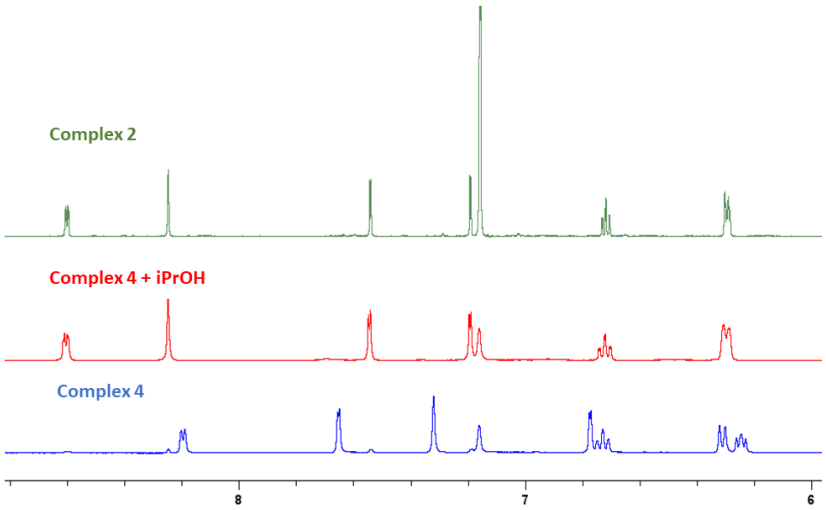

Figure 2.8 ^{1}H NMR spectrum (600 MHz, C_6D_6, 298 K) complex **4** with 1 equiv. of ^{i}PrOH.

The NMR experiments performed with magnesium complexes **2** and **4** showed the formation of several species under the reaction conditions used for the polymerizations. This could be the reason of the low control was observed during polymerizations.

2.2.4 Degradation studies

Chemical recycling of polymers has recently become a key objective for the sustainability of plastics in a circular economy. The controlled degradation of PLA through transesterification reactions with methanol provide methyl lactate, a very valuable chemical. In recent years, several homoleptic zinc complexes with phenoxy-imine or phenoxy-amine ligands bearing additional neutral donors (from primary amine to tertiary amine) have been investigated as catalysts for the chemical degradation of PLLA.[13] Considering the importance of this topic and the high tendency of the synthesized complexes to promote transesterification reactions, they were also studied for the degradation reaction of PLLA, by alcoholysis.

The main reaction conditions and results were summarized in **Table 2.2**. Initially, complexes **1**-**5** were tested for the degradation of a commercial sample of PLLA (Mn = 50000 gmol^{-1} Đ = 1.2) dissolved in a THF / MeOH solution at room temperature. According to the literature, under these conditions the degradation of PLA proceeds via random splitting of the internal bonds that lead to oligomers which are then converted to methyl lactate (Me-La). All parameters for monitoring the reaction, namely conversion (X_{Int}), selectivity ($S_{Me\text{-}La}$) and yield ($Y_{Me\text{-}La}$) of Me-La were evaluated by ^{1}H NMR analysis of the methine region. Under these conditions, the heteroleptic zinc complex **3** revealed to be the most active, quantitatively degrading the PLA in 2 h. The homoleptic zinc and magnesium complexes (**1** and **2** respectively) showed the same activity while complex **4** was completely inactive due to its susceptibility to the presence of protic species (entries 1-4, **Table 2.2**).

Table 2.2
Methanolysis Data of PLAs with complexes **1**-**5**.

Entry[a]	cat	time (h)	T (°C)	Solvent	X_{Int}[b]	$S_{Me\text{-}La}$[b]	$Y_{Me\text{-}La}$[b]
1	**1**	7	25	THF	86	34	29
2	**2**	7	25	THF	83	26	21
3	**3**	2	25	THF	100	74	74
4	**4**	24	25	THF	0	0	0

5	**5**	24	25	THF	0	0	0
6	**1**	0.25	65	-	61	100	59
7	**2**	1	65	-	39	100	39
8	**3**	0.25	65	-	67	100	67
9	**4**	1	65	-	15	100	15

[a]All reactions were carried out by using 5 µmol of Zn catalyst (0.6 mol % relative to ester linkages) in 1.8 mL of THF, with 0.2 mL of MeOH at room temperature. [b]Determinated by ^{1}H NMR. [c]2 mL of MeOH.

No activity was reached with the zinc complex **5** confirming the key role of the additional pyridine donor also in the degradation reactions (entry 5, **Table 2.2**). As already reported by Jones, in the case of homoleptic complexes, the pendant amine groups in the ancillary ligands could have an active role both during the polymerization reactions and during the degradation process of PLA. In particular, during the degradation by metanolysis, the pendant arm could potentially aid the proton-transfer steps by activating the external nucleophile (**Scheme 2.6**).[13]

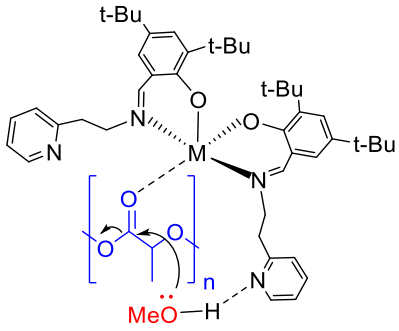

Scheme 2.6 Mechanism of degradation of PLA with focus on the role of the pyridine pendant arm.

The degradation reactions under solvent-free conditions were performed using absolute MeOH at a temperature of 65 °C (entries 6-9, **Table 2.2**). Despite the insolubility of the polymer in MeOH, selective degradation of more than 60 % of the PLLA sample to Me-La was achieved with zinc complexes **1** and **3** after only 15 min. Under these conditions, all the complexes were selective in the formation of Me-La, as a consequence of a degradation mechanism that proceeds by a progressive erosion of the polymer chain starting from the chain ends.[17]

2.3 Conclusion

In this *Chapter*, zinc and magnesium complexes supported by pyridyl phenoxy-imine ligands typified by different coordination geometries have been described. All complexes were active both in the ROP of lactide and in the methanolysis of PLA showing different activities depending on their structural parameters. In the ROP of L-LA high activity and efficient control were observed for zinc catalysts even under industrially relevant conditions. Mechanistic studies on active species have demonstrated the formation of species with defined identities for zinc complexes. Otherwise, the magnesium complexes are affected by several equilibria which generate a mixture of active species in the polymerization medium resulting in an uncontrolled process. The zinc complexes were also found to be the most active in the degradation reaction of polylactide by methanolysis. These data support the hypothesis that the nature of the metal has a crucial role on catalyst activity and polymerization control. These studies were useful to provide indications about a functional design of the catalytic species in terms of structure of the ancillary ligand, nature of the metal center and coordination geometry to promote synthesis and degradation of PLA.

2.4 Experimental part

Materials and methods

Moisture and air-sensitive materials were manipulated under nitrogen using Schlenk techniques or an MBraun Labmaster glovebox. Toluene and methanol were refluxed over Na and distilled under nitrogen. Tetrahydrofuran (THF) was refluxed over Na and benzophenone and distilled under nitrogen. Monomers (Sigma-Aldrich) were purified before use.

$CDCl_3$, C_7D_8 and C_6D_6 were purchased from Eurisotop and used as received. All other reagents and solvents were purchased from Aldrich and used without further purification.

Instruments and measurements

NMR spectra of polymers were performed at room temperature on Bruker Avance 300, 400 or 600 spectrometers (^{1}H: 300.13, 400.13, 600.13 MHz; ^{13}C: 75.47, 100.62, 150.92 MHz, respectively). The resonances are reported in ppm (δ) and the coupling constants in Hz (J) and are referenced to the residual solvent peak at δ = 7.16 ppm for C_6D_6 and δ = 7.27 for $CDCl_3$. Spectra recording was performed using Bruker-TopSpin v2.1 software. Data processing was performed using TopSpin v2.1 or MestReNova v6.0.2 software.

The average molecular masses and the molecular weight dispersities (Đ) of the obtained polylactide samples were determined by GPC in THF as the mobile phase at a flow rate of 1 mL min^{-1}. The utilized GPCmax VE-2001 from Viscotek was a combination of an HPLC pump, two Malvern Viscotek T columns (porous styrene divinylbenzene copolymer) with a maximum pore size of 500 and 5000 a, a refractive index detector (VE-3580), and a viscometer (Viscotek 270 Dual Detector). Polystyrene standards were used for calibration. The evaluation of the molar masses was carried out with a universal method or with a conventional method in combination with multiplying a factor of 0.58 for PLA.

MALDI mass spectra were recorded using a Bruker solariX XR Fourier transform ion cyclotron resonance (FT-ICR) mass spectrometer (Bruker Daltonik GmbH, Bremen, Germany) equipped with a 7 T refrigerated actively shielded superconducting magnet (Bruker Biospin, Wissembourg, France). The samples were prepared at the concentration of 1.0 mg mL^{-1} in THF, while the matrix (DCTB) was mixed at a concentration of 10.0 mg mL^{-1}.

Synthesis and characterization of the ligand LH

The ligand was synthetized by condensation of the 2-(2-pyridyl) ethylamine (0.496 g 4.06 mmol) with the 3,5-di-tert-butyl-2-hydroxybenzaldehyde (0.958 g 4.06 mmol). The reaction was performed in reflux of 30 mL of methanol overnight. The solvent was removed under vacuum, forming an orange oil. Yield 98 %

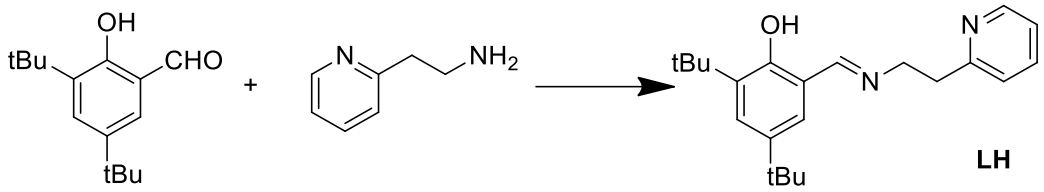

Scheme 2.7 Synthesis of the ligand LH

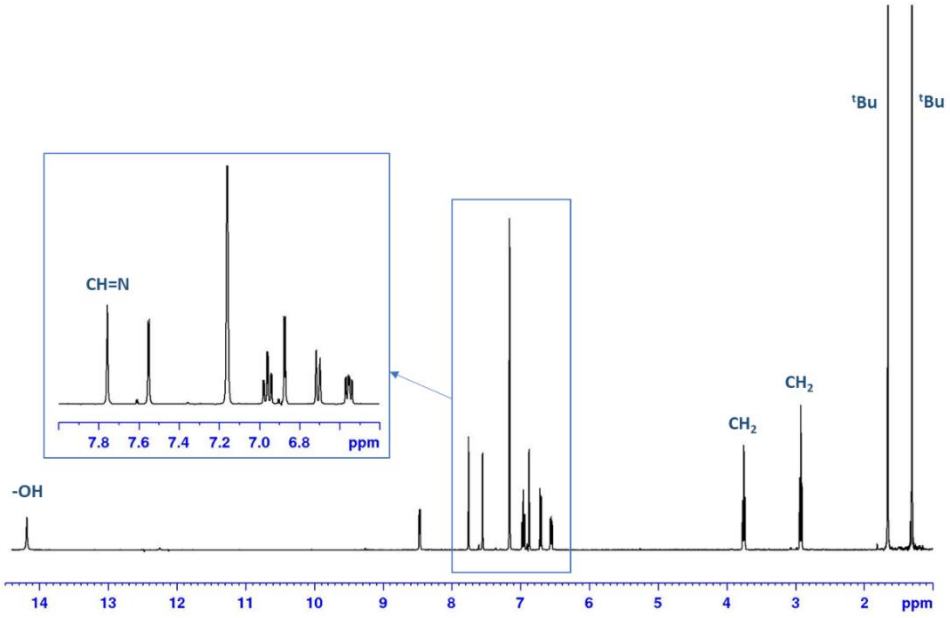

Figure 2.9 ^{1}H NMR spectrum (400 MHz, C_6D_6, 298 K) ligand LH.

^{1}H NMR (400 MHz, C_6D_6, 298 K): δ 14.2 (s, 1H, -OH), 8.45 (dd, J_1 = 4.8 Hz, J_2 = 1.7 Hz, 1H, Py-H), 7.75 (s, 1H, CH=N), 7.56 (d, J = 2.4 Hz, 1H, Ph-H), 6.95 (dt, J_1 = 7.5Hz, J_2 = 2.1 Hz, 1H, Py-H), 6.87 (d, J = 2.4 Hz, 1H, Ph-H), 6.70 (d, J = 7.7 Hz, 1H, Py-H), 6.55 (dt, J_1 = 7.2 Hz, J_2 = 2.1 Hz, 1H, Py-H), 3.75 (dt, J_1 = 7.2 Hz, J_2 = 1.0 Hz, 2H, CH_2), 2.92 (t, J = 7.1Hz, 2H, CH_2), 1.66 (s, 9H, ^{t}Bu), 1.30 (s, 9H, ^{t}Bu).

Synthesis and characterization of the complex 1

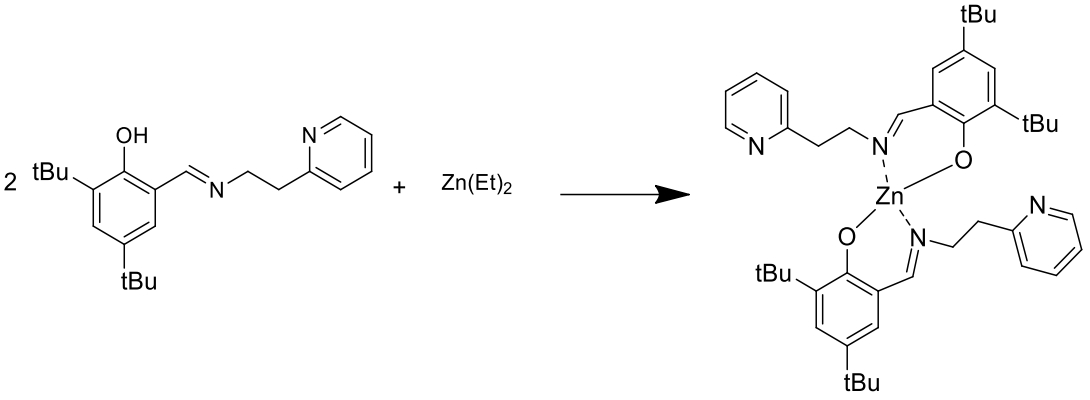

Scheme 2.8 Synthesis of complex **1**.

To a stirred solution containing diethylzinc (0.072 g, 0.600 mmol) in dry benzene (4.0 mL) was added dropwise a solution of the ligand precursor LH (0.407 g, 1.20 mmol) in dry benzene (2.0 mL). The solution was stirred for 2 hours at room temperature. The solvent was removed under vacuum, forming a yellow solid. The formation of the desired species was confirmed by NMR analysis. Yield: 97 %

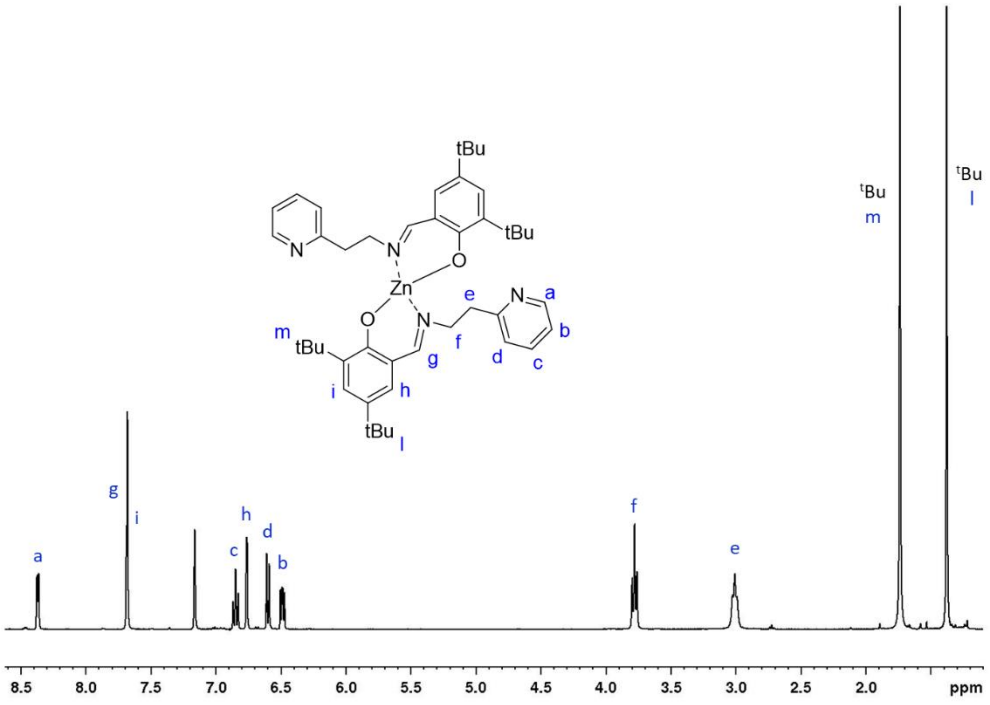

Figure 2.10 ^{1}H NMR spectrum (400 MHz, C_6D_6, 298 K) complex **1**.

^{1}H NMR (400 MHz, C_6D_6, 298 K): δ 8.37 (d, J = 4.8 Hz, 1H, Ha), 7.67 (m, 2H, Hi-g), 6.84 (dt, J_1 = 7.6 Hz, J_2= 1.8 Hz, 1H, Hc), 6.76 (d, J= 2.6 Hz, 1H, Hh), 6.59 (d, J = 7.8 Hz, 1H, Hd), 6.48 (t, J = 6.1 Hz, 1H, Hb), 3.77 (t, J = 7.4 Hz, 2H, Hf), 3.01 (m, 2H, He), 1.73 (s, 9H, ^{t}Bum), 1.37 (s, 9H, ^{t}Bul).

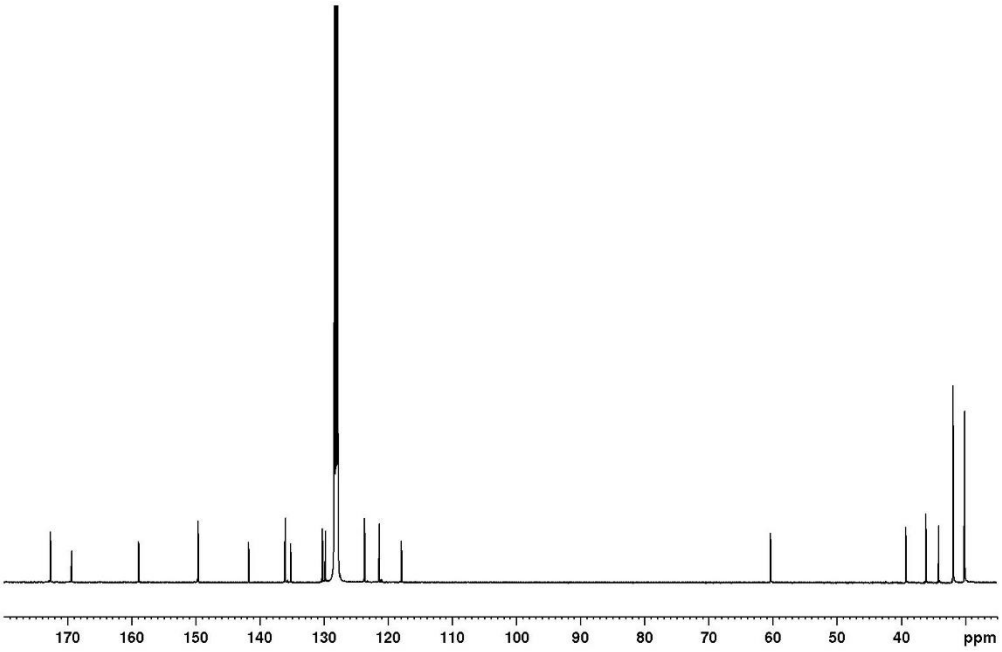

Figure 2.11 ^{13}C NMR spectrum (400 MHz, C_6D_6, 298 K) complex **1**.

^{13}C NMR (100 MHz, C_6D_6, 298 K): δ 172.6, 169.4, 158.9, 149.6, 141.7, 136.0, 135.2, 130.2, 129.8, 123.7, 121.4, 117.9, 60.3, 39.2, 36.0, 34.1, 31.9, 30.0.

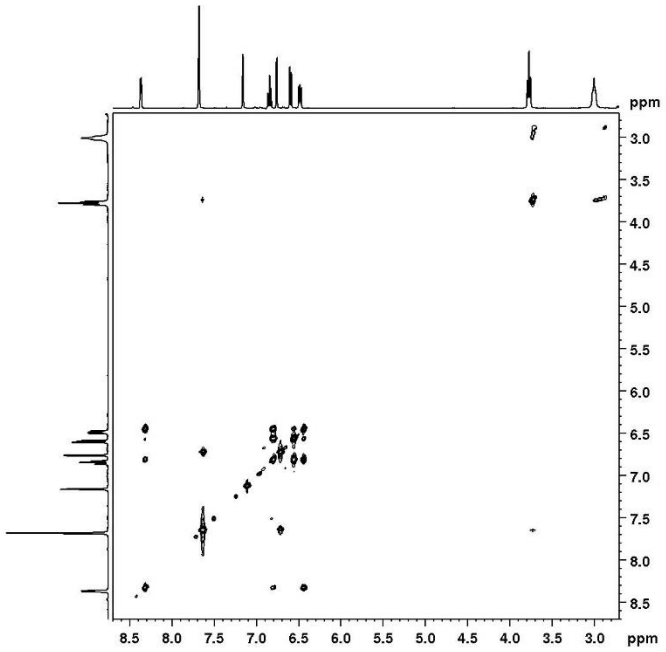

Figure 2.12 COSY spectrum (400 MHz, C_6D_6, 298 K) complex **1**.

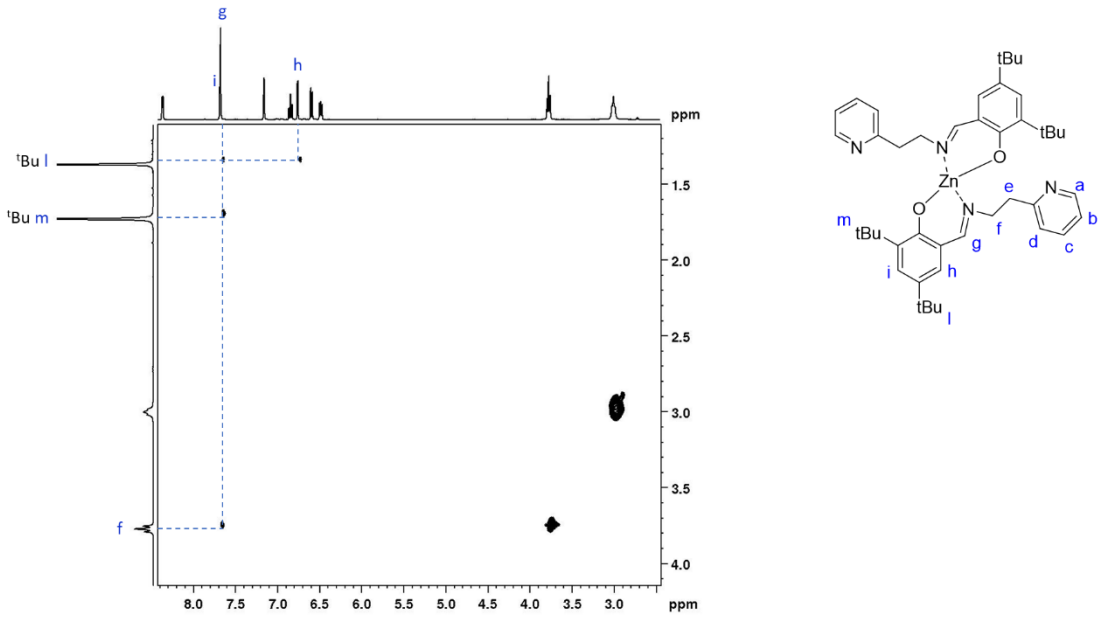

Figure 2.13 NOESY spectrum (400 MHz, C_6D_6, 298 K) complex **1**.

Synthesis and characterization of the complex 2

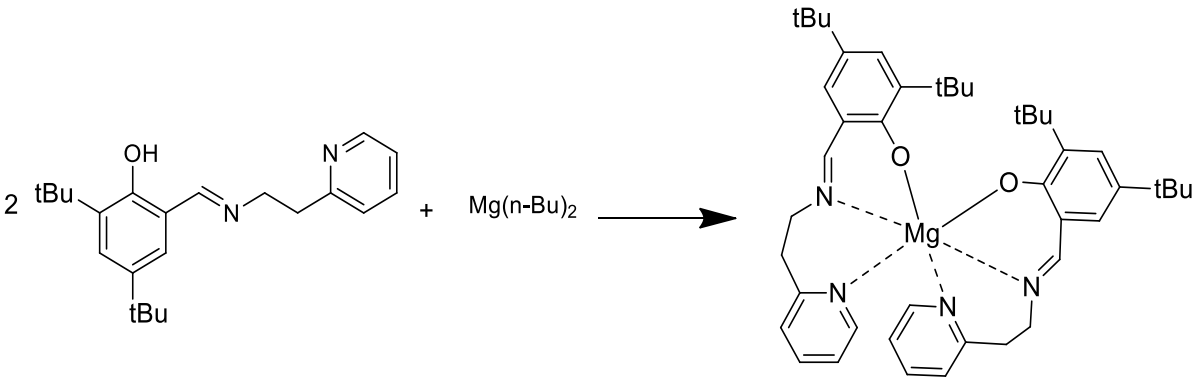

Scheme 2.9 Synthesis of complex **2**.

To a stirred solution containing di-n-butylmagnesium solution 0.5 M in heptane (0.850 g, 0.61 mmol) in dry benzene (3.5 mL) was added dropwise a solution of the ligand precursor L1 (0.404 g, 1.19 mmol) in dry benzene (2.5 mL). The solution was stirred for 2 hours at room temperature. The solvent was removed under vacuum, forming a yellow solid and washed with hexane. The formation of the desired species was confirmed by NMR analysis. Yield: 91 %

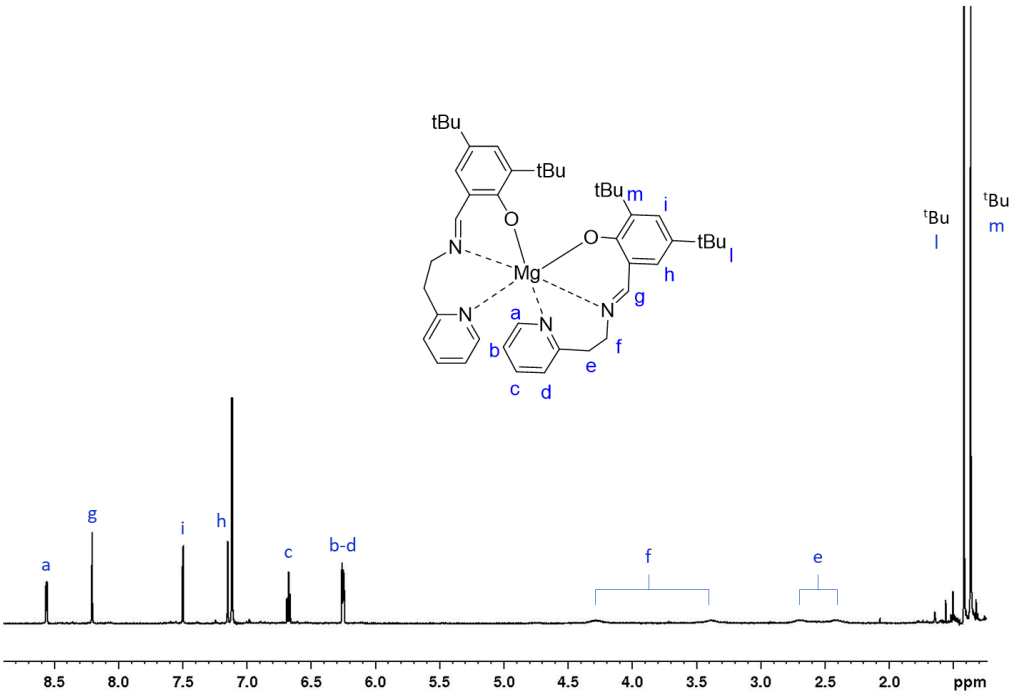

Figure 2.14 ^{1}H NMR spectrum (600 MHz, C_6D_6, 298 K) complex **2**.

^{1}H NMR (600 MHz, C_6D_6, 298 K): δ 8.56 (dd, J_1 = 5.9 Hz, J_2 = 2.1 Hz, 1H, Ha), 8.20 (s, 1H, Hg), 7.49 (d, J = 2.8 Hz, 1H, Hl), 7.15 (d, J = 2.8 Hz, 1H, Hh), 6.67 (dt, J_1 = 7.6 Hz, J_2 = 1.8 Hz, 1H, Hc), 6.25 (m, 2H, Hb-d), 4.28 (m, 1H, Hf), 3.38 (m, 1H, Hf), 2.68 (m, 1H, He), 2.41 (m, 1H, He), 1.41 (s, 9H, ^{t}Bum), 1.36 (s, 9H, ^{t}Bul).

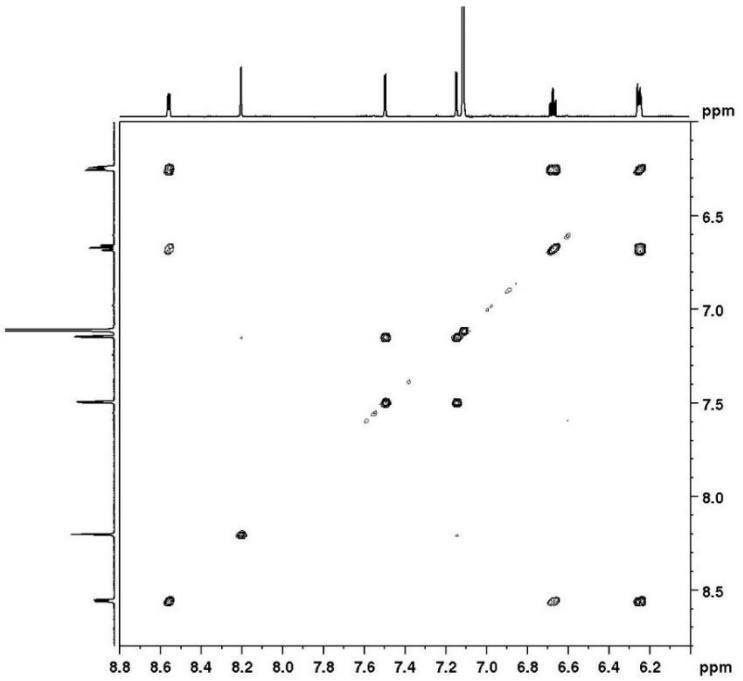

Figure 2.15 COSY NMR spectrum (600 MHz, C_6D_6, 298 K) complex **2**.

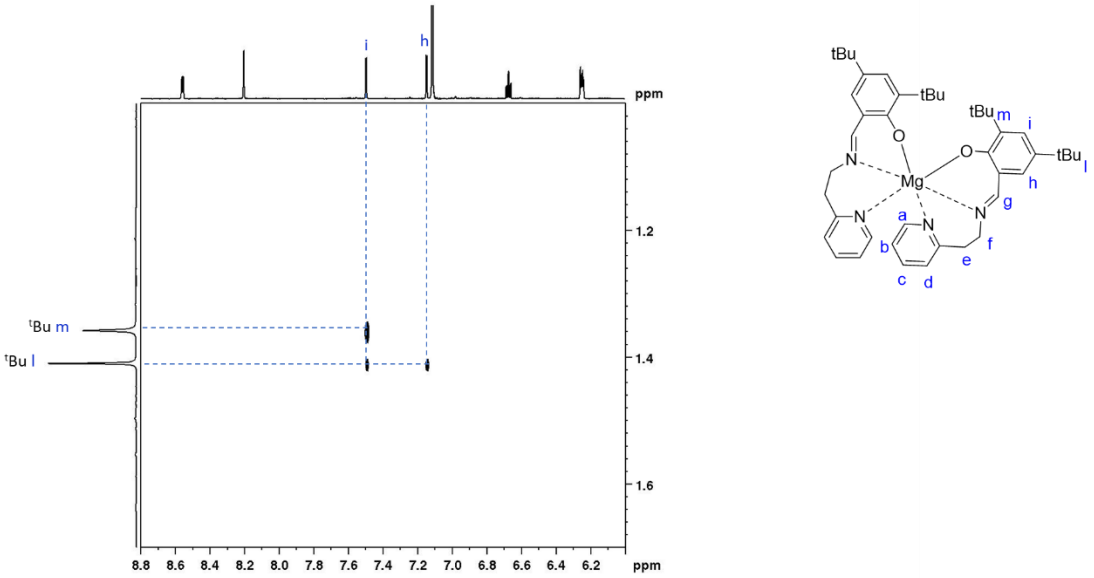

Figure 2.16 NOESY NMR spectrum (600 MHz, C_6D_6, 298 K) complex **2**.

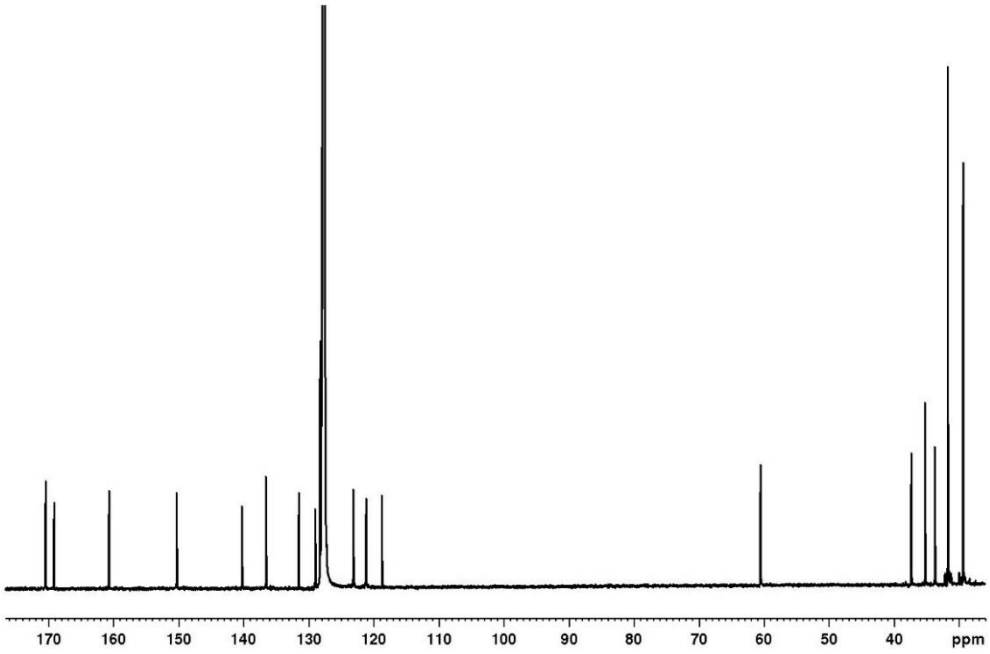

Figure 2.17 ^{13}C NMR spectrum (150 MHz, C_6D_6, 298 K) complex **2**.

^{13}C NMR (150 MHz, C_6D_6, 298 K): δ 170.4, 169.1, 160.6, 150.2, 140.2, 136.5, 131.5, 128.9, 128.2, 123.1, 121.2, 118.7, 60.5, 37.3, 35.2, 33.7, 31.5, 29.3.

Synthesis and characterization of the complex 3

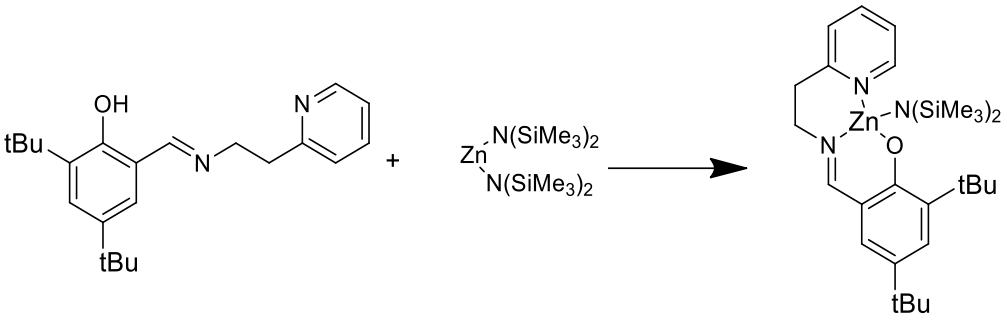

Scheme 2.10 Synthesis of complex **3**.

To a stirred solution containing Zinc bis[bis(trimethylsilyl)amide] (0.572 g, 1.48 mmol) in dry benzene (4.0 mL) was added dropwise a solution of the ligand precursor LH (0.500 g, 1.48 mmol) in dry benzene (2.0 mL). The solution was stirred for 3 hours at room temperature. The solvent was removed under vacuum, forming an orange solid. The formation of the desired species was confirmed by NMR analysis. Yield 85 %

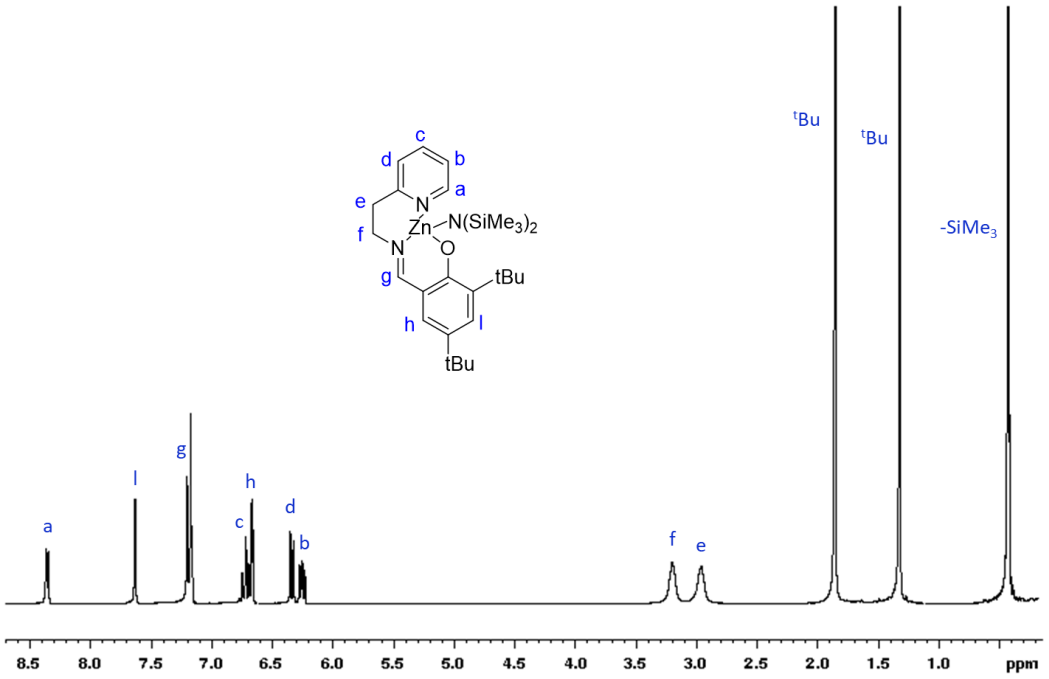

Figure 2.18 ^{1}H NMR spectrum (300 MHz, C_6D_6, 298 K) complex **3**.

^{1}H NMR (300 MHz, C_6D_6, 298 K): δ 8.35 (dd, J_1 = 5.2 Hz, J_2 = 0.87 Hz, 1H, Ha), 7.63 (d, J = 2.7 Hz, 1H, Hl), 7.20 (s, 1H, Hg), 6.71 (dt, J_1 = 7.7 Hz, J_2 = 1.7 Hz, 1H, Hc), 6.66 (d, J = 2.7 Hz, 1H, Hh), 6.33 (d, J = 7.8 Hz, 1H, Hd), 6.25 (dt, J_1 = 7.5 Hz, J_2 = 1.1 Hz, 1H, Hb), 3.19 (m, 2H, Hf), 2.95 (m, 2H, He), 1.85 (s, 9H, ^{t}Bu), 1.31 (s, 9H, ^{t}Bu), 0.41 (s, 18H, $SiMe_3$).

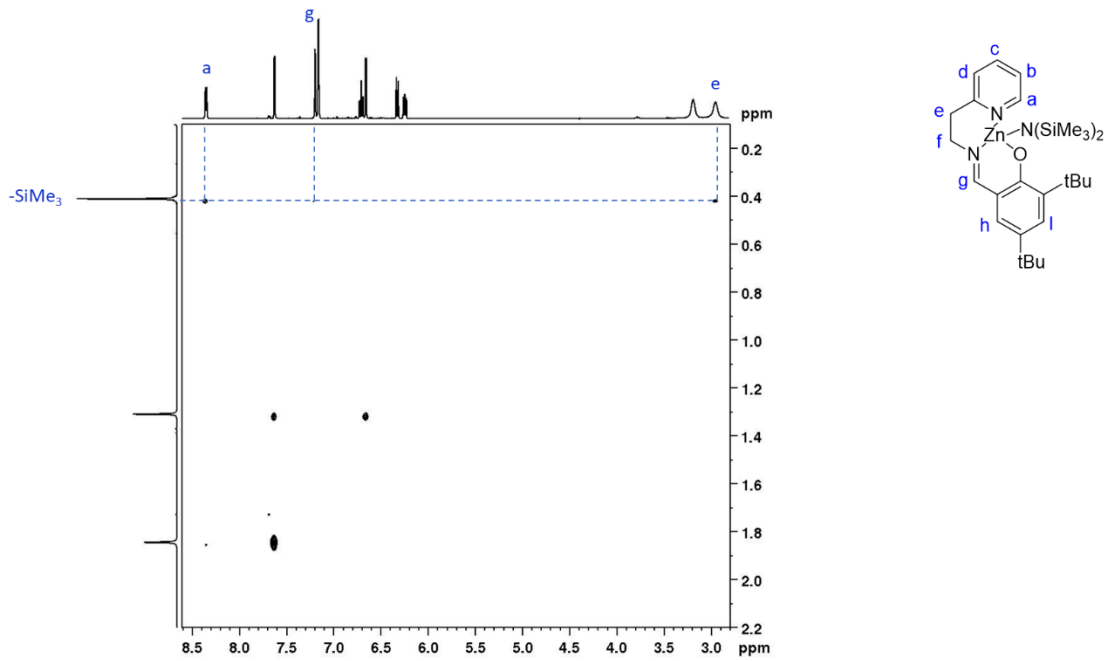

Figure 2.19 NOESY spectrum (400 MHz, C_6D_6, 298 K) complex **3**.

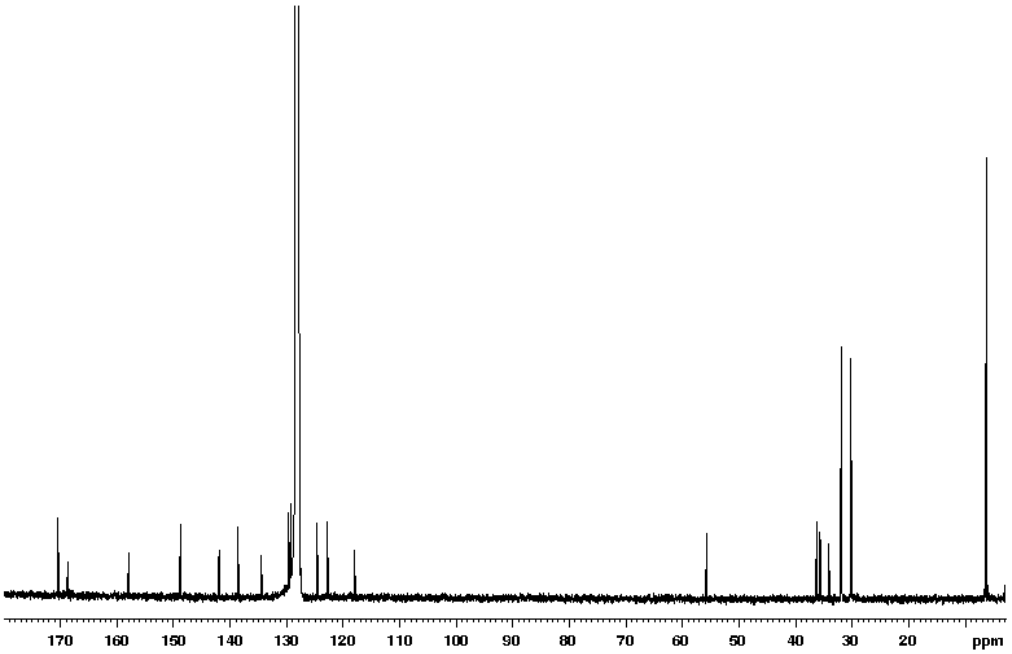

Figure 2.20 ^{13}C NMR spectrum (100 MHz, C_6D_6, 298 K) complex **3**.

^{13}C NMR (100 MHz, C_6D_6, 298 K): δ 170.4, 168.7, 157.9, 148.8, 141.9, 138.9, 134.4, 129.6, 129.3, 124.5, 122.7, 118.0, 55.6, 36.1, 35.5, 34.0, 31.7, 30.0, 6.10.

Synthesis and characterization of the complex 4

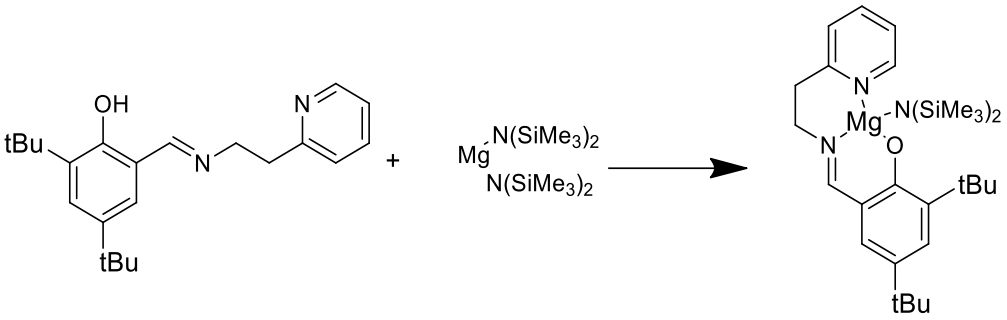

Scheme 2.11 Synthesis of complex **4**.

To a stirred solution containing the ligand precursor LH (0.099 g, 0.29 mmol) in dry benzene (2.0 mL) was added dropwise a solution of magnesium bis(hexamethyldisilazide) (0.101 g, 0.29 mmol) in dry benzene (3.0 mL). A few drops of THF were added and then the solution was stirred for 2 hours at room temperature. The solvent was removed under vacuum, forming a yellow solid. The formation of the desired species was confirmed by NMR analysis. Yield: 90 %

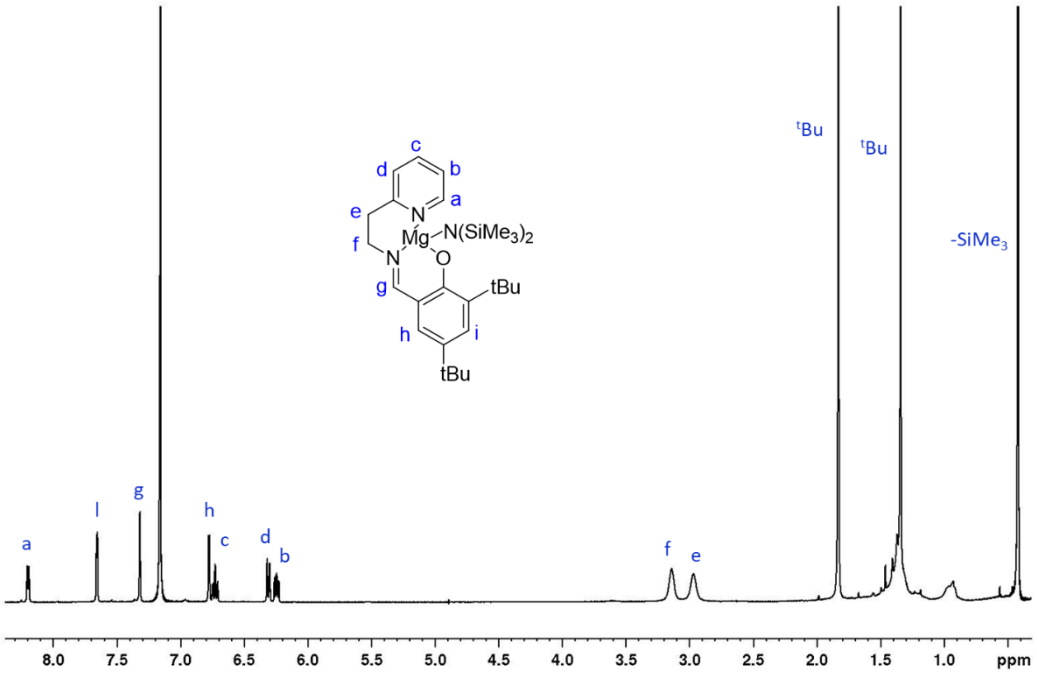

Figure 2.21 ^{1}H NMR spectrum (400 MHz, C_6D_6, 298 K) complex **4**.

^{1}H NMR (600 MHz, C_6D_6, 298 K): δ 8.20 (d, J_1 = 5.0 Hz, 1H, Ha), 7.65 (d, J = 2.5 Hz, 1H, Hh), 7.32 (s, 1H, Hg), 6.77 (d, J = 2.5 Hz, 1H, Hi), 6.72 (t, J = 7.8 Hz, 1H, Hc), 6.30 (d, J = 7.7 Hz, 1H, Hd), 6.24 (t, J = 6.58 Hz ,1H, Hb), 3.14 (s, 2H, Hf), 2.96 (m, 2H, He), (s, 9H, ^{t}Bu), 1.33 (s, 9H, ^{t}Bu), 0.4 (s, 18H, $SiMe_3$)

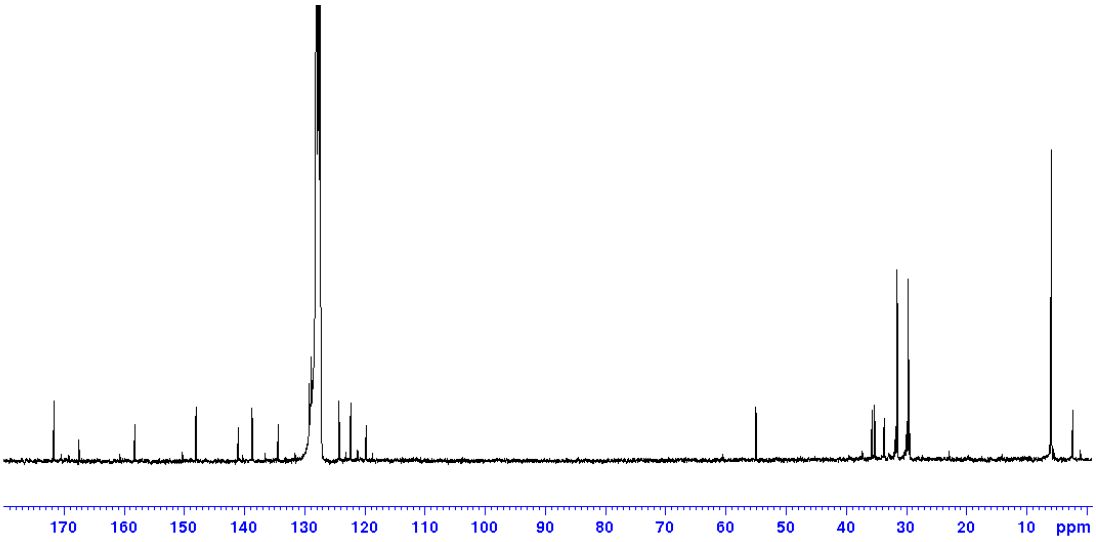

Figure 2.22 ^{13}C NMR spectrum (75 MHz, C6D6, 298 K) complex **4**.

^{13}C NMR (75 MHz, C_6D_6, 298 K): δ 171.6, 167.4, 158.2, 148.0, 141.0, 138.6, 134.3, 128.0, 127.7, 127.3, 124.2, 122.3, 119.7, 54.9, 35.8, 35.2, 33.6, 31.4, 29.6, 5.8.

Synthesis and characterization of the complex 5

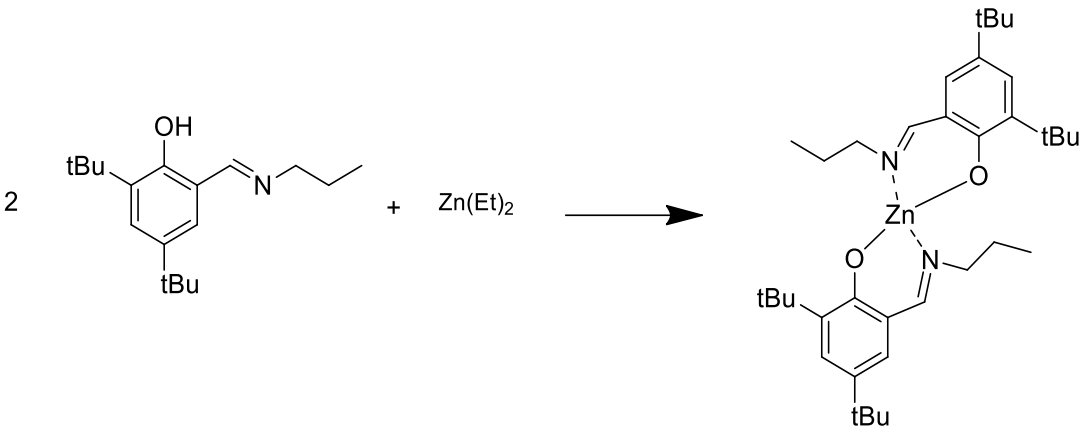

Scheme 2.12 Synthesis of complex **5**.

To a stirred solution containing the ligand precursor (0.734 g, 0.266 mmol) in dry benzene (2.0 mL) was added dropwise a solution of $ZnEt_2$ (0.165 g, 1.33 mmol) in dry benzene (4.0 mL), then the solution was stirred for 2 hours at room temperature. The solvent was removed under vacuum, forming a yellow solid. The formation of the desired species was confirmed by NMR analysis. Yield: 88 %

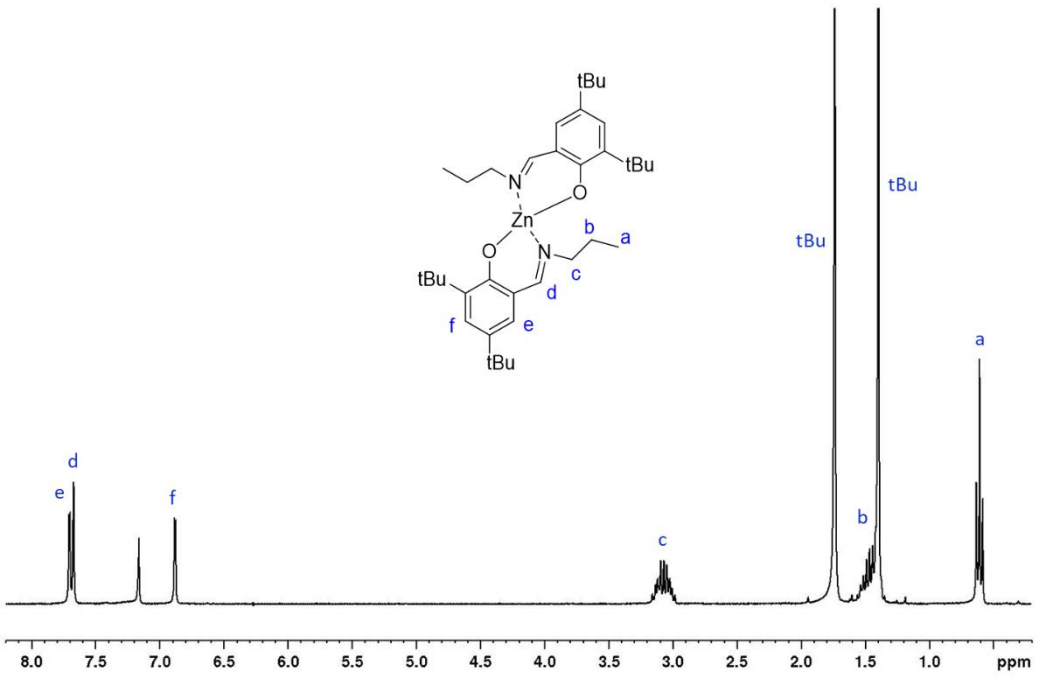

Figure 2.23 ^{1}H NMR spectrum (300MHz, C_6D_6, 298 K) complex **5**.

^{1}H NMR (300 MHz, C_6D_6, 298 K): δ 7.70 (d, J = 2.6 Hz, 1H, He), 7.67 (s, 1H, Hd), 6.87 (dt, J = 2.6 Hz, 1H, Hf), 3.07 (m, 2H, Hc), 1.73 (s, 9H, ^{t}Bu), 1.46 (m, 2H, Hb), 1.38 (s, 9H, ^{t}Bu), 0.60 (t, J = 7.4 Hz, 3H, Ha).

General procedure for the polymerization of lactide

The polymerization experiments conducted at room temperature were carried out in a glove box, under inert conditions. In a Braun Labmaster glovebox, a magnetically stirred reactor flask was charged with lactide. The complex and ROH (iPrOH for polymerizations at 25 °C and BnOH for polymerization at 80 °C) were added in a 2 mL vial and the mixture was stirred for 5 min; then dichloromethane or toluene was added, and the monomer was transferred in. During the reaction, small aliquots of the reaction mixture were sampled, dissolved in $CDCl_3$, and analyzed by ^1H NMR spectroscopy. At the end of the polymerization, the product was precipitated in hexane, then filtered and dried in a vacuum oven. The polymer was characterized by NMR spectroscopy, MALDI MS and/or GPC analysis. For the polymerization experiment carried out under industrial relevant conditions, the complex and 1 equiv. of BnOH (0.1 M solution of BnOH in toluene) were added in a 2 mL vial and the mixture was stirred for 5 min; then transferred in the monomer and, finally, mixed to more equiv. of BnOH. The Schlenk flask was closed, pulled out of the glove box and immersed in a thermostated oil bath at the temperature of 130 °C or 150°C. After the reaction time, the polymerization was stopped using dichloromethane. The solvent was removed under reduced pressure and the polymer was dried and characterized.

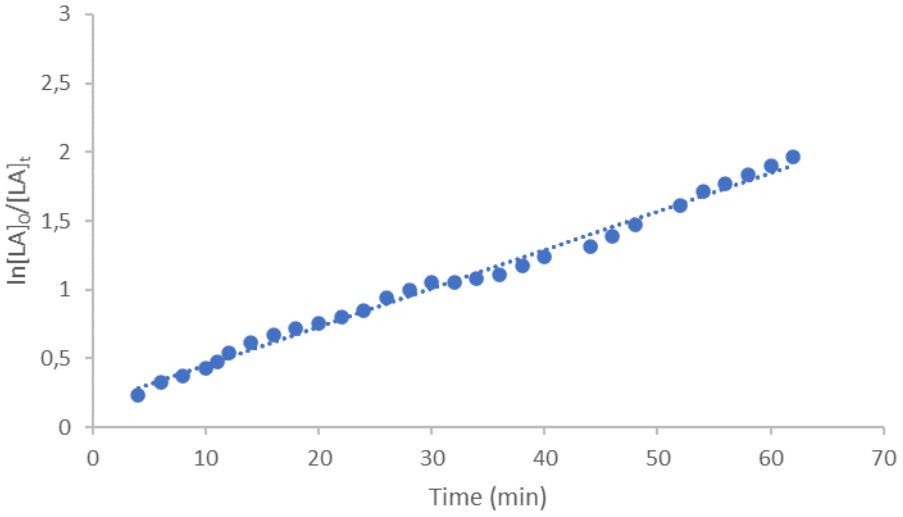

Figure 2.24 Kinetic plot for ROP of L-LA promoted by complex **1** depicting reaction orders of unity with respect to the monomer concentration. Reaction conditions: Zn = 5μmol; [L-LA] : [**1**] : [BnOH] = 100:1:1; T=298 K; 0.5 mL of CD_2Cl_2. Pseudofirst-order rate is 0.028 min^{-1} at 25 °C (R^2 = 0.992).

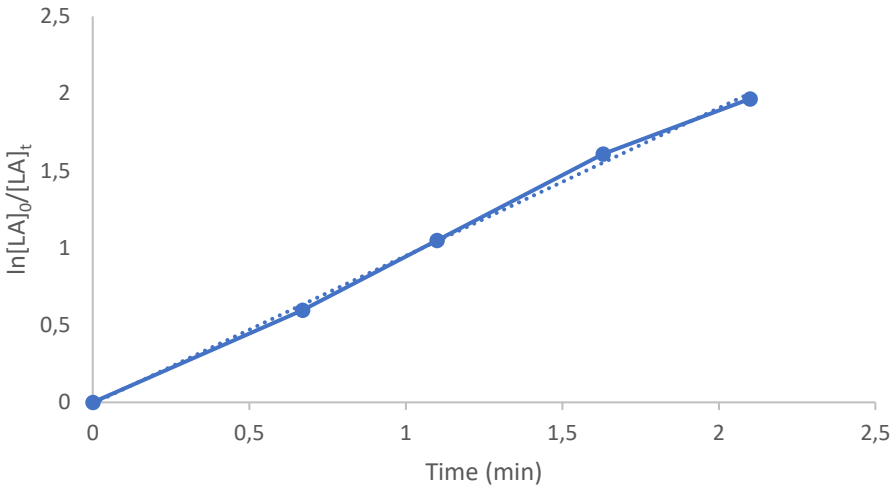

Figure 2.25 Kinetic plot for ROP of L-LA promoted by complex **3** depicting reaction orders of unity with respect to the monomer concentration. Reaction conditions: Zn = 5µmol; [L-LA] : [**3**] : [BnOH] = 100:1:1; T=298 K; 0.5 mL of CH_2Cl_2. Pseudofirst-order rate is 0.957 min^{-1} at 25 °C (R^2 = 0.9976).

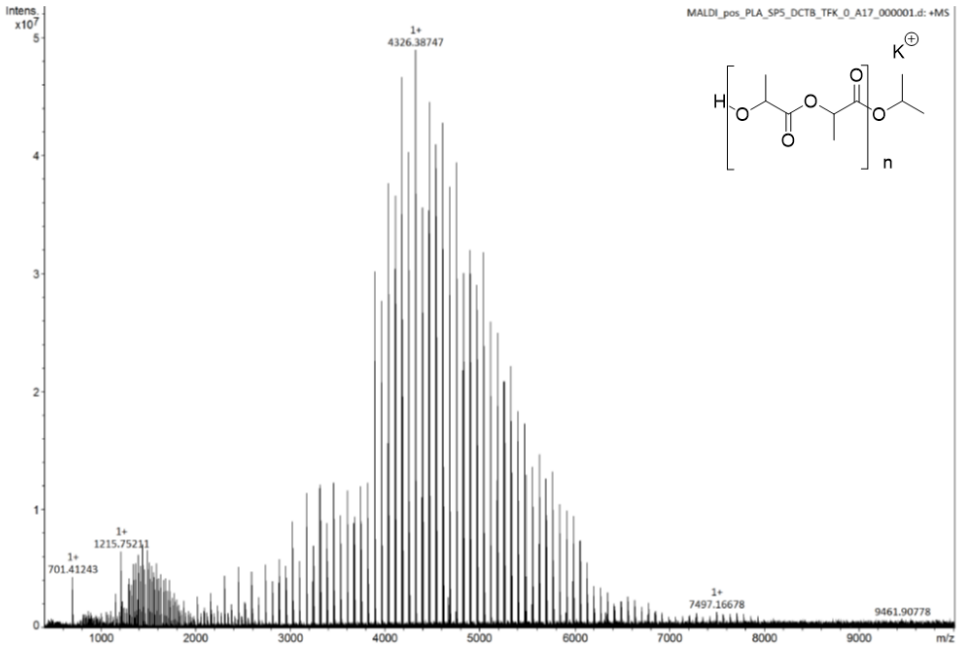

Figure 2.26 MALDI-FT-ICR MS spectrum of PLA synthesizes by complex **1** (2 h after the complete consume of monomer).

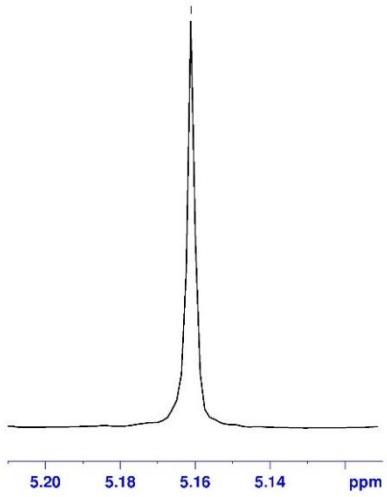

Figure 2.27 Methine region of the homonuclear decoupled ^{1}H NMR spectrum ($CDCl_3$, 298K, 400MHz) of a PLLA sample (entry 11 Table **2.1**).

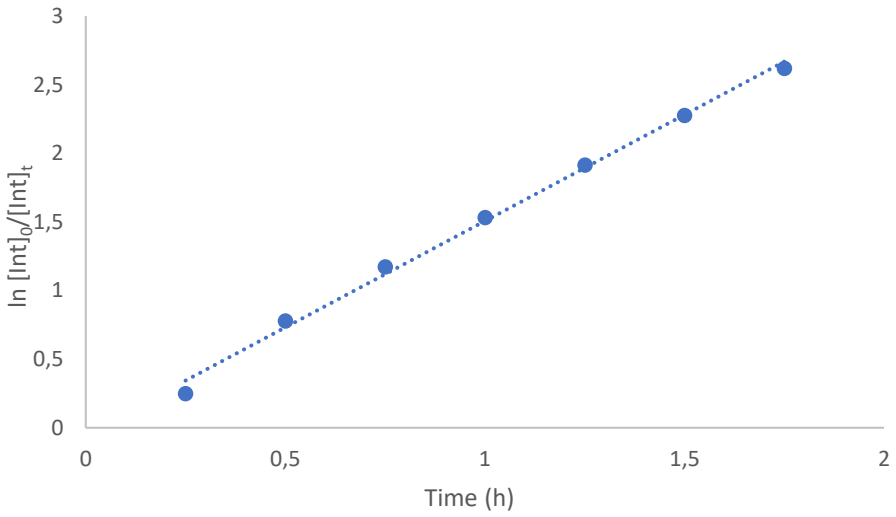

Figure 2.28 Kinetic plot of the degradation of polylactide vs the reaction time. Reaction conditions: ($[PLA]_0$ = 0.21 M; [polyester linkages]/[1] = 60; 0.45 mL of CD_2Cl_2; 0.05 mL of MeOH. Pseudo first-order rate is 1.55 h^{-1} at 25 °C (R^2 = 0.9959).

General procedure for the degradation of polylactide

The degradation experiments conducted in solution were carried out in a glove box, under inert condition. In a Braun Labmaster glovebox, a magnetically stirred reactor flask was charged with polylactide and MeOH. The complex was dissolved in THF and added to the polymer. The reaction mixture was stirred at room temperature. At desired times, small aliquots of the reaction mixture were sampled, dissolved in $CDCl_3$ or CD_2Cl_2 and analyzed by ^1H NMR spectroscopy. At the end of the degradation the reaction was stopped with CH_2Cl_2 and dried under vacuum. For the degradation experiment carried out under solvent free condition, the complex was dissolved in MeOH and added to the polymer. The reaction mixture was stirred at room temperature. At desired times, small aliquots of the reaction mixture were sampled, dissolved in $CDCl_3$ or C_6D_6 and analyzed by ^1H NMR spectroscopy. At the end of the degradation the reaction was stopped with CH_2Cl_2 and dried under vacuum.

NMR experiment for the mechanistic studies

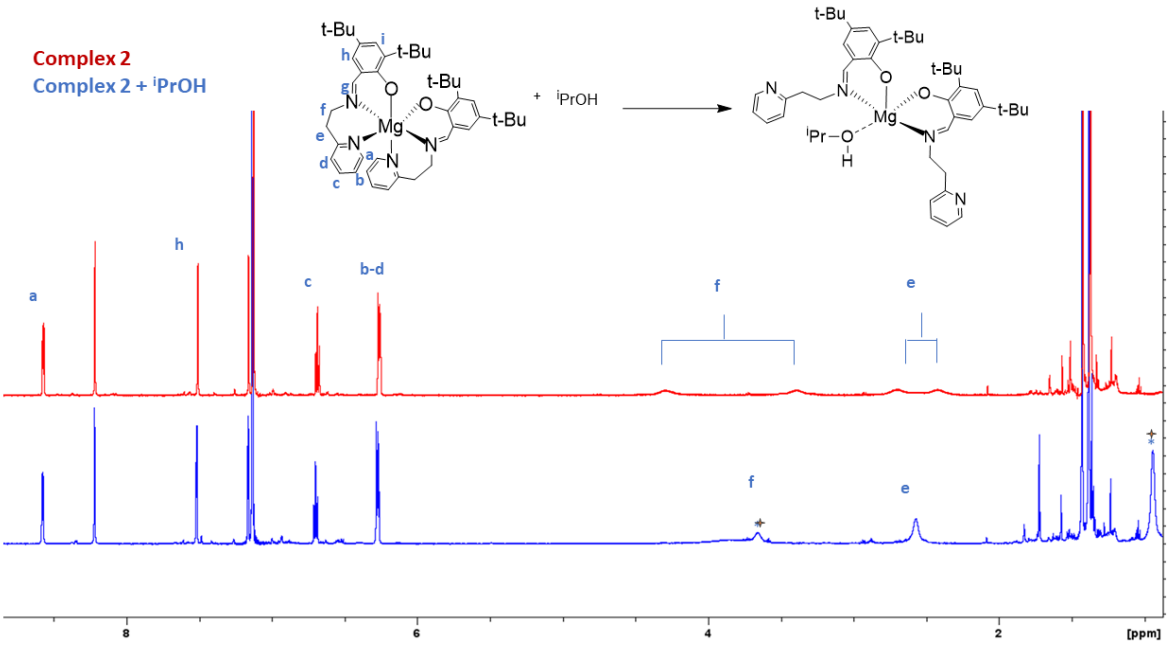

Figure 2.25 ^1H NMR spectrum (600MHz, C_6D_6, 298 K) complex **2** with 1 equiv. of iPrOH.

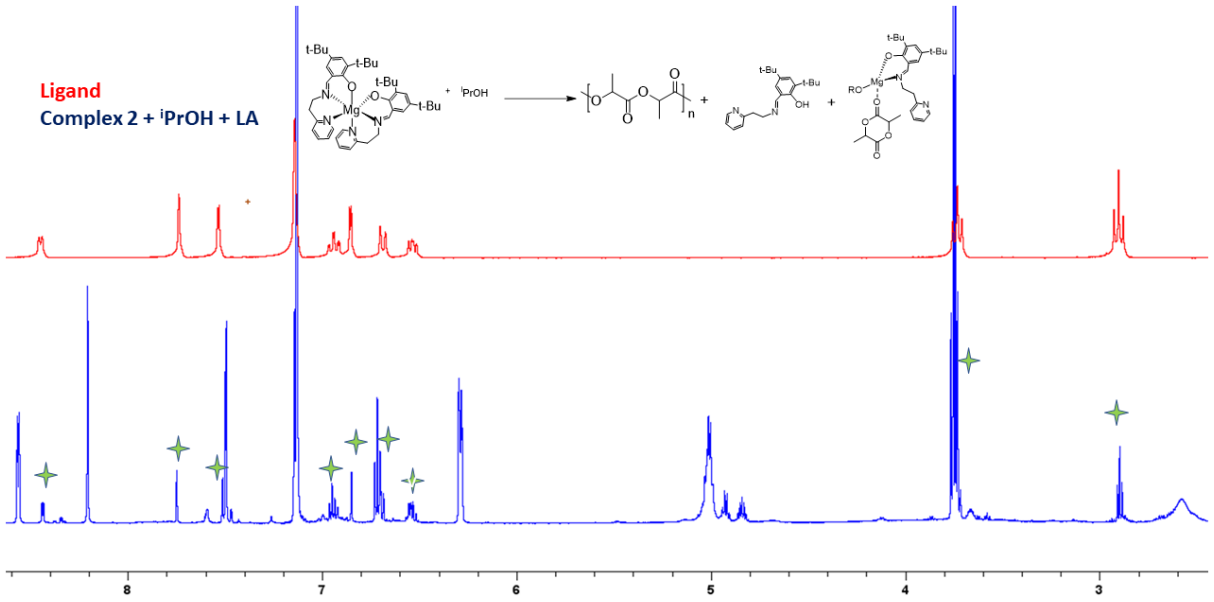

Figure 2.26 ^{1}H NMR spectrum (600MHz, C_6D_6, 298 K) complex **2** with iPrOH and 5 equiv. of L-LA.

References

[1] Ho, K.-L. G., Pometto, A. L., Gadea-Rivas, A., Briceno, J. A., Rojas, A. Degradation of Polylactic Acid (PLA) Plastic in Costa Rican Soil and Iowa State University Compost Rows. *Journal of Environmental Polymer Degradation* **7**, 173-177 (1999).

[2] [a]Chisholm, M. H., Galluci, J. C., Zhen, H. & Huffman, J. C. Three-coordinate zinc amide and phenoxide complexes supported by a schiff base ligand. *Inorganic Chemistry* **40**, 5051–5054 (2001).
[b]Gong, Y., Ma, H. High performance benzoimidazolyl-based aminophenolate zinc complexes for isoselective polymerization of: Rac -lactide. *Chemical Communications* **55**, 10112–10115 (2019).
[c]Rosen, T., Popowski, Y., Goldberg, I., Kol, M. Zinc Complexes of Sequential Tetradentate Monoanionic Ligands in the Isoselective Polymerization of rac-Lactide. *Chemistry - A European Journal* **22**, 11533–11536 (2016).
[d]Chen, H. Y., Tang, H. Y., Lin, C. C. Ring-opening polymerization of lactides initiated by zinc alkoxides derived from NNO-tridentate ligands. *Macromolecules* **39**, 3745–3752 (2006).
[e]Hu, J., Kan, C., Ma, H. Exploring Steric Effects of Zinc Complexes Bearing Achiral Benzoxazolyl Aminophenolate Ligands in Isoselective Polymerization of rac-Lactide. *Inorganic Chemistry* **57**, 11240–11251 (2018).

[3] [a]Wang, H., Yang, Y., Ma, H. Stereoselectivity switch between zinc and magnesium initiators in the polymerization of rac -lactide: Different coordination chemistry, different stereocontrol mechanisms. *Macromolecules* **47**, 7750–7764 (2014).
[b]Chamberlain, B. M. et al. Polymerization of lactide with zinc and magnesium β-diiminate complexes: Stereocontrol and mechanism. *Journal of American Chemical Society* **123**, 3229–3238 (2001).
[c]Rosen, T., Rajpurohit, J., Lipstman, S., Venditto, V., Kol, M. Isoselective Polymerization of rac-Lactide by Highly Active Sequential {ONNN} Magnesium Complexes. *Chemistry - A European Journal* **26**, 17183–17189 (2020).

[4] [a]Zhu, Y., Romain, C., Williams, C. K. Selective Polymerization Catalysis: Controlling the Metal Chain End Group to Prepare Block Copolyesters. *Journal of American Chemical Society* **137**, 12179–12182 (2015).
[b]Rosen, T., Goldberg, I., Venditto, V., Kol, M. Tailor-Made Stereoblock Copolymers of Poly(lactic acid) by a Truly Living Polymerization Catalyst. *Journal of American Chemical Society* **138**, 12041–12044 (2016).

[5] [a]Thevenon, A., Romain, C., Bennington, M. S., White, A. J. P., Davidson, H. J., Brooker, S., Williams, C. K. Dizinc Lactide Polymerization Catalysts: Hyperactivity by Control of Ligand Conformation and Metallic Cooperativity. *Angewandte Chemie* **128**, 8822–8827 (2016).
[b]Williams, C. K., Breyfogle, L. E., Choi, S. K., Nam, W., Young, V. G., Hillmyer, M. A., Tolman, W. B. A highly active zinc catalyst for the controlled polymerization of lactide. *Journal of American Chemical Society* **125**, 11350–11359 (2003).
[c]Soobrattee, S., Zhai, X., Nyamayaro, K., Diaz, C., Kelley, P., Ebrahimi, T., Mehrkhodavandi, P. Dinucleating Amino-Phenolate Platform for Zinc Catalysts: Impact on Lactide Polymerization. *Inorganic Chemistry* **59**, 5546–5557 (2020).

[6] [a]Hermann, A., Hill, S., Metz, A., Heck, J., Hoffmann, A., Hartmann, L., Herres-Pawlis, S. Next Generation of Zinc Bisguanidine Polymerization Catalysts towards Highly Crystalline, Biodegradable Polyesters. *Angewandte Chemie* **59**, 21778–21784 (2020).
[b]D'Alterio, M. C., D'Auria, I., Gaeta, L., Tedesco, C., Brenna, S., Pellecchia, C. Are Well Performing Catalysts for the Ring Opening Polymerization of l -Lactide under Mild Laboratory Conditions Suitable for the Industrial Process? The Case of New Highly Active Zn(II) Catalysts. *Macromolecules* **55**, 5115–5122 (2022).
[c]McKeown, P., McCormick, S. N., Mahon, M. F., Jones, M. D. Highly active Mg(II) and Zn(II) complexes for the ring opening polymerisation of lactide. *Polymer Chemistry* **9**, 5339–5347 (2018).

[7] Piemonte, V., Sabatini, S., Gironi, F. Chemical Recycling of PLA: A Great Opportunity Towards the Sustainable Development? *Journal of Polymers and the Environment* **21**, 640–647 (2013).

[8] [a]Lamberti, F. M., Román-Ramírez, L. A., Wood, J. Recycling of Bioplastics: Routes and Benefits. *Journal of Polymers and the Environment* **28**, 2551–2571 (2020).
[b]Rahimi, A. R., Garciá, J. M. Chemical recycling of waste plastics for new materials production. *Nature Reviews Chemistry* **1**, (2017).

[9] [a]Lamberti, F. M., Román-Ramírez, L. A., Mckeown, P., Jones, M. D. & Wood, J. Kinetics of alkyl lactate formation from the alcoholysis of poly(lactic acid). *Processes* **8**, 738-751 (2020).
[b]Román-Ramírez, L. A., Powders, M., McKeown, P., Jones, M. D., Wood, J. Ethyl Lactate Production from the Catalytic Depolymerisation of Post-consumer Poly(lactic acid). *Journal of Polymers and the Environment* **28**, 2956–2964 (2020).

[10] McKeown, P., Jones, M. D. The Chemical Recycling of PLA: A Review. *Sustainable Chemistry* **1**, 1-22 (2020).

[11] [a]Whitelaw, E. L., Davidson, M. G., Jones, M. D. Group 4 salalen complexes for the production and degradation of polylactide. *Chemical Communications* **47**, 10004–10006 (2011).
[b]Fliedel, C., Vila-Viçosa, D., Calhorda, M. J., Dagorne, S., Avilés, T. Dinuclear zinc-N-heterocyclic carbene complexes for either the controlled ring-opening polymerization of lactide or the controlled degradation of polylactide under mild conditions. *ChemCatChem* **6**, 1357–1367 (2014).
[c]Payne, J., McKeown, P., Mahon, M. F., Emanuelsson, E. A. C., Jones, M. D. Mono-and dimeric zinc(II) complexes for PLA production and degradation into methyl lactate-a chemical recycling method. *Polymer Chemistry* **11**, 2381–2389 (2020).
[d]Román-Ramírez, L. A., McKeown, P., Jones, M. D., Wood, J. Poly(lactic acid) Degradation into Methyl Lactate Catalyzed by a Well-Defined Zn(II) Complex. *ACS Catalysis* **9**, 409–416 (2019).

[12] [a]McKeown, P., Román-Ramírez, L. A., Bates, S., Wood, J., Jones, M. D. Zinc Complexes for PLA Formation and Chemical Recycling: Towards a Circular Economy. *ChemSusChem* **12**, 5233–5238 (2019).
[b]Payne, J., McKeown, P., Driscoll, O., Kociok-Köhn, G., Emanuelsson, E. A. C., Jones, M. D. Make or break: Mg(II)-and Zn(II)-catalen complexes for PLA production and recycling of commodity polyesters. *Polymer Chemistry* **12**, 1086–1096 (2021).

[13] Román-Ramírez, L. A., McKeown, P., Jones, M. D., Wood, J. Poly(lactic acid) Degradation into Methyl Lactate Catalyzed by a Well-Defined Zn(II) Complex. *ACS Catalysis* **9**, 409–416 (2019).

[14] D'Aniello, S., Laviéville, S., Santulli, F., Simon, M., Sellitto, M., Tedesco, C., Thomas, C. M., Mazzeo, M. Homoleptic phenoxy-imine pyridine zinc complexes: efficient catalysts for solvent free synthesis and chemical degradation of polyesters. *Catalysis Science & Technology* **12**, 6142-6154 (2022).

[15] Rittinghaus, R. D., Schäfer, P. M., Albrecht, P., Conrads, C., Hoffmann, A., Ksiazkiewicz, A. N., Bienemann, O., Pich, A., Herres-Pawlis, S. New Kids in Lactide Polymerization: Highly Active and Robust Iron Guanidine Complexes as Superior Catalysts. *ChemSusChem* **12**, 2161–2165 (2019).

[16] Román-Ramírez, L. A., McKeown, P., Jones, M. D., Wood, J. Poly(lactic acid) Degradation into Methyl Lactate Catalyzed by a Well-Defined Zn(II) Complex. *ACS Catalysis* **9**, 409–416 (2019).

[17] Santulli, F., Lamberti, M., Mazzeo, M. A Single Catalyst for Promoting Reverse Processes: Synthesis and Chemical Degradation of Polylactide. *ChemSusChem* **14**, 5470–5475 (2021).

CHAPTER 3

Heteroleptic zinc complexes for the synthesis and degradation of polylactide

The results described in this Chapter have been published in:

Santulli, F., Lamberti, M., Mazzeo, M. A Single Catalyst for Promoting Reverse Processes: Synthesis and Chemical Degradation of Polylactide. *ChemSusChem* **14**, 5470-5475 (2021).

3.1 Introduction

As reported in the *Introduction*, the development of both new environmentally friendly materials and efficient technologies for plastic recycling are necessary actions to achieve a circular economy and solve the problem of plastic pollution.[1]

Polylactide (PLA) is a biodegradable plastic derived from renewable resources. Thanks to its good mechanical and gas barrier properties, it may express its potentiality as alternative to the traditional oil derived plastics for short single use. However, despite its potential sustainability, there are some challenges to its life cycle.

PLA is industrially produced by ring-opening polymerization of lactide promoted by a highly toxic tin catalyst. Furthermore, although PLA is a biodegradable material, its end-of-life fate is currently not well planned. Nowadays, PLA disposal is performed under composting conditions of high temperature and high humidity, requiring long reaction times. The products that are released are CO_2 and water, thus losing the high value associated with the polymer. There are other polymer recycling options that could provide greater benefits in both environmental and economic terms.

Chemical degradation by alcoholysis is emerging as a powerful method for recycling PLA. Occurs through transesterification reactions, producing value-added molecules such as alkyl lactates. These can be useful on their own or used to reform lactic acid, and thus close the PLA cycle.

There are numerous catalytic systems based on non-toxic metals such as magnesium[2], zinc[3] and aluminum[4] which have demonstrated a high efficiency in the synthesis of PLA. However, examples of catalyst for the chemical degradation of PLA by alcoholysis are rare.

In *Chapter 2*, homoleptic and heteroleptic zinc and magnesium complexes supported by phenoxy-imine bearing an additional pyridine moiety were investigated. All the complexes were used in both the synthesis and chemical degradation of PLA. The heteroleptic zinc complex was the most active in both reactions, furthermore high performances were observed when pyridine was present as an additional donor. In this *Chapter* new heteroleptic pyridyl phenoxy-imine zinc complexes with several *para*- and *ortho*-substituents have been synthesized, characterized, and used for the ROP of lactide both in solution and under industrially conditions. The behavior of the catalysts in the degradation of PLA have also been described.

3.2 Results and discussion

3.2.1 Synthesis and characterization

A series of pyridyl phenoxy-imine proligands (L_1H-L_5H) bearing different substituents on the phenolate rings were obtained via simple condensation reactions (**Scheme 3.1**) in yields always higher than 85 %. The ligands were characterized by ^{1}H and ^{13}C NMR spectroscopy (**Figures 3.6-3.9**).

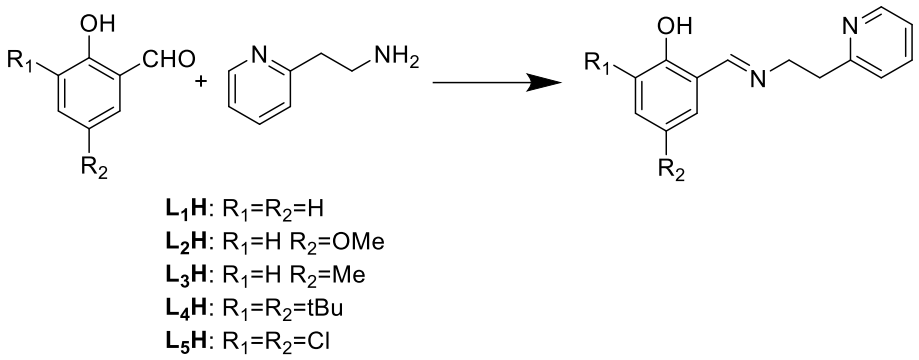

L_1H: R_1=R_2=H
L_2H: R_1=H R_2=OMe
L_3H: R_1=H R_2=Me
L_4H: R_1=R_2=tBu
L_5H: R_1=R_2=Cl

Scheme 3.1 Synthesis of ligands L_1H-L_5H.

The ^1H NMR spectrum of the L_1H ligand is shown below as an example. Diagnostic resonances in ^1H NMR spectrum were the singlet at δ = 7.67 ppm for the imine proton, the singlet at δ = 13.6 ppm for the phenolic proton and the doublet at δ = 8.46 ppm for the proton adjacent to the pyridine nitrogen. Two distinct triplets at δ = 3.68 and δ = 2.86 ppm for the methylene protons of the pyridine pendant arm were observed. (**Figure 3.1**).

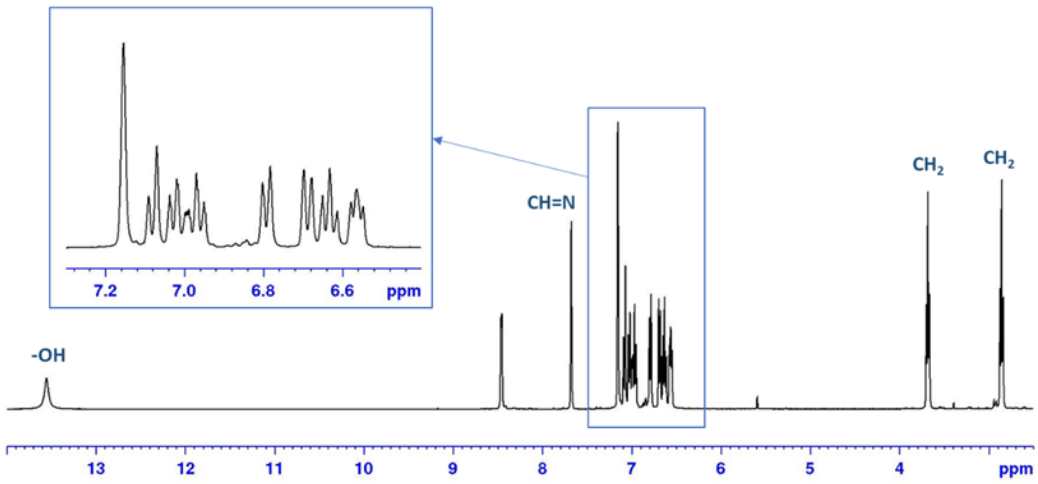

Figure 3.1 ^1H NMR spectrum (300 MHz, C_6D_6, 298 K) ligand L_1H.

To understand the effect of the pyridine donor, ligand L_6H was also synthesized by condensation reaction between N,N-dimethyl ethylenediamine and 3,5-bis(tert-butyl)-2-hydroxybenzaldehyde (**Scheme 3.2**).

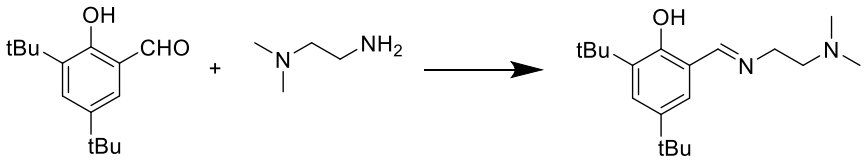

Scheme 3.2 Synthesis of ligand L_6H.

The confirmation of the reaction was observed by the appearance of a new signal at δ = 7.84 ppm relative to the imino proton (**Figure 3.2**). Again, the phenoxy proton is observed as a down-field peak (δ = 14.3 ppm) and the methylene groups of the amino arm resonate as two triplets at δ = 3.29 ppm and δ = 2.89 ppm.

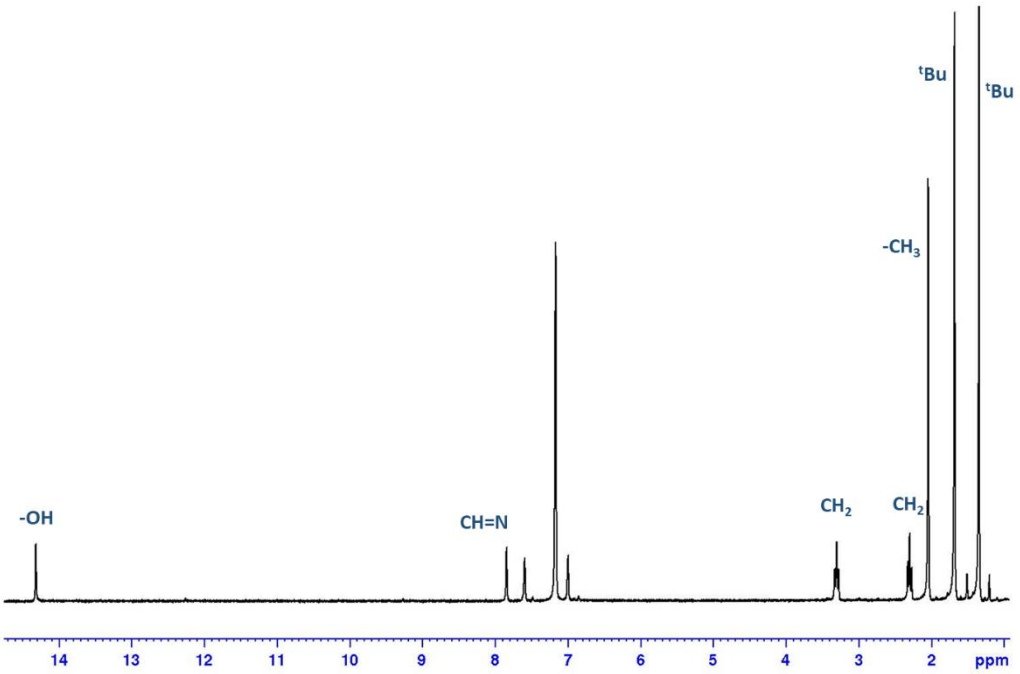

Figure 3.2 ^{1}H NMR spectrum (250 MHz, C_6D_6, 298 K) ligand L_6H.

The Zn(II) complexes **1-6** were obtained by direct reaction between $Zn[N(SiMe_3)_2]_2$ and the tridentate Schiff base ligand L_1H-L_6H in toluene or benzene (**Scheme 3.3**). The complexes were characterized by mono- and bi-dimensional NMR analysis (**Figures 3.11-3.30**).

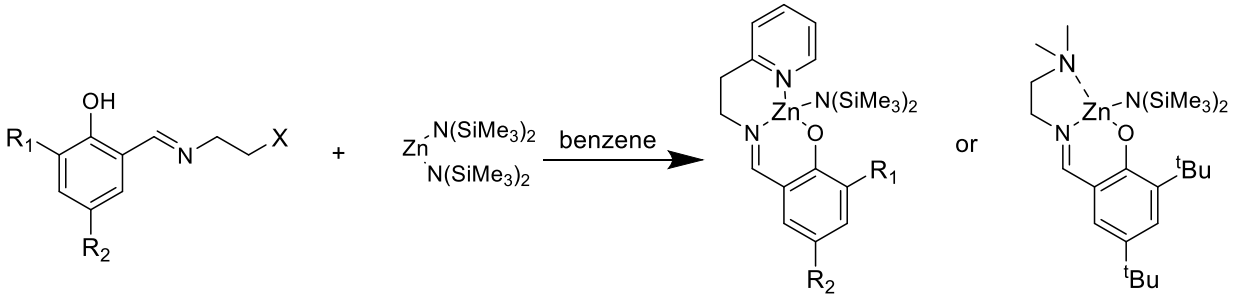

L_1H: $R_1=R_2=H$ X=*ortho*-pyridine
L_2H: $R_1=H$ $R_2=OMe$ X=*ortho*-pyridine
L_3H: $R_1=H$ $R_2=Me$ X=*ortho*-pyridine
L_4H: $R_1=R_2=tBu$ X=*ortho*-pyridine
L_5H: $R_1=R_2=Cl$ X=*ortho*-pyridine
L_6H: $R_1=R_2=tBu$ $X=N(Me)_2$

1: $R_1=R_2=H$
2: $R_1=H$ $R_2=OMe$
3: $R_1=H$ $R_2=Me$
4: $R_1=R_2={}^{t}Bu$
5: $R_1=R_2=Cl$

6

Scheme 3.3 Synthesis of complexes **1-6**.

For the complex **1**, the ^{1}H, and ^{13}C spectra, performed both in C_6D_6 (**Figure 3.3**) and CD_2Cl_2, showed sharp and well resolved resonances for the pyridyl imino-phenolate ligand and the bis-(trimethylsilyl)amide group of the zinc complex which were consistent with a monomeric structure in solution for which no change to the zinc coordination on the NMR timescale was observed. Reliable evidence of coordination of the pyridine moiety to the metal center was shown by the low-field ^{1}H-NMR shift of proton in the *ortho* position of the pyridyl ring ($\delta = 8.46$ ppm) in comparison to the same resonance for the free ligand ($\delta = 8.31$ ppm) and by the NOESY measurement in which the *ortho* proton of the pyridyl fragment was strongly correlated to the protons of the bis-(trimethylsilyl)amide group (**Figure 3.13**).

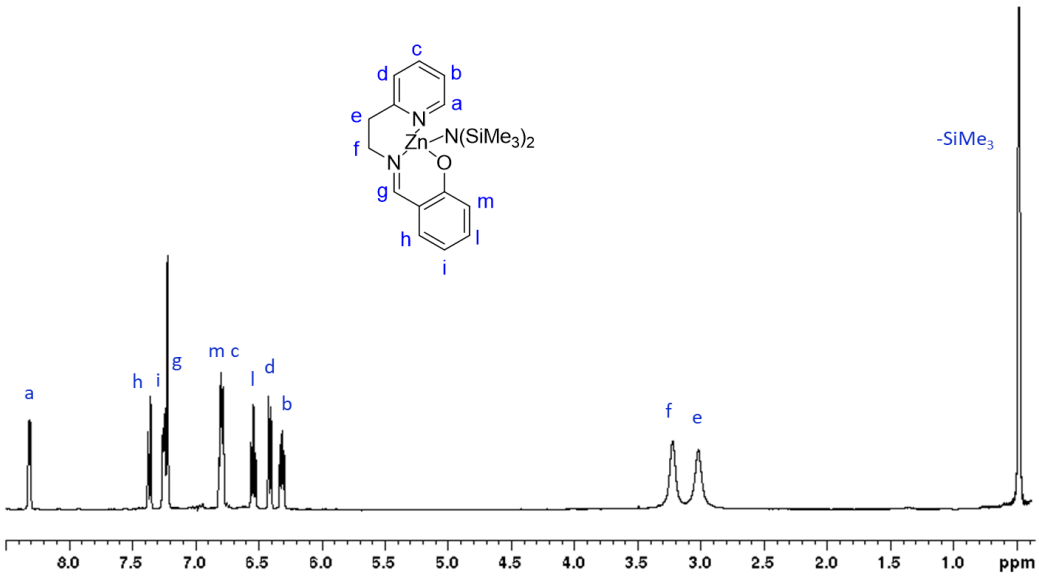

Figure 3.3 ^{1}H NMR spectrum (400 MHz, C_6D_6, 298 K) complex **1**.

The nuclearity of complex was further assessed via diffusion-ordered NMR spectroscopy (DOSY) and the result indicated that the complex has a monomeric structure in solution. (**Figure 3.16**). TGA analysis showed high thermal stability of complex **1** for more than one hour at 150 °C (**Figure 3.20**).

A similar situation was observed for the other phenoxy-amino complexes.

3.2.2 Polymerization studies

All complexes synthesized were used as catalysts in the ROP of *rac*-LA in solution at room temperature. Representative results are summarized in **Table 3.1**.

Table 3.1
Polymerization Data of *rac*-LA with complexes **1-7**.

Entry[a]	cat	iPrOH (eq.)	time (min)	Conv (%)	TOF (h^{-1})	M_{nGPC}[b] (KDa)	Đ[b]	M_{nth}[c] (KDa)
1	**1**	-	8	61	460	2.7	1.7	8.8
2	**1**	1	2	80	2420[d]	12.0	1.1	11.5
3	**2**	1	2	77	2300[d]	11.5	1.2	11.1
4	**3**	1	2	84	2520[d]	12.2	1.1	12.1
5	**4**	1	2	56	1700	8.7	1.2	8.1
6	**5**	1	2	24	720	11.8	1.1	11.5
7	**6**	1	2	56	1700	8.5	1.2	8.1

[a]All polymerizations were carried out by using 5 µmol of catalysts in 2 mL of CH_2Cl_2 and 100 equiv. of *rac*-LA. [b]Experimental Mn and Đ values of the polymers were determined by gel-permeation chromatography (GPC) in THF relative to polystyrene standards and multiplied by a correction factor of 0.58. [c]Calculated according to the monomer conversion: M_{nth} (KDa) = 144.14 $gmol^{-1}$ × ([LA]/[ROH]) × conversion of LA. [d]TOF calculated after 0.5 min.

An initial polymerization test of *rac*-LA was performed at room temperature in dichloromethane. Under these conditions, **1** showed a turnover frequency (TOF) of 460 h^{-1} (entry 1, **Table 3.1**). By adding 1 equiv. of alcohol, the activity increased considerably reaching a TOF of 2650 h^{-1} (entry 2, **Table 3.1**). From the tests, a clear effect of the nature of the substituents emerged, indeed complexes **2** and **3** (entries 3 - 4, **Table 3.1**), in which electron donating groups were present on the *para* positions of the phenoxy moiety, were very active. A slight decrease in reactivity were observed when very bulky groups (complex **4**) or electron withdrawing groups (complex **5**) were introduced (entries 5 and 6 respectively, **Table 3.1**). During polymerization, the nature of

the neutral donor appeared to have no significant effect. Indeed, complexes **4** and **6** showed the same activities (entries 5 and 7, **Table 3.1**).

Complex **1** was further investigated using other reaction conditions reported in the **Table 3.2**.

Table 3.2
Polymerization Data of lactides with complex **1**.

Entry[a]	Mon	[LA]/[1]/[ROH]	time (min)	T (°C)	Conv (%)	TOF (h^{-1})	M_{nGPC}[b] (KDa)	Đ[b]	M_{nth}[c] (KDa)
1	*rac*-LA	400/1/1	1	25	77	28320[g]	49.5	1.14	44.4
2	L-LA	400/1/1	1	25	70	25920[g]	45.1	1.12	40.3
3	L-LA	400/1/40	2	25	97	14880[g]	1.80	1.10	1.44
4	L-LA	400/1/100	2	25	67	8040	0.9	1.10	0.4
5[d]	L-LA	1000/1/2	2	25	56	16800	37.8	1.30	40.3
6[e]	L-LA	1000/1/2	2	25	68	20400	31.2	1.37	48.9
7[f]	L-LA	1000/1/0	4	150	23	3450	46.9/28.2	bimodal	33.2
8[f]	L-LA	1000/1/10	1	150	100	60000	9.7	1.38	14.4
9[f]	L-LA	1000/1/50	0.5	150	100	120000	3.1	1.91	2.9
10[f]	L-LA	5000/1/50	5	150	82	49200	8.9	1.44	11.5

[a]All reactions were carried out by using 10 µmol of catalyst **1** at 25 °C in CH_2Cl_2 (2 mL), ROH was ^{i}PrOH for runs at 25 °C and BnOH for runs at 150 °C. [b]Experimental M_n (corrected using factor of 0.58) and $Đ$ values were determined by GPC analysis in THF using polystyrene standards. [c]Calculated M^{th}(KDa) =144.14 x ([LA]/[ROH]) x conversion of LA.[d]LA purified by a single crystallization [e]Unpurified LA. [f]Technical grade purity LA, solvent free. [g]TOF calculated after 0.5 min.

Using a higher amount of monomer, complex **1** showed very high activity reaching a TOF higher than 25000 h^{-1} using both *rac*-LA and L-LA (entries 1 and 2, **Table 3.2**). Increasing the alcohol/ complex ratio up to 100 equiv. (entries 3 – 4, **Table 3.2**), in the so called "immortal" conditions, the high activity of catalyst was preserved. The MALDI-FT-ICR MS analysis of samples revealed single series of peaks with a constant peak spacing of 144 Da indicating the complete absence of transesterification side reactions (**Figures 3.32 -3.34**). The chain end groups were those expected: BnO- or iPrO- and -H groups as observed also by ^{1}H NMR spectroscopy (**Figure 3.31**) depending on the nature of the alcohol used.

To align with industrial practices and demonstrate the robust nature of the catalyst, subsequent polymerization experiments were performed by using poorly purified or unpurified monomer (entries 5 and 6, **Table 3.2**) and we were delighted to observe no decline of the catalyst performance (TOF = 20400 h^{-1}) and only a minimal impact on the dispersity of the molecular masses of the obtained polymers.

Subsequently, additional polymerization tests were carried out with L-LA of technical grade purity at 150 °C with a monomer/ complex ratio up to 5000: 1 (entries 7-10, **Table 3.2**) obtaining very high activities in all cases and TOF up to 120000 h^{-1}. In the absence of alcohol, a bimodal distribution of the molecular weights was observed (entry 7, **Table 3.2**), while all polymers obtained with complex **1**/ROH showed monomodal distributions with narrow dispersities (Đ) and molecular weights values coherent with the theoretical ones thus suggesting a good control of the polymerization process even under these challenging conditions.

About microstructures of the obtained polymers, perfectly isotactic PLAs were obtained by L-LA even carrying out the polymerizations at high temperatures indicating the absence of epimerization phenomena (**Figure 3.33**). Coherently, differential scanning calorimetry (DSC) analysis of sample produced showed melting temperatures of 164.1 °C, a value indicative of a PLLA with high crystallinity (**Figure 3.35**).

3.2.3 Degradation studies

The chemical degradation of PLA via transesterification by methanol or ethanol allows the formation of valuable low-molecular-weight compounds, such as methyl and ethyl lactate (Me-La and Et-La), respectively.

Initially, complex **1** was investigated in the methanolysis of several samples of PLA, different for stereoregularity [isotactic poly(L-LA) and atactic poly(*rac*-LA)] or for molecular weights. Some commercial products were also selected. The details of the PLA samples tested are summarized in **Table 3.6**.

All degradation reactions were performed at room temperature with 0.6 mol % catalyst with respect to the repeating units of polymer and by using unpurified solvent and alcohol. The monitoring of the degradation reaction was performed by regular sampling and ^{1}H NMR spectroscopy analysis (**Figure 3.4**) of the reaction. In the spectral region between $\delta = 4.00$ ppm and $\delta = 5.20$ ppm, four different signals were evident, attributable to methine protons of the chain end units of PLA oligomers, of the internal repeating units and of Me-La. Conversion of internal methine units (X_{Int}), Me-La selectivity ($S_{Me\text{-}La}$) and Me-La yield ($Y_{Me\text{-}La}$) were chosen as representative parameters for a comparative analysis with the studies reported by Sobota[5] and Jones[6].

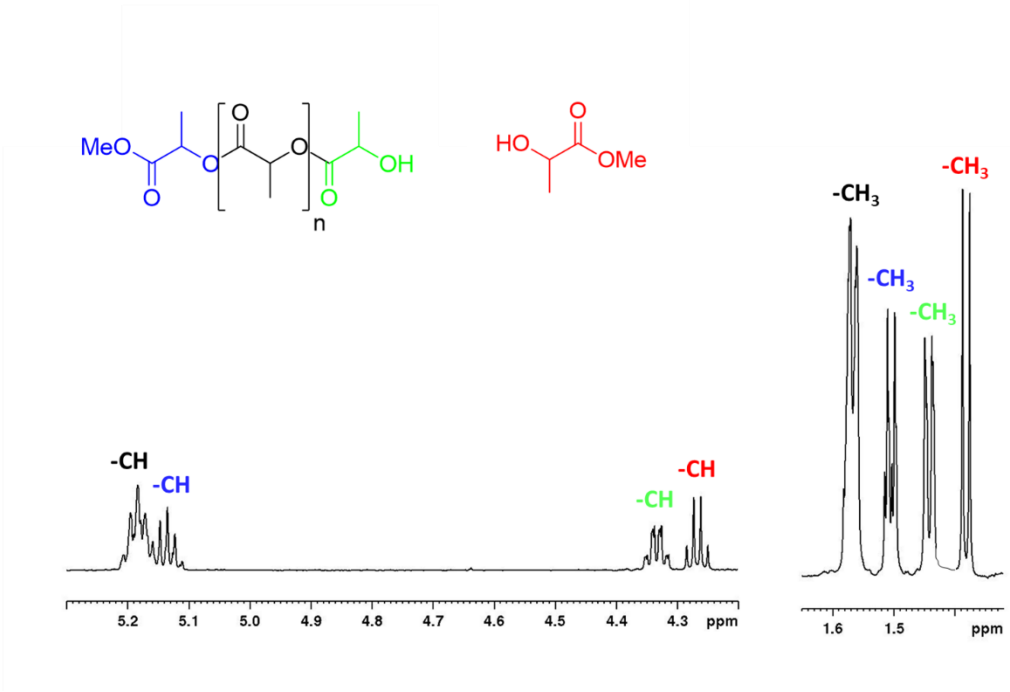

Figure 3.4 ^{1}H NMR spectrum (CD_2Cl_2, 298 K, 400 MHz) of a degradation reaction of PLLA.

The zinc complex **1** revealed high activity in the degradation of isotactic PLLA samples with molecular weights ranging from 14.0 to 90.0 KDa, and in all cases the quantitative degradation of polymers was achieved after 1 h at room temperature (entries 1-4, **Table 3.3**).

Table 3.3

Methanolysis Data of PLAs performed in THF solution with complex **1**.

Entry[a]	Sample	Mn (KDa)	time (h)	X_{Int}[b]	$S_{Me\text{-}La}$[b]	$Y_{Me\text{-}La}$[b]
1	PLLA	30	1	100	61	61
2	PLLA	48	1	100	74	74
3	PLLA	92	1	100	77	77
4	PLLA	14	1	97	95	92
5	P(*rac*-LA)	13	1	44	35	16
6	P(*rac*-LA)	44	1 2	75 88	69 89	52 78
7[d]	PLLA	30	2 4.5	89 97	38 61	34 60
8[d]	PLA cup	58	2 4.5	100 100	47 100	47 100
9[d]	PLA filament	20	2 4.5	84 100	26 62	22 62

[a]All reactions were carried out by using 5 µmol of catalyst **1** (0.6 mol % relative to ester linkages) in 1.8 mL of THF, with 0.2 mL of MeOH (6 times relative to ester linkages). [b]Mn = experimental molecular weight (GPC). [c]Determinated by ^{1}H NMR spectroscopy. [d]reaction performed in air.

The good performances of complex **1** were preserved even when the reactions were performed in the presence of air, indeed only a little decrease of the degradation rate was observed (entries 1 vs 7, **Table 3.3**).

To demonstrate the applicability of this complex in recycling processes of post-consumer PLA samples, degradation experiments of an end-of-life PLA-plastic cup and a PLA filament for 3D printing were performed in the presence of air following the conditions described in entry 7 of **Table 3.3**. The PLA-plastic cup was rapidly converted to Me-La after about 4 h at room temperature (entry 8, **Table 3.3**). Lower activity was observed with 3D printing filament, reasonably as consequence of the presence of unknown additives present in the sample (entry 9, **Table 3.3**).

The NMR monitoring (**Figure 3.5**) showed that degradation process occurred via a two-step process (THF solution of **Scheme 3.3**) in which a random scission of the polymer chains in the initial stages led to the formation of oligomeric species that are progressively converted into Me-La.

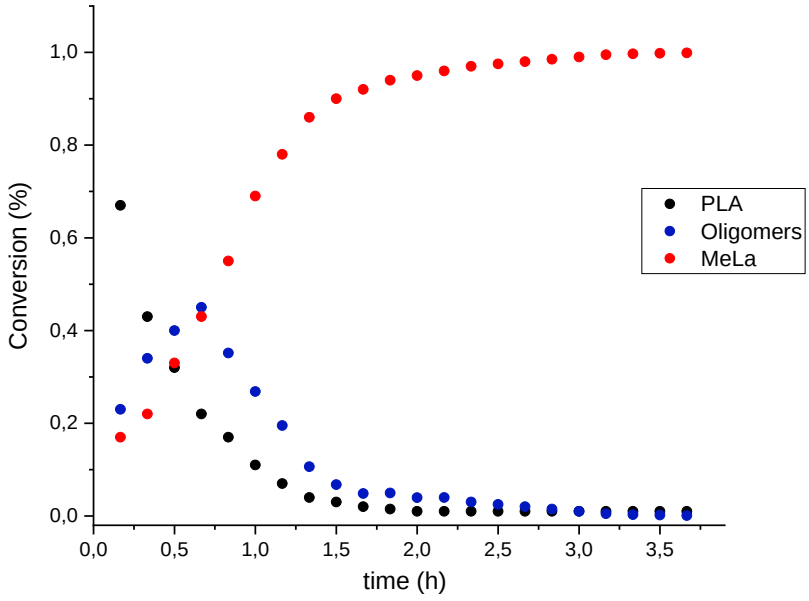

Figure 3.5 Kinetic profile for degradation of a PLLA sample. Reaction condition $[PLLA]_0$ = 0.44 M; $[polyester\ linkages]_0/[\mathbf{1}]_0$ = 60; THF-d8 (0.45 mL) as solvent; MeOH 0.05 mL.

For reactions performed in THF solution, the degradation rate revealed to be not depending on the molecular weight of PLA samples (see runs 1-4, **Table 3.3**), coherently with a mechanism of random scission of the polymeric chain (THF solution of **Scheme 3.3**). In this mechanism the zinc acts as a Lewis acid and activates a carbonyl group of the chain for a nucleophilic attack by the alkoxide labile group or an external alcohol. Surprisingly, the degradation rate was influenced by the tacticity of the polymer (see entry 4 vs 5, and entry 2 vs 6, **Table 3.3**), and it was faster for the isotactic than for atactic PLAs. Probably, the formation of different diastereoisomeric zinc species during the degradation phenomena may be responsible for the observed differences.

The NMR analysis of PLLA degradation performed in THF-d8 or CD_2Cl_2 revealed a linear relationship of $\ln[PLLA]_0/[PLLA]_t$ against the time indicative of a first-order kinetics with a k_{app} values of 2.3 h^{-1} at 25 °C (**Figure 3.36**).

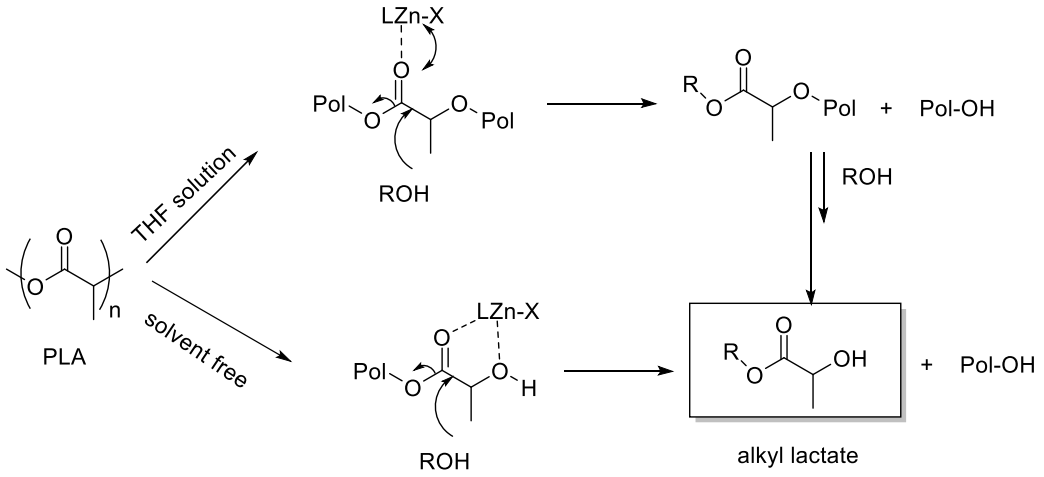

Scheme 3.3 Alcoholysis of PLA via random scission of the chains (THF solution) or by chain-end cutting (solvent-free condition).

Subsequently, the alcoholysis experiments were performed without the use of additional solvents (**Table 3.4**).

Table 3.4

Alcoholysis Data of PLAs under solvent free conditions, with complex **1**.

Entry[a]	Sample	ROH	Mn[b] (KDa)	time (h)	X_{Int}[c]	$S_{R\text{-}La}$[c]	$Y_{R\text{-}La}$[c]
1	P(*rac*-LA)	MeOH	38	1	100	100	100
2	PLLA	MeOH	30	3 8	51 100	100 100	51 100
3	PLLA	MeOH	48	3 8	36 75	100 100	36 75
4	PLLA	MeOH	92	3 8	25 79	100 100	25 79
5	PLLA	MeOH	160	24	100	100	100
6	PLLA	EtOH	92	24	100	80	80
7[d]	PLLA	EtOH	92	13	100	100	100

[a]All reactions were carried out by using 5 µmol of catalyst **1** (0.6 mol % relative to ester the linkages) with 2 mL of ROH at 25 °C. [b]Mn = experimental molecular weights (GPC). [c]Determinated by ^{1}H NMR spectroscopy. [d]Reaction performed at reflux temperature of EtOH.

The degradation in neat alcohol of P(*rac*-LA) proceeded very quickly: after 1 hour the complete conversion into Me-La was observed (entry 1, **Table 3.4**). As expected, for the crystalline PLLA the degradation time was longer because of its scarce permeability to the methanol, and it was significantly dependent on the molecular weights (see entries 2-5, **Table 3.4**). However, the complete degradation of a very high molecular weight PLLA (160.0 KDa) was achieved after 24 h at room temperature (entry 5, **Table 3.4**).

During NMR monitoring of the methanolysis performed in the absence of solvent (**Figure 3.6**) the oligomers were not observed during the process, revealing a different mechanism (solvent-free condition, **Scheme 3.3**) in which the degradation had occurred via a progressive erosion of the chain ends with the direct formation of Me-La. This could be due to the easier accessibility of polymer chain end groups because of hydrogen bond interaction with alcohol. A pseudo first-order kinetic plot was obtained also for the solvent free degradation of polylactide (**Figure 3.39**).

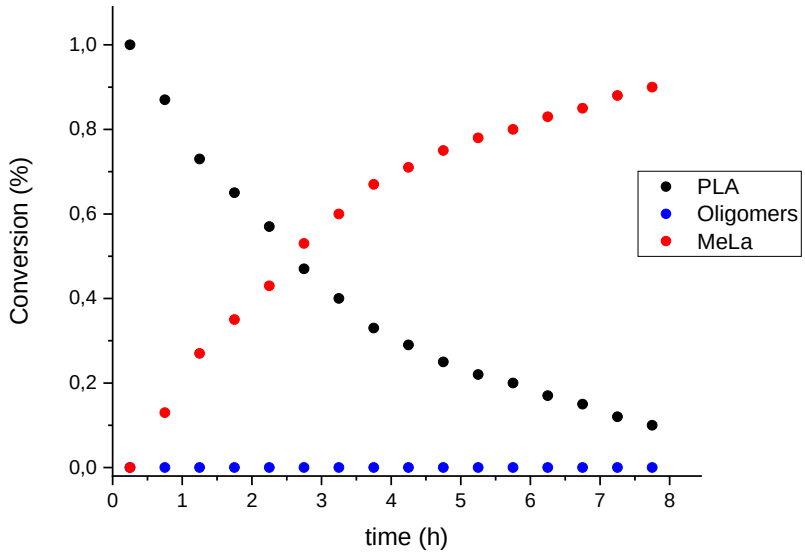

Figure 3.6 Kinetic profile for degradation of a PLLA sample. Reaction condition $[PLLA]_0$ = 0.44 M; [polyester linkages]$_0$/[**1**]$_0$ = 60; MeOH 0.50 mL.

The ethanolysis reaction resulted to be slower than methanolysis; however, after 24 h at room temperature the degradation of the polymer was complete with an 80 % yield of Et-La; at reflux temperature, only 13 h were necessary to quantitatively convert the polymer to Et-La (entries 6 and 7, **Table 3.4**).

The other complexes (**2-7**) were also used in the methanolysis reaction of PLLA (M_n = 30 KDa) in THF solution and in the presence of air (**Table 3.5**).

Table 3.5 Methanolysis Data of PLAs with complexes **1-6**.

Entry[a]	cat	time (h)	X_{Int}[b]	$S_{Me\text{-}La}$[b]	$Y_{Me\text{-}La}$[b]
1	**1**	2	89	38	34
2	**2**	2	49	24	12
3	**3**	2	51	23	12
4	**4**	2	62	16	10
5	**5**	2 4.5	39 64	0 23	0 15
6	**6**	24	41	24	10

[a]All reactions were carried out in air by using 5 µmol of catalysts (0.6 mol % relative to ester linkages) in 1.8 mL of THF, with 0.2 mL of MeOH at room temperature. [b]Determinated by ^{1}H NMR.

The complex **1**, without substituents was the most active and, conversely to what occurred in the polymerization reaction, the presence of *para*-methyl or *para*-methoxy substituents on the phenoxy group of the ligand resulted in lower activities (entries 2 and 3, **Table 3.5**). Once again, very bulky groups or electron withdrawing groups inhibited the efficiency of the complexes **4** and **5** even more (entries 4 and 5, **Table 3.5**). In the degradation reaction, the neutral donor group seems to be fundamental, indeed by comparing complexes with the same substituents on the phenoxy portion, the same yield of Me-La was obtained after 2 h with complex **4** bearing the additional pyridine donor, while 24 h were necessary with complex **6** with the pendant

amine group (entry 4 vs 6, **Table 3.5**). With all the other complexes, only Me-La is obtained after 24h with a yield of 100 %.

3.3 Conclusion

Several pyridyl phenoxy-imine zinc complexes with different substituents have been prepared and used as catalysts for the ROP of lactides in solution at room temperature. Complexes with *para*-electron donor groups on the phenoxy moiety showed higher activities, on the other hand the *ortho*- and *para*- bulk substituents or electron withdrawing groups made the reaction slower. Excellent activity and efficient control were observed with complex **1** (without substituents) even under industrially relevant conditions such as high temperature, low catalyst loading and by using unpurified monomers. The activities obtained classify this system among the most efficient ones reported in literature and comparable to the industrial catalyst $Sn(Oct)_2$.

The same complex was successfully employed for the degradation of high molecular weight and crystalline PLLA and of post-consumer PLA products. Different mechanisms were hypnotized when several degradation conditions were adopted. In THF solution, the degradation occurred via a two-step process in which random scission of the polymer chains led to the formation of oligomers that are progressively converted into alkyl lactate; while under solvent-free conditions, the degradation occurred via a progressive erosion of the chain ends with the direct formation of alkyl lactate. In the degradation reaction, the presence of the additional pyridine donor led higher activities.

In the degradation reaction, different substituents on the phenoxy moiety didn't result in activity differences. Contrarily, the presence of the pyridine group made the complex about one order of magnitude more active than the complex with an amino group as a neutral donor arm. Probably the additional donor group plays an important role in the degradation reaction, instead it was indifferent during polymerization reaction.

3.4 Experimental part

Materials and methods

Moisture and air-sensitive materials were manipulated under nitrogen using Schlenk techniques or an MBraun Labmaster glovebox. Toluene and methanol were refluxed over Na and distilled under nitrogen. Benzene was refluxed over Na and benzophenone and distilled under nitrogen. Monomers (Sigma-Aldrich) were purified before use.

$CDCl_3$, CD_2Cl_2 and C_6D_6 were purchased from Eurisotop and used as received. All other reagents and solvents were purchased from Aldrich and used without further purification.

Instruments and measurements

NMR spectra of polymers were performed at room temperature on Bruker Avance 250, 300, 400 or 600 spectrometers (^{1}H: 250.13, 300.13, 400.13, 600.13 MHz; ^{13}C: 62.57, 75.47, 100.62, 150.92 MHz, respectively). The resonances are reported in ppm (δ) and the coupling constants in Hz (J) and are referenced to the residual solvent peak at δ = 7.16 ppm for C_6D_6, δ = 7.27 for $CDCl_3$ and δ = 5.32 for CD_2Cl_2. Spectra recording was performed using Bruker- TopSpin v2.1 software. Data processing was performed using TopSpin v2.1 or MestReNova v6.0.2 software.

The average molecular masses and the molecular weight dispersities (Đ) of the obtained polylactide samples were determined by GPC in THF as the mobile phase at a flow rate of 1 mL min^{-1}. The utilized GPCmax VE-2001 from Viscotek was a combination of an HPLC pump, two Malvern Viscotek T columns (porous styrene divinylbenzene copolymer) with a maximum pore size of 500 and 5000, a refractive index detector (VE-3580), and a viscometer (Viscotek 270 Dual Detector). Polystyrene standards were used for calibration. The evaluation of the molar masses was carried out with a universal method or with a conventional method in combination with a multiplying factor of 0.58 for PLA.

MALDI mass spectra were recorded using a Bruker solariX XR Fourier transform ion cyclotron resonance (FT-ICR) mass spectrometer (Bruker Daltonik GmbH, Bremen, Germany) equipped with a 7 T refrigerated actively shielded superconducting magnet (Bruker Biospin, Wissembourg, France). The samples were prepared at the concentration of 1.0 mg mL^{-1} in THF, while the matrix (DCTB) was mixed at a concentration of 10.0 mg mL^{-1}.

Synthesis and characterization of the ligands L_1H-L_5H

The ligands were synthetized by condensation of the 2-(2-pyridyl) ethylamine with the salicyl aldehydes bearing different substituents on the ortho and para positions. The reactions were performed in reflux of ethanol overnight. The solvent was removed under vacuum, forming an orange oil in almost quantitative yields (80-85 %). The success of performed reactions was confirmed by ^{1}H NMR experiments, which spectra are illustrated in the following figures:

^{1}H NMR (400 MHz, C_6D_6, 298 K) ligand L_1H.: δ 13.6 (s, 1H, -OH), 8.46 (d, J = 4.1 Hz, 1H, Py-H), 7.67 (s, 1H, CH=N), 7.08 (d, J = 8.2 Hz, 1H, Ph-H), 7.02 (dt, J_1 = 7.2 Hz, J_2 = 1.5 Hz, 1H, Ph-H), 6.96 (dt, J_1 = 7.5 Hz, J_2 = 1.7 Hz, 1H, Py-H), 6.79 (d, J = 7.6 Hz, 1H, Ph-H), 6.69 (d, J = 7.6 Hz, 1H, Py-H), 6.63 (dt, J_1 = 7.2 Hz, J_2 = 1.1 Hz, 1H, Ph-H), 6.56 (d, J = 7.2 Hz, 1H, Py-H), 3.68 (t, J = 6.9 Hz, 2H, CH_2), 2.86 (t, J = 6.9 Hz, 2H, CH_2).

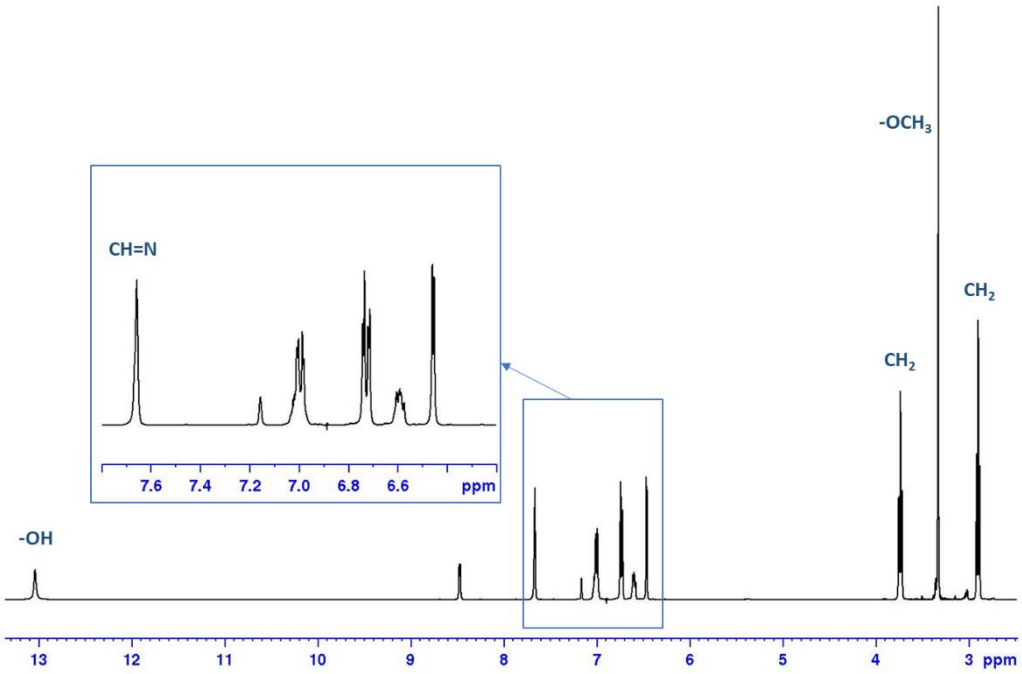

Figure 3.7 ^{1}H NMR spectrum (400 MHz, C_6D_6, 298 K) ligand L_2H.

^{1}H NMR (400 MHz, C_6D_6, 298 K): δ 13.0 (s, 1H, -OH), 8.46 (d, J = 4.8 Hz, 1H, Py-H), 7.66 (s, 1H, CH=N), 7.00 (m, 2H, Ph-H + Py-H), 6.72 (m, 2H, Ph-H + Py-H), 6.59 (m, 1H, Py-H), 6.46 (d, J = 3.0 Hz, 1H, Ph-H), 3.72 (t, J = 6.9 Hz, 2H, CH_2), 3.32 (s, 3H, OCH_3), 2.89 (t, J = 6.9 Hz, 2H, CH_2).

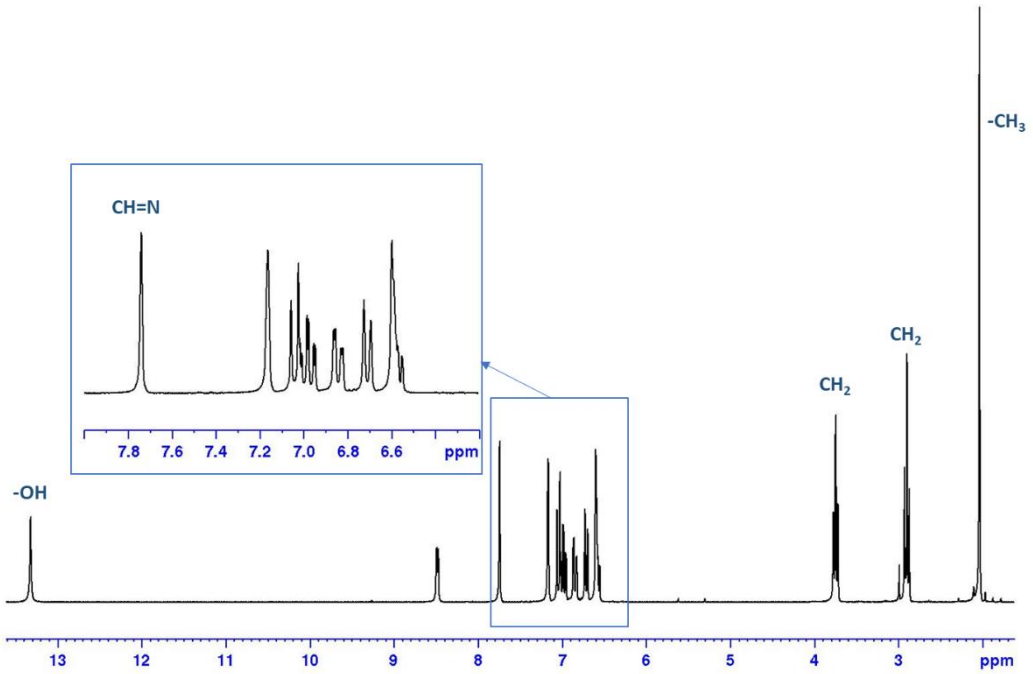

Figure 3.8 ^{1}H NMR spectrum (250 MHz, C_6D_6, 298 K) ligand L_3H.

^{1}H NMR (250 MHz, C_6D_6, 298 K): δ 13.3 (s, 1H, -OH), 8.47 (d, J = 4.8 Hz, 1H, Py-H), 7.74 (s, 1H, CH=N), 7.04 (d, J = 8.4 Hz, 1H, Ph-H), 6.98 (t, J = 7.6 Hz, 1H, Py-H), 6.84 (dd, J_1 = 8.3 Hz, J_2 = 1.9 Hz, 1H, Py-H), 6.71 (d, J = 7.9 Hz, 1H, Ph-H), 6.58 (m, 2H, Py-H + Ph-H), 3.73 (t, J = 6.9 Hz, 2H, CH_2), 2.89 (t, J = 6.9 Hz, 2H, CH_2), 2.03 (s, 3H, CH_3).

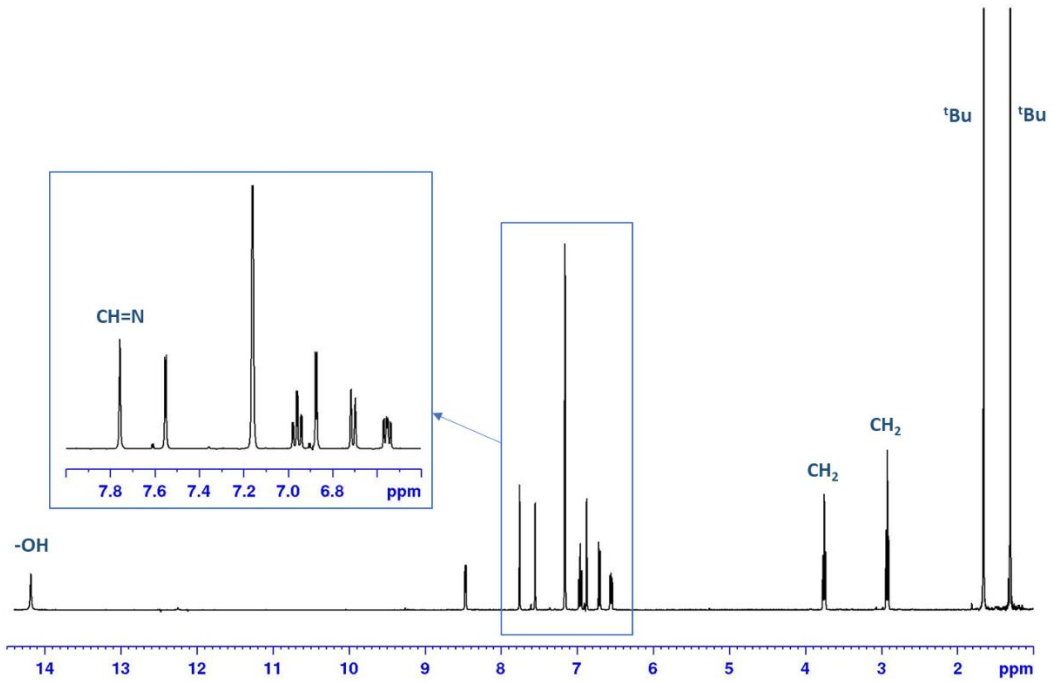

Figure 3.9 ^{1}H NMR spectrum (400 MHz, C_6D_6, 298 K) ligand L_4H.

^{1}H NMR (400 MHz, C_6D_6, 298 K): δ 14.2 (s, 1H, -OH), 8.45 (dd, J_1 = 4.8 Hz, J_2 = 1.7 Hz, 1H, Py-H), 7.75 (s, 1H, CH=N), 7.56 (d, J = 2.4 Hz, 1H, Ph-H), 6.95 (dt, J_1 = 7.5 Hz, J_2 = 2.1 Hz, 1H, Py-H), 6.87 (d, J = 2.4 Hz,

1H, Ph-H), 6.70 (d, J = 7.7 Hz, 1H, Py-H), 6.55 (dt, J_1 = 7.2 Hz, J_2 = 2.1 Hz, 1H, Py-H), 3.75 (dt, J_1 = 7.2 Hz, J_2 = 1.0 Hz, 2H, CH_2), 2.92 (t, J = 7.1 Hz, 2H, CH_2), 1.66 (s, 9H, ^{t}Bu), 1.30 (s, 9H, ^{t}Bu).

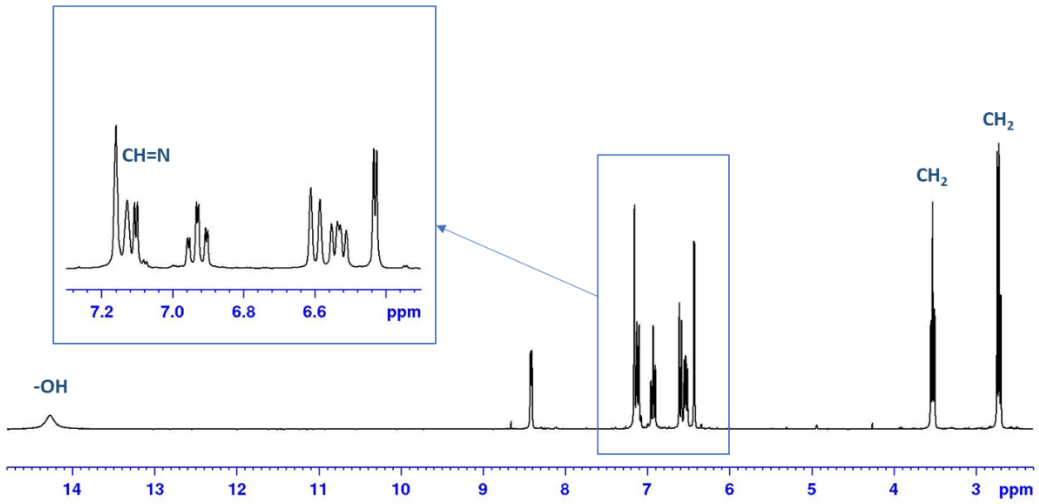

Figure 3.10 ^{1}H NMR spectrum (300 MHz, C_6D_6, 298 K) ligand L_5H.

^{1}H NMR (300 MHz, C_6D_6, 298 K): δ 14.3 (s, -OH, 1H), 8.41 (d, J = 4.8 Hz, 1H, Py-H), 7.12 (s, 1H, CH=N), 7.10 (d, J = 2.5 Hz, 1H, Ph-H), 6.93 (dt, J_1 = 7.6 Hz, J_2 = 1.8 Hz, 1H, Py-H), 6.60 (d, J = 7.7 Hz, 1H, Py-H), 6.53 (t, J = 7.7 Hz, 1H, Py-H), 6.43 (d, J = 2.5 Hz, 1H , Ph-H), 3.53 (t, J = 6.8 Hz, 2H, CH_2), 2.72 (t, J = 6.5 Hz, 2H, CH_2).

Synthesis and characterization of the ligand L_6H

The ligand was synthetized by condensation of the N,N-dimethyl ethylenediamine (0.173 g, 1.97 mmol) with the 3,5-bis(tert-butyl)-2-hydroxybenzaldehyde (0.462 g, 1.95 mmol). The reaction weas performed in reflux of ethanol overnight. The solvent was removed under vacuum, forming an orange oil in almost quantitative yields (96 %). The success of performed reaction was confirmed by ^{1}H NMR experiments, which spectrum is illustrated in the following figure:

^{1}H NMR (250 MHz, C_6D_6, 298 K) ligand L_6H: δ 14.3 (s, 1H, -OH), 7.84 (s, 1H, CH=N), 7.58 (d, J = 2.1 Hz, 1H, Ph-H), 6.99 (d, J = 2.1 Hz, 1H, Ph-H), 3.29 (t, J = 6.8 Hz, 2H, CH_2), 2.89 (t, J = 6.8 Hz, 2H, CH_2), 2.04 (s, 6H, CH_3), 1.68 (s, 9H, ^{t}Bu), 1.34 (s, 9H, ^{t}Bu).

Synthesis and characterization of the complexes 1-5

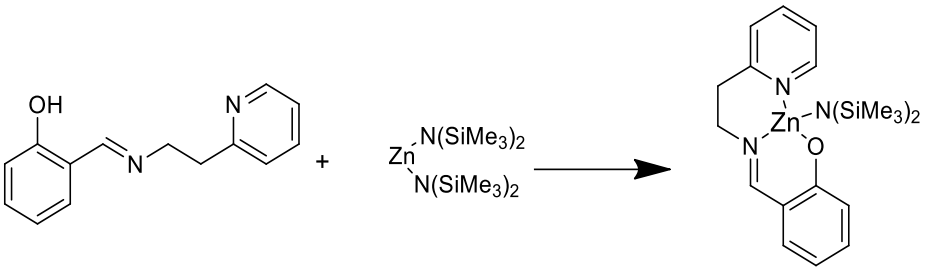

Scheme 3.4 Synthesis of complex **1**.

To a stirred solution containing Zinc bis[bis(trimethylsilyl)amide] (0.798 g, 2.0 mmol) in dry benzene (4.0 mL) was added dropwise a solution of the ligand precursor L_1H (0.453 g, 2.0 mmol) in dry benzene (2.0 mL). The solution was stirred for 3h at room temperature. The solvent was removed under vacuum, forming a red solid. The formation of the desired species was confirmed by NMR analysis (**Figures 3.11-3.19**). Yield: 80 %

^{1}H NMR (400 MHz, C_6D_6, 298 K) of complex **1**: δ 8.31 (d, J = 5.2 Hz, 1H, Ha), 7.36 (d, J = 8.6 Hz, 1H, Hh), 7.25 (m, 1H, Hi), 7.22 (s, 1H, Hg), 6.80 (m, 2H, H_m-Hc), 6.53 (t, J = 7.8 Hz, 1H, Hl), 6.40 (d, J = 7.8 Hz, 1H, Hd), 6.31 (t, J = 6.5 Hz, 1H, Hb), 3.22 (m, 2H, Hf). 3.01 (m, 2H, He), 0.47 (s, 18H, -$SiMe_3$).

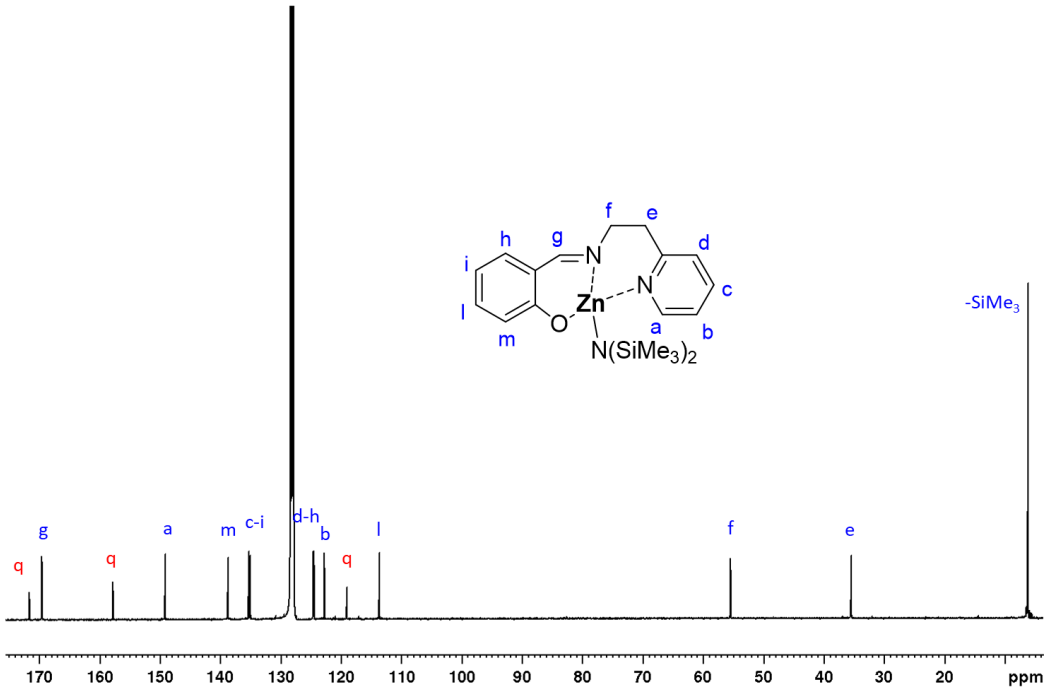

Figure 3.11 ^{13}C NMR spectrum (100 MHz, C_6D_6, 298 K) complex **1**.

^{13}C NMR (100 MHz, C_6D_6, 298 K): δ 171.6 (Cq), 169.5 (Cg), 157.8 (Cq), 149.1 (Ca), 138.7 (Cm), 135.2 (Cc), 135.0 (Ci), 124.6 (Cd), 124.4 (Ch), 122.8 (Cb), 119.0 (Cq), 113.6 (Cl), 55.4 (Cf), 35.4 (Ce), 6.12(-$SiMe_3$).

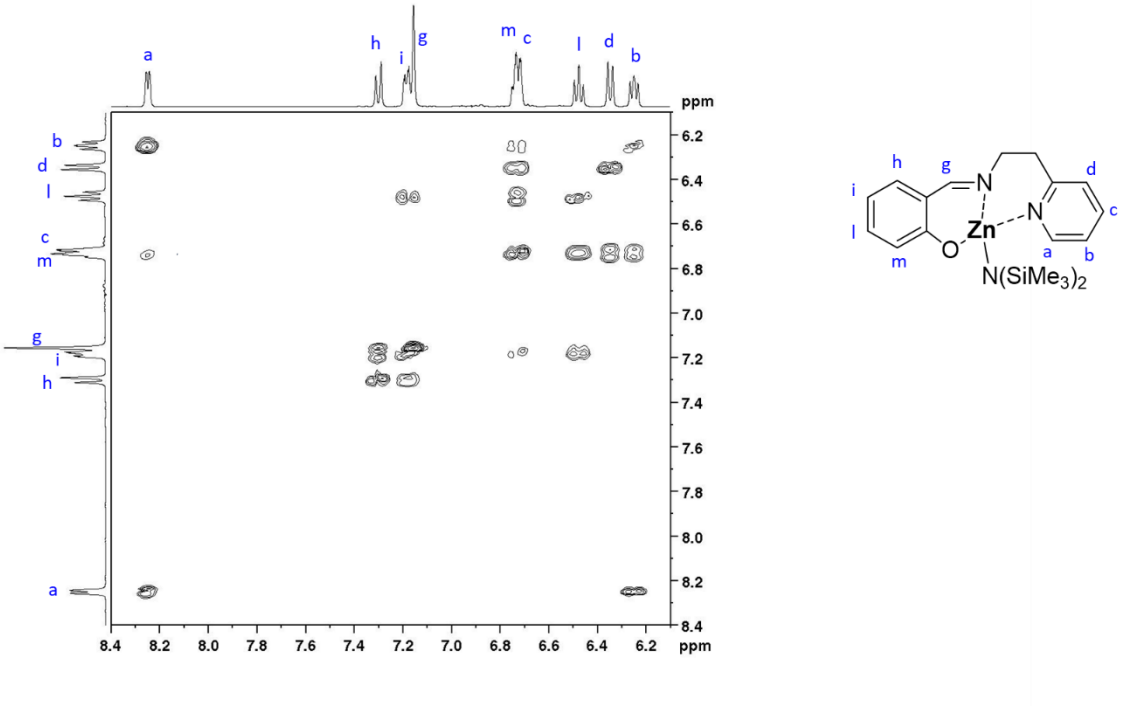

Figure 3.12 Aromatic region of COSY NMR spectrum (400 MHz, C_6D_6, 298 K) complex **1**.

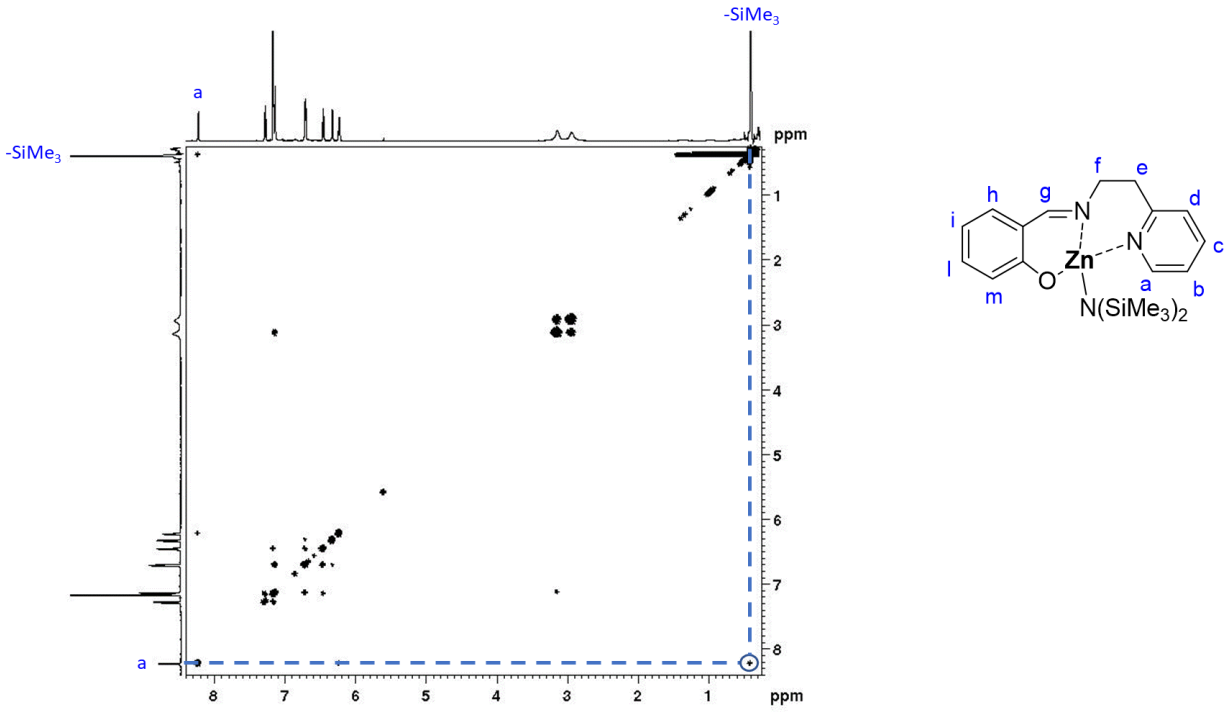

Figure 3.13 NOESY NMR spectrum (600 MHz, C_6D_6, 298 K) complex **1**.

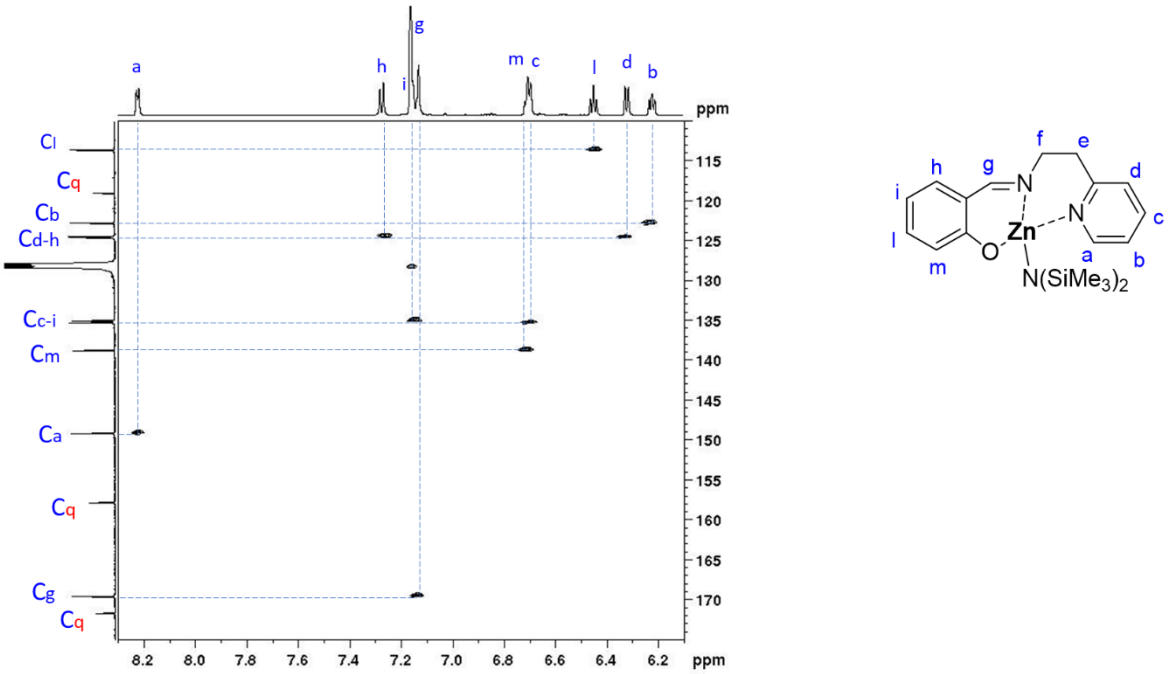

Figure 3.14 Aromatic region of HSQC NMR spectrum (600 MHz, C_6D_6, 298 K) complex **1**.

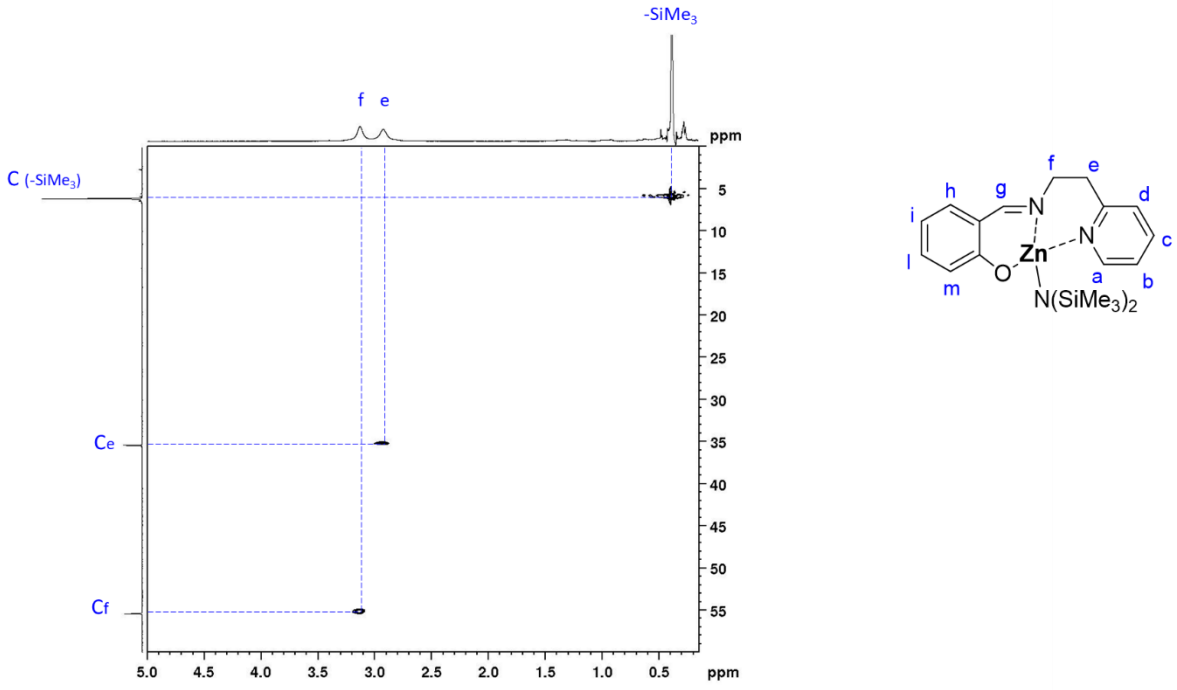

Figure 3.15 Aliphatic region of HSQC NMR spectrum (600 MHz, C_6D_6, 298 K) complex **1**.

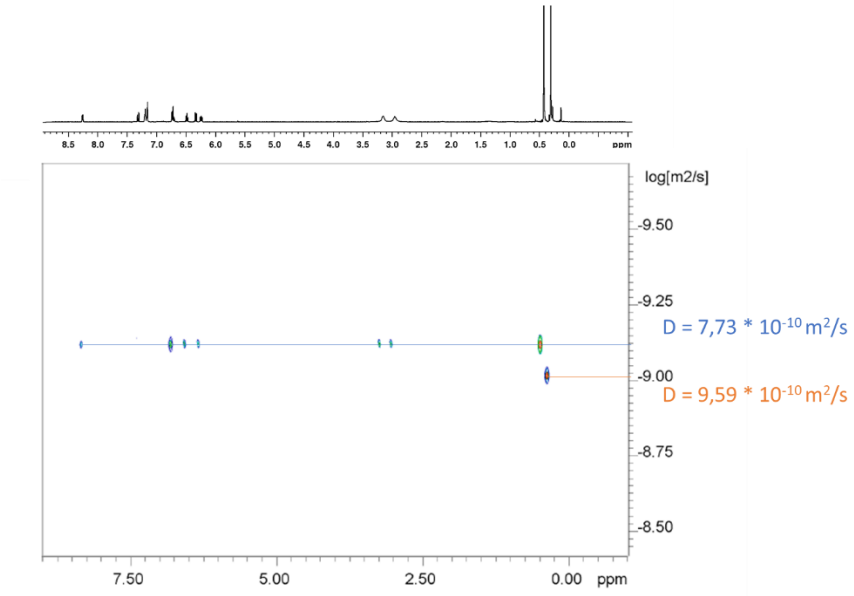

Figure 3.16 DOSY NMR spectrum (400 MHz, C_6D_6, 298 K) of complex **1** (D = 7.73 10^{-10} m^2/s) in the presence of tetrakis(trimethylsilyl)silane TMSS as standard (D = 9.59 10^{-10} m^2/s).

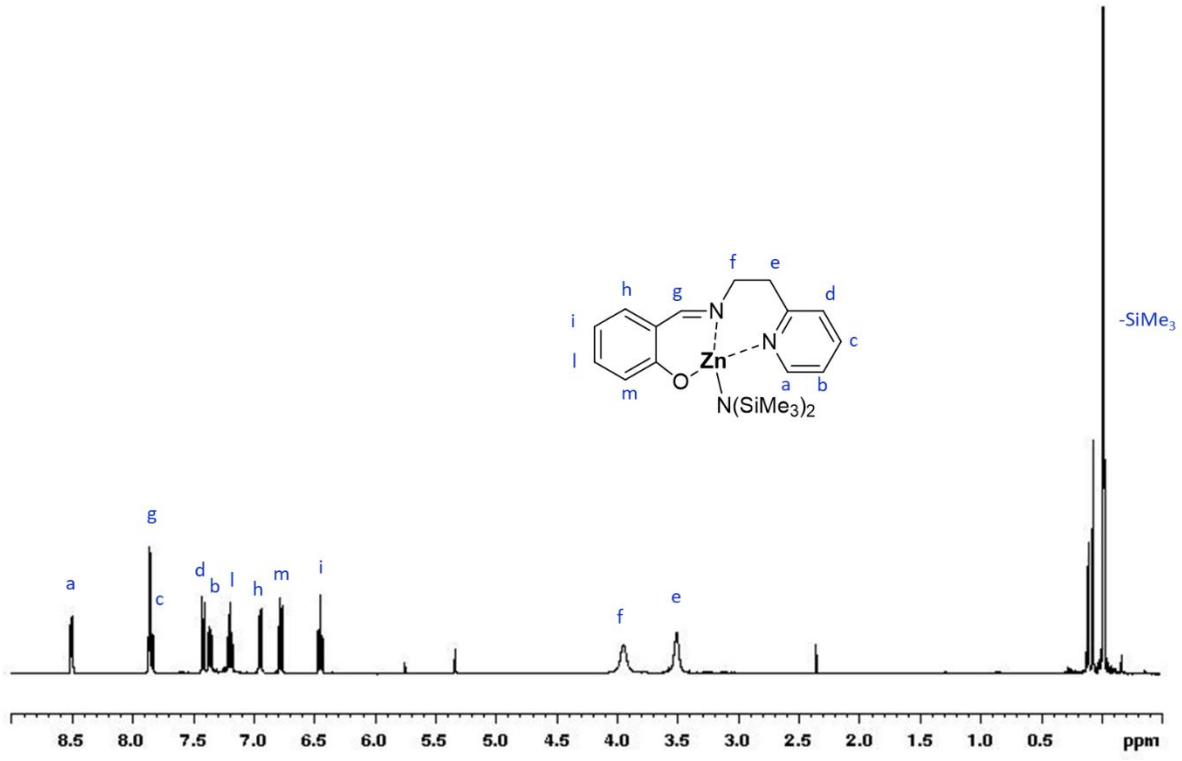

Figure 3.17 ^1H NMR spectrum (400 MHz, $CDCl_2$, 298 K) complex **1**.

^1H NMR (400 MHz, CD_2Cl_2, 298 K): δ 8.49 (d, J = 5.2 Hz, 1H, Ha), 7.84 (m, 2 H, Hg-Hc), 7.41 (d, J = 7.8 Hz, 1H, Hd), 7.35 (t, J = 6.5 Hz, 1H, Hb), 7.18 (t, J = 8.7 Hz, 1H, Hl), 6.94 (dd, J_1 = 7.8 Hz, J_2 = 1.7 Hz, 1H, Hh), 6.76 (d, J = 8.6 Hz, 1H, Hm), 6.44 (t, J = 7.8 Hz, 1H, Hi), 3.93 (m, 2H, Hf). 3.49 (m, 2H, He), -0.0336 (s, 18H, -$SiMe_3$).

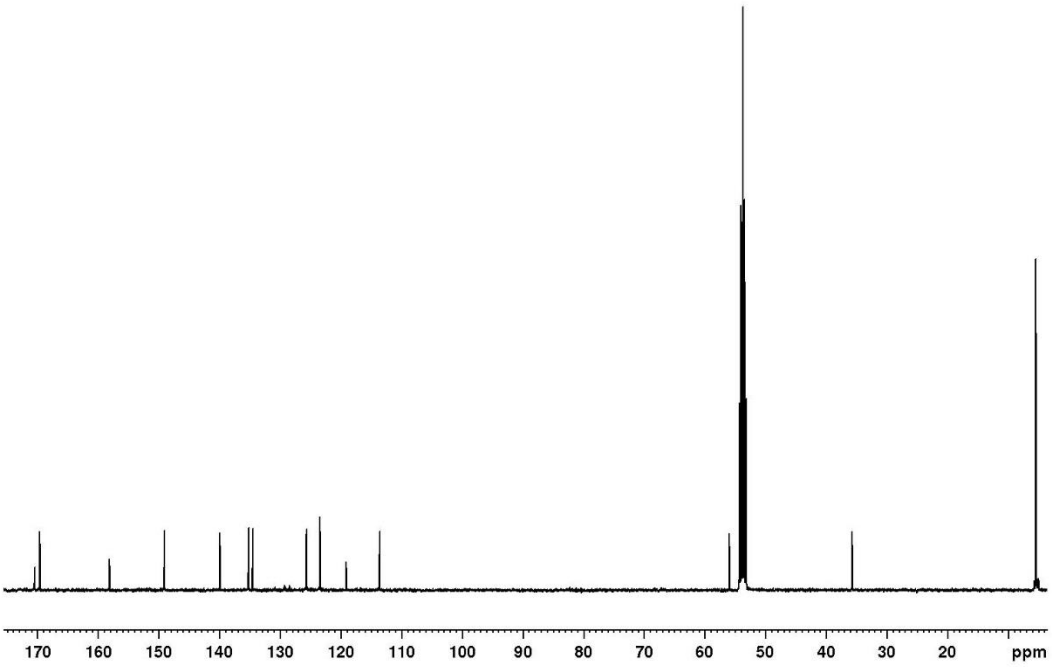

Figure 3.18 ^{13}C NMR spectrum (400 MHz, CD_2Cl_2, 298 K) of complex **1**.

^{13}C NMR (100 MHz, CD_2Cl_2, 298 K): δ 170.4, 169.6, 158.1, 149.0, 139.9, 135.1, 134.5, 125.6, 123.4, 123.3, 119.1, 113.6, 55.9, 35.7, 5.40.

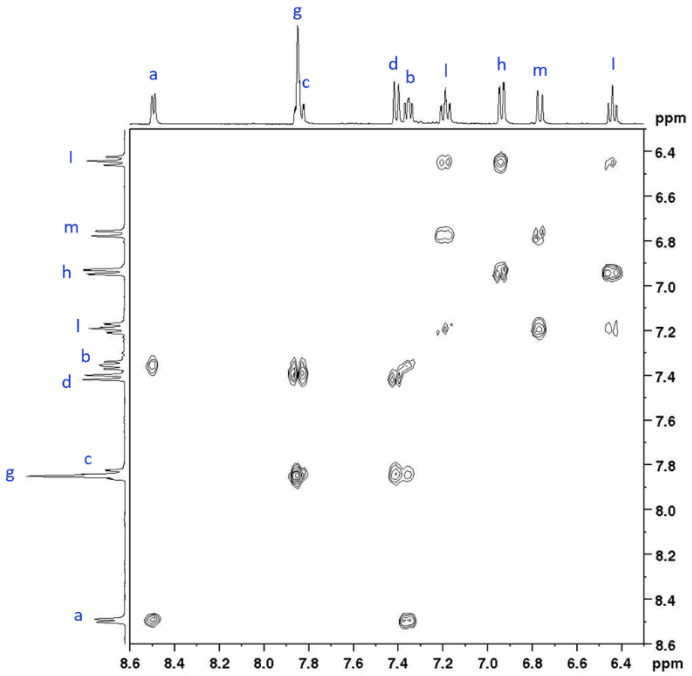

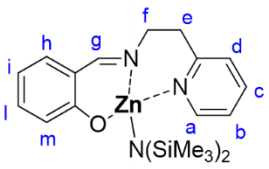

Figure 3.19 Aromatic region of COSY NMR spectrum (400 MHz, CD_2Cl_2, 298 K) of complex **1**.

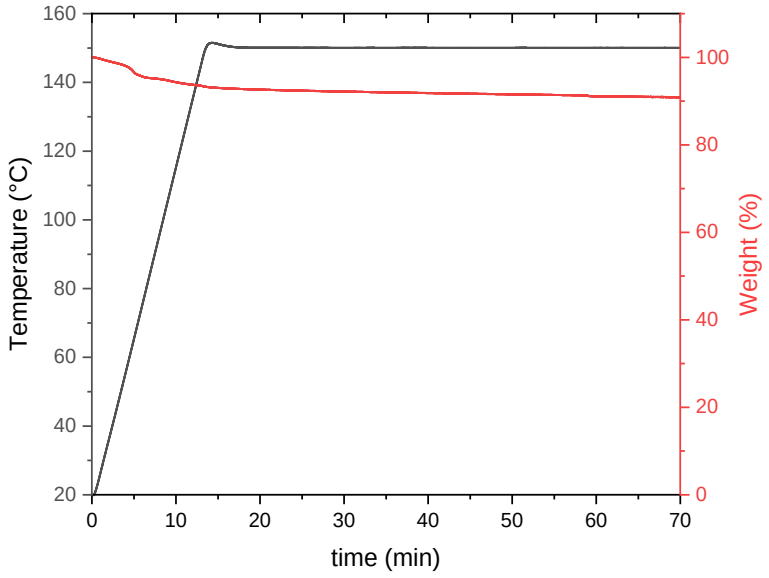

Figure 3.20 TGA measurement of the complex **1** at 150 °C.

Synthesis and characterization of the complex 2

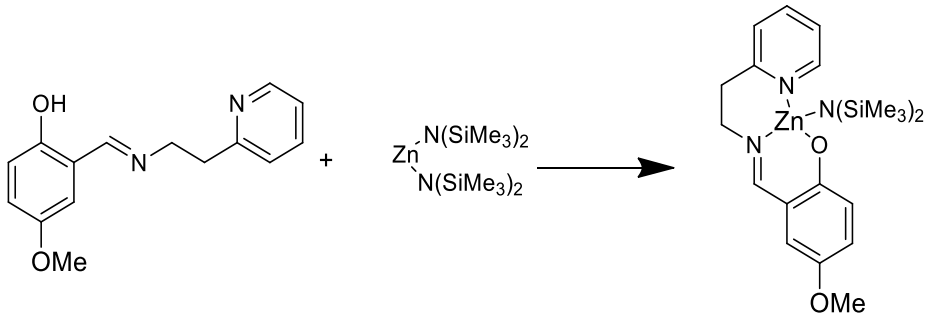

Scheme 3.5 Synthesis of complex **2**.

To a stirred solution containing Zinc bis[bis(trimethylsilyl)amide] (0.572 g, 1.48 mmol) in dry benzene (4.0 mL) was added dropwise a solution of the ligand precursor L_2H (0.500 g, 1.48 mmol) in dry benzene (2.0 mL). The solution was stirred for 3 hours at room temperature. The solvent was removed under vacuum, forming an orange solid. The formation of the desired species was confirmed by NMR analysis. Yield 65 %

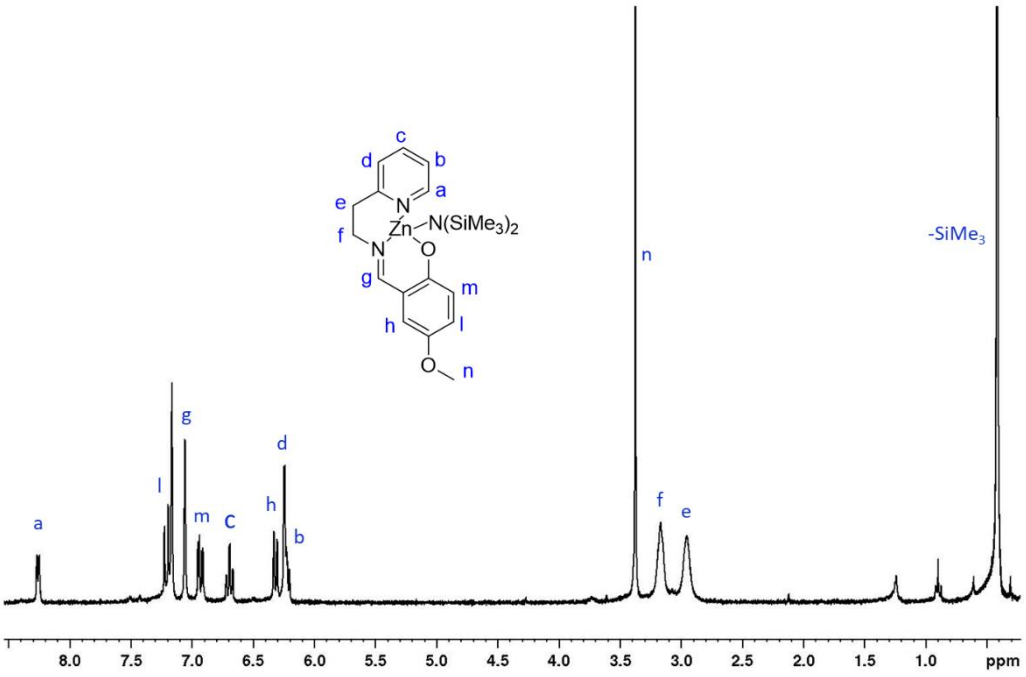

Figure 3.21 1H NMR spectrum (300 MHz, C_6D_6, 298 K) complex **2**.

^{1}H NMR (300 MHz, C_6D_6, 298 K): δ 8.26 (d, J = 5.2 Hz, 1H, Ha), 7.20 (d, J = 9.2 Hz, 1H, Hl), 7.05 (s, 1H, Hg), 6.93 (dd, J_1 = 9.2 Hz, J_2 = 3.3 Hz, 1H, Hm), 6.69 (t, J = 7.6 Hz, 1H, Hc), 6.31 (d, J = 7.6 Hz, 1H, Hh), 6.22 (m, 2H, Hd - Hb), 3.37 (s, 3H, Hn), 3.16 (m, 2H, Hf), 2.95 (m, 2H, He), 0.41 (s, 18H, -$SiMe_3$).

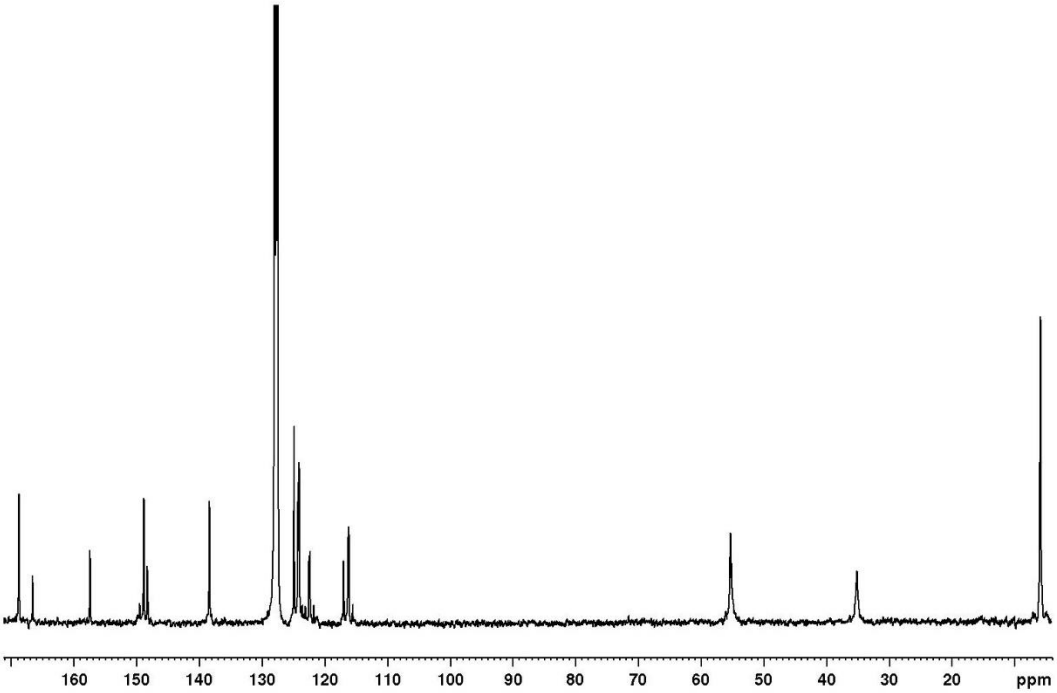

Figure 3.22 ^{13}C NMR spectrum (100 MHz, C_6D_6, 298 K) complex **2**.

^{13}C NMR (100 MHz, C_6D_6, 298 K): δ 168.7, 166.5, 157.4, 148.8, 148.2, 138.3, 124.8, 124.1, 122.3, 117.0, 116.2, 116.1, 55.3, 55.1, 35.0, 5.8.

Synthesis and characterization of the complex 3

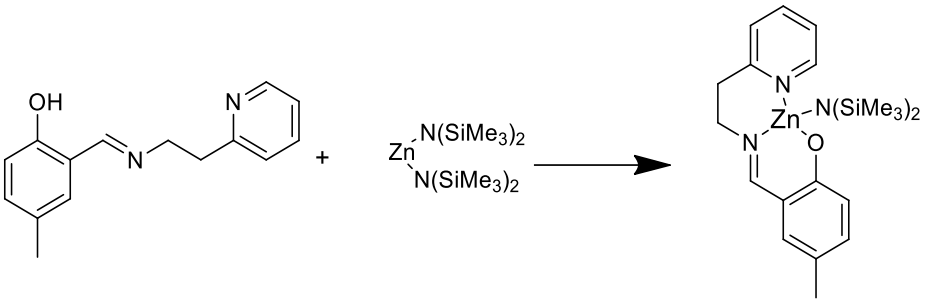

Scheme 3.6 Synthesis of complex **3**

To a stirred solution containing Zinc bis[bis(trimethylsilyl)amide] (0.193 g, 0.500 mmol) in dry benzene (2.0 mL) was added dropwise a solution of the ligand precursor L_3H (0.120 g, 0.500 mmol) in dry benzene (2.0 mL). The solution was stirred for 3h at room temperature. The solvent was removed under vacuum, forming an orange solid. The formation of the desired species was confirmed by NMR analysis. Yield 85 %

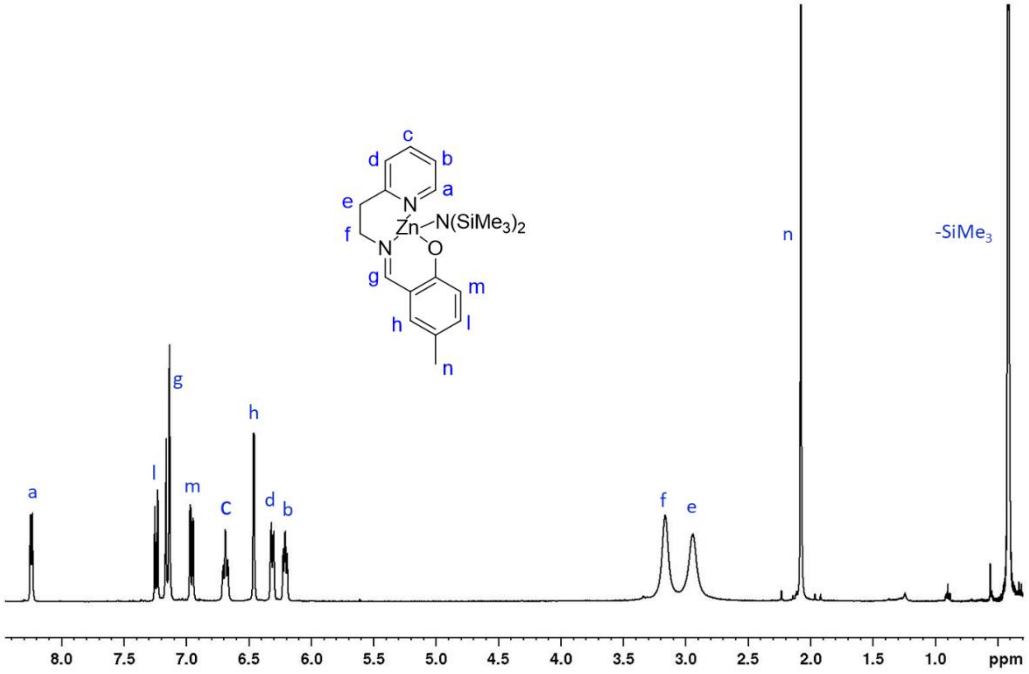

Figure 3.23 ^{1}H NMR spectrum (400 MHz, C_6D_6, 298 K) complex **3**.

^{1}H NMR (400 MHz, C_6D_6, 298 K): δ 8.23 (d, J = 5.2 Hz, 1H, Ha), 7.23 (d, J = 8.6 Hz, 1H, Hl), 7.13 (s, 1H, Hg), 6.95 (dd, J_1 = 8.7 Hz, J_2 = 2.4 Hz, 1H, Hm), 6.68 (t, J = 7.7 Hz, 1H, Hc), 6.30 (d, J = 7.8 Hz, 1H, Hd), 6.21 (t, J = 5.8 Hz, 1H, Hb), 3.16 (m, 2H, Hf), 2.94 (m, 2H, He), 2.07 (s, 3H, Hn), 0.41 (s, 18H, -$SiMe_3$).

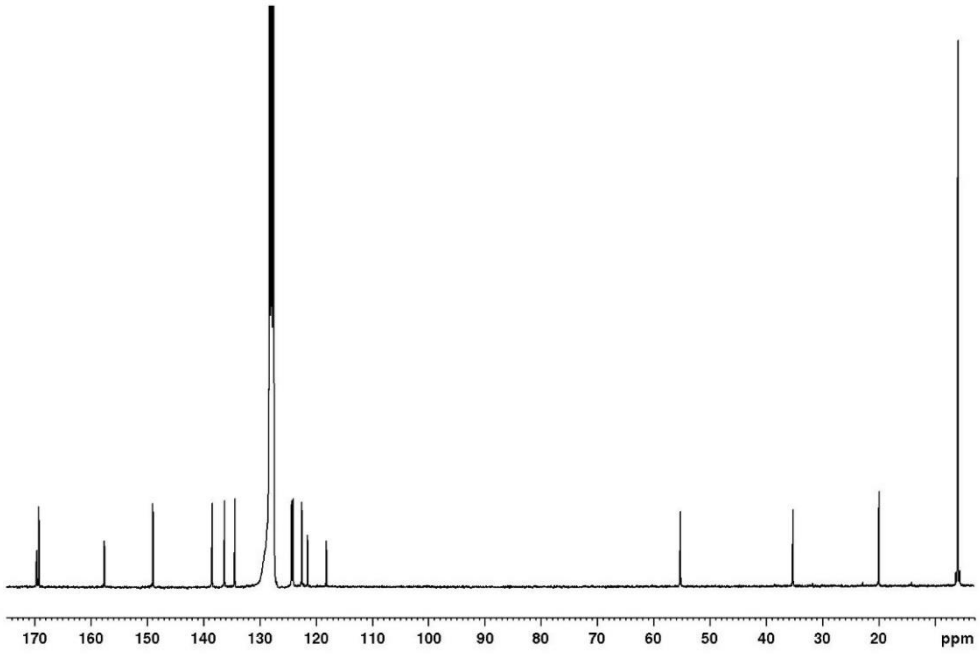

Figure 3.24 ^{13}C NMR spectrum (100 MHz, C_6D_6, 298 K) complex **3**.

^{13}C NMR (75 MHz, C_6D_6, 298 K): δ 169.5, 169.2, 157.5, 148.9, 138.4, 136.2, 134.3 124.3, 124.0, 122.4, 121.4, 118.1, 55.2, 35.2, 19.9, 5.86.

Synthesis and characterization of the complex 4

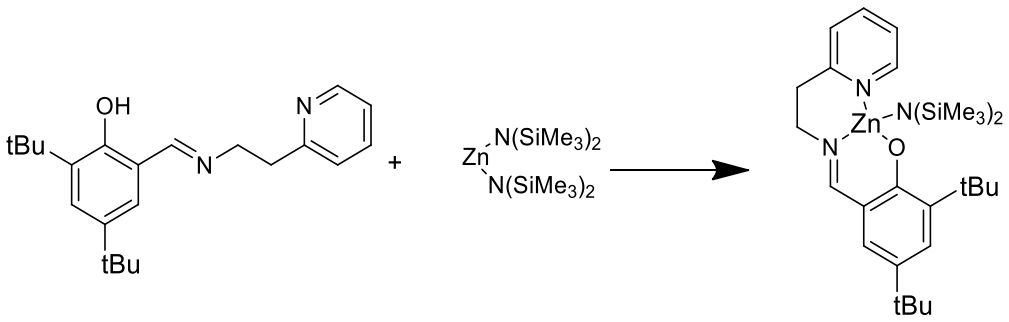

Scheme 3.7 Synthesis of complex **4**

To a stirred solution containing Zinc bis[bis(trimethylsilyl)amide] (0.572 g, 1.48 mmol) in dry benzene (4.0 mL) was added dropwise a solution of the ligand precursor L_4H (0.500 g, 1.48 mmol) in dry benzene (2.0 mL). The solution was stirred for 3 hours at room temperature. The solvent was removed under vacuum, forming an orange solid. The formation of the desired species was confirmed by NMR analysis. Yield 88 %

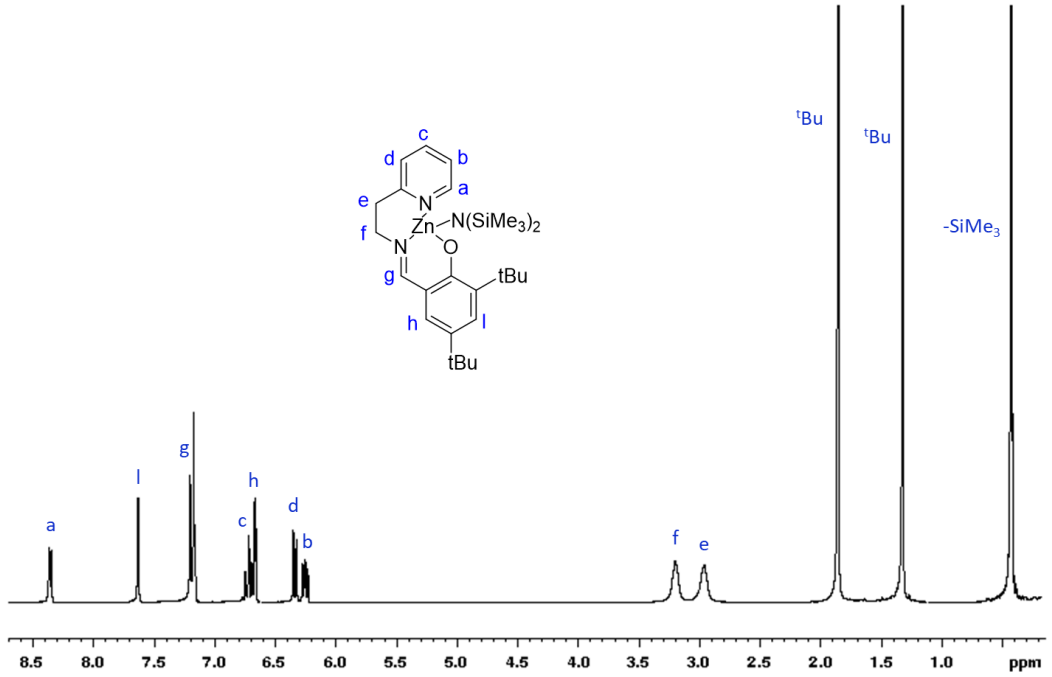

Figure 3.25 1H NMR spectrum (300 MHz, C_6D_6, 298 K) complex **4**

^{1}H NMR (300 MHz, C_6D_6, 298 K): δ 8.35 (dd, J_1 = 5.2 Hz, J_2 = 0.87 Hz, 1H, Ha), 7.63 (d, J = 2.7 Hz, 1H, Hl), 7.20 (s, 1H, Hg), 6.71 (dt, J_1 = 7.7 Hz, J_2 = 1.7 Hz, 1H, Hc), 6.66 (d, J = 2.7 Hz, 1H, Hh), 6.33 (d, J = 7.8 Hz, 1H, H_d), 6.25 (dt, J_1 = 7.5 Hz, J_2 = 1.1 Hz, 1H, H_b), 3.19 (m, 2H, Hf), 2.95 (m, 2H, He), 1.85 (s, 9H, ^{t}Bu), 1.31 (s, 9H, ^{t}Bu), 0.41 (s, 18H, -$SiMe_3$).

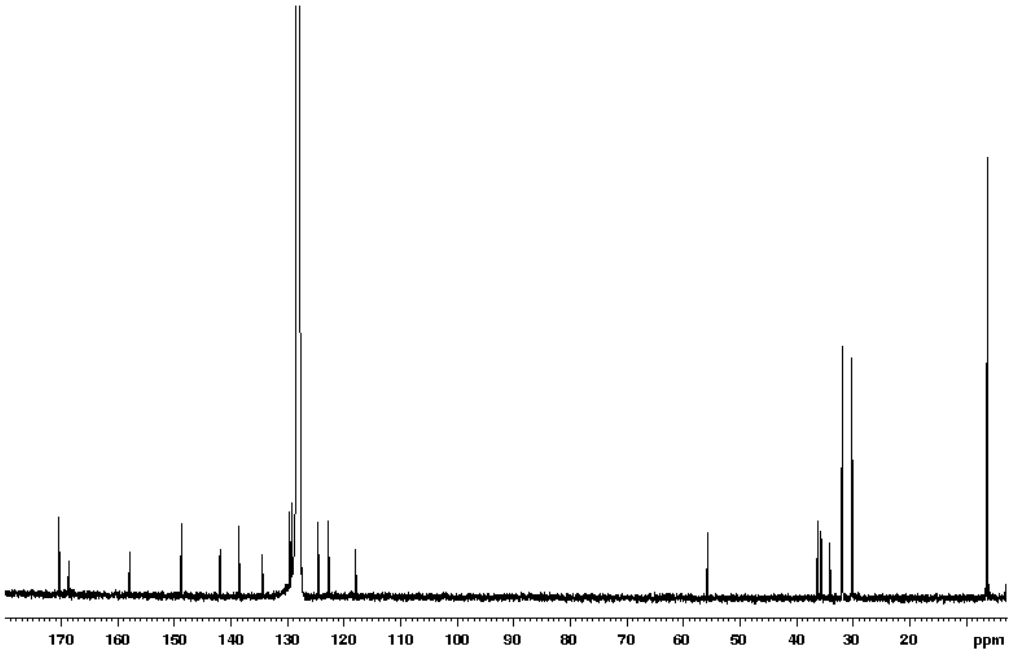

Figure 3.26 ^{13}C NMR spectrum (100 MHz, C_6D_6, 298 K) complex **4**.

^{13}C NMR (100 MHz, C_6D_6, 298 K): δ 170.4, 168.7, 157.9, 148.8, 141.9, 138.9, 134.4, 129.6, 129.3, 124.5, 122.7, 118.0, 55.6, 36.1, 35.5, 34.0, 31.7, 30.0, 6.10.

Synthesis and characterization of the complex 5

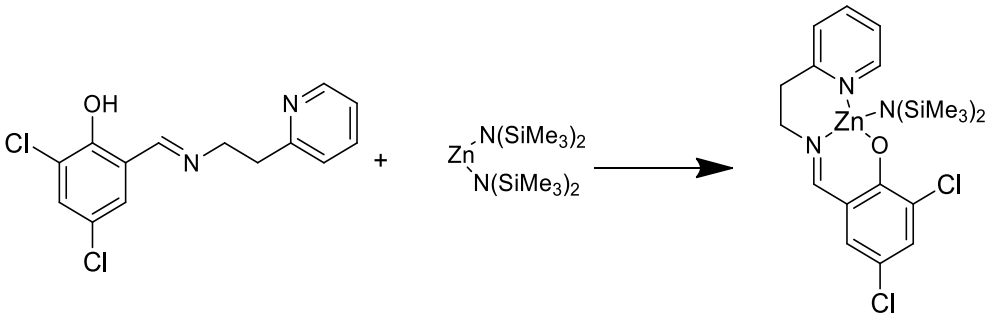

Scheme 3.8 Synthesis of complex **5**.

To a stirred solution containing Zinc bis[bis(trimethylsilyl)amide] (0.826 g, 2.14 mmol) in dry benzene (4.0 mL) was added dropwise a solution of the ligand precursor L_5H (0.633 g, 2.14 mmol) in dry benzene (2.0 mL). The solution was stirred for 3h at room temperature. The solvent was removed under vacuum, forming a red solid. The formation of the desired species was confirmed by NMR analysis. Yield: 70 %

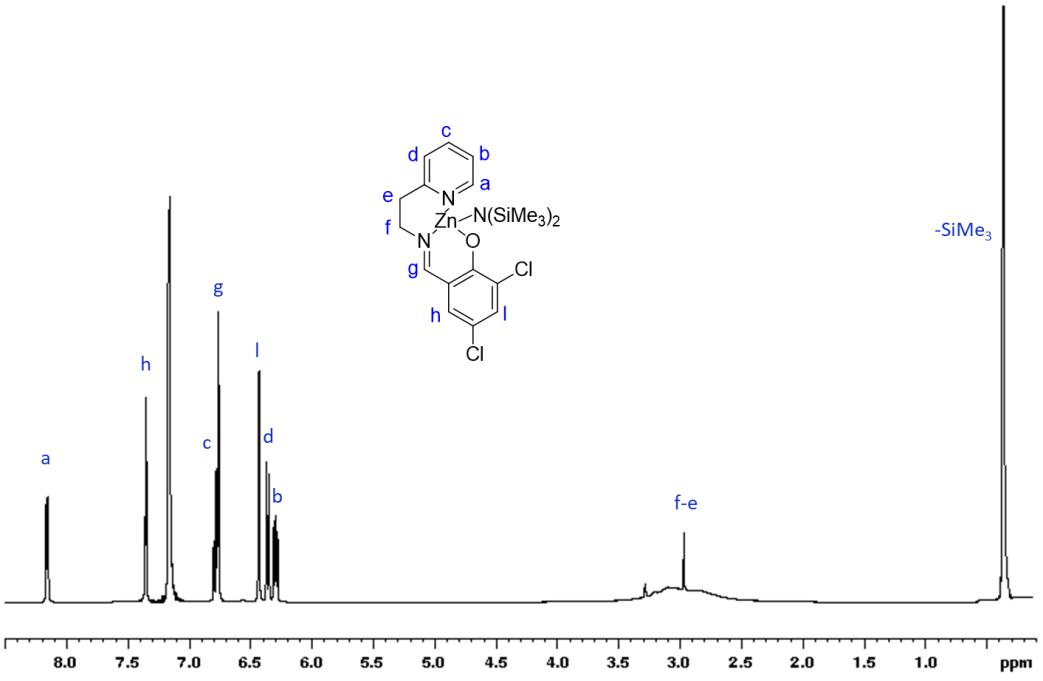

Figure 3.27 ^{1}H NMR spectrum (400 MHz, C_6D_6, 298 K) complex **5**.

^{1}H NMR (400 MHz, C_6D_6, 298 K): δ 8.15 (d, J = 4.5 Hz, 1H, H_a), 7.35 (d, J = 2.8 Hz, 1H, Hh), 6.77 (dt, J_1 = 7.7 Hz, J_2 = 1.7 Hz, 1H, Hc), 6.75 (s, 1H, Hg), 6.43 (d, J = 2.8 Hz, 1H, Hl), 6.35 (d, J = 7.8Hz, 1H, Hd), 6.29 (dt, J_1 = 7.5 Hz, J_2 = 1.0 Hz, 1H, Hb), 2.94 (m, 4H, Hf-He), 0.35 (s, 18H, -$SiMe_3$).

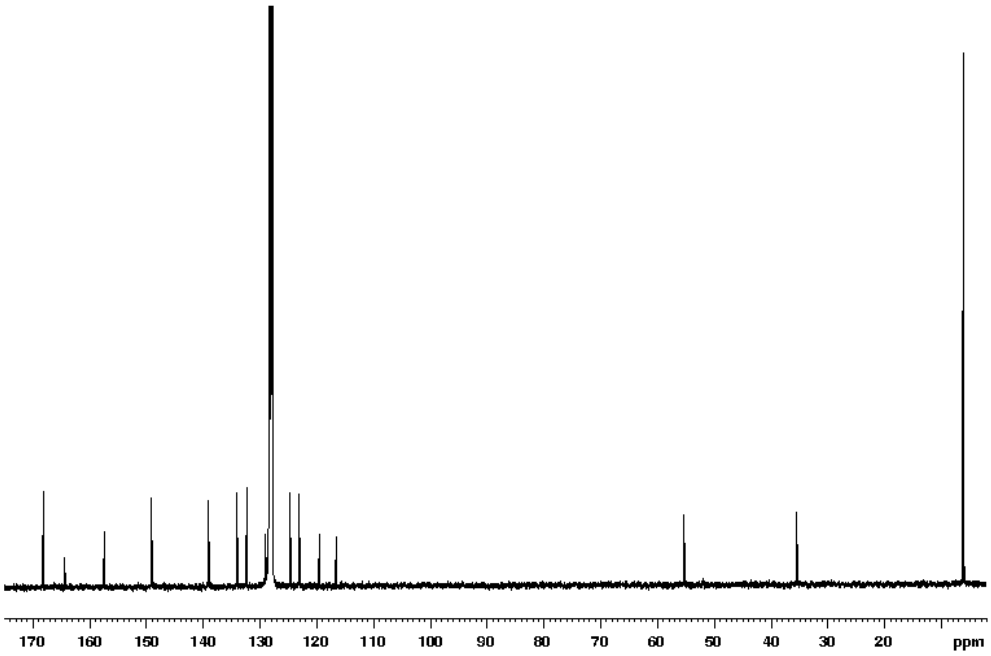

Figure 3.28 ^{13}C NMR spectrum (100 MHz, C_6D_6, 298 K) complex **5**.

^{13}C NMR (100 MHz, C_6D_6, 298 K): δ 168.1, 164.3, 157.4, 149.1, 139.0, 134.0, 132.2, 128.9, 124.6, 123.0, 119.5, 116.5, 55.2, 35.4, 6.02.

Synthesis and characterization of the complex 6

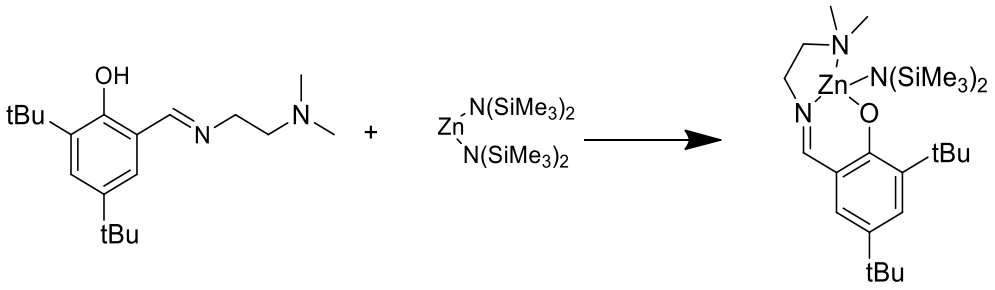

Scheme 3.9 Synthesis of complex **6**.

To a stirred solution containing Zinc bis[bis(trimethylsilyl)amide] (0.520 g, 1.30 mmol) in dry benzene (4.0 mL) was added dropwise a solution of the ligand precursor L6 (0.393 g, 1.30 mmol) in dry benzene (2.0 mL). The solution was stirred for 3 hours at room temperature. The solvent was removed under vacuum, forming an orange solid. The formation of the desired species was confirmed by NMR analysis. Yield 93 %

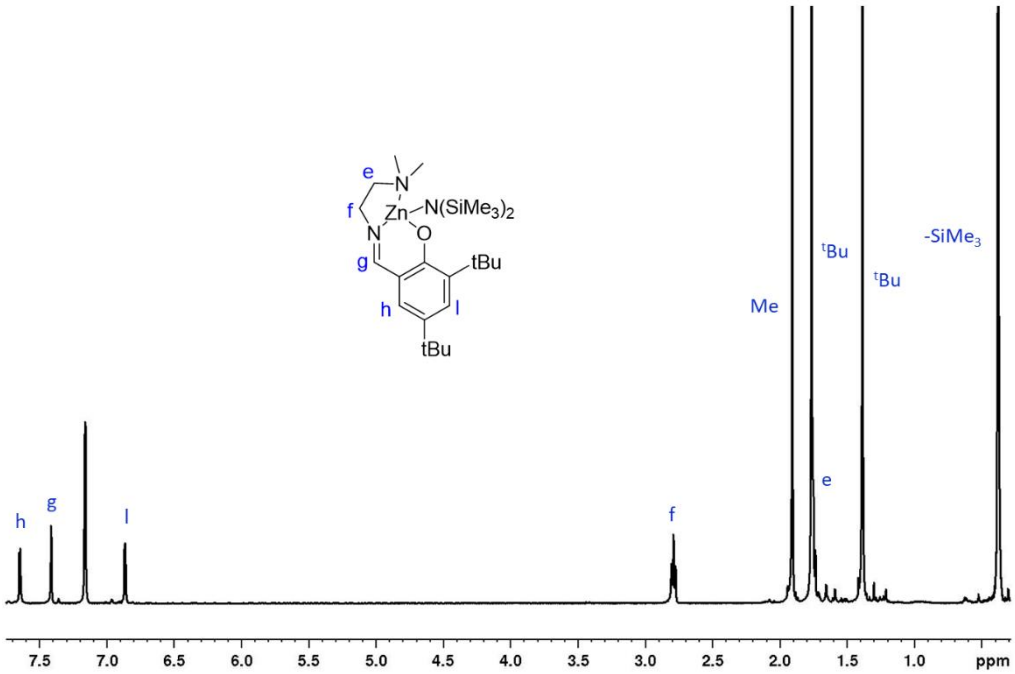

Figure 3.29 ^{1}H NMR spectrum (400 MHz, C_6D_6, 298 K) complex **6**.

^{1}H NMR (400 MHz, C_6D_6, 298 K): δ 7.64 (d, J = 2.6 Hz, 1H, Hh), 7.41 (s, 1H, Hg), 6.86 (d, J = 2.7 Hz, 1H, Hl), 2.79 (t, J = 6.0 Hz, 2H, Hf), 1.90 (s, 6H, Me), 1.76 (m, 11H, He - ^{t}Bu), 1.38 (s, 9H, ^{t}Bu), 0.38 (s, 18H, -$SiMe_3$).

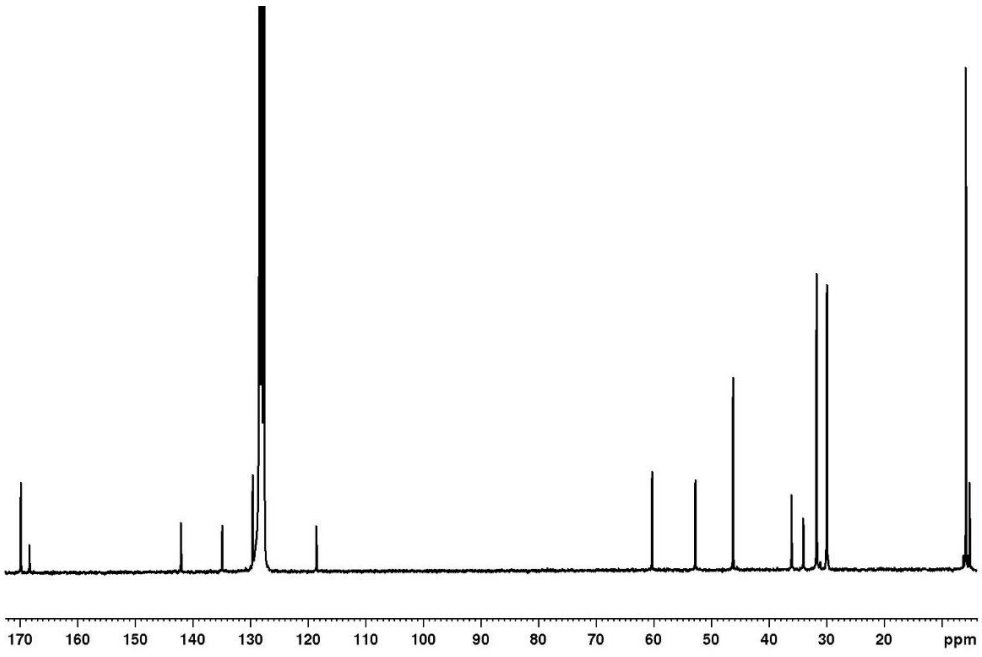

Figure 3.30 ^{13}C NMR spectrum (75 MHz, C_6D_6, 298 K) complex **6**.

^{13}C NMR (75 MHz, C_6D_6, 298 K): δ 169.8, 168.3, 142.0, 134.8, 129.6, 118.5, 60.4, 52.7, 46.2, 36.0, 34.0, 31.7, 30.3, 5.8.

General procedure for the polymerization of lactide

The polymerization experiments conducted at room temperature were carried out in a glove box, under inert conditions. In a Braun Labmaster glovebox, a magnetically stirred reactor flask was charged with lactide. The complex and ^{i}PrOH (0.1 M of iPrOH in dichloromethane) were added in a 2 mL vial and the mixture was stirred for 5 min; then transferred in the monomer. The polymerization was stopped using dichloromethane, after taking the vial out of the glove box. The product was precipitated in hexane, then filtered and dried in a vacuum oven. The polymer was characterized by NMR spectroscopy, MALDI MS and/or GPC analysis. For the polymerization experiment carried out under industrial relevant conditions, the complex and 1 equiv. of BnOH (0.1 M solution of BnOH in toluene) were added in a 2 mL vial and the mixture was stirred for 5 min; then transferred in the monomer and, finally, mixed to more equiv. of BnOH. The Schlenk flask was closed, pulled out of the glove box and immersed in a thermostated oil bath at the temperature of 150°C. After the reaction time, the polymerization was stopped using dichloromethane. The solvent was removed under reduced pressure and the polymer was dried and characterized.

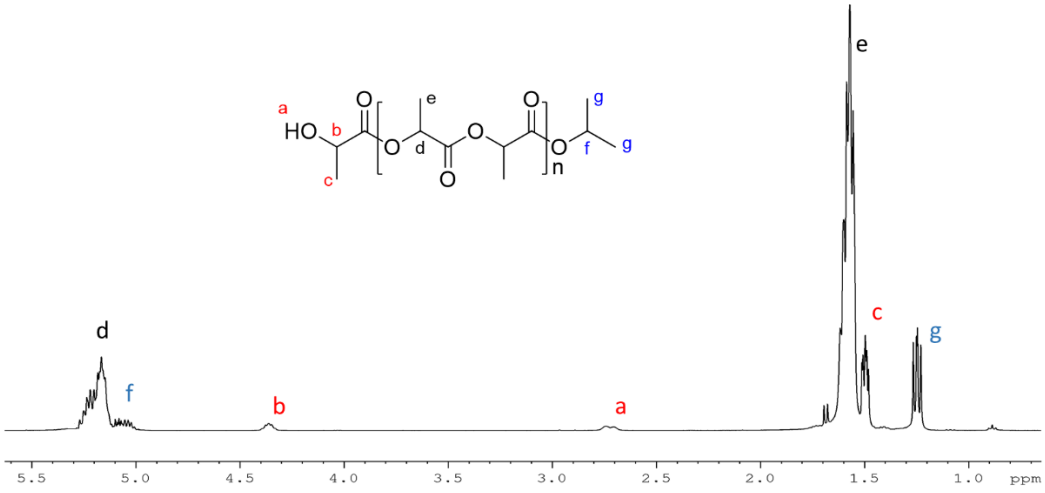

Figure 3.31 ^{1}H NMR spectrum (400 MHz, $CDCl_3$, 298 K) polylactide.

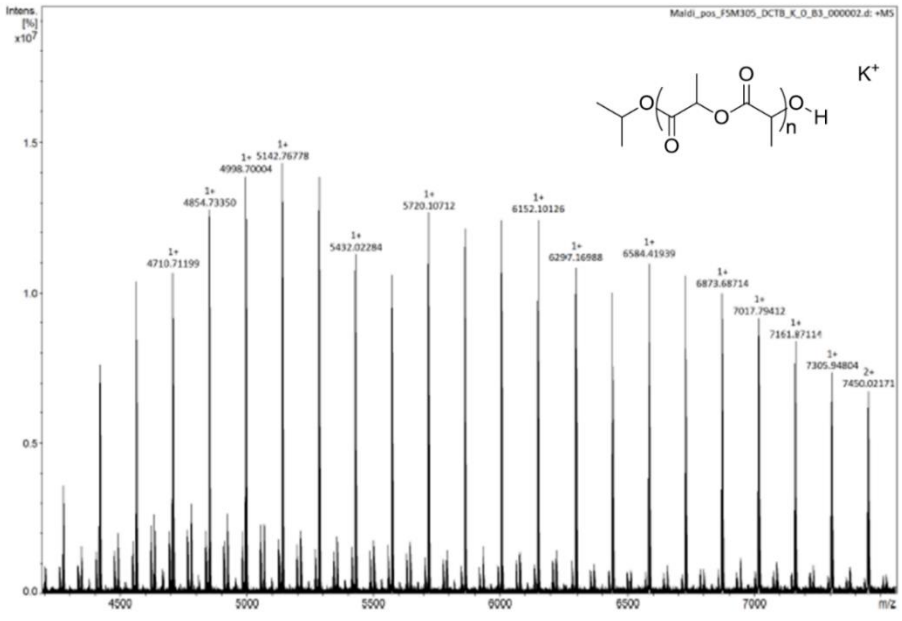

Figure 3.32 MALDI-FT-ICR MS of PLLA sample, entry 2 **Table 3.1**.

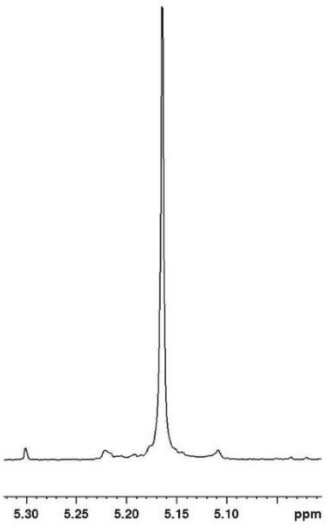

Figure 3.33 Methine region of the homonuclear decoupled ^{1}H NMR spectrum ($CDCl_3$, RT, 400MHz) of a PLLA sample (entry 10 **Table 3.2**).

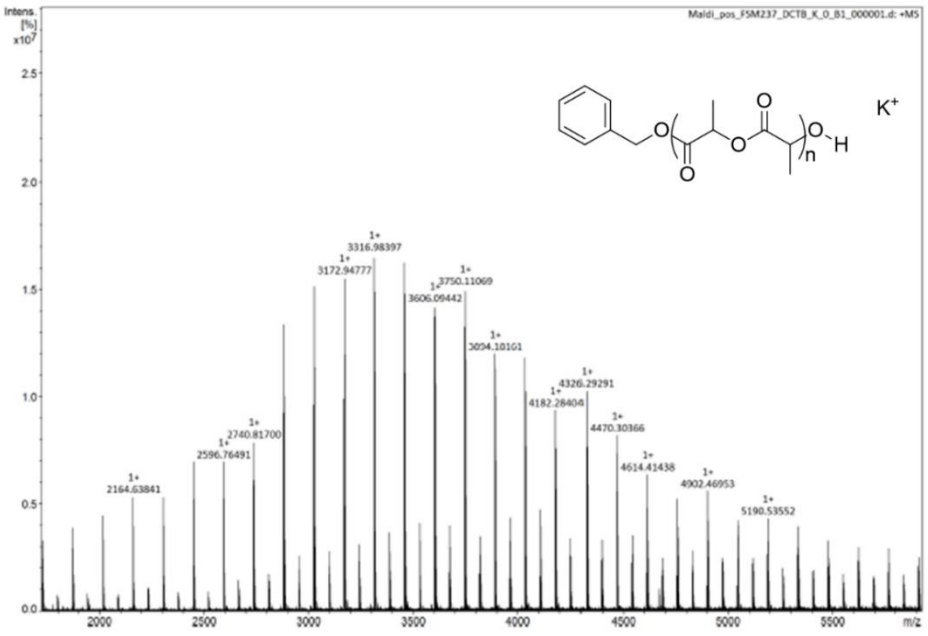

Figure 3.34 MALDI-FT-ICR MS of PLLA sample (entry 9 **Table 3.2**).

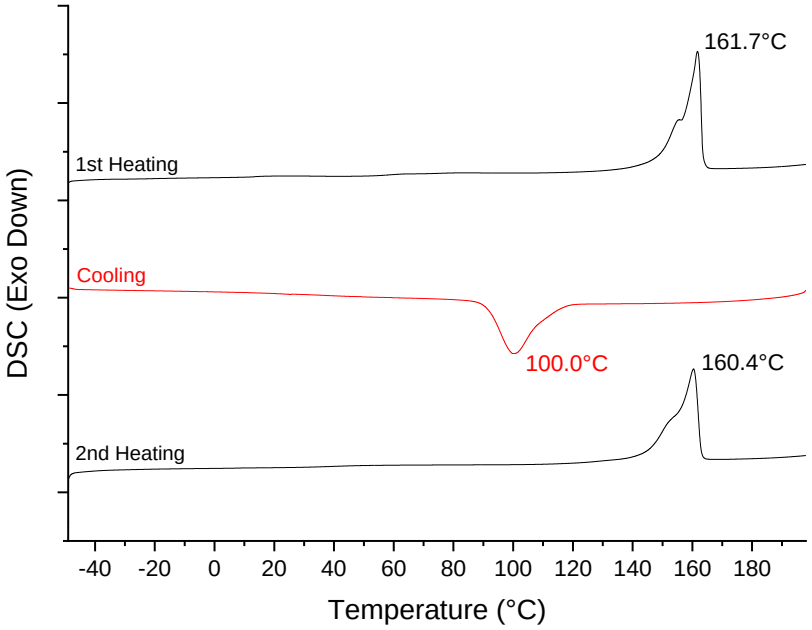

Figure 3.35 DSC measurement of a PLLA sample (entry 8 **Table 3.2**).

General procedure for the degradation of polylactide

The degradation experiments conducted in solution were carried out in a glove box, under inert condition. In a Braun Labmaster glovebox, a magnetically stirred reactor flask was charged with polylactide and MeOH. The complex was dissolved in THF and added to the polymer. The reaction mixture was stirred at room temperature. At desired times, small aliquots of the reaction mixture were sampled, dissolved in $CDCl_3$ or CD_2Cl_2 and analyzed by ^1H NMR spectroscopy. At the end of the degradation the reaction was stopped with CH_2Cl_2 and dried under vacuum. For the degradation experiment carried out under solvent free condition, the complex was dissolved in MeOH or EtOH and added to the polymer. The reaction mixture was stirred at room temperature. At desired times, small aliquots of the reaction mixture were sampled, dissolved in $CDCl_3$ or C_6D_6 and analyzed by ^1H NMR spectroscopy. At the end of the degradation the reaction was stopped with CH_2Cl_2 and dried under vacuum.

Table 3.6

Number average molecular weight (Mn), dispersity (Đ) and Tf of PLA samples used for degradation reactions.

PLA sample	Mn (KDa)	Đ	T_f (°C)
PLLA	160	1.2	179
P(*rac*-LA)	13	1.1	
PLLA	30	1.1	171
PLLA	48	1.8	170
PLLA	92	1.5	178
PLLA cup	58	1.9	150
PLLA filament	20	2.9	168

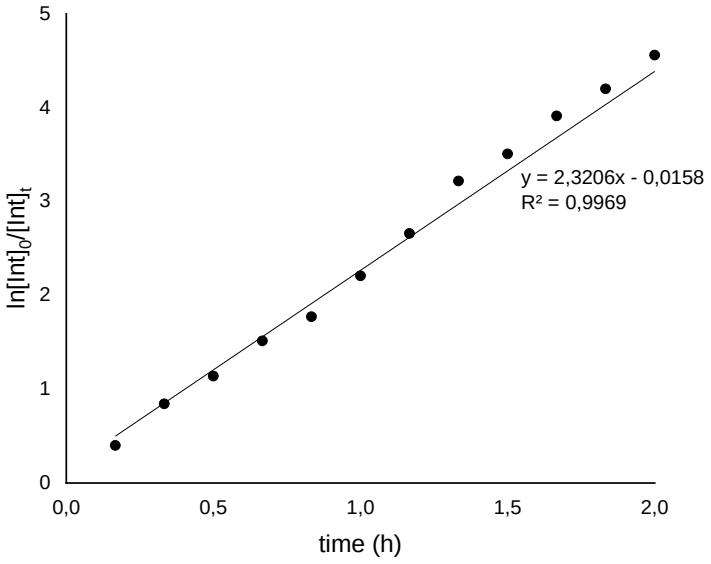

Figure 3.36 Kinetic plot of the degradation of polylactide vs the reaction time. Reaction condition: $([PLLA]_0$ = 0.44 M; $[\text{polyester linkages}]_0/[\mathbf{1}]_0 = 60$; CD_2Cl_2 (0.45 mL) as solvent; MeOH 0.05 mL). Pseudo first-order rate is 2.32 h^{-1} at 25 °C (R^2 = 0.9969).

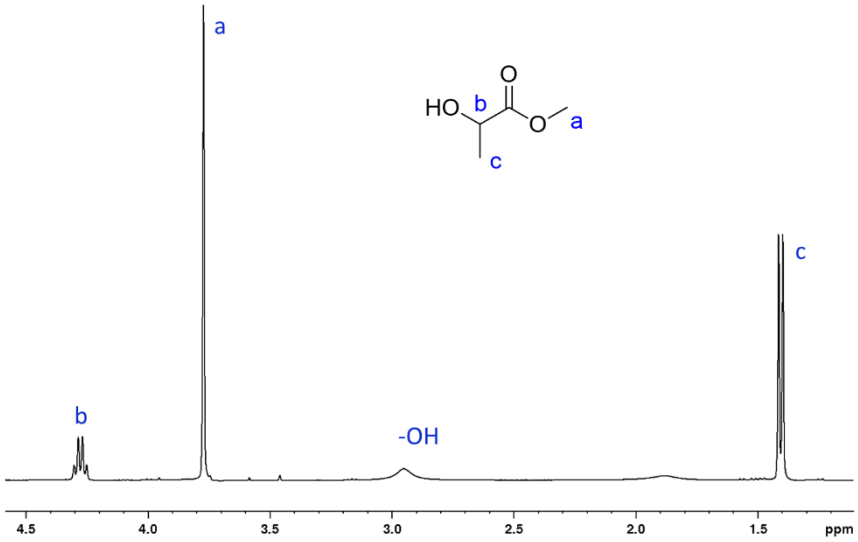

Figure 3.37 ^{1}H NMR spectrum (400 MHz, $CDCl_3$, 298 K) of methyl-lactide (Me-La).

^{1}H NMR (400 MHz, $CDCl_3$, 298 K): δ 4.27 (q, J = 6.7 Hz, 1H, Hb), 3.77 (s, 3H, Ha), 2.95 (br, 1H, -OH), 1.40 (d, J = 6.8 Hz, 3H, Hc).

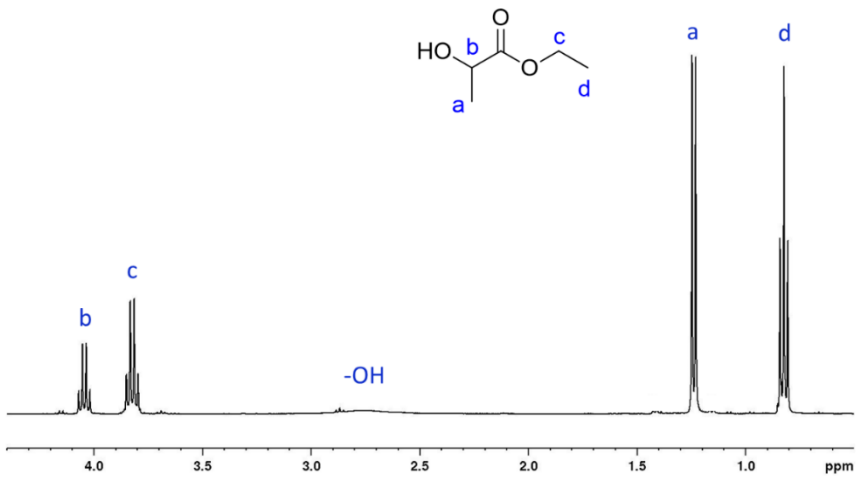

Figure 3.38 ^{1}H NMR spectrum (400 MHz, C_6D_6, 298 K) of ethyl-lactide (Et-La).

^{1}H NMR (400 MHz, C_6D_6, 298 K): δ 4.04 (q, J = 6.9 Hz, 1H, Hb), 3.82 (q, J = 7. 2Hz, 2H, Hc), 2.76 (br, 1H, -OH), 1.23 (d, J = 6.9 Hz, 3H, Ha), 0.82 (t, J = 7.1 Hz, 3H, Hd).

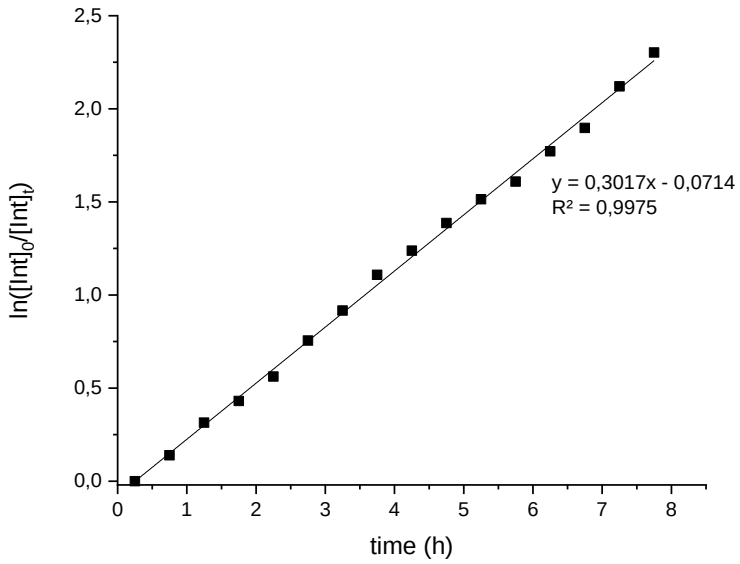

Figure 3.39 Kinetic plot of the degradation reaction of polylactide vs the reaction time. Reaction condition: ($[PLLA]_0$ = 0.44 M; $[polyester\ linkages]_0/[\mathbf{1}]_0$ = 60; MeOH 0.50 mL). Pseudo first-order rate is 0.30 h^{-1} at 25 °C (R^2 = 0.9975).

References

[1] [a]Rahimi, A. R., Garciá, J. M. Chemical recycling of waste plastics for new materials production. *Nature Reviews Chemistry* **1**, 0046 (2017).
[b]Coates, G. W., Getzler, Y. D. Y. L. Chemical recycling to monomer for an ideal, circular polymer economy. *Nature Reviews Material*s **5** 501–516 (2020).

[2] Rosen, T., Rajpurohit, J., Lipstman, S., Venditto, V. & Kol, M. Isoselective Polymerization of rac-Lactide by Highly Active Sequential {ONNN} Magnesium Complexes. *Chemistry - A European Journal* **26**, 17183–17189 (2020).

[3]Thevenon, A. *et al.* Dizinc Lactide Polymerization Catalysts: Hyperactivity by Control of Ligand Conformation and Metallic Cooperativity. *Angewandte Chemie* **128**, 8822–8827 (2016).

[4] Robert, C. *et al.* Mechanistic Aspects of the Polymerization of Lactide Using a Highly Efficient Aluminum(III) Catalytic System. *Journal of American Chemical Society* **139**, 6217–6225 (2017).

[5] Petrus, R., Bykowski, D. & Sobota, P. Solvothermal Alcoholysis Routes for Recycling Polylactide Waste as Lactic Acid Esters. *ACS Catalysis* **6**, 5222–5235 (2016).

[6] Román-Ramírez, L. A., McKeown, P., Jones, M. D. & Wood, J. Poly(lactic acid) Degradation into Methyl Lactate Catalyzed by a Well-Defined Zn(II) Complex. *ACS Catalysis* **9**, 409–416 (2019).

CHAPTER 4

Commercial metal amides for the chemical degradation of polyesters

The results described in this Chapter have been published in:

Santulli, F., Lamberti, M., Annunziata, A., Lastra, R. C., Mazzeo, M. The Contribution of Commercial Metal Amides to the Chemical Recycling of Waste Polyesters. *Catalysts* **12**, 1193-1204 (2022).

4.1 Introduction

Most of the plastic that is produced every year is placed on the market for single-use products which, together with the absence of a correct strategy for managing their end-of-life fate, have caused dramatic environmental pollution problems. In recent years, scientific research has focused on the development of both more sustainable, biodegradable and / or renewable plastics, and on strategies for their chemical recycling.[1]

Ring-opening polymerization (ROP) of lactones to provide degradable aliphatic polyesters, such as polylactide (PLA) has received growing interest.[2] In the last two decades, the process has been investigated, and has seen the use of almost all the metals of the periodic table. Most catalysts have required the presence of delicate and complicate ancillary ligands and to one or more labile ligands that act as initiating groups.[3] However, their synthesis can increase the cost of the catalysts and therefore reduce their application value in practical industry. Therefore, the use of non-toxic metal-based catalysts with simple and/or commercially accessible structures is highly desirable.

In addition to investing in environmentally friendly processes to produce sustainable polymers, effective methods for their end-of-life treatment need to be considered.[4] The mechanical recycling of polyesters involves the loss of the properties of the final product causing a downgrading of their reuse.[5] Conversely, the conversion of the waste polymer into molecules of higher value, by chemical degradation, is a particularly interesting strategy.[6] For example, transesterification of PLA in the presence of MeOH or EtOH produces methyl lactate (Me-La) and ethyl lactate (Et-La), respectively.[7] These are used as green solvents to replace petroleum-based ones, being biodegradable and non-toxic.[8] In general, alkyl lactates are already used in various fields such as the pharmaceutical, food, and polymer industries.

In the literature, simple amides or alkoxides of several metals have been tested as catalysts for the ROP of lactide. Wang et al. reported zinc bis[bis(trimethylsilyl)amide] $Zn[N(SiMe_3)_2]_2$ as catalyst to synthesize different sustainable polyesters with controlled molecular weights but also for the degradation of polylactide or mixed commercial plastics to obtain precious molecules.[9] Inspired by these results, in this *Chapter*, the catalytic behavior of other commercially available amides of non-toxic and low-cost metals (**Scheme 4.1**) in the degradation reactions of polylactide (PLLA) is reported. Furthermore, these studies have also been extended to the chemical degradation, by glycolysis, of polyethylene terephthalate (PET), the most important commercial polyester used mainly to produce disposable products.

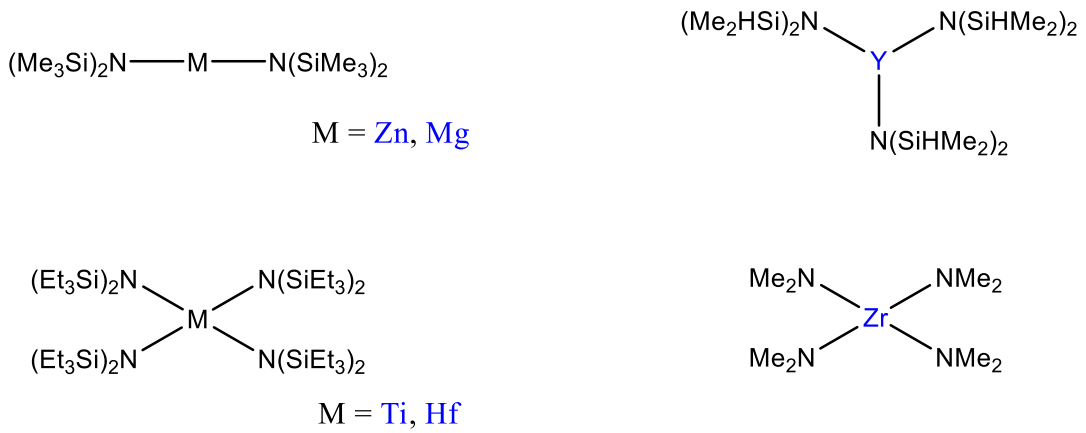

Scheme 4.1 Metal amides used in *this Chapter*.

4.2 Results and discussion

4.2.1 Methanolysis of PLA

Depolymerisation of PLA promoted by alcohols proceeds by transesterification reactions in which the metal center acts as Lewis acid activating the carbonylic groups of the polymer chain, more susceptible to the nucleophilic attack of the alcohol, such as methanol (**Scheme 4.2**). In this Chapter we investigated the behaviour of several commercially available metal amides in the degradation reaction of end-of-life plastic cups.

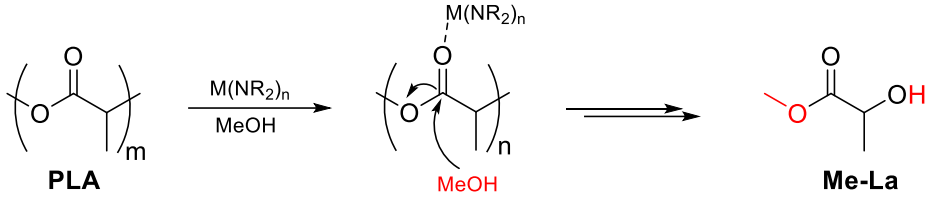

Scheme 4.2 Chemical degradation of PLA by methanolysis.

Initially, the degradation reactions were carried out using commercial PLA plastic cups with a molecular mass of 58 KDa at room temperature in the presence of absolute MeOH, and without the use of added solvents to minimize the environmental impact.

Degradation progress was monitored by ^{1}H NMR spectroscopic analysis. This technique allows to quantify the conversion of internal units of methine (X_{Int}), the selectivity of Me-La ($S_{Me\text{-}La}$) and the yield of Me-La ($Y_{Me\text{-}La}$) which have been calculated by integrating the diagnostic signals in the methine region (**Figure 4.1**).

Table 4.1 Methanolysis Data of PLLA by metal amides.

Entry[a]	cat	time (h)	X_{Int}[b]	$S_{Me\text{-}La}$[b]	$Y_{Me\text{-}La}$[b]
1	Zn	2	39	100	39
2	Mg	2	90	100	90
3	Y	19	98	100	98
4	Ti	24	100	89	89
5	Zr	8	11	69	8
6	Hf	2	10	52	5

[a]All reactions were carried out by using 10 µmol of catalyst (1 mol % relative to ester linkages) in 1.0 mL of MeOH at room temperature.
[b]Determinated by ^{1}H NMR.

Among the catalysts investigated, Mg amide appeared to be the most active, capable of quantitatively degrading PLA after 2 h (entry 2, **Table 4.1**). Its activity was significantly higher than that of Zn complex which, for the same time, achieved a conversion of 40 % (entry 1, **Table 4.1**). Complete degradation of the polymer was observed with Y amide too, but taking 10 times more time (entry 3, **Table 4.1**). Finally, the amides of group 4 show significantly lower activity than the other metals (entries 4-6, **Table 4.1**) and the Zr amide was found to be the worst of all.

Generally, the degradation of PLA occurs through a two-step process in which the polymer undergoes a random scission of the polymer chains into oligomeric species that are progressively converted into Me-La. Under these conditions, the Zn, Mg and Y catalysts promoted selective processes in which the polymer chain is directly converted in the final product (the selectivity of Me-La was 100 %). This behavior was already observed for the heteroleptic zinc complexes described in *Chapter 3* that, in the absence of solvent, promoted a mechanism in which the degradation occurs through a progressive aggression of the chain ends with the direct formation of Me-La.[10]

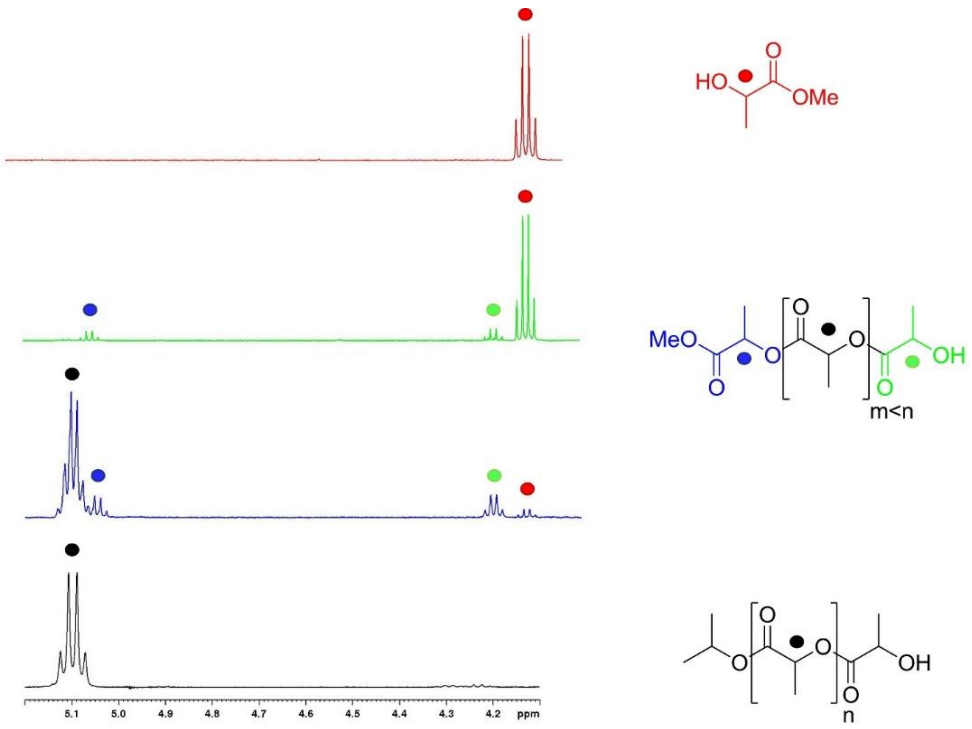

Figure 4.1 ^{1}H NMR ($CDCl_3$, 400 MHz, 298 K) monitoring of PLA methanolysis with assignment of internal (black), chain ends (blue and green), and Me-La (red) methine groups (entry 3, **Table 4.1**).

4.2.2 Ethanolysis of PLA

The same metal compounds were used in the degradation of PLA in the presence of ethanol (**Scheme 4.3**). The final product of ethanolysis of PLA is ethyl lactate (Et-La), described as a biodegradable 'green' solvent with low toxicity, that has a market value higher than PLA itself.[11]

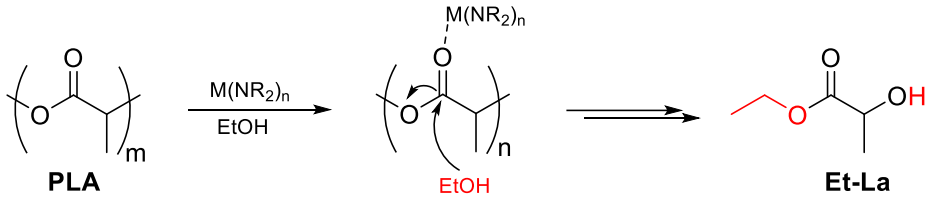

Scheme 4.3 Chemical degradation of PLA by ethanolysis.

Degradation progress was monitored by ^{1}H NMR spectroscopic analyses in the ethanolysis too, calculating the conversion of the internal units of methine (X_{Int}), the selectivity of Et-La ($S_{Et\text{-}La}$) and the yield of Et-La ($Y_{Et\text{-}La}$) integrating diagnostic signals in the methine region (**Figure 4.2**).

As expected, the ethanolysis of PLA was definitively a slower process than when performed in pure methanol (entries 1-6, **Table 4.2**) because the more sterically hindered alkyl group disadvantages attachment to the carbonyl group.[12] At room temperature, almost quantitative conversions were obtained for the amides of Zn, Mg and Y after 24 h. Also in this case, the lowest activities were observed with group 4 metals, especially with Zr and Hf.

Table 4.2 Ethanolysis Data of PLLA by metal amides.

Entry[a]	cat	T (°C)	X_{Int}[b]	$S_{Me\text{-}La}$[b]	$Y_{Me\text{-}La}$[b]
1	Zn	25	100	83	83
2	Mg	25	93	98	91
3	Y	25	100	91	91
4	Ti	25	75	39	29
5	Zr	25	3	51	2
6	Hf	25	5	0.2	1
7	Zn	80	100	100	100
8	Mg	80	57	50	29
9	Y	80	17	100	17
10	Ti	80	100	100	100
11	Zr	80	100	100	100
12	Hf	80	89	54	48
13	Y	60	57	58	33
14	Zr	60	41	68	28

[a]All reactions were carried out by using 70 μmol of catalyst (1 mol % relative to ester linkages), 500 mg of PLLA sample, in 10 mL of EtOH for 24 h. [b]Determinated by ^{1}H NMR.

At higher temperature, the reactivity trend was significantly different: the Zn amide preserved its activity while an important downfall was observed for Mg and Y catalysts (entries 7-12, **Table 4.2**). The Mg amide showed a performance significantly poorer than the bis [amino (phenoxy-imine)] complexes reported by Jones and Wood,[12] this could suggest that the presence of ancillary ligands is important to stabilize the metal center when drastic reaction conditions are applied.

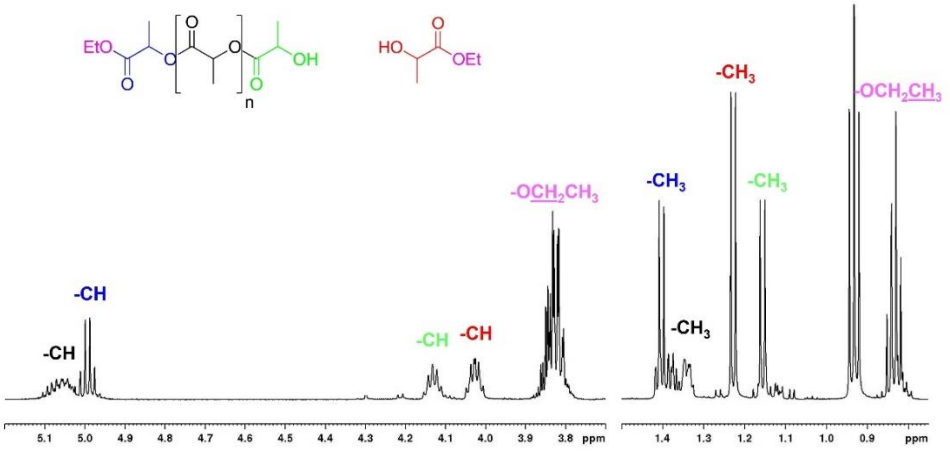

Figure 4.2 ^{1}H NMR (C_6D_6, 400 MHz, 298 K) monitoring of PLA ethanolysis with assignment of internal (black), chain ends (blue and green), and Et-La (red) alkyl protons.

Interestingly, at higher temperature, the group 4 metal compounds improved their performances. Additional experiments performed at the intermediate temperature of 60 °C (entries 13 and 14, **Table 4.2**), confirmed the opposite effect of the temperature on the catalytic activity of Y and Zr catalysts (**Figure 4.3**). These results showed that the trend in the performances of the explored catalysts is strongly depending on the reaction conditions, likely because of the different thermal stability of the active species involved in the polymerization process.

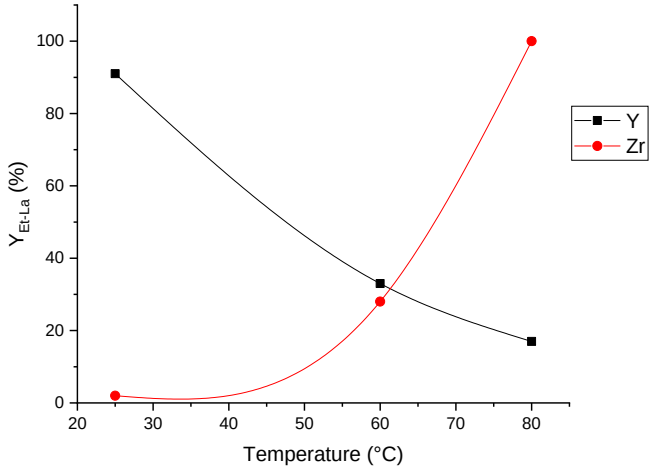

Figure 4.3 Yield of Et-La by Zr and Y amides at different temperatures.

To exclude the presence of epimerization side-reactions by deprotonation of the β-CH group by amides, the ethylactate samples obtained by degradation processes were analyzed by optical rotation measurements in CH_2Cl_2 at 22 °C. The full coherence between the $[\alpha]_{22}^{D}$ value of the ethylactate sample obtained in entry 2 of **Table 4.2** ($[\alpha]_{22}^{D}$ = -0.2169) and that of the commercial product (ethyl L-lactide ($[\alpha]_{22}^{D}$ = -0.2919) confirmed the absence of side reactions of epimerization.

4.2.3 Glycolysis of PET

Following PLA degradation success, we decided to extend our studies to the alcoholysis reaction of other polyesters of high commercial interest such as polyethylene terephthalate (PET). Currently PET accounts for about 23 % of plastic use for short-time packaging; thus, the improvement of strategies for its recycling is of fundamental importance. The degradation of PET by glycolysis is an efficient procedure to convert PET waste into a bis(2-hydroxyethyl) terephthalate (BHET), which is the monomeric unit for the synthesis of PET by polycondensation (**Scheme 4.4**).

A variety organocatalysts,[13] ionic liquids (ILs),[14] deep eutectic solvents (DES),[15] metal salt[16] and discrete metal-based complexes[17] have been reported for the chemical degradation of PET. Usually, because of its scarce solubility and high stability, the alcoholysis of PET requires severe reaction conditions such as high temperature and pressure and elevated percentage of catalyst.

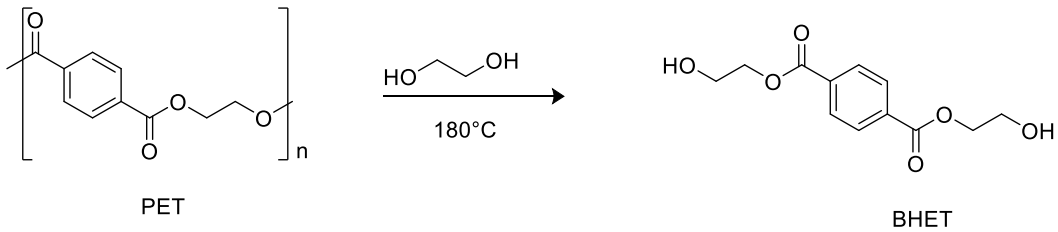

Scheme 4.4 Glycolysis of PET with production of BHET.

All metal amides reported in **Scheme 4.1** were investigated in the degradation of a commercial sample of PET (Mn = 42000 g mol^{-1}, Đ = 1.7). The reactions were performed in the absence of additional solvents at 180 °C and were stopped when the complete dissolution of solid PET was observed. The conversion of PET (Conv)

was evaluated as ratio of the weight of the decomposed PET (i.e., the difference between the initial weight of PET and the weight of residual PET) and the weight of initial sample of PET. The yield (Y_{BHET}) and selectivity (S_{BHET}) in the production of BHET were estimated as described in the *Experimental Part*.

The degradation products were extracted with distilled water and crystallized from cold water. The purity of the BHET obtained by degradation was evaluated by ^{1}H NMR spectroscopy (**Figure 4.4**) and mass spectrometry using either electrospray (ESI) or matrix-assisted laser desoption (MALDI) ionization methods (**Figure 4.5**).

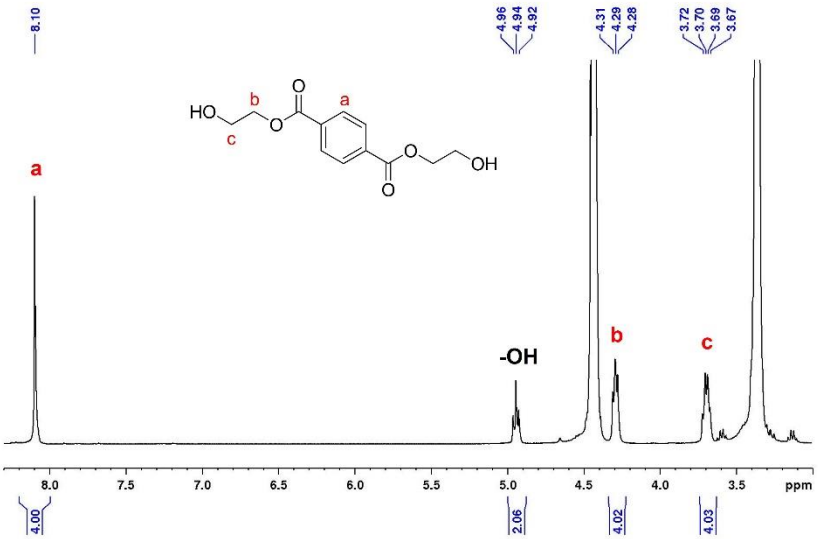

Figure 4.4 ^{1}H NMR (DMSO, 400 MHz, 298 K) of BHET obtained via crystallization.

In the ESI-FT-ICR MS spectrum three peaks were evident, two were related to [BHET + Na^+] m/z =277.06 and [BHET + H^+] m/z =255.08 ions and the other one corresponding to [BHET - H_2O + H^+] ion. In the MALDI-FT-ICR MS spectrum a single peak was evident for the [BHET - H_2O + H^+] ion m/z =237.07

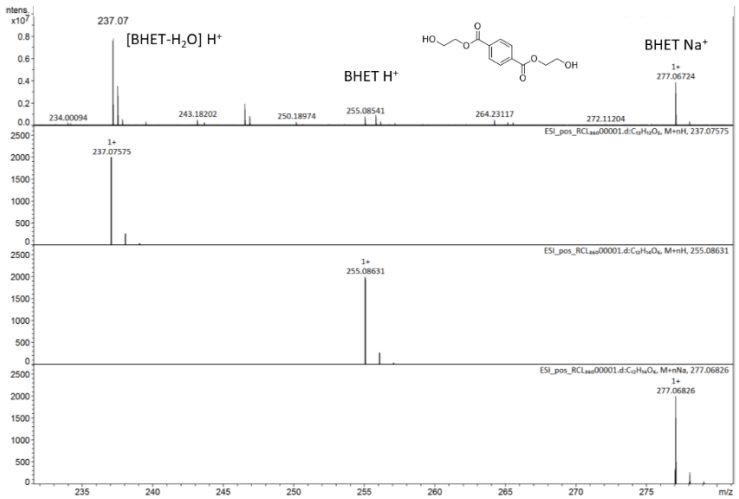

Figure 4.5 ESI-FT-ICR MS spectra of BHET obtained via crystallization.

Among the investigated catalysts, Zn, Mg and Y amides were able to convert the whole PET amount almost quantitatively after 1 h. However, the best results were obtained with Zr amide, which reached a good percentage of degradation (86 %) and very high selectivity (78 %) in the production of BHET, with values that are comparable with the best results obtained with metal catalysts.[18]

Table 4.3 Glycolysis Data of PET under solvent free conditions at 180 °C.

Entry[a]	cat	Conv (%)	Y_{BHET} (%)	S_{BHET} (%)
1	Zn	92	26	24
2	Mg	96	24	22
3	Y	96	58	26
4	Ti	52	15	8
5	Zr	86	78	65
6	Hf	73	28	21

[a]All reactions were carried out by using 200 mg of PET (Mn = 42000 g mol^{-1}), 0.8 mL of EG (27.8 equiv. relative to the ester bonds) and catalyst (0.013 equiv. relative to the ester bonds) at 180 °C for 1 h.

Since, in the presence of a large amount of alcohol, the metal amides are reasonably converted into the related metal alkoxides, a comparison experiment was performed by using $Zr(OEt)_4$ as catalyst, under the same reaction conditions. In this case, a much lower percentage of PET degradation was achieved (19 %).

The very good performances showed by Zr amide, in comparison to related alkoxide, could be a consequence of the nature of the active species and/ or of the co-presence of free amine produced *in situ* that could activate the alcohol by hydrogen bond interaction as supposed for bicomponent catalysts formed by metal halides and amines described by Dove.[19] To the best of our knowledge, these studies represent the first example of systematic exploration of the commercial metal amides in the PET glycolysis.

4.3 Conclusion

In this *Chapter* the study of the catalytic behavior of commercial metal amides in the chemical degradation by alcoholysis of polylactide (PLA) and polyethylene terephthalate (PET) is described. In the degradation of PLA, performed with methanol or ethanol at room temperature, the Mg amide showed the highest activity followed by Zn and Y amides, while the amides of group 4 metals were scarcely efficient. In the ethanolysis of PLA and in the glycolysis of PET conducted at higher temperatures, the good activity of the Zn amide was preserved while for Mg and Y amides a significant decrease was observed. Surprisingly, in the glycolysis of PET the Zr amide revealed to be the best catalyst enabling 78 % BHET yield within 1 h at 180 °C, a result that is comparable to the best ones described in the literature for metal catalysts. The obtained results highlighted that simple non-toxic metal compounds can represent a valid tool to efficiently promote the sustainable recycling of exhausted polymeric materials into chemical products of synthetic interest, furnishing useful information about the catalytic potentialities of metals that are non-traditionally investigated in these catalytic processes.

4.4 Experimental part

Materials and method

All manipulations of air- and/or water-sensitive compounds were carried out under a dry nitrogen atmosphere using a Braun Labmaster glovebox or standard Schlenk line techniques. Glassware and vials used in the polymerization were dried in an oven at 120 °C overnight and exposed three times to vacuum–nitrogen cycles. Methanol and ethanol were refluxed over Na and distilled under nitrogen. Deuterated solvents, DMSO, C_6D_6 and $CDCl_3$ were purchased from Eurisotop and were dried over molecular sieves. All other reagents and solvents were purchased from Aldrich and used without further purification. The metal amides were purchased from Aldrich and used as received. L-lactide were purchased from Aldrich and crystallized by dry toluene and afterward stored at −20 °C in a glovebox. All other chemicals were commercially available and used as received unless otherwise stated.

The NMR spectra were recorded on Bruker Advance 300, 400 and 600 MHz spectrometers (^{1}H: 300.13, 400.13, 600.13 MHz) at 25 °C, unless otherwise stated. Chemical shifts (δ) are expressed as parts per million and coupling constants (J) in hertz. The resonances are reported in ppm (δ) and the coupling constants in Hz (J) and are referenced to the residual solvent peak at δ = 2.50 ppm for DMSO, δ = 7.27 ppm for $CDCl_3$, δ = 7.16 ppm for C_6D_6.

MALDI mass spectra were recorded using a Bruker solariX XR Fourier transform ion cyclotron resonance (FT-ICR) mass spectrometer (Bruker Daltonik GmbH, Bremen, Germany) equipped with a 7 T refrigerated actively shielded superconducting magnet (Bruker Biospin, Wissembourg, France). The samples were prepared at the concentration of 1.0 mg mL^{-1} in THF, while the matrix (DCTB) was mixed at a concentration of 10.0 mg mL^{-1}.

General procedure for the degradation of polylactide

The depolymerization reaction was carried out under an inert atmosphere. In a Braun Labmaster glovebox, a magnetically stirred reactor vessel (10 mL) was charged with polylactide. In a vial (4mL) the metal-complex was dissolved in MeOH or EtOH and added to the polymer. The reaction mixture was stirred at room temperature. At desired times, small aliquots of the reaction mixture were sampled, dissolved in DMSO, $CDCl_3$ or C_6D_6 and analyzed by ^1H NMR spectroscopy. At the end of the depolymerization the reaction was stopped with CH_2Cl_2 and dried under vacuum. The conversion of PLA, methyl lactate and oligomers were calculated from ^1H NMR, by the following equations:

$$\text{Conversion } X_{int} = \frac{Int_0 - Int}{Int_0}$$

$$\text{Selectivity } S_{MeLa} = \frac{MeLa}{Int_0 - Int}$$

$$\text{Yield } Y_{MeLa} = S_{MeLa} X_{Int}$$

General procedure for the degradation of polyethylene terephthalate

For each experiment, 0.200 g PET particles, the opportune volume of ethylene glycol, and the predicted amount of catalyst were added to a 25 mL reaction tube with a magnetic stirrer. Glycolysis reactions were carried out at 180 °C for one hour. After this time the reaction mixture was cooled to room temperature and about 12 mL of distilled water were added, the resulting mixture was stirred and then filtered to eliminate the residual PET that was dried at 60 °C in vacuo to constant weight. The water solution was concentrated and stored at 4 °C for the night. The crystals of BHET were recovered by filtration, dried and weighted.

The conversion of PET is calculated by the following equation:

$$\text{Conversion } \% = \frac{W_0 - W_r}{W_0} \times 100$$

where W_0 is the initial weight of PET and W_r is the weight of residual PET.

The water solution was concentrated by using a vacuum rotary evaporator at 70 °C and then refrigerated at 0 °C for 12 hours to obtain white crystals of pure BHET.

Selectivity and yield of BHET were calculated according to the following equations:

$$\text{Selectivity BHET } \% = \frac{mol\ BHET_{crystals}}{mol\ PET_{soluble}} \times 100$$

$$\text{Yield BHET } \% = \frac{mol\ BHET_{crystals}}{mol\ PET_{inizial}} \times 100$$

References

[1] [a]Schneiderman, D. K., Hillmyer, M. A. 50th Anniversary Perspective: There Is a Great Future in Sustainable Polymers. *Macromolecules* **50**, 3733–3749 (2017).
[b]Filiciotto, L., Rothenberg, G. Biodegradable Plastics: Standards, Policies, and Impacts. *ChemSusChem* **14**, 56–72 (2021).
[c]Ragauskas, A. J., Williams, C. K., Davison, B. H., Britovsek, G., Cairney, J., Eckert, C. A., Frederick, W. J., Hallett, J. P., Leak, D. J., Liotta, C. L., Mielenz, J. R., Murphy, R. R., Templer, R., Tschaplinski, T. The Path Forward for Biofuels and Biomaterials. Science **311**, 484-489 (2006).

[2] Zhang, X., Fevre, M., Jones, G. O., Waymouth, R. M. Catalysis as an Enabling Science for Sustainable Polymers. *Chemical Reviews*, **118** 839–885 (2018).

[3] [a]Gao, J., Zhu, D., Zhang, W., Solan, G. A., Ma, Y., Sun, W-H. Recent progress in the application of group 1, 2 & 13 metal complexes as catalysts for the ring opening polymerization of cyclic esters. *Inorganic Chemistry Frontiers* **6** 2619–2652 (2019).
[b]Santoro, O., Zhang, X., Redshaw, C. Synthesis of biodegradable polymers: A review on the use of schiff-base metal complexes as catalysts for the ring opening polymerization (ROP) of cyclic esters. *Catalysts* **10** 1–49 (2020).
[c]Chamberlain, B. M., Cheng, M., Moore, D. R., Ovitt, T. M., Lobkovsky, E. B., Coates, G. W. Polymerization of lactide with zinc and magnesium β-diiminate complexes: Stereocontrol and mechanism. *Journal of the American Chemical Society* **123**, 3229–3238 (2001).
[d]Wang, H., Yang, Y., Ma, H. Stereoselectivity switch between zinc and magnesium initiators in the polymerization of rac -lactide: Different coordination chemistry, different stereocontrol mechanisms. *Macromolecules* **47**, 7750–7764 (2014).
[e]Thomas, C. M. Stereocontrolled ring-opening polymerization of cyclic esters: Synthesis of new polyester microstructures. *Chemical Society Reviews* **39**, 165–173 (2010).

[4] [a]Coates, G. W., Getzler, Y. D. Y. L. Chemical recycling to monomer for an ideal, circular polymer economy. *Nature Reviews Materials*, **5** 501–516 (2020).
[b]Kaur, G., Uisan, K., Ong, K. L., Ki Lin, C. S. Recent Trends in Green and Sustainable Chemistry & Waste Valorisation: Rethinking Plastics in a circular economy. *Current Opinion in Green and Sustainable Chemistry* **9** 30–39 (2018).

[5] Beltrán, F. R., Lorenzo, V., Acosta, J., de la Orden, M. U., Martínez Urreaga, J. Effect of simulated mechanical recycling processes on the structure and properties of poly(lactic acid). *Journal of Environment Management* **216**, 25–31 (2018).

[6] McKeown, P., Jones, M. D. The Chemical Recycling of PLA: A Review. Sustainable Chemistry **1,** 1-22 (2020).

[7] Lamberti, F. M., Román-Ramírez, L. A., Mckeown, P., Jones, M. D., Wood, J. Kinetics of alkyl lactate formation from the alcoholysis of poly(lactic acid). *Processes* **8**, (2020).

[8] Calvo-Flores, F. G., Monteagudo-Arrebola, M. J., Dobado, J. A., Isac-García, J. Green and Bio-Based Solvents. *Topics in Current Chemistry* **376** (2018).

[9] [a]Yang, R., Xu, G., Dong, B., Guo, X., Wang, Q. Selective, Sequential, and 'one-Pot' Depolymerization Strategies for Chemical Recycling of Commercial Plastics and Mixed Plastics. *ACS Sustainable Chemistry & Engineering* **10**, 9860–9871 (2022).
[b]Yang, R., Xu, G., Lv, C., Dong, B., Zhou, L., Wang, Q. $Zn(HMDS)_2$ as a Versatile Transesterification Catalyst for Polyesters Synthesis and Degradation toward a Circular Materials Economy Approach. *ACS Sustainable Chemistry & Engineering* **8**, 18347–18353 (2020).

[10] Santulli, F., Lamberti, M., Mazzeo, M. A Single Catalyst for Promoting Reverse Processes: Synthesis and Chemical Degradation of Polylactide. *ChemSusChem* **14**, 5470-5475 (2021).

[11] [a]Payne, J., Jones, M. D. The Chemical Recycling of Polyesters for a Circular Plastics Economy: Challenges and Emerging Opportunities. *ChemSusChem* **14** 4041–4070 (2021).
[b]Lamberti, F. M., Román-Ramírez, L. A., Wood, J. Recycling of Bioplastics: Routes and Benefits. *Journal of Polymers and the Environment* **28** 2551–2571 (2020).

[12] Román-Ramírez, L. A., Powders, M., McKeown, P., Jones, M. D., Wood, J. Ethyl Lactate Production from the Catalytic Depolymerisation of Post-consumer Poly(lactic acid). *Journal of Polymer and the Environment* **28**, 2956–2964 (2020).

[13] [a]Jehanno, C., Flores, I., Dove, A. P., Müller, A. J., Ruipérez, F., Sardon, H. Organocatalysed depolymerisation of PET in a fully sustainable cycle using thermally stable protic ionic salt. *Green Chemistry* **20**, 1205–1212 (2018).
[b]Jehanno, C., Pérez-Madrigal, M. M., Demarteau, J., Sardon, H., Dove, A. P. Organocatalysis for depolymerisation. *Polymer Chemistry* **10** 172–186 (2019).
[c]Wang, Q., Yao, X., Tang, S., Lu, X., Zhanga, X., Zhang, S. Urea as an efficient and reusable catalyst for the glycolysis of poly(ethylene terephthalate) wastes and the role of hydrogen bond in this process. *Green Chemistry* **14**, 2559–2566 (2012).
[d]Fukushima, K., Coulembier, O., Lecuyer, J. M., Almegren, H. A., Alabdulrahman, A. M., Alsewailem, F. D., Mcneil, M. A., Dubois, P., Waymouth, R. M., Horn, H. W., Rice, J. E., Hedrick, J. L. Organocatalytic depolymerization of poly(ethylene terephthalate). *Journal of Polymer Science Part A: Polymer Chemistry* **49**, 1273–1281 (2011).

[14] [a]Wang, H., Li, Z. X., Liu, Y. Q., Zhang, X. P., Zhang, S. J. Degradation of Poly(Ethylene Terephthalate) Using Ionic Liquids. *Green Chemistry* **11**, 1568−1575 (2009).
[b]Wang, H., Liu, Y. Q., Li, Z. X., Zhang, X. P., Zhang, S. J., Zhang, Y. Q. Glycolysis of Poly(Ethylene Terephthalate) Catalyzed by Ionic Liquids. *European Polymer Journal* **45**, 1535−1544 (2009).
[c]Yue, Q. F., Xiao, L. F., Zhang, M. L., Bai, X. F. The Glycolysis of Poly(ethylene terephthalate) Waste: Lewis Acidic Ionic Liquids as High Efficient Catalysts. *Polymers* **5**, 1258–1271 (2013).

[15] Musale, R. M., Shukla, S. R. Deep eutectic solvent as effective catalyst for aminolysis of polyethylene terephthalate (PET) waste. *International Journal of Plastics Technology* **20**, 106–120 (2016).

[16] Pingale, N. D., Palekar, V. S., Shukla, S. R. *Journal of Applied Polymer Science* **115**, 249–254 (2010).
Lo´pez-Fonseca, R., Duque-Ingunza, I., De Rivas, B., Flores-Giraldo, L., Gutierrez-Ortiz, J. I. *Chemical Engineering Journal* **168**, 312–320 (2011).
Chen, F., Yang, F., Wang, G., Li, W. *Journal of Applied Polymer Science* **131**, 41053 (2014).

[17] [a]Troev, K., Grancharov, G., Tsevi, R., Gitsov, I. Erratum: A Novel Catalyst for the Glycolysis of Poly(ethylene terephthalate). *Journal of Applied Polymer Science* **90**, 1148-1152 (2003).
[b]Payne, J., McKeown, P., Driscoll, O., Kociok-Köhn, G., Emanuelsson, E. A. C., Jones, M. D. Make or break: Mg(II)-and Zn(II)-catalen complexes for PLA production and recycling of commodity polyesters. *Polymer Chemistry* **12**, 1086–1096 (2021).

[18] Payne, J., McKeown, P., Driscoll, O., Kociok-Köhn, G., Emanuelssonc, E. A. C., Jones, M. D. Make or break: Mg(II)-and Zn(II)-catalen complexes for PLA production and recycling of commodity polyesters. *Polymer Chemistry* **12**, 1086–1096 (2021).

[19] Delle Chiaie, K. R., McMahon, F. R., Williams, E. J., Price, M. J., Dove, A. P. Dual-catalytic depolymerization of polyethylene terephthalate (PET). *Polymer Chemistry* **11**, 1450–1453 (2020).

CHAPTER 5

Zinc complexes bearing dinucleating bis(imino-pyridine)binaphthol ligands

The results described in this Chapter are part of a manuscript in preparation:

Santulli, F., Bruno, F., Mazzeo, M., Lamberti M. Zinc complexes bearing dinucleating bis(imino-pyridine)binaphthol ligands: highly active and robust catalysts for the lactide polymerization.

5.1 Introduction

Polylactic acid (PLA) is considered an environmentally friendly polymer being both a bio-based and biodegradable polymer. It is a derivative of lactic acid which is produced from renewable resources such as wheat, straw and corn.[1] Moreover, PLA can be decomposed into water and carbon dioxide by microbes, although under specific conditions.[2]

The most efficient method to obtain PLA is the ring-opening polymerization (ROP) of lactide promoted by metal complexes.[3] However, to respect the sustainability criteria, the whole productive process must be carefully designed, for example by selecting catalysts with high efficiency and low toxicity, able to work in the absence of solvents and not requiring expensive purification processes of the substrates.

Zinc is an excellent candidate to produce sustainable polymers because of its high activity, low price with a lack of color and toxicity.[4] Indeed, conspicuous number of zinc complexes bearing different ancillary ligands have been reported as active catalysts in the ROP of lactides. Recent literature studies have shown that complexes with more than one metal center, which work synergistically, can show a peculiar catalytic behavior compared to monometallic analogs.[5] This concept evokes the modes of action of many metalloenzymes: specific and highly selective biocatalysts containing two or more metal ions in the active sites.[6]

Among the related complexes, active catalysts in the synthesis of PLA are pentadentate and hexadentate bis(diamino)- and bis(diimino)-phenolate dinuclear zinc complexes reported by Tolman and Williams[7] and subsequently by Mehrkhodavandi[8], various dizinc complexes bearing NNO-scorpionate ligands explored by Otero.[9] To date, the most active catalyst for the ROP of lactide in solution is a bis(imino)diphenylamido dizinc complex, reported in 2016 by Williams et al.[10], which showed TOF up to 60000 h^{-1} and worked efficiently under immortal conditions or at very low catalyst loading too.

Despite the numerous reported zinc catalysts that show remarkable activity in the ROP of LA, only few examples are able to preserve their efficiency under the conditions required for the industrial synthesis of PLA, i.e. at high temperature and in the presence of large amounts of protic chain transfer agents.[11] A detailed comparison between the activities of the zinc complexes active under these more challenging conditions, is not possible since the explored reaction conditions are different (i.e. the temperature, the monomer equivalents, the presence of a cocatalyst) and, above all, only some authors have tested the abilities of the synthesized complexes in the presence of unpurified lactide.

In this work, we report the synthesis of new hexadentate ligands in which two pyridyl phenoxy-imine portions, seen in the previous *Chapters*, are connected to each other by means of a binaphthyl backbone. This structure was purposely designed to host two metal centers in their coordinative pockets. The corresponding dinuclear zinc complexes have been used in lactide polymerization experiments carried out under several conditions demonstrating the high activity and robustness of the catalytic systems. In addition, mechanistic studies were conducted to obtain information on the nature of the active catalytic species.

5.2 Results and discussion

5.2.1 Synthesis and characterization

The bis(imino pyridine)binaphthol ligands (S)-LH_2 and *rac*-LH_2 were obtained in methanol at room temperature by condensation of two equivalents of 2-(2-pyridyl)ethylamine with the (S)- and *rac*-3,3'-diformyl BINOL, properly synthesized according to a procedure reported in the literature (**Scheme 5.1**).[12]

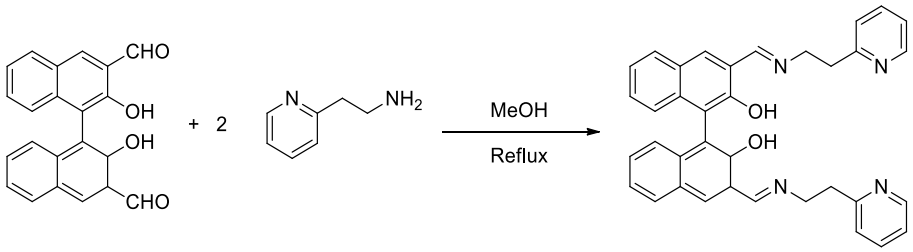

Scheme 5.1 Synthesis of the ligands (S)-LH_2 and *rac*-LH_2.

(S)-LH_2 ligand was fully characterized by mono- and bi- dimensional NMR analysis in C_6D_6 (**Figure 5.1 and 5.7-5.10**) and MALDI-FT-ICR MS analysis (**Figure 5.11**).

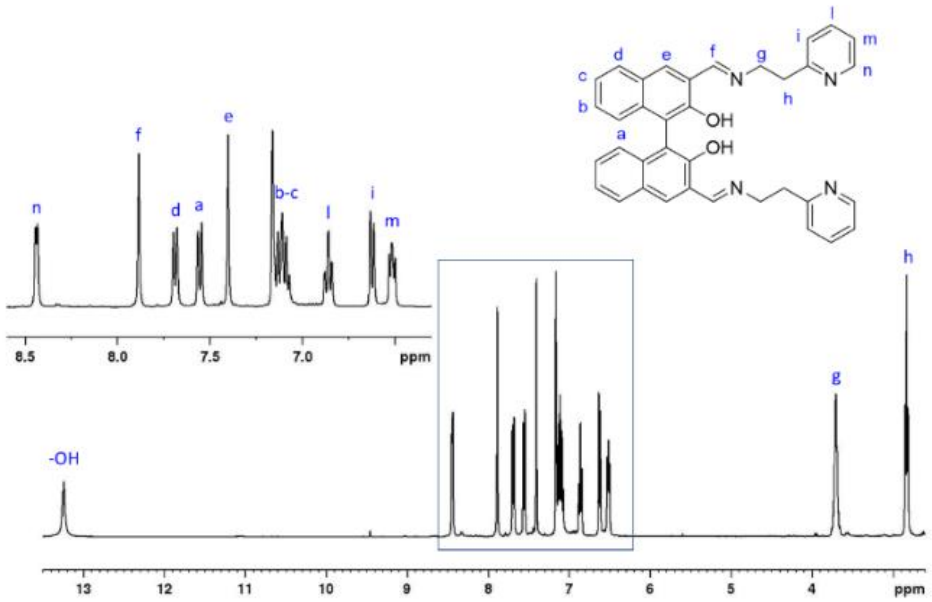

Figure 5.1 ^{1}H NMR spectrum of ligand (S)-LH_2 (400 MHz, C_6D_6, 298 K).

Direct reaction of the hexadentate ligand (S)-LH_2 with 2 equiv. of zinc bis[bis(trimethylsilyl)amide] $Zn[N(SiMe_3)_2]_2$ in benzene gave the corresponding dizinc complex (**Scheme 5.2**). After 2 h at room temperature the benzene was removed under vacuum and the product was washed with hexane to remove any impurities, including the bis(trimethylsilyl) amine formed as a co-product. The dizinc complex (S)-**1** appeared as an orange powder (73 % of yield) which was characterized by an exhaustive NMR analysis (**Figures 5.12-5.17**).

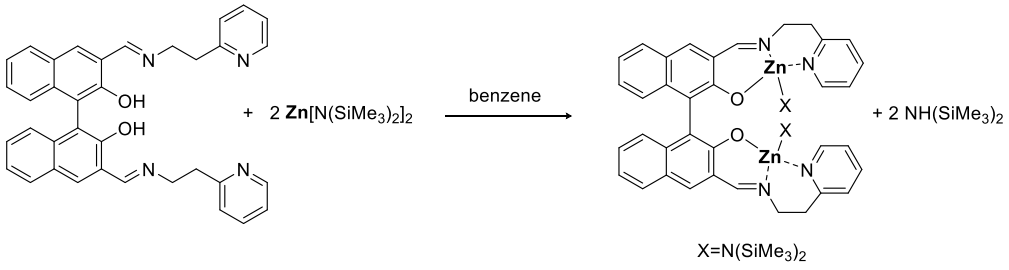

Scheme 5.2 Synthesis of zinc complexes (S)-**1** and *rac*-**1**.

^{1}H NMR spectrum of complex (S)-1 (**Figure 5.2**) showed the disappearance of the -OH signal of the ligand and the appearance of a new peak, centered at δ = 0.19 ppm integrating for 36 protons, attributable to the

hydrogens of the silylamido groups. Moreover, the narrow triplets observed for the methylene protons of the ethylene bridge (NCH_2CH_2Ar) in the ligand spectrum, split in three broad signals at δ = 3.21, 3.02 and 2.81 ppm, integrating, respectively, for four, two and two protons (protons denoted with letters g and h in **Figure 5.2**). All the other signals of the protons of the ligand skeleton were easily recognizable, most of them shifting upfield with respect to the same signals in the ^{1}H NMR spectrum of the free ligand. Interestingly, the number of the signals indicated the presence in solution of a symmetric species. 2D NMR experiments (**Figures 5.13-5.16**) suggested the formation of the binuclear zinc complex sketched in **Scheme 5.3**, in which ligand LH_2 binds each zinc center by two six-membered chelate rings, thus zinc atoms are tetracoordinate.

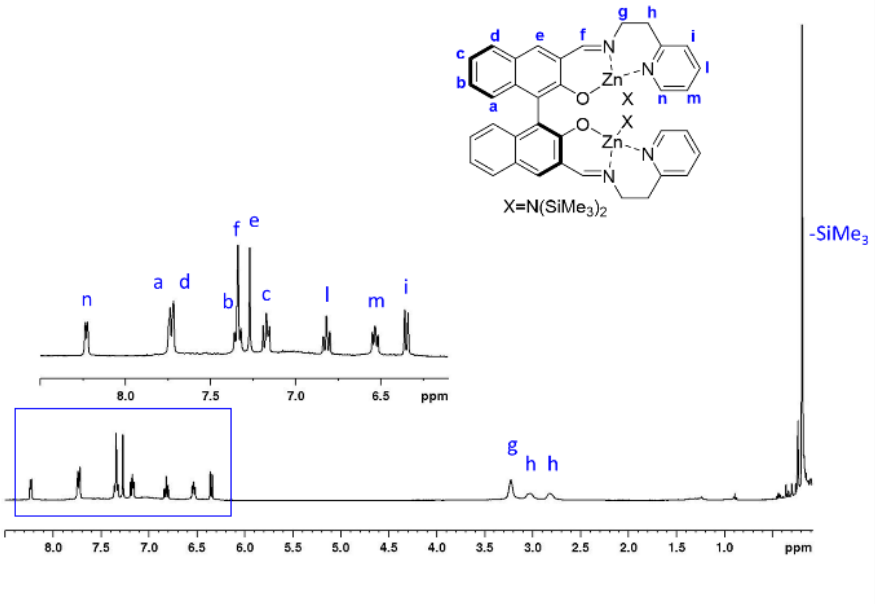

Figure 5.2 ^{1}H NMR spectrum of complex (S)-**1** (400 MHz, C_6D_6, 298 K).

^{1}H NMR spectrum of the zinc complex at 70 °C shows partially coalesced signals for the methylene protons, as usually observed for fluxional systems (**Figures 5.18-5.19**). At the same time both the signals of the iminic proton and of the α-proton of the pyridine shift downfield with respect to the same signals in the RT spectrum. This last observation suggests a weaker coordination of both types of nitrogen atoms to the zinc centers at higher temperature.

Next, we performed the synthesis of the dizinc complex from the racemic form of ligand, *rac*-LH_2. In this case, we observed the formation of complex *rac*-**1**, with a ^{1}H NMR spectrum not superimposable to that observed for complex (S)-**1** (**Figure 5.3**).

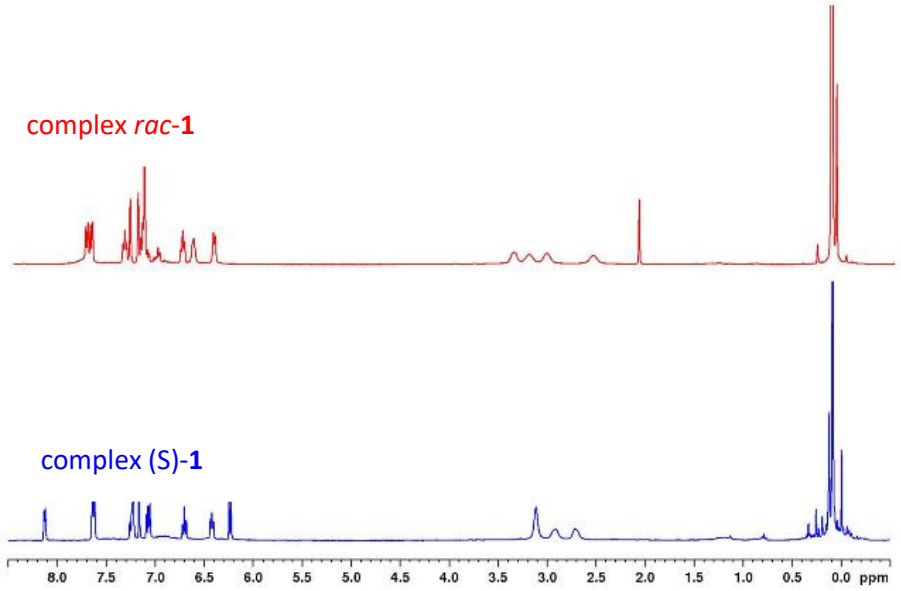

Figure 5.3. ^{1}H NMR spectra of complexes (S)-**1** (blue) and *rac*-**1** (red) (400 MHz, C_6D_6, 298 K).

In particular, unlike complex (S)-**1**, the NMR spectrum of complex *rac*-**1** shows: four signals for the methylene protons, the α-proton of the pyridine appears as a broad signal overlapped with other aromatic protons, in addition to some other shifts of the aromatic signals (**Figures 5.20-5.23**).

As a possible explanation for the observed differences, it has been hypothesized that different dimeric species are formed in solution. In particular, we hypnotized that in the case of the racemic mixture *rac*-**1**, the two enantiomers interact each other forming a heterochiral dimer, while for the chiral complex (S)-**1**, a homochiral dimer is formed.[13] The formation of two diastereomeric dimeric species could explain the differences observed in the ^{1}H NMR spectra of *rac*-**1** and (S)-**1** at room temperature. Interestingly, when we performed the ^{1}H NMR spectra of complexes *rac*-**1** and (S)-**1** at higher temperature (70 °C), the spectra were identical (**Figures 5.18-5.24**). It is presumable that the dimeric structures of the complexes dissociate into the monomeric enantiomers under this condition. The formation of the dimers presumably occurs through the establishment of bridging bonds between the zinc atoms of the monomeric species by the nitrogen atoms of the amide groups[14] or the pyridine moieties (**Scheme 5.4**).

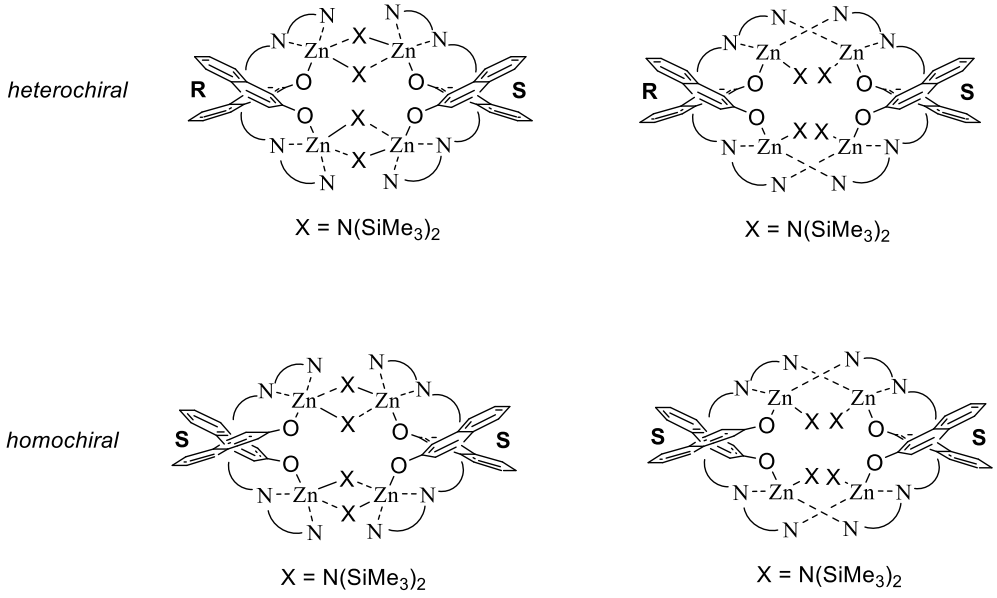

Scheme 5.4 Hypothesized sketched structures of the heterochiral dimer *rac*-**1** and of the homochiral dimer (S)-**1**.

To verify the effective formation of the dimers, NMR diffusion experiments were performed in the presence of an internal reference molecule (tetrakismethylsilylsilane, TMSS). 2D DOSY-^{1}H NMR measurements[15] provide insight into the translational diffusion coefficient of the molecular species in solution, and it has already been used for characterizing various organometallics, supramolecular and polymer structures in solution. [16] Using the semiempirical equation,[17] whereby the ratio between the diffusion coefficients of two species is the inverse of the square roots of their masses, molecular weights 1.5 times higher than the theoretical one were estimated for both complexes (**Figures 5.16-5.23**). Thus, we assumed the existence of an equilibrium between the monomeric and dimeric species both for the chiral complex and for the racemic form.[18]

5.2.2 Polymerization studies

Bimetallic zinc complexes *rac*-**1** and (S)-**1** were tested as catalysts for the ROP of lactides under several reaction conditions (**Table 5.1**). The conversion was evaluated by ^{1}H NMR analysis of small aliquots withdrawn during the reactions. The obtained polymers were characterized by MALDI-FT-ICR MS and ^{1}H NMR analyses.

Table 5.1 Ring-opening polymerization of lactides by complexes (S)-**1** and *rac*-**1**.

Entry[a]	monomer (equiv.)	cat	Cocat (eq.)	Solvent (mL)	time	Conv[b] (%)	TOF (h^{-1})	Mn_{th}[c] (KDa)	Mn_{GPC}[d] (KDa)	Đ[d]
1	*rac*-LA (200)	(S)-**1**	-	DCM (2)	0.25 h 1.5 h	5 75	40 100	21.6	37.7	1.76
2	*rac*-LA (200)	*rac*-**1**	-	DCM (2)	0.25 h 1.5 h 3.5 h	0 54 90	- 72 51	26.0	55.6	1.46
3	*rac*-LA (200)	(S)-**1**	^{i}PrOH (2)	DCM (2)	2 min 4 min	56 72	3360 2160	8.1 10.4	7.3 9.3	1.03 1.03
4	*rac*-LA (200)	*rac*-**1**	^{i}PrOH (2)	DCM (2)	4 min	78	2350	11.2	9.1	1.11
5	L-LA (200)	(S)-**1**	^{i}PrOH (2)	DCM (2)	4 min	71	2130	10.2	8.7	1.15
6	L-LA (200)	*rac*-**1**	^{i}PrOH (2)	DCM (2)	4 min	80	2400	11.5	12.1	1.17
7[e]	*rac*-LA (500)	(S)-**1**	BnOH (2)	THF (2.5)	5 min	50	3000	18.0	9.7	1.27
8[e]	*rac*-LA (500)	(S)-**1**	BnOH (2)	DCM (2.5)	5 min	29	1740	10.4	6.4	1.08
9[e]	*rac*-LA (500)	(S)-**1**	BnOH (2)	toluene (2.5)	5 min 1 h 5 h	67 100	4020	24.1	22.6 22.3 12.8	1.05 2.00 2.38
10[f]	*rac*-LA (500)	(S)-**1**	^{i}PrOH (2)	toluene (2)	4 min	84	6300	30.3	16.9	1.05
11[g]	L-LA (5000)	(S)-**1**	BnOH (50)	-	40 min	36	2700	5.2	3.6	1.3
12	*rac*-LA (200)	(S)-**1**a	^{i}PrOH (2)	DCM (2)	18 h 48 h	60 71	6 3	10.2	4.14	1.23
13	*rac*-LA (200)	$Zn(O^iPr)_2$		DCM (2)	10 min 1 h	37 100	444	28.8	25.2	1.19

[a]All polymerizations were carried out by using 8 µmol of complexes *rac*/(S)-**1** in 2 mL of solvent at 25 °C. [b]Conversion of lactides as determined by ^{1}H NMR spectral data. [c]Calculated according to the monomer conversion: M_{nth} (KDa) = 144.14 $gmol^{-1}$ × ([LA]/[ROH]) × conversion of LA. [d]Experimental Mn and Đ values of the polymers were determined by gel-permeation chromatography (GPC) in THF relative to polystyrene standards and multiplied by a correction factor of 0.58. [e]4.0 µmol of complex (S)-1. [f]Temperature of 70 °C. [g]Temperature of 190 °C.

Complex (S)-**1** was able to polymerize 150 equiv. of *rac*-LA in 1.5 h at 25 °C, in dichloromethane as solvent. Under the same conditions, complex *rac*-**1** showed a lower conversion (entries 1 vs 2, **Table 5.1**). Kinetic plots for these polymerization experiments are reported in **Figure 5.26**. Both complexes *rac*-**1** and (S)-**1** showed first-order rates in lactide with a k_{obs} for (S)-**1** about twice that of *rac*-**1**. Moreover, for complex *rac*-**1**, a longer induction period was observed. The induction period is likely related to a slow initiating rate on the amido

group bound to the zinc center. In agreement with this observation, the PLA samples obtained in these polymerization tests showed experimental molecular weights higher than the theoretical values and dispersity indexes higher than 1.5. The slower rate observed for complex *rac*-**1** with respect to (S)-**1**, both for the initiation and the propagation, could be attributable to the different structure of the dimeric species, although further studies are needed to clarify this aspect.

The subsequent polymerization tests were carried out in the presence of an alcohol as a cocatalyst. By adding 2 equiv. of ^{i}PrOH to both complexes, the activity raised considerably converting about 150 equiv. of *rac*-LA in only 4 min (entries 3-4, **Table 5.1**). In addition, under these conditions, both complexes exhibit similar activities and a good control over the polymerization process in terms of molecular weight and dispersity.

Next, we explored the behavior of complexes (S)-**1** and *rac*-**1** with the enantiomerically pure monomer, L-LA (entries 5-6, **Table 5.1**). Also in this case, the activities were similar for both complexes and comparable to those obtained in the presence of the racemic monomer (entries 3 vs 6, **Table 5.1**) thus suggesting the lack of a preference of the enantiomeric catalysts towards one of the monomer enantiomers. In line with this observation, the ^{1}H homodecoupled spectra of the obtained PLAs, showed atactic polymers with only a slight isotactic bias. In particular, for the PLA sample obtained by *rac*-LA with complex (S)-**1** at 25 °C (entry 3, **Table 5.1**), an isotactically enriched microstructure with a α value of 66 % was observed. Upon lowering the polymerization temperature to -20 °C (entry 1, **Table 5.2**) the polymer microstructure did not change significantly, on the other hand a small increase in the stereocontrol (α = 72 %) was registered in the case of the polymerization reaction carried out without the co-initiator (entry 1, **Table 5.1**) (**Figures 5.28-5.31**).

Subsequently, the effect of the solvent on the activity of complex (S)-**1** in combination with BnOH, was studied in the presence of 500 equiv. of *rac*-LA (entries 7-9, **Table 5.1**). The activity remained very high also under these conditions and with all the tested solvents, following the order: toluene > THF > DCM. Worth of note, a very low dispersity with a good agreement between theoretical and experimental weights was found in toluene. In order to study the kinetics of the polymerization reactions carried out in the presence of the co-initiator, a polymerization experiment conducted under the conditions of entry 8 (**Table 5.1**), was followed by ^{1}H NMR analysis of reaction mixture samples taken every 2 min. Under these conditions, a kinetic of the first order with respect to the monomer and the absence of the induction period were highlighted, the k_{obs} resulted 0.0404 min^{-1} (**Figure 5.27**).

Then, we performed two polymerization reactions (entries 2-3, **Table 5.2**) promoted by complex (S)-**1** in combination with both ^{i}PrOH and BnOH, and with a ratio of [*rac*-LA]/[Zn] = 50 to carefully analyze the polymer chain-end by NMR spectroscopy studies and MALDI-FT-ICR MS spectrometry. Both NMR and MALDI-FT-ICR MS analyses of these polymeric samples (**Figures 5.32-5.37**) showed the formation of PLA with -H and -BnO/^{i}PrO (depending on the employed initiator) end groups. The presence of one symmetrical series with a peak spacing of 144 Da indicated the absence of side reactions. Interestingly, extending the reaction time beyond the complete conversion of the monomer (entry 3 after 15 min, **Table 5.2**), a minor series of peaks with a separation of 72 Da appeared in the MALDI-FT-ICR MS spectrum. Additional reaction time (entry 3 after 45 min, **Table 5.2**) led to a multimodal distribution with a peak spacing of 72 Da (**Figure 5.37**). The whole picture indicates that the catalyst selectively promotes the polymerization reaction as long as the monomer is present in the reaction mixture while, in the absence of lactide, the zinc active species catalyzes fast transesterification reactions of the polymer chains. With the aim to get more information on the transesterification reactions we studied other polymeric samples, obtained under different reaction conditions, which were left under stirring in the reaction medium beyond the time necessary for the ROP of the whole monomer. GPC analysis of aliquots taken at different times, indicated a decrease in molecular masses accompanied by an increase in dispersities (entry 4, **Table 5.2**), in addition MALDI-FT-ICR MS analysis showed the formation of low molecular cyclic fractions, thus suggesting the occurrence of intramolecular transesterifications as well. In order to maximize the transesterification reactions, we studied a polymeric sample obtained at higher reaction temperature (entry 8, **Table 5.2**), in this case, the exclusive formation of cyclic polymers was observed, as indicated by MALDI-FT-ICR MS analysis (**Figure 5.38**) and by the good agreement between MALDI and GPC molecular masses.

Finally, the performance of complex *rac*-**1** was evaluated under industrially conditions: a polymerization experiment was carried out without solvent, at elevated temperature (190 °C), low catalyst loading, BnOH as a co-initiator and, more relevant, with not purified L-LA monomer (entry 11, **Table 5.1**). At a 5000 : 1 : 50 ratio of L-LA : *rac*-**1** : BnOH, the polymerization of L-LA promoted by complex *rac*-**1** was very efficient, reaching a 36 % of conversion after 40 min, thus suggesting the robustness of this zinc catalyst even under these conditions. MALDI-FT-ICR MS analysis of PLA showed a polymer with -H and -BnO end groups and each peak is at a constant spacing of 144 Da indicating the absence of side reactions, despite this challenging conditions (**Figure 5.40**).

5.2.3 Mechanistic studies

Polymerization reactions promoted by zinc complexes and an alcohol as catalytic systems, were conducted by mixing in situ the zinc amido derivative with ^{i}PrOH or BnOH for 15 min before monomer addition. In order to get information on the active species, the reaction between the zinc–amido complex (S)-**1** with 1 equiv. of ^{i}PrOH per zinc, was carried out in a J-Young NMR tube in C_6D_6 as solvent (**Scheme 5.5** pathway a). In few min at room temperature, the ^{1}H NMR spectrum showed the consumption of the amido complex and the formation of a new product (**Figure 5.41**). After the purification of this new species, the ^{1}H NMR suggested the formation of the monometallic zinc complex (S)-**1a** in which the ligand acts as a hexadentate ligand wrapped around one zinc center. The same reaction was carried out in THF-d8 (**Figure 5.43**). Even in this case the spectrum suggested the formation of species (S)-**1a**. After few min, the formation of a precipitate was observed. However, by adding 20 equiv. of L-LA, the ^{1}H NMR spectrum showed the formation of the polymer while the reaction mixture become homogeneous (**Figure 5.44**).

The nature of the monometallic zinc species (S)-**1a** was confirmed synthesizing it by reaction of ligand (S)-LH_2 with 1 equiv. of diethyl zinc $Zn(Et)_2$ (**Scheme 5.5** pathway b). The evolution of ethane EtH was evident, in addition the spectrum showed ten signals in the aromatic region and four multiplets in the range δ = 2.8-3.8 ppm, attributable to the diastereotopic protons of the methylene groups (**Figure 5.45**), thus suggesting a C_2 symmetry also for this species and a strong coordination of the imine and pyridine nitrogen atoms to the zinc center.

To verify the activity of the monometallic species (S)-**1a** in the ring-opening polymerization of lactide, it was tested in combination with 2 equiv. of ^{i}PrOH under the same reaction conditions of entry 4 in **Table 5.1**. (S)-**1**a employed 18 h to polymerize 120 equiv. of lactide, thus showing a very low activity at room temperature in a dichlorometane solution (entry 12, **Table 5.1**).

Taking into account that zinc bis(isopropoxide) is generated during the reaction of the amido complex with ^{i}PrOH, we carried out a new experiment to evaluate its activity. Zinc isopropoxide $Zn(O^{i}Pr)_2$ is a polymeric, insoluble derivative, however, it can be obtained in a pure, soluble form by alcoholysis of $Zn[N(SiMe_3)_2]_2$ according to reaction c in **Scheme 5.5**.[19] In our case, this reaction has the additional advantage to generate even the bis(trimethylsilyl)amine $HN(SiMe_3)_2$ compound which is another product of the in situ reaction between the amido complex and the ^{i}PrOH. In other words, the products of this reaction constitute the ideal system for a blank test of our polymerization reactions. Thus, a polymerization experiment was carried out by using freshly $Zn(O^{i}Pr)_2$ prepared and working in the same conditions of **entry 4** (200 equiv. *rac*-LA, 2 mL DCM, 25 °C). A conversion of 37 % of *rac*-LA was evaluated after 10 min (entry 13, **Table 5.1**), thus showing an activity one order of magnitude lower than the activity of the catalytic system constituted by complex (S)-**1** and ^{i}PrOH. In summary, both the homoleptic species (S)-**1a** and the mixture of the $Zn(O^{i}Pr)_2$ with the $HN(SiMe_3)_2$ are less active than the system formed in situ by reaction of the amido complex (S)-**1** with ^{i}PrOH, thus suggesting that the high activity observed in the ROP of lactides is the result of a cooperation between these species. The observed high activity could also be the result of the establishment of a Schlenk-like equilibrium among complex (S)-**1a**, zinc isopropoxide and the isopropoxide derivative of the zinc complex, following the addition of the lactide monomer.

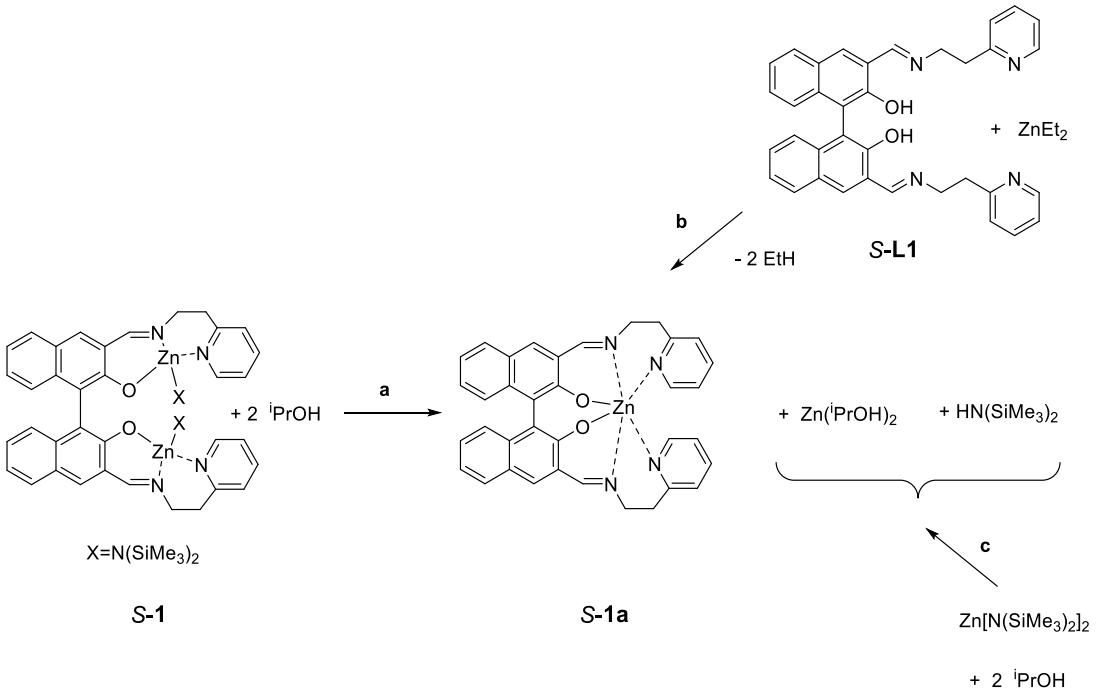

Scheme 5.5 Schematic pathways of the reactions carried out in C_6D_6 in J-Young NMR tubes, addressed to unravel the nature of the active species in the ROP of lactide.

5.3 Conclusion

In this *Chapter*, the synthesis of a hexadentate ligand with an original structure has been reported. Enantiomerically pure and racemic version of the ligand were converted in the corresponding zinc bimetallic complexes by direct reaction with the zinc amide precursor. Satisfyingly, both complexes showed very high activity in the ring-opening polymerization of L-LA and *rac*-LA with turnover frequencies (TOF) around 4000 h^{-1} which reached a value of 6200 h^{-1} at 70 °C, allowing the classification of this catalytic system among the most active reported in the literature. Noteworthy, the activity remains high even when working under industrial conditions, i.e. at 190 °C, with a high number of alcohol equiv. and, above all, in the presence of technical grade L-LA, thus demonstrating the robustness and the versatility of the catalysts.

The characterization of the polymers by MALDI, GPC and NMR analysis, showed a good control of the molecular weights, chain end groups dependent on the alcohol used as cocatalyst, and a bias toward isotacticity. In addition, while transesterification reactions were absent during the polymerization reactions, the catalyst proved to be very efficient also in promoting these reactions when the monomer is no longer present in the reaction mixture. Interestingly, while at room temperature intermolecular transesterifications appear to be the predominant reactions, by increasing the reaction temperature, the catalytic system completely switches towards intramolecular transesterifications, allowing the full monomer conversion to low molecular weights cyclic polymers.

NMR-scale reactions carried out to obtain information on the active species, have shown the formation of the monometallic species by reaction of the amide adduct with ^{i}PrOH. Furthermore, it has been observed that both the monometallic species and $Zn(O^{i}Pr)_2$ alone have lower activities than that observed for the synthesized complex thus suggesting either the cooperation between these two metallic species or the existence of a Schlenk-type equilibrium between the two aforementioned species and the isopropoxy derivative of the bimetallic complex. Reasonably, the high reaction rate of these catalytic systems prevented us from directly observing this species via NMR, while the results obtained lead us to hypothesize its existence.

5.4 Experimental part

Materials and methods

Moisture and air-sensitive materials were manipulated under nitrogen using Schlenk techniques or an MBraun Labmaster glovebox. Toluene and methanol were refluxed over Na and distilled under nitrogen. Tetrahydrofuran (THF) was refluxed over Na and benzophenone and distilled under nitrogen. Monomers (Sigma-Aldrich) were purified before use.

$CDCl_3$, C_7D_8 and C_6D_6 were purchased from Eurisotop and used as received. All other reagents and solvents were purchased from Aldrich and used without further purification.

Instruments and measurements

NMR spectra of polymers were performed at room temperature on Bruker Avance 300, 400 or 600 spectrometers (^{1}H: 300.13, 400.13, 600.13 MHz; ^{13}C: 75.47, 100.62, 150.92 MHz, respectively). The resonances are reported in ppm (δ) and the coupling constants in Hz (J) and are referenced to the residual solvent peak at δ = 7.16 ppm for C_6D_6 and δ = 7.27 ppm for $CDCl_3$. Spectra recording was performed using Bruker- TopSpin v2.1 software. Data processing was performed using TopSpin v2.1 or MestReNova v6.0.2 software.

The average molecular masses and the molecular weight dispersities (Đ) of the obtained polylactide samples were determined by GPC in THF as the mobile phase at a flow rate of 1 mL min^{-1}. The utilized GPCmax VE-2001 from Viscotek was a combination of an HPLC pump, two Malvern Viscotek T columns (porous styrene divinylbenzene copolymer) with a maximum pore size of 500 and 5000 a, a refractive index detector (VE-3580), and a viscometer (Viscotek 270 Dual Detector). Polystyrene standards were used for calibration. The evaluation of the molar masses was carried out with a universal method or with a conventional method in combination with multiplying a factor of 0.58 for PLA.

MALDI mass spectra were recorded using a Bruker solariX XR Fourier transform ion cyclotron resonance (FT-ICR) mass spectrometer (Bruker Daltonik GmbH, Bremen, Germany) equipped with a 7 T refrigerated actively shielded superconducting magnet (Bruker Biospin, Wissembourg, France). The samples were prepared at the concentration of 1.0 mg mL^{-1} in THF, while the matrix (DCTB) was mixed at a concentration of 10.0 mg mL^{-1}.

Synthesis and characterization of ligand (S)-LH_2

PREPARATION AND CHARACTERIZATION OF 2,2'-bis(methoxymethoxy)-1,1'-binaphthalene

The synthesis is a modified literature procedure. Under nitrogen, (S)-(−)-1,1′-Bi(2-naphthol) (5.16 g, 19.6 mmol) was dissolved in 25 mL of N, N-dimethylformamide DMF dry. In a schlenk flask, sodium hydride (1.88 g, 78.4 mmol) was suspended in DMF dry (30 mL) and the flask was cooled to 0 °C. The solution was slowly added to the suspension obtaining a yellow solution. After stirring for 10 min to 0 °C, chloromethyl methyl ether (6.0 mL, 78.4 mmol) was added slowly to the solution, obtaining a white solution. The flask was warmed to room temperature and the mixture was allowed to stir for 3 h. The reaction was quenched with H_2O and was extracted with diethyl ether. The combined organic extracts were washed with brine and dried over $MgSO_4$. The solvent was removed under vacuum and the compound was purified for crystallization in diethyl ether, obtaining white crystals. Yield 77 %

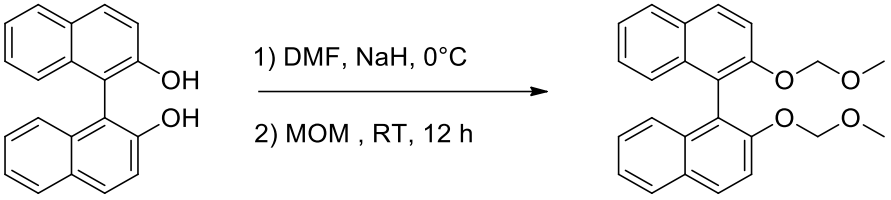

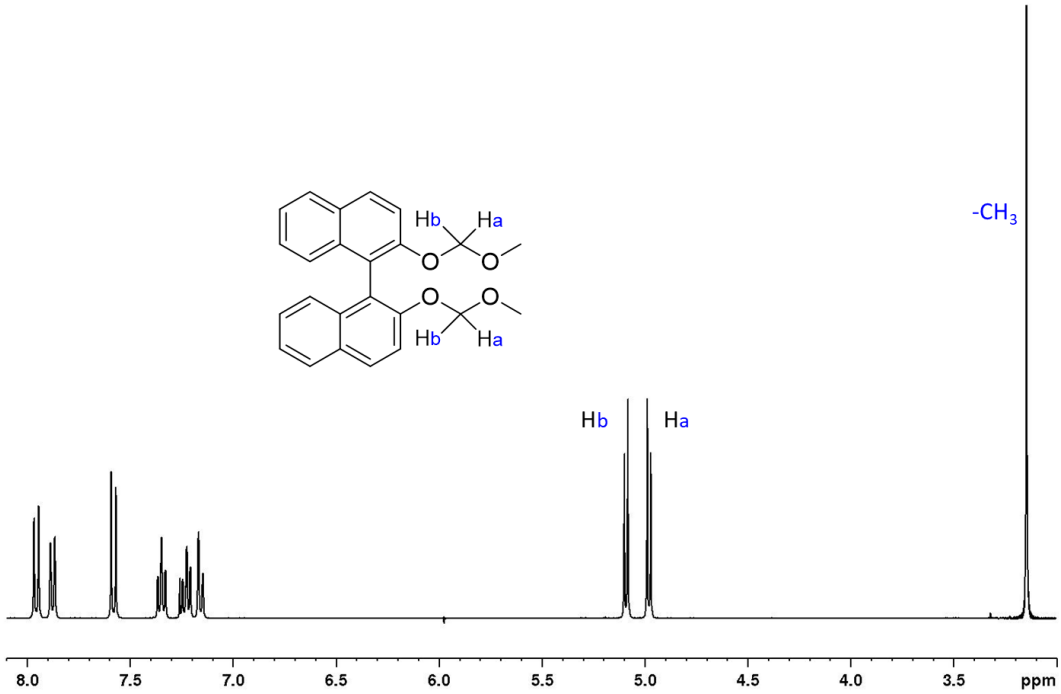

Figure 5.4 ^1H NMR spectrum (400 MHz, $CDCl_3$, 298 K) of 2,2'-bis(methoxymethoxy)-1,1'-binaphthalene.

^1H NMR (400 MHz, $CDCl_3$, 298 K): δ 7.97 (d, J = 9.2 Hz, 2H, ArH), 7.88 (d, J = 8.0 Hz, 2H, ArH), 7.58 (d, = 9.2 Hz, 2H, ArH), 7.35 (td, J_1 = 6.8 Hz, J_2 = 1.2 Hz, 2H, ArH), 7.23 (td, J_1 = 8.4 Hz, J_2 = 1.2 Hz, 2H, ArH), 7.16 (d, J = 8.4 Hz, 2H, ArH), 5.09 (d, J = 6.8 Hz, 2Hb), 4.98 (d, J = 6.8 Hz, 2Ha), 3.15 (s, 6H, $-CH_3$).

PREPARATION AND CHARACTERIZATION OF 2,2'-bis(methoxymethoxy)-[1,1'-binaphthalene]-3,3'-dicarbaldehyde

Under nitrogen, 2,2'-bis(methoxymethoxy)-1,1'-binaphthalene (1.7 g, 4.50 mmol) was dissolved in THF dry (70 mL) and the flask was cooled to 0 °C. n-Butyllithium (2.5 M in hexane, 6.0 mL, 15.0 mmol) was dropwise to the solution and the mixture was allowed to stir for 3 h to room temperature, obtaining a grey suspension. After the mixture was cooled again to 0 °C, DMF (1.3 mL, 16.4 mmol) was added slowly. The flask was warmed to room temperature and the mixture was allowed to stir overnight. The reaction was quenched with saturated NH_4Cl (35 ml) and was extracted with ethyl acetate. The combined organic extracts were washed with brine and dried over $MgSO_4$. The solvent was removed under vacuum and the compound was purified by column chromatography over silica gel eluted with 10 % ethyl acetate in toluene. Yield 35 %

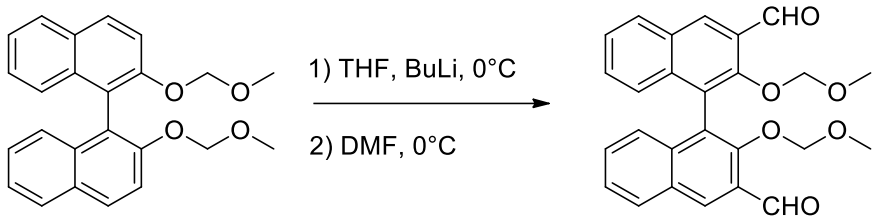

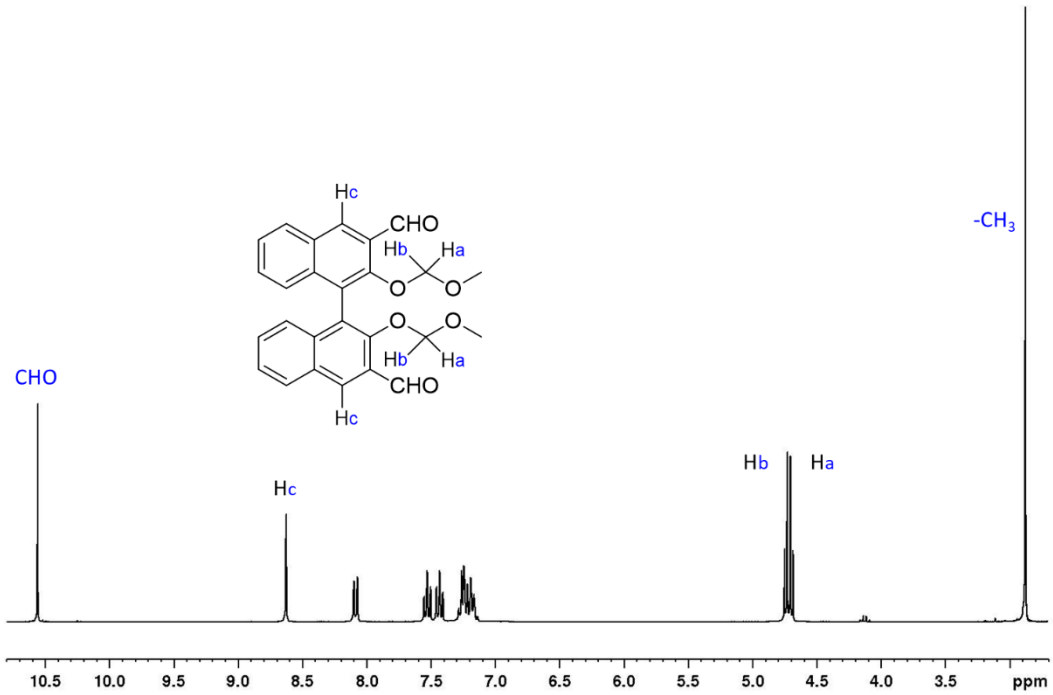

Figure 5.5 ^{1}H NMR spectrum (300 MHz, $CDCl_3$, 298 K) of 2,2'-bis(methoxymethoxy)-[1,1'-binaphthalene]-3,3'-dicarbaldehyde.

^{1}H NMR (300 MHz, $CDCl_3$, 298 K): δ 10.5 (s, 2H, -CHO), 8.62 (s, 2Hc), 8.08 (dd, J_1 = 8.1 Hz, J_2 = 0.6 Hz, 2H, ArH), 7.52 (td, J_1 = 6.9 Hz, J_2 = 1.2 Hz, 2H, ArH), 7.42 (td, J_1 = 8.4 Hz, J_2 = 1.4 Hz, 2H, ArH), 7.24 (d, J = 9.0 Hz, 2H, ArH), 4.74 (d, J = 6.0 Hz, 2Hb), 4.70 (d, J = 6.3 Hz, 2Ha), 2.87 (s, 6H, -CH_3).

PREPARATION AND CHARACTERIZATION OF 2,2'-dihydroxy-[1,1'-binaphthalene]-3,3'-dicarbaldehyde

2,2'-bis(methoxymethoxy)-[1,1'-binaphthalene]-3,3'-dicarbaldehyde (0.32 g, 0.739 mmol) was dissolved in THF (5 ml) and the flask was warmed to 0 °C. HCl (12 M, 3.0 mL, 36.0 mmol) was added slowly to the solution and the mixture was allowed to stir at room temperature for 3 h. The reaction was extracted with ethyl acetate. The combined organic extracts were washed with saturated $NaHCO_3$, and brine and dried over $MgSO_4$. The solvent was removed under vacuum obtaining a yellow solid. Yield 82 %

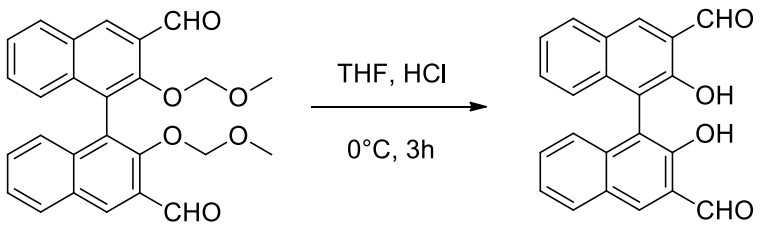

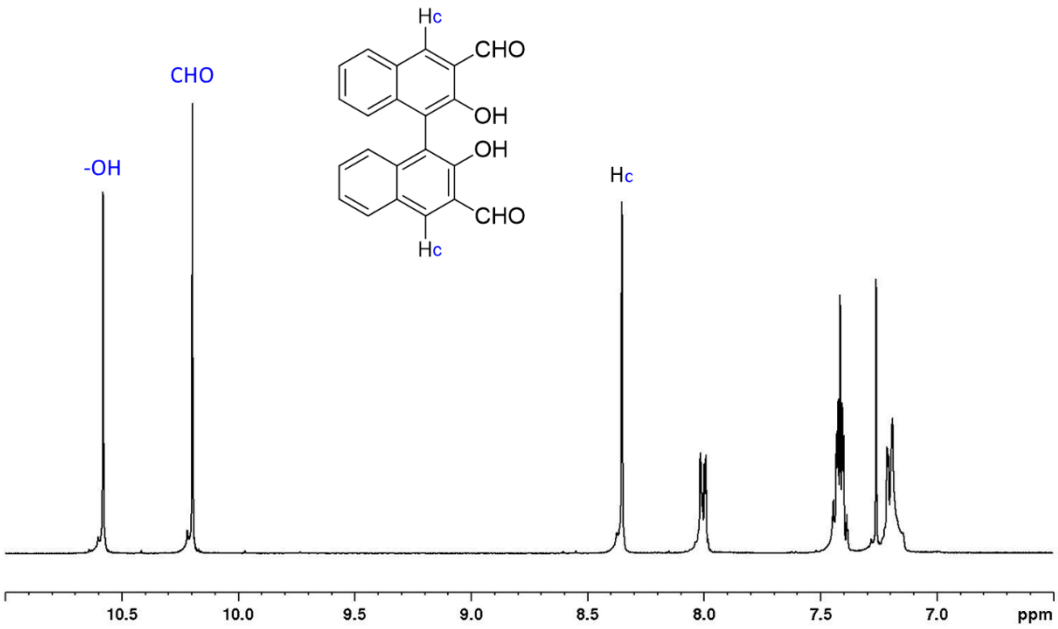

Figure 5.6 ^{1}H NMR spectrum (300 MHz, $CDCl_3$, 298 K) of 2,2'-dihydroxy-[1,1'-binaphthalene]-3,3'-dicarbaldehyde.

^{1}H NMR (300 MHz, $CDCl_3$, 298 K): δ 10.6 (s, 2H, -OH), 10.2 (s, 2H, -CHO), 8.35 (s, 2Hc), 7.99 (m, 2H, ArH), 7.41 (m, 4H, ArH), 7.20 (m, 2H, ArH).

PREPARATION AND CHARACTERIZATION OF ligand (S)-LH_2

2,2'-dihydroxy-[1,1'-binaphthalene]-3,3'-dicarbaldehyde (0.20 g, 0.599 mmol) was dissolved in MeOH dry (10 ml) and the 2-(2-pyridine)ethylamine (0.15 g, 1.20 mmol) was added. The solution was allowed to stir overnight at reflux. The solvent was removed under vacuum, obtaining the desired product as an orange oil. Yield 62 %

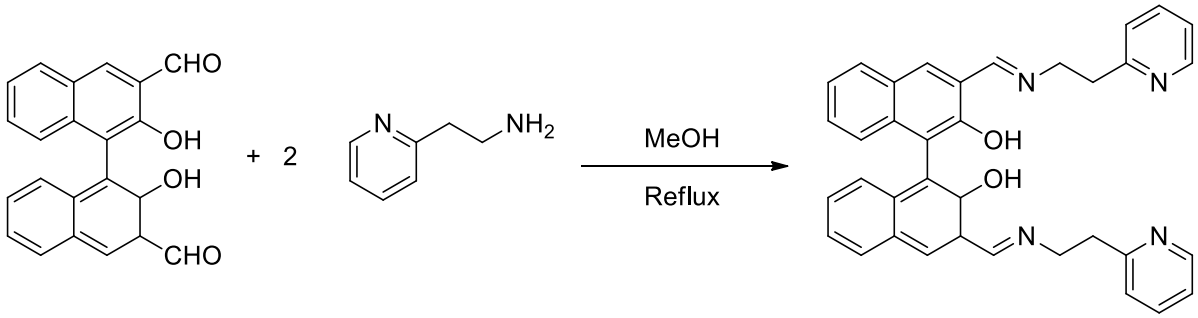

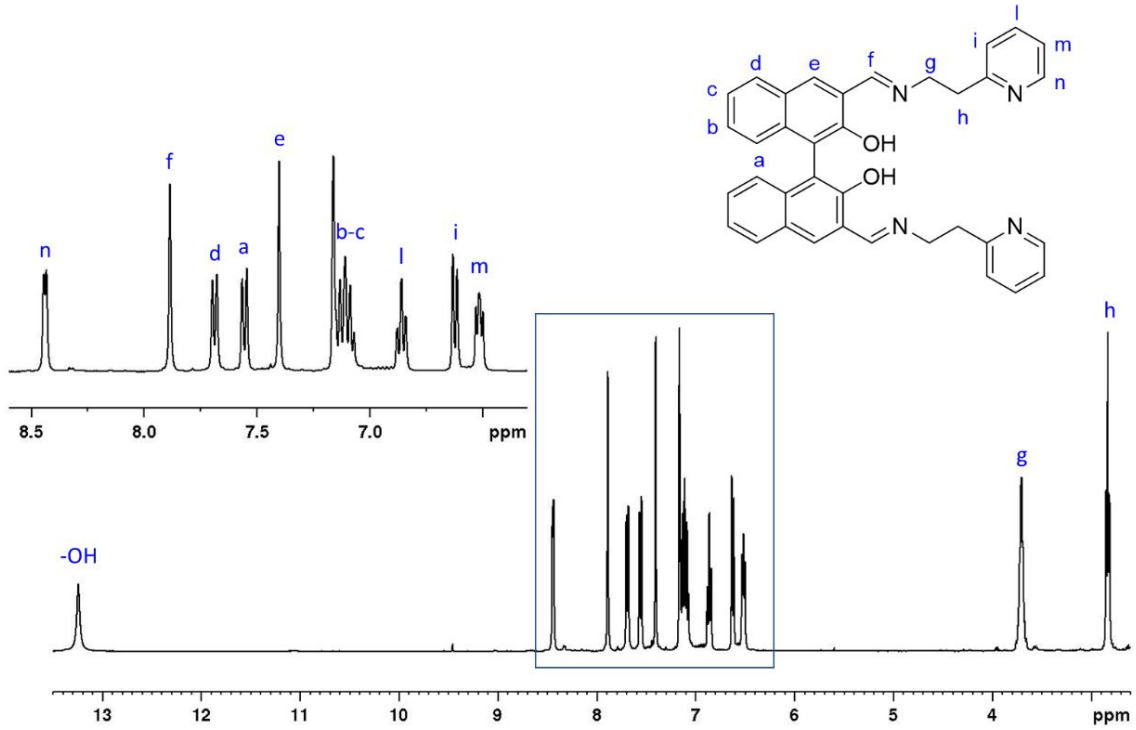

Figure 5.7 ^{1}H NMR spectrum (400 MHz, C_6D_6, 298 K) of ligand (S)-LH_2.

^{1}H NMR (400 MHz, C_6D_6, 298 K): δ 13.2 (s, 2H, -OH), 8.44 (d, J = 4.4 Hz, 2H, Hn), 7.88 (s, 2H, Hf), 7.68 (d, J = 7.8 Hz, 2H, Hd), 7.55 (d, J = 8.1 Hz, 2H, Ha), 7.40 (s, 2H, He), 7.10 (m, 4H, Hb-Hc), 6.85 (t, J = 6.8 Hz, 2H, Hl), 6.62 (d, J = 7.7 Hz, 2H, Hi), 6.51 (t, J = 6.8 Hz, 2H, Hm), 3.70 (m, 4H, Hg), 2.83 (t, J = 6.8 Hz, 4H, Hh).

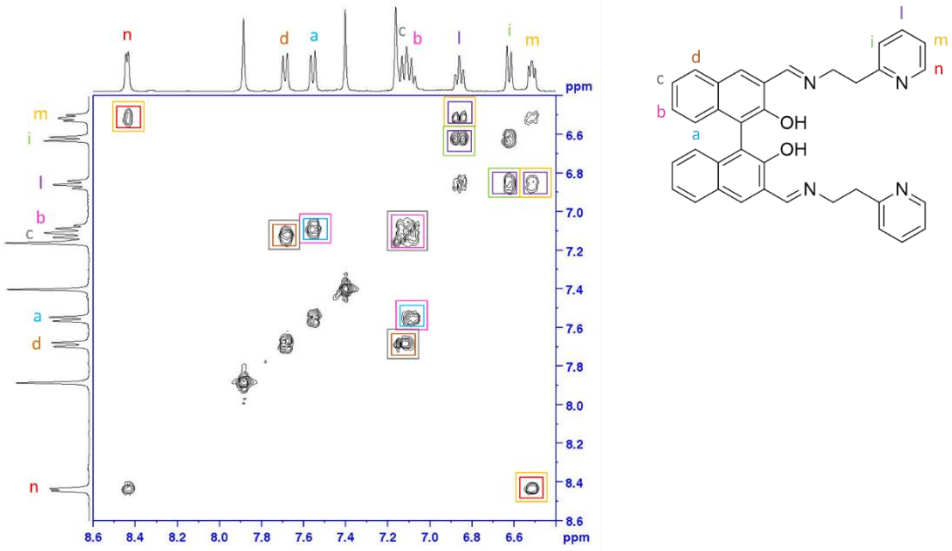

Figure 5.8 COSY spectrum (400 MHz, C_6D_6, 298 K) of ligand (S)-LH_2.

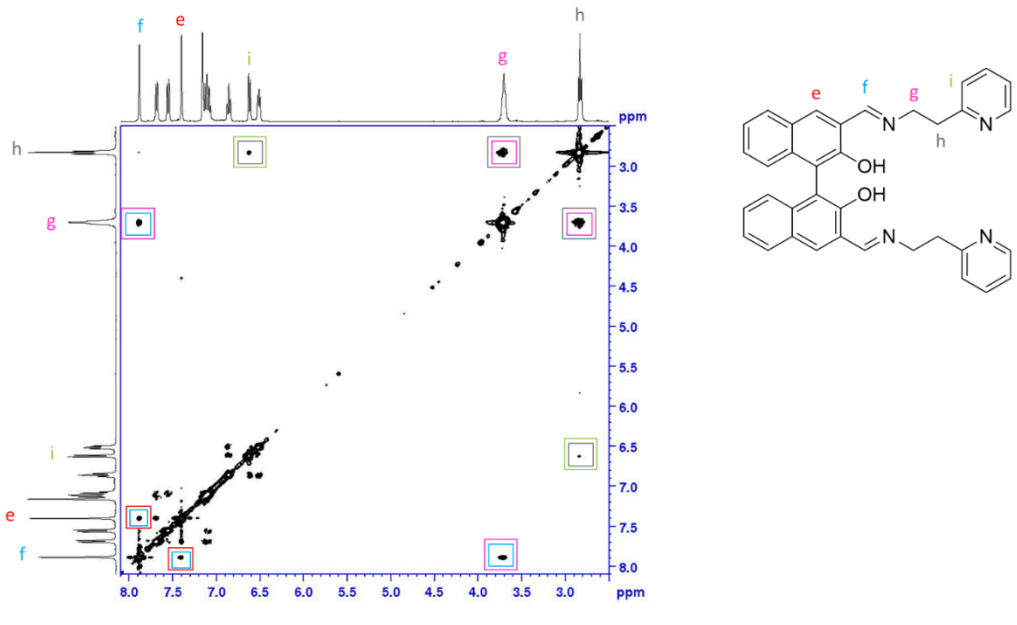

Figure 5.9 NOESY spectrum (400 MHz, C_6D_6, 298 K) of ligand (S)-LH_2.

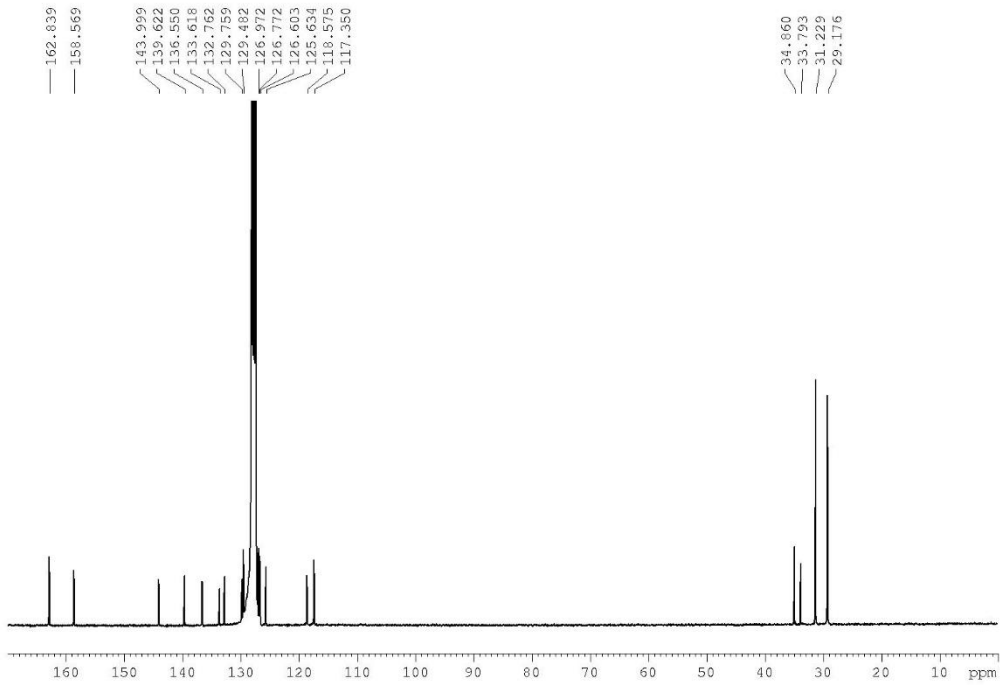

Figure 5.10 ^{13}C NMR spectrum (75 MHz, C_6D_6, 298 K) of ligand (S)-LH_2.

^{13}C NMR (75 MHz, C_6D_6, 298 K): δ 162.8, 158.6, 144.0, 139.6, 136.5, 133.6, 132.8, 129.8, 129.5, 127.0, 126.8, 126.6, 125.6, 118.6, 117.4, 34.9, 33.8, 31.2, 29.2.

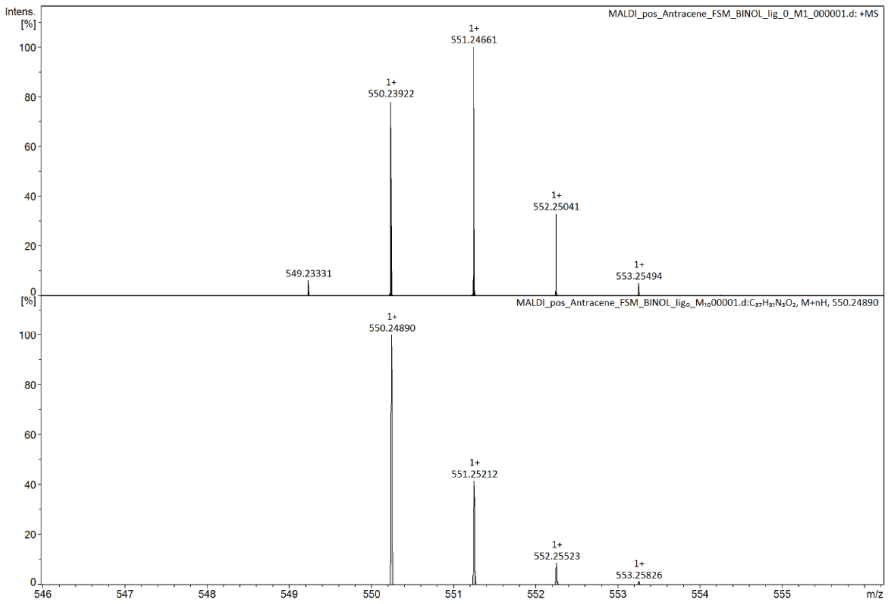

Figure 5.11 MALDI-FT-ICR MS spectrum of ligand (S)-LH_2.

Synthesis and characterization of complex (S)-1

In a glove box, zinc bis[bis(trimethylsilyl)amide] (0.29 g, 0.726 mmol) was dissolved in benzene (0.5 ml). Ligand (S)-LH_2 (0.20 g, 0.363 mmol) was dissolved in benzene (6 ml) and was slowly added to the solution of the zinc complex. The solution was allowed to stir for 2 h. The solvent was removed under vacuum, and the residue was washed with hexane. The desired product is an orange powder. Yield 73 %

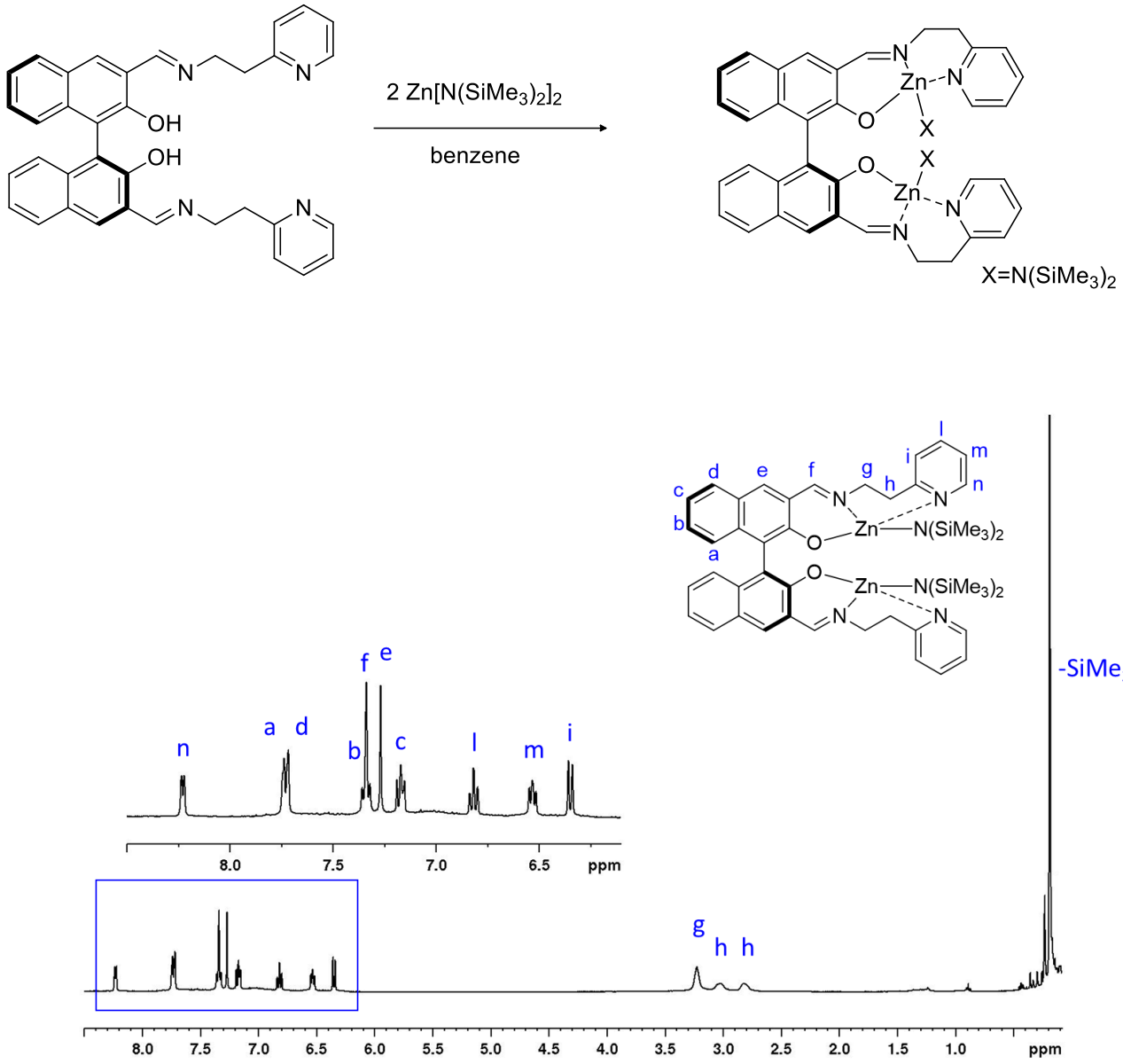

Figure 5.12 ^{1}H NMR spectrum (400 MHz, C_6D_6, 298 K) of complex (S)-**1**.

^{1}H NMR (400 MHz, C_6D_6, 298 K): δ 8.23 (d, J = 5.0 Hz, 2H, Hn), 7.74 (m, 4H, Ha-Hd), 7.34 (m, 4H, Hb-Hf), 7.27 (s , 2H, He), 7.17 (t, J = 7.7 Hz, 2H, Hc), 6.81 (t, J = 7.7 Hz, 2H, Hl), 6.53 (t, J = 6.4 Hz, 2H, Hm), 6.34 (d, J = 7.7 Hz, 2H, Hi), 3.22 (m, 4H, Hg), 3.02 (m, 2H, Hh), 2.80 (m, 2H, Hh), 0.19 (s, 18H, -N($SiMe_3$)$_2$).

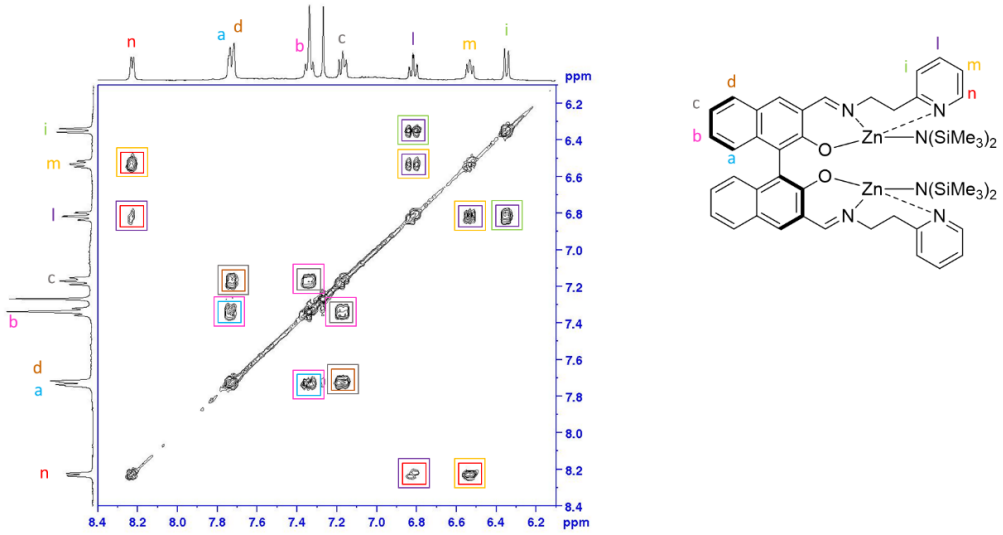

Figure 5.13 COSY spectrum (400 MHz, C_6D_6, 298 K) of complex (S)-**1**.

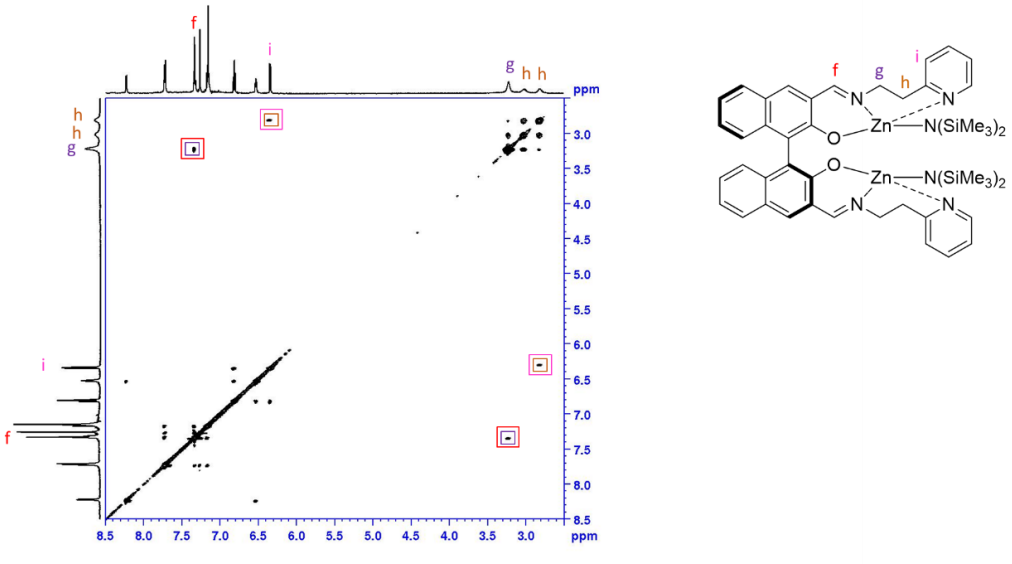

Figure 5.14 Aromatic region of NOESY spectrum (400 MHz, C_6D_6, 298 K) of complex (S)-**1**.

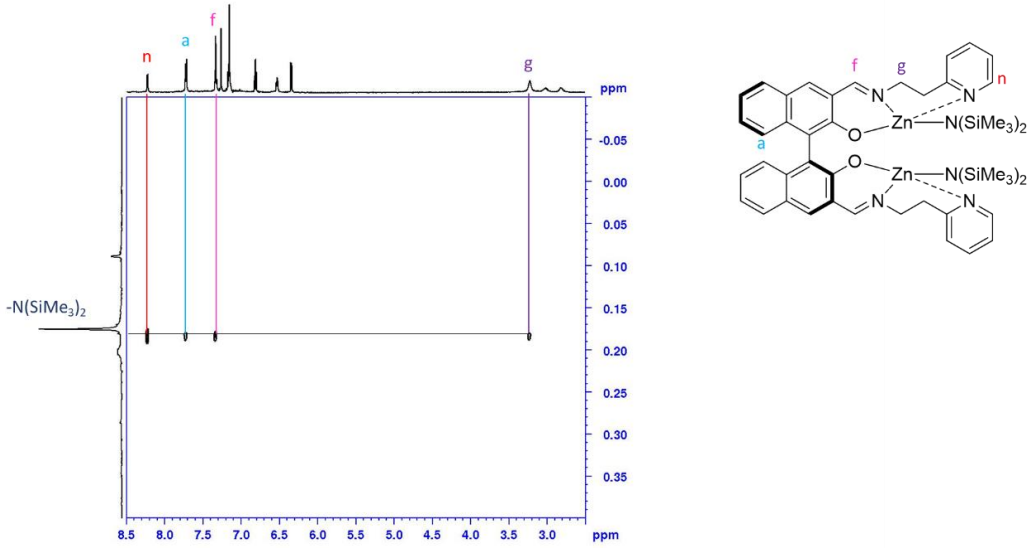

Figure 5.15 NOESY spectrum (400 MHz, C_6D_6, 298 K) of complex (S)-**1**.

DOSY-NMR experiment details[17]

A measurement of diffusion has been carried out by observing the attenuation of the NMR signals during a pulsed field gradient experiment using the double stimulated echo pulse sequence. In particular, 2D DOSY PGSE NMR spectra were performed on a Bruker Avance 600 spectrometer at 298 K without spinning. Tetrakistrimethylsilylsilane (TMSS) was added as the internal standard. The dependence of the resonance intensity (*I*) on the gradient strength (*G*) is described by the following equation:

$$I = I_0 \exp\{-D\gamma^2 G^2 \delta^2 (\Delta - \delta/3)\}$$

where *I* is the observed intensity (attenuated signal intensity), I_0 is the reference intensity (unattenuated signal intensity), *D* is the diffusion coefficient, γ is the nucleus gyromagnetic ratio, *G* is the gradient strength, δ is the gradient duration, and Δ is the diffusion delay. The parameters δ and Δ were kept constant during the experiments, whereas *G* varied from 5 to 95% in 32 steps.

The molecular masses in solution (m) were simply estimated using Graham's law of diffusion: $D = K\sqrt{\frac{T}{m}}$, where the constant K depends on geometric factors, including the area over which the diffusion is occurring. By assuming a constant temperature and that K is the same for both species in solution, the relative diffusion rate of two species a and b is given by the equation shown below:

$$\frac{D_a}{D_b} = \sqrt{\frac{m_b}{m_a}}$$

This allows the calculation of an unknown molecular mass. The experimentally determined values of D are shown in **Figure 5.16**.

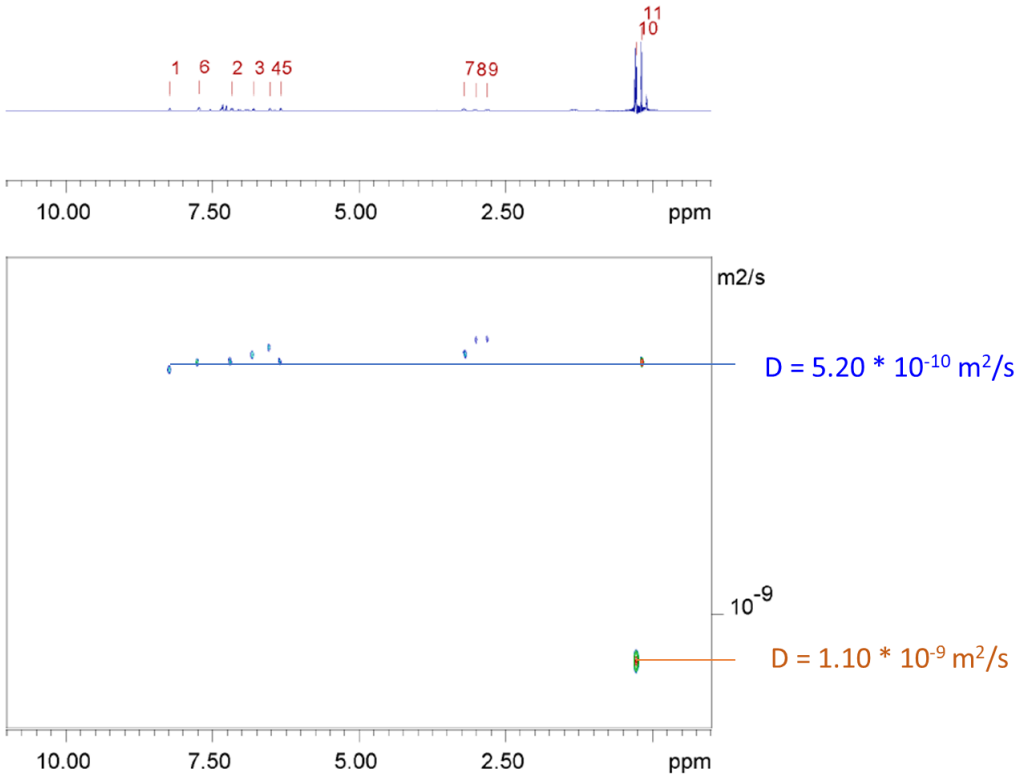

Figure 5.16 DOSY spectrum (600 MHz, C_6D_6, 298 K) of complex (S)-**1** ($D = 5.20\ 10^{-10}$ $m^2\ s^{-1}$) in the presence of tetrakis(trimethylsilyl)silane TMSS as standard ($D = 1.10\ 10^{-9}$ $m^2\ s^{-1}$).

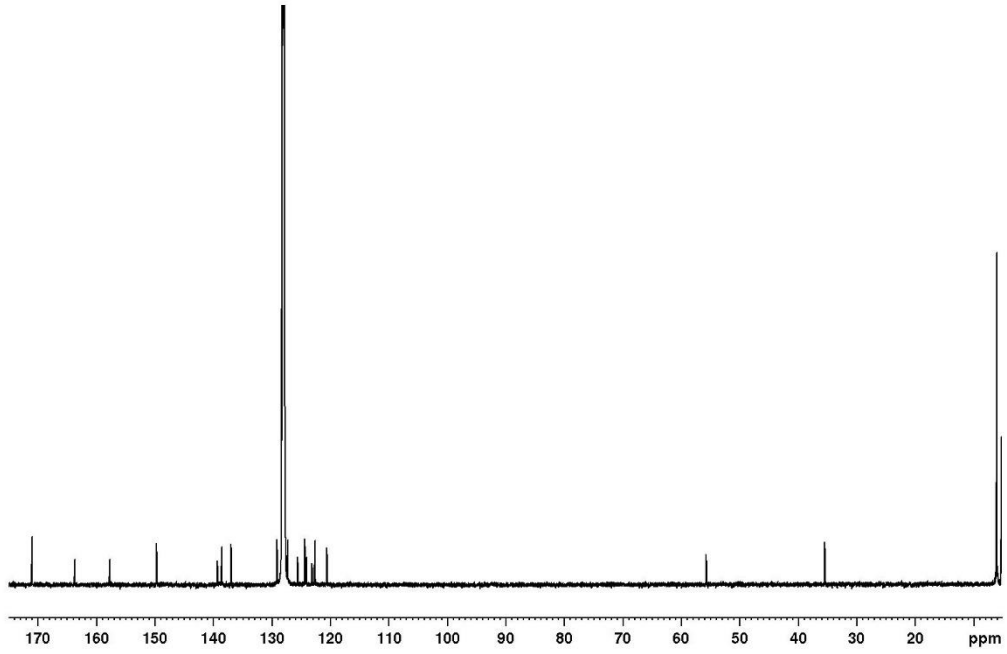

Figure 5.17 ^{13}C NMR spectrum (100 MHz, C_6D_6, 298 K) of complex (S)-**1**.

^{13}C NMR (100 MHz, C_6D_6, 298 K): δ 171.0, 163.7, 157.7, 149.6, 139.3, 138.5, 136.9, 129.1, 127.2, 125.5, 124.3, 124.0, 123.1, 122.6, 120.5, 55.7, 35.4, 6.0.

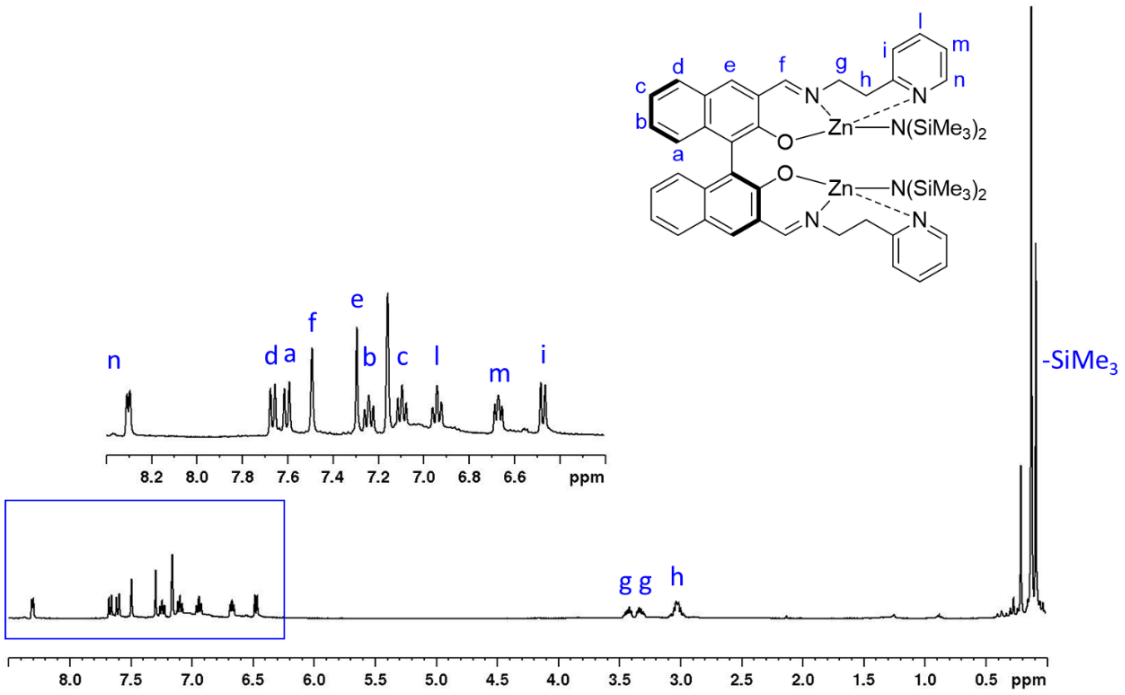

Figure 5.18 ^{1}H NMR spectrum (400 MHz, C_6D_6, 343 K) of complex (S)-**1**.

^{1}H NMR (400 MHz, C_6D_6, 343 K): δ 8.30 (d, J = 5.0 Hz, 2H, Hn), 7.66 (d, J = 8.2 Hz, 2H, Hd), 7.60 (d, J = 8.7 Hz, 2H, Ha), 7.49 (s, 2H, Hf), 7.29 (s, 2H, He), 7.24 (t, J = 7.3 Hz, 2H, Hb), 7.09 (t, J = 7.4 Hz, 2H, Hc), 6.94 (t, J = 7.6 Hz, 2H, Hl), 6.67 (t, J = 6.2 Hz, 2H, Hm), 6.47 (d, J = 7.7 Hz, 2H, Hi), 3.41 (m, 2H, Hg), 3.32 (m, 2H, Hg), 3.01 (m, 4H, Hh), 0.12 (s, 18H, -N($SiMe_3$)$_2$).

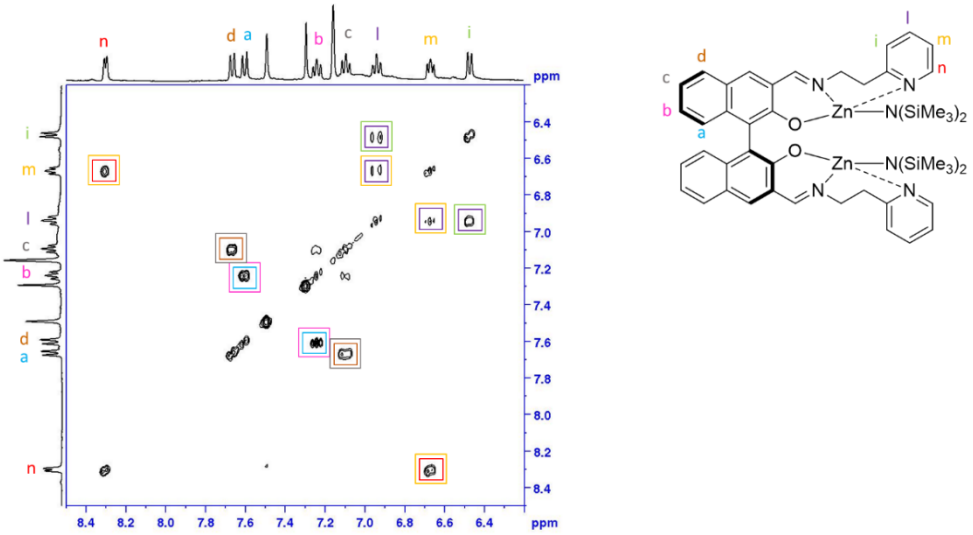

Figure 5.19 *COSY* spectrum (400 MHz, C_6D_6, 343 K) of complex (S)-**1**.

Synthesis and characterization of complex *rac*-1

The preparation procedure was the same as that of complex (*S*)-**1** with the use of ligand *rac*-LH_2 as the starting material.

In a glove box, zinc bis[bis(trimethylsilyl)amide] (0.22 g, 0.545 mmol) was dissolved in benzene (0.5 ml). Ligand *rac*-LH_2 (0.15 g, 0.272 mmol) was dissolved in benzene (5 ml) and was slowly added to the solution of the zinc complex. The solution was allowed to stir for 2 hours. The solvent was removed under vacuum, and the residue was washed with hexane. The desired product is a red powder. Yield 80 %

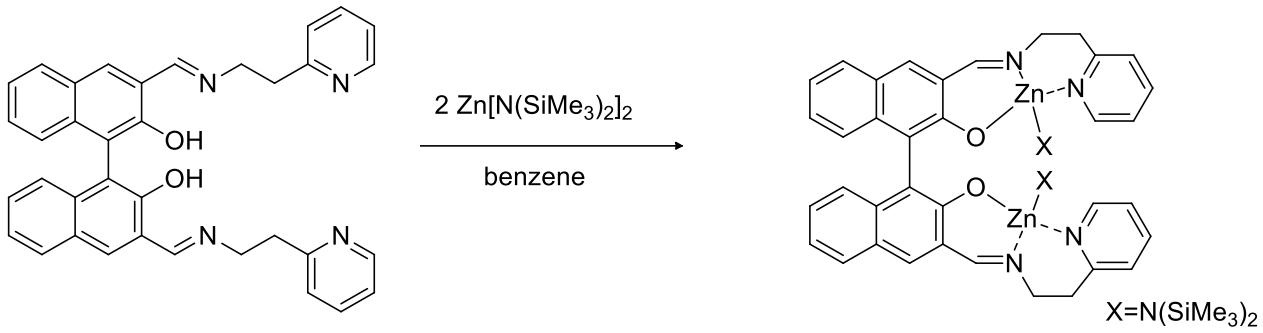

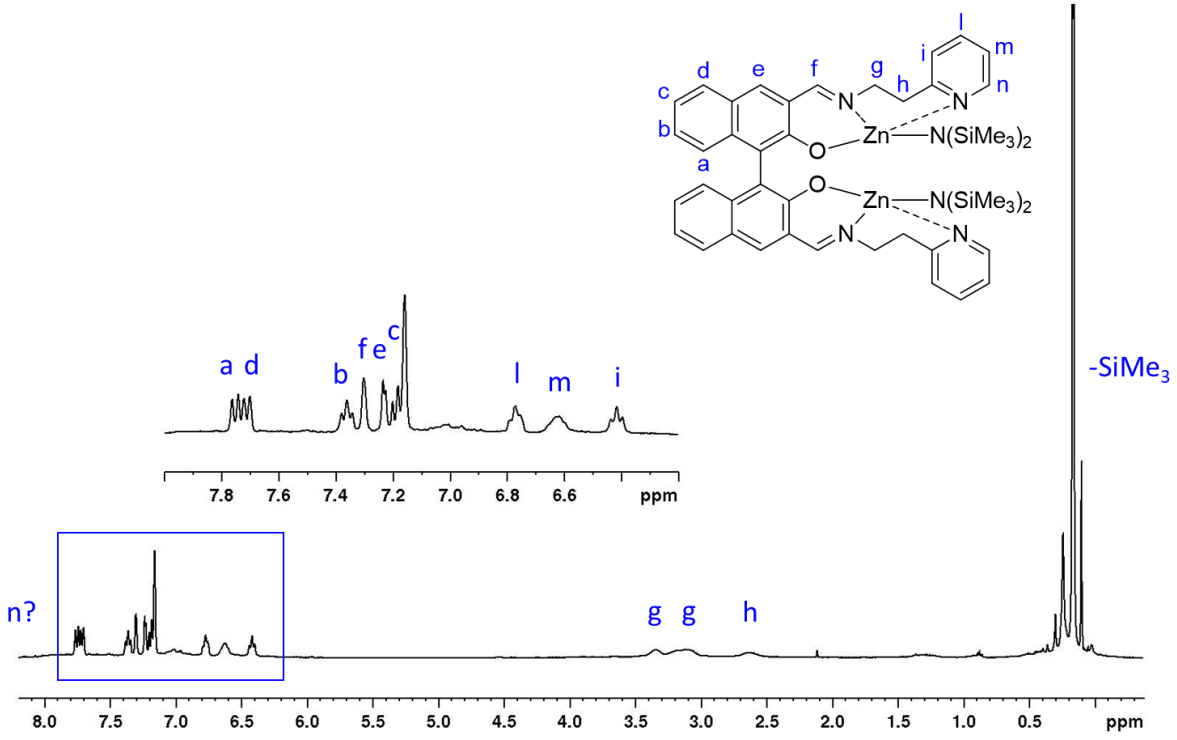

Figure 5.20 ^{1}H NMR spectrum (600 MHz, C_6D_6, 298 K) of complex *rac*-**1**.

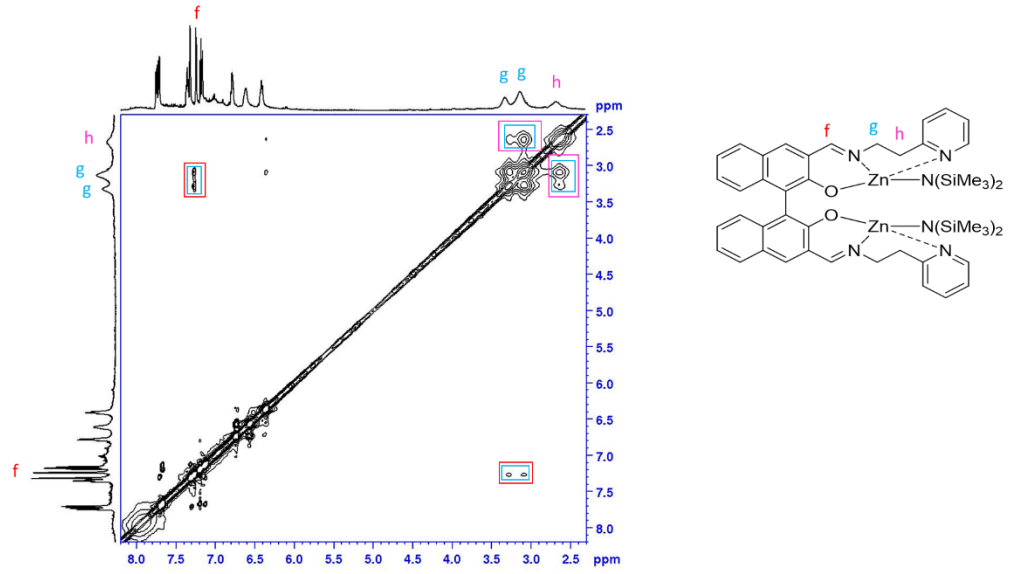

Figure 5.21 NOESY spectrum (600 MHz, C_6D_6, 298 K) of complex *rac*-**1**.

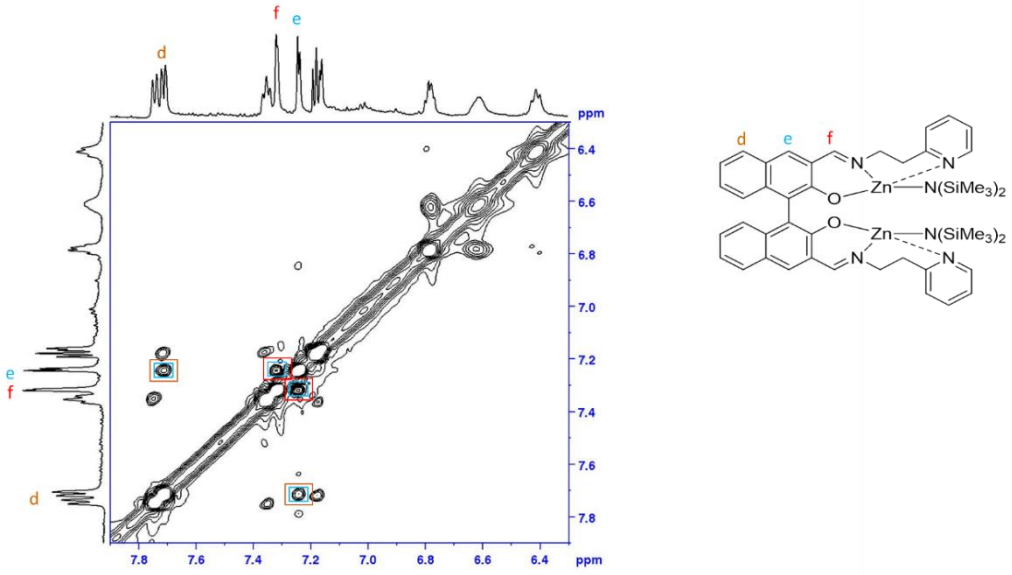

Figure 5.22 Aromatic region NOESY spectrum (600 MHz, C_6D_6, 298 K) of complex *rac*-**1**.

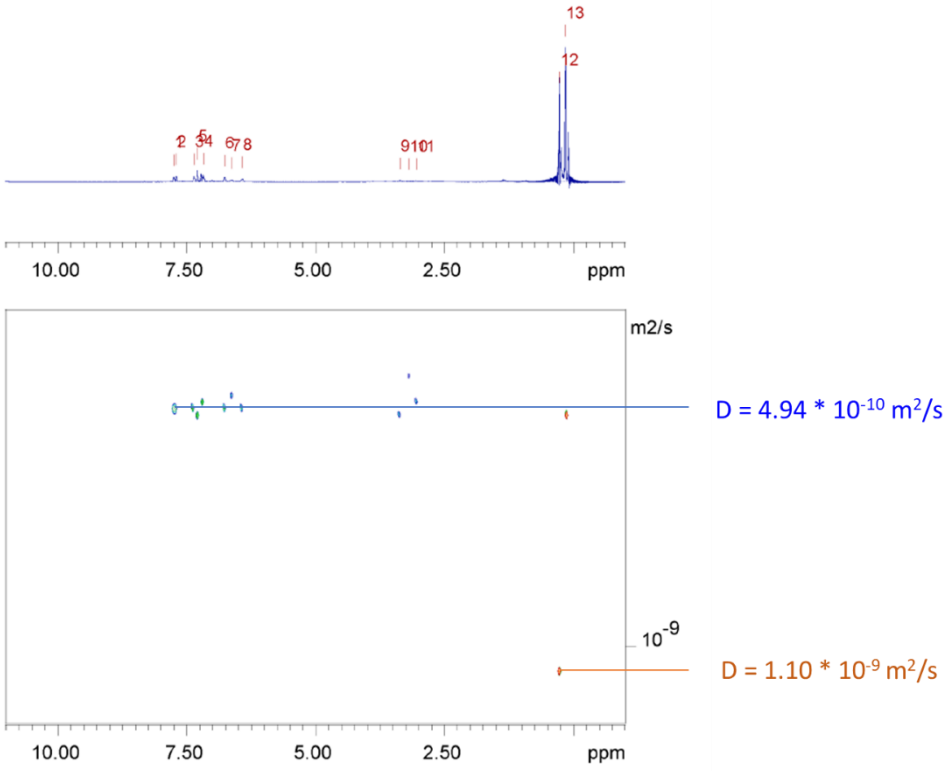

Figure 5.23 DOSY spectrum (600 MHz, C_6D_6, 298 K) of complex *rac*-**1** (D = 4.94 10^{-10} m^2 s^{-1}) in the presence of tetrakis(trimethylsilyl)silane TMSS as standard (D = 1.10 10^{-9} m^2 s^{-1}).

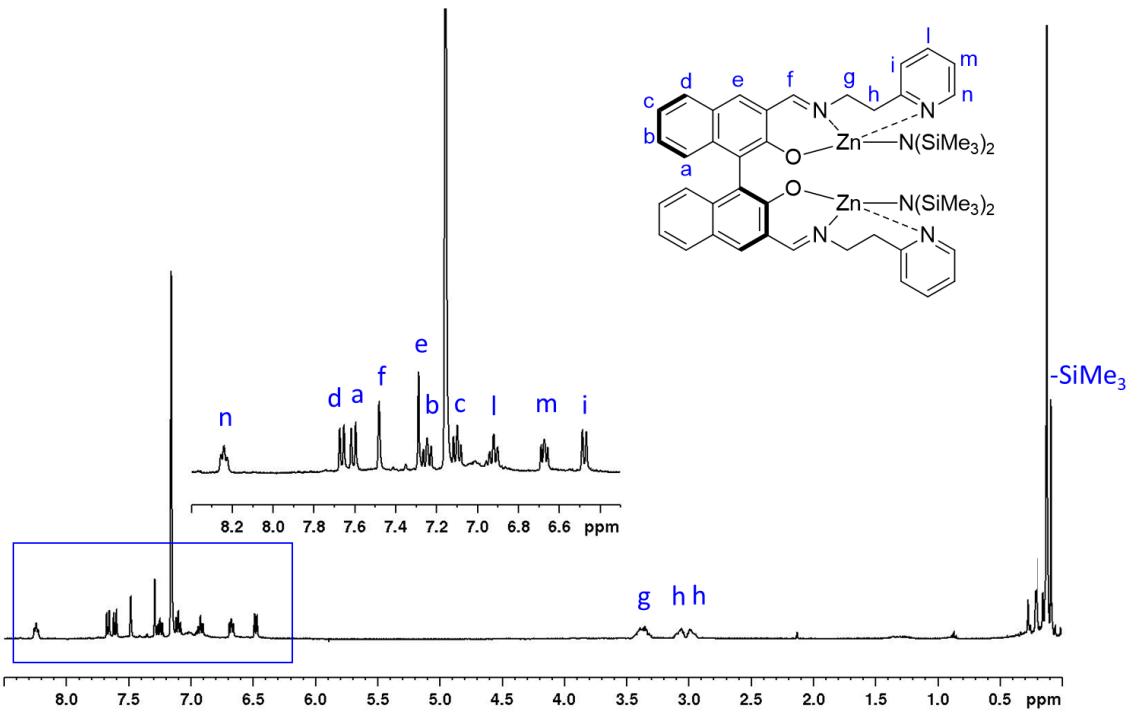

Figure 5.24 ^{1}H NMR spectrum (600 MHz, C_6D_6, 343 K) of complex *rac*-**1**.

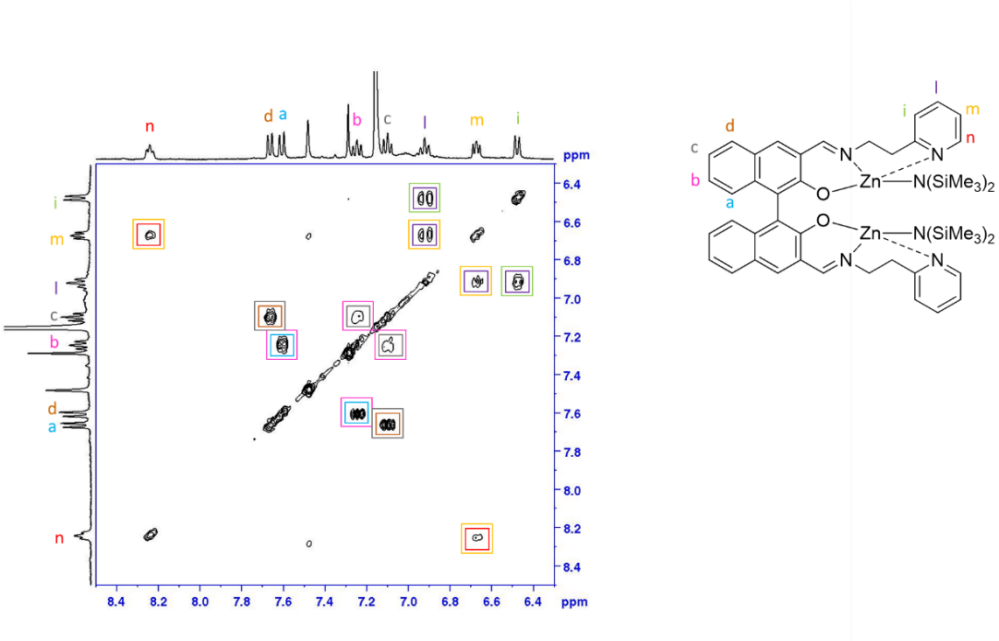

Figure 5.25 COSY spectrum (400 MHz, C_6D_6, 343 K) of complex *rac*-**1**.

Kinetic Studies

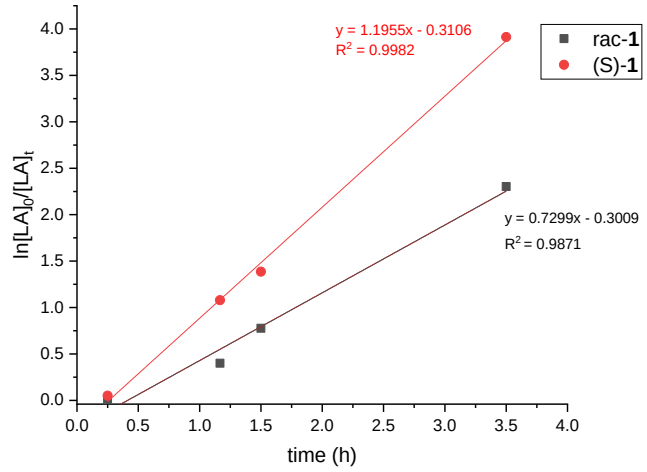

time (h)	Conversion (%)	
	rac-**1**	(S)-**1**
0.25	0	5
1.16	33	66
1.50	54	75
3.50	90	98

Figure 5.26 Kinetic plot of the *rac*-LA conversion vs the reaction time, using *rac*-**1** and (S)-**1**. Reaction conditions: Zn = 8 μmol; [*rac*-LA] : [**Zn**] = 200:1; T = 298 K. Pseudofirst-order rate is k_{obs} = 1.1955 h^{-1} at 25 °C (R^2 = 0.9982) with *rac*-**1**, and k_{obs} = 0.7299 h^{-1} at 25 °C (R^2 = 0.9871) with (S)-**1**.

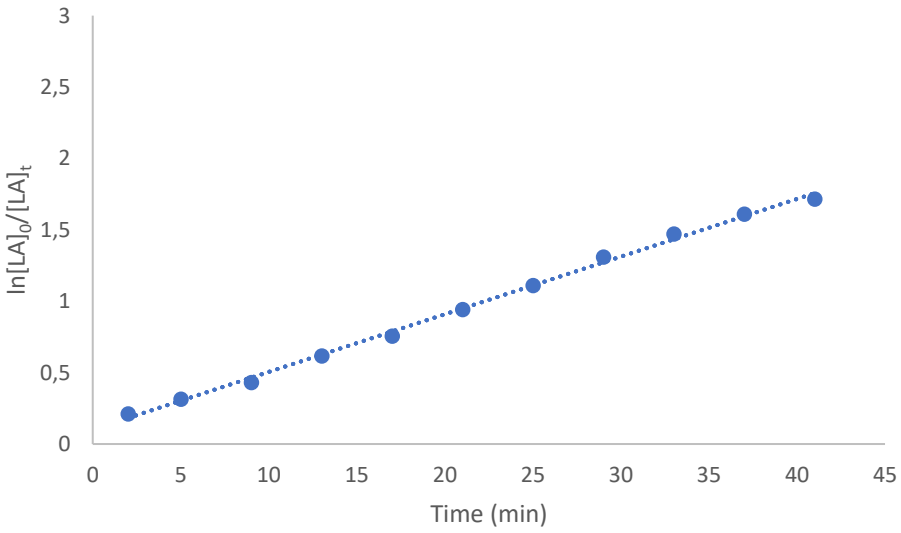

Figure 5.27 Kinetic plot of the *rac*-LA conversion vs the reaction time. Reaction conditions: Zn = 8 μmol; [*rac*-LA] : [(S)-**1**] : [BnOH] = 500:1:4; T = 298 K. Pseudofirst-order rate is k_{obs} = 0.0404 min^{-1} at 25 °C (R^2 = 0.9972) in CH_2Cl_2 solution.

General procedure for the polymerization of lactide

The polymerization experiments conducted at room temperature were carried out in a glove box, under inert conditions. In a Braun Labmaster glovebox, a magnetically stirred reactor flask was charged with lactide. The complex (8.5 mg, $8.0 \cdot 10^{-6}$ mol) and 2 equiv. of ROH (0.1 M of iPrOH or BnOH in the solvent) were added in a 2 mL vial and the mixture was stirred for 15 min, then transferred in the monomer. The polymerization was stopped using dichloromethane, after taking the vial out of the glove box. The solvent was removed under reduced pressure, the polymer was dried in a vacuum oven and characterized by NMR spectroscopy, MALDI MS and/or GPC analysis. For the polymerization experiment carried out under industrial conditions, the zinc complex (5.0 mg, $5.0 \cdot 10^{-6}$ mol) and the monomer (3.60 g, $2.5 \cdot 10^{-2}$ mol) were transferred into a 50 ml Schlenk flask. Subsequently, BnOH ($2.5 \cdot 10^{-4}$ mol) was added: after that, the Schlenk flask was closed, pulled out of the glove box and immersed in a thermostated oil bath at the temperature of 150°C. After the reaction time, the polymerization was stopped using dichloromethane. The solvent was removed under reduced pressure and the polymer was dried and characterized.

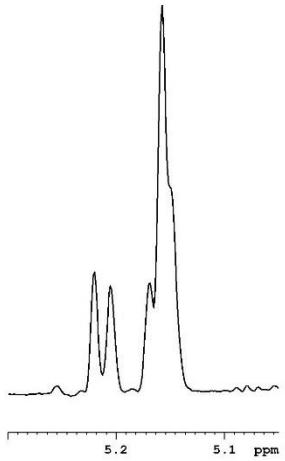

Figure 5.28 Methine region of the homonuclear decoupled ^{1}H NMR spectrum ($CDCl_3$, RT, 400 MHz) of PDLLA (entry 3 **Table 5.1**).

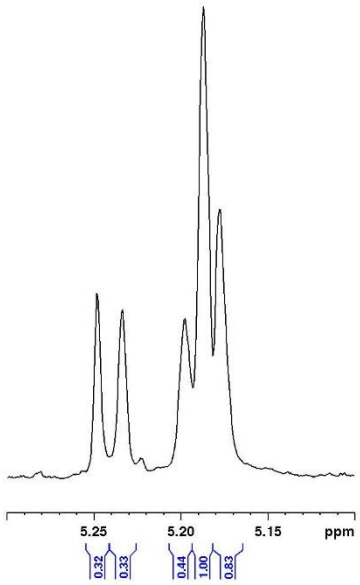

Figure 5.29 Methine region of the homonuclear decoupled ^{1}H NMR spectrum ($CDCl_3$, RT, 400 MHz) of PDLLA (entry S1, **Table 5.2**).

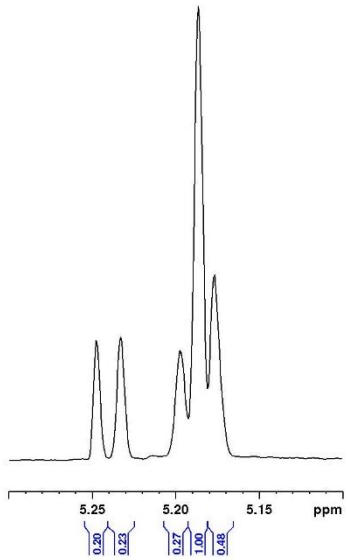

Figure 5.30 Methine region of the homonuclear decoupled ^{1}H NMR spectrum ($CDCl_3$, RT, 600 MHz) of PDLLA (entry 1, **Table 5.1**).

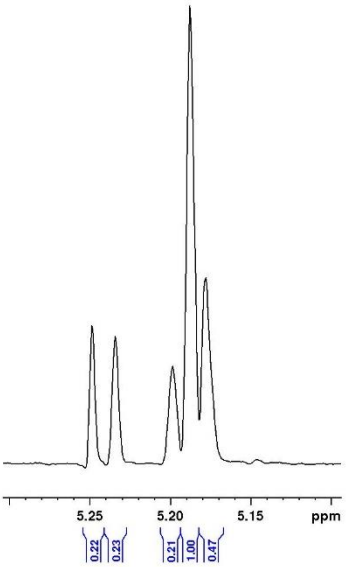

Figure 5.31 Methine region of the homonuclear decoupled ^{1}H NMR spectrum ($CDCl_3$, RT, 600 MHz) of PDLLA (entry 2, **Table 5.1**).

Table 5.2 Polymerization reactions of *rac*-LA under several conditions.

Entry	Mon (equiv)	Cocat (equiv)	Solvent (mL)	Temp (°C)	Time (min)	Conv (%)[a]	M_n^{th} (KDa)[b]	M_n^{MALDI} (KDa)[c]	M_n^{GPC} (KDa)[d]	Đ [d]
S1	*rac*-LA (100)	^{i}PrOH (2)	DCM (2)	-20	40’	44	3.2	-	-	-
S2	*rac*-LA (50)	^{i}PrOH (2)	DCM (2)	RT	1’	74	2.7	-	-	-
S3	*rac*-LA (50)	BnOH (2)	toluene (2)	RT	2	100	3.6	4.9	-	-
					15	-	-	-		
					45	-	-	-	0.4	2.7
S4	*rac*-LA (500)	BnOH (2)	toluene (2.5)	RT	5	67	24.1	-	22.6	1.05
					60	-	36.0	1.6	22.3	2.00
					5h	-		-	12.8	2.38
S5	*rac*-LA (500)	^{i}PrOH (2)	toluene (2)	RT	5	43	15.5	-	-	-
					10	87	31.3	-	-	-
					1h	100	-	2.4	17.0	2.09
S6	*rac*-LA (200)	BnOH (2)	toluene (2)	70	3h	100	-	2.3	1.4	4.9
S7	*rac*-LA (200)	BnOH (2)	toluene (2)	70	24’	100	-	2.5	2.8	3.8
S8	*rac*-LA (500)	BnOH (2)	toluene (5)	RT	17h	100	-	1.9	13.9	1.8
S9	*rac*-LA (500)	BnOH (2)	toluene (5)	RT	17h	100	-	1.7	26.0	1.5

General conditions: Complex (S)-1 = 8.0 µmol. [a] Conversion of lactides as determined by ^{1}H NMR spectral data. [b] M_n^{th} (in g · mol^{-1}) = 144.13 × ([LA]$_0$/[ROH]) × conversion LA. [c] Mn^{MALDI} (KDa) were deteminated by MALDI-FT-ICR MS in THF. [d] M_n^{GPC} (KDa) and Đ values were determined by GPC in THF against polystyrene standards and corrected using the factor 0.58 M_n^{GPC}.

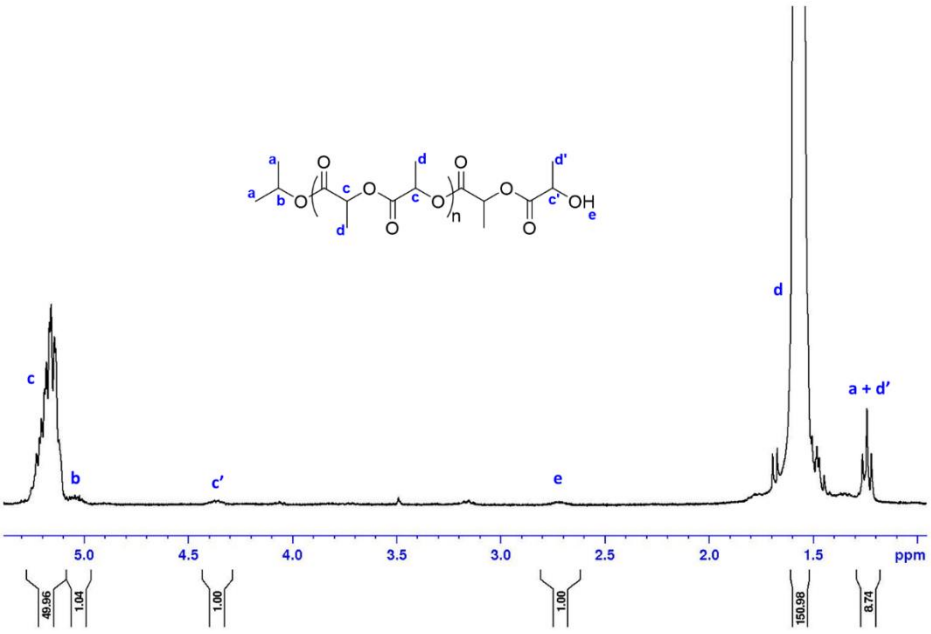

Figure 5.32 ^{1}H NMR spectrum (400 MHz, $CDCl_3$, 298 K) of PDLLA (entry 2, **Table 5.2**).

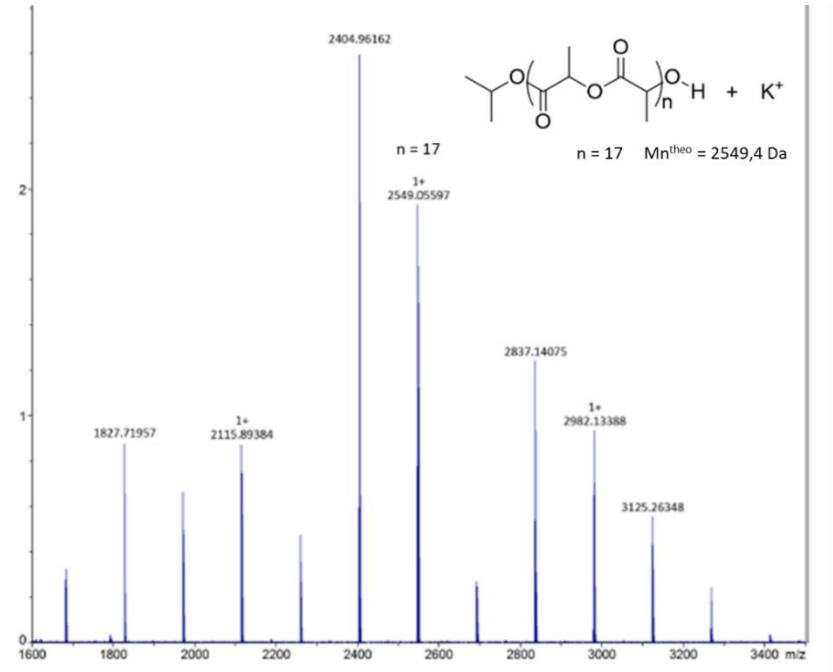

Figure 5.33 MALDI-FT-ICR MS spectrum of PDLLA (entry 2 after 0.5 min, **Table 5.2**).

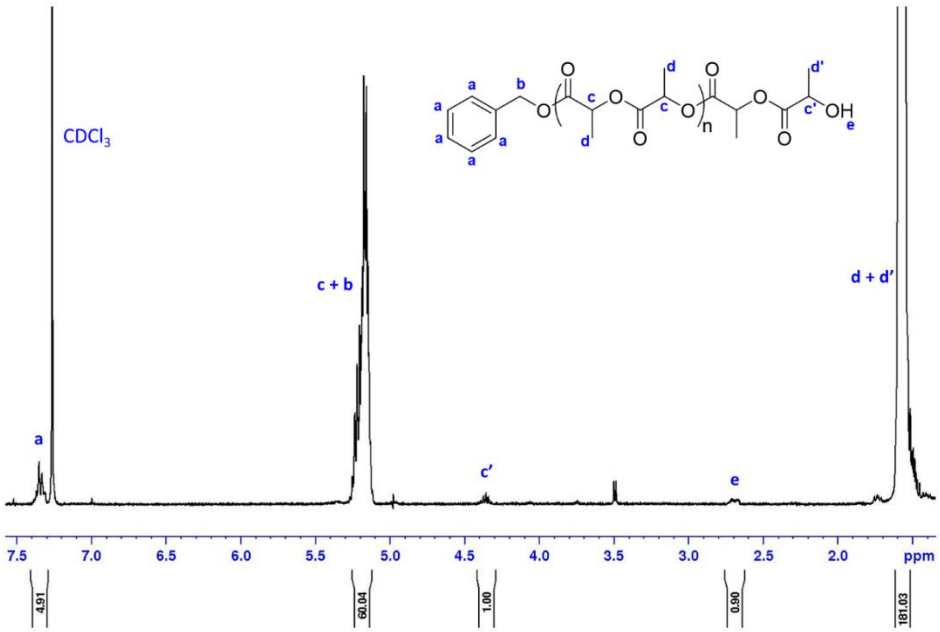

Figure 5.34 ^{1}H NMR spectrum (400 MHz, $CDCl_3$, 298 K) of PDLLA (entry 3, **Table 5.2**).

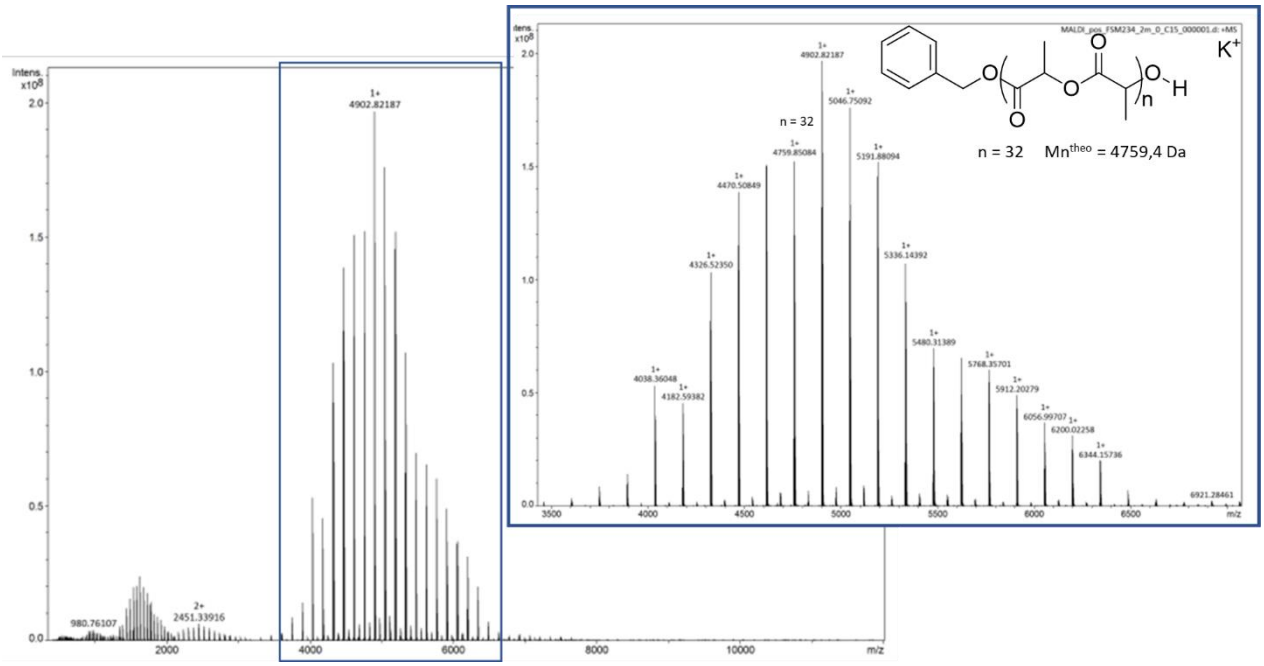

Figure 5.35 MALDI-FT-ICR MS spectrum of PDLLA (entry 3 after 0.5 min, **Table 5.2**).

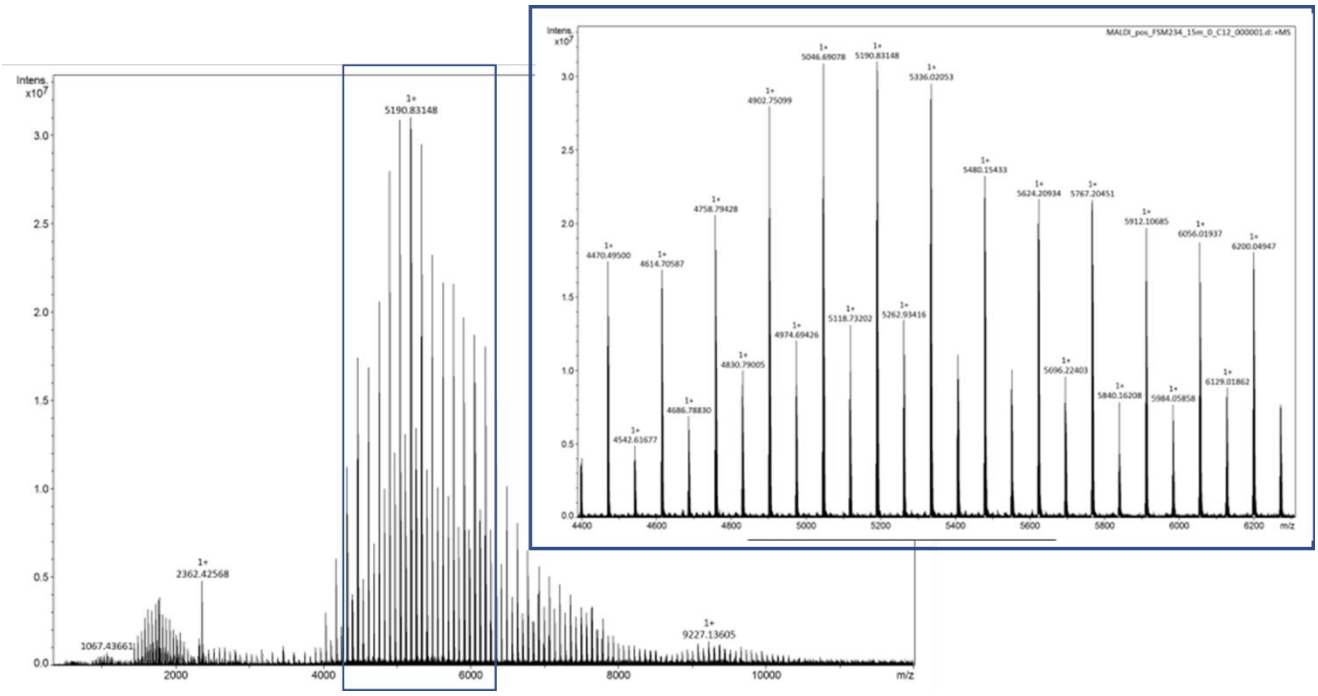

Figure 5.36 MALDI-FT-ICR MS spectrum of PDLLA (entry 3 after 15 min, **Table 5.2**).

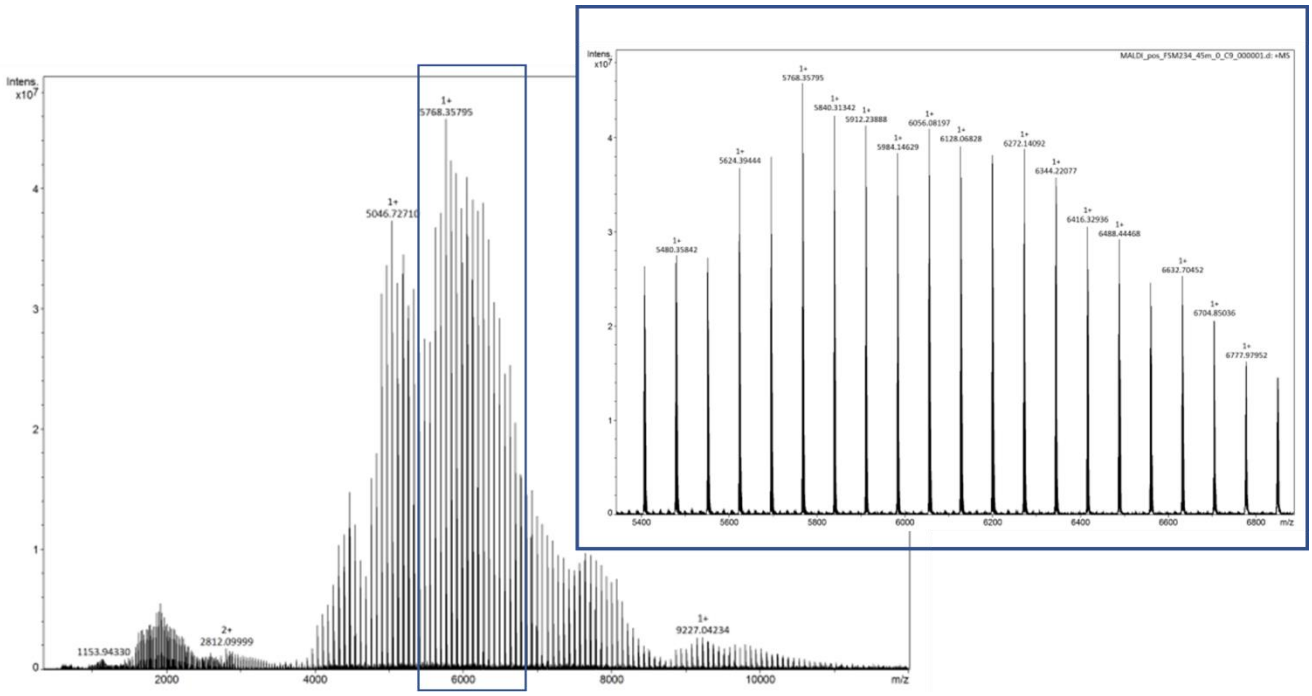

Figure 5.37 MALDI-FT-ICR MS spectrum of PDLLA (entry 3 after 45 min, **Table 5.2**).

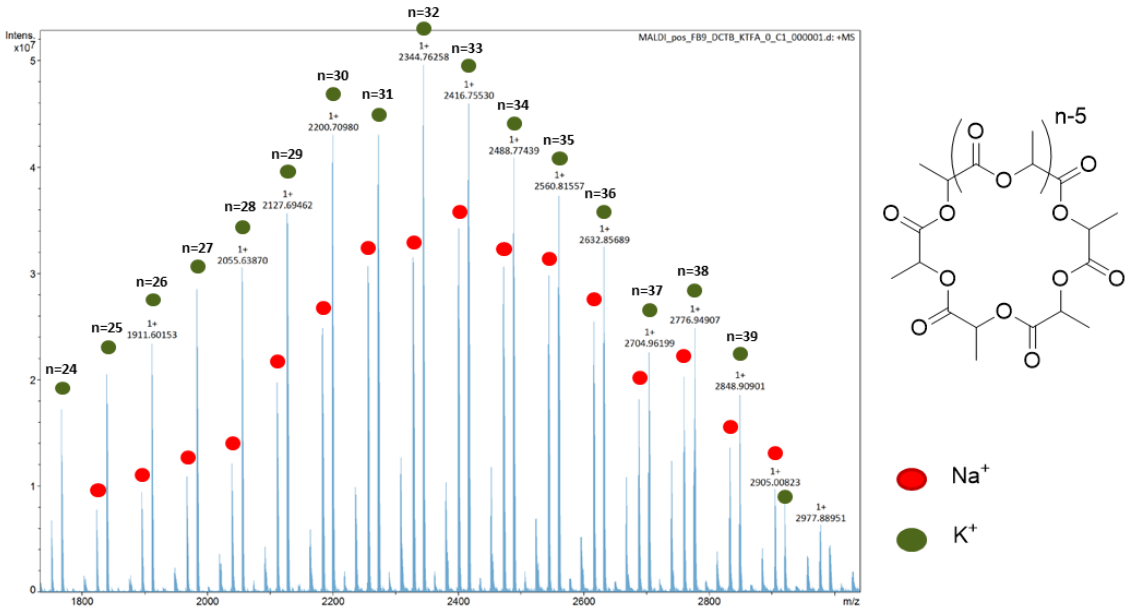

Figure 5.38 MALDI-FT-ICR MS spectrum of PDLLA (entry 8, **Table 5.2**).

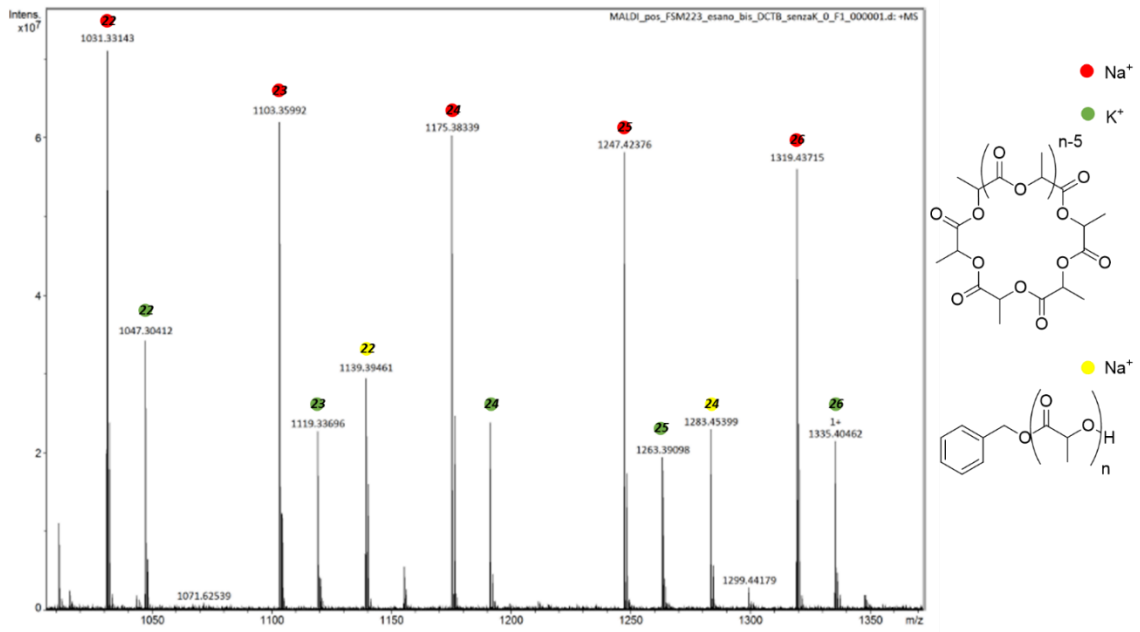

Figure 5.39 MALDI-FT-ICR MS spectrum of PLLA (entry 9, **Table 5.2**).

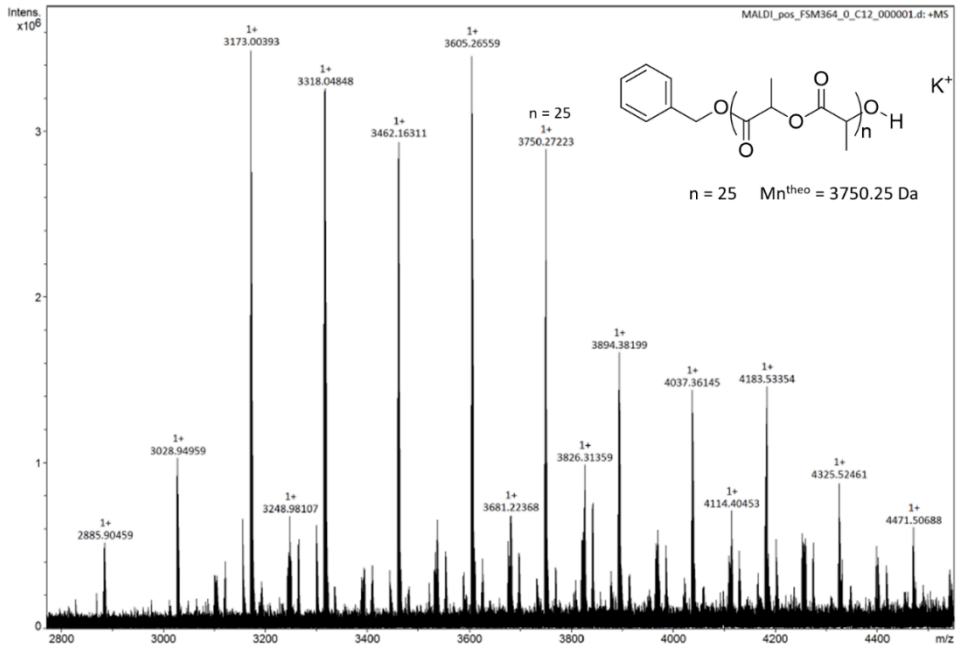

Figure 5.40 MALDI-FT-ICR MS spectrum of PLLA (entry 11, **Table 5.1**).

Mechanistic studies

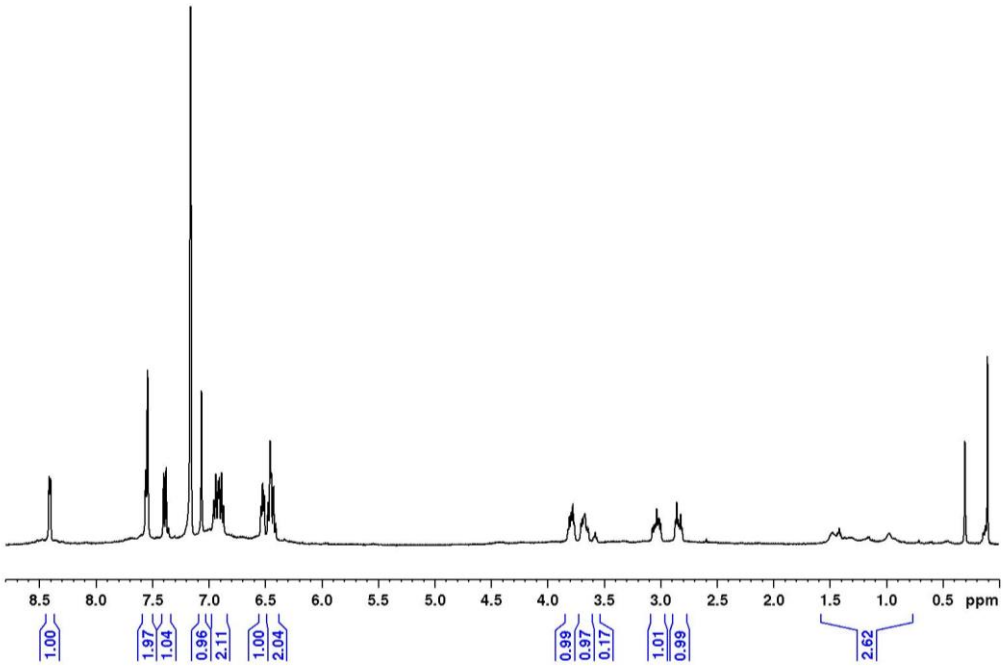

Figure 5.41 ^{1}H NMR spectrum (400 MHz, C_6D_6, 298 K) of complex (S)-**1** + 2 equiv. iPrOH.

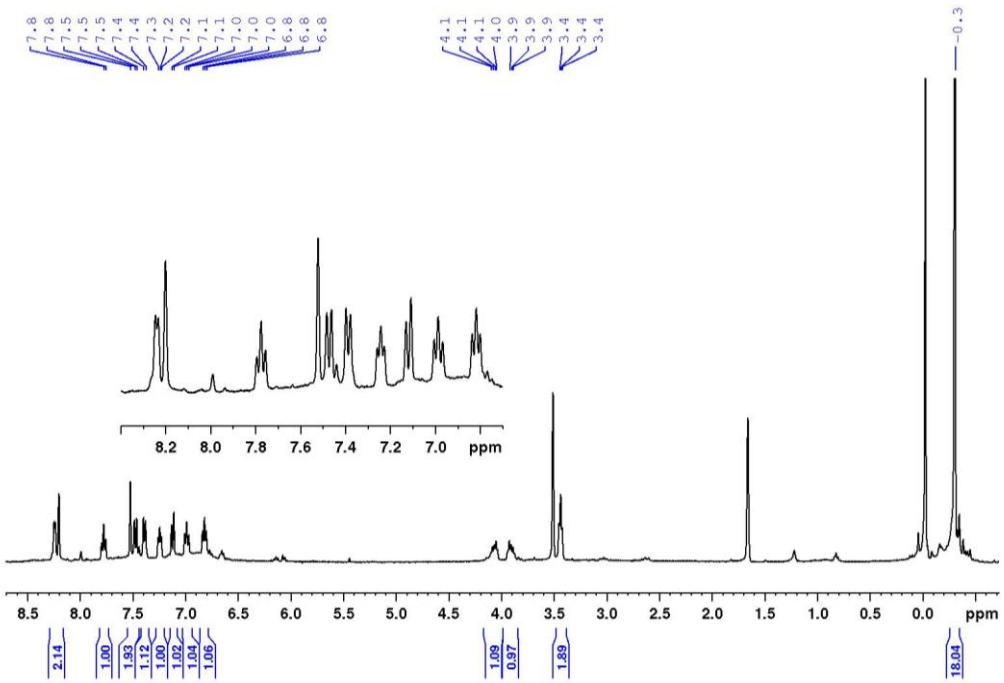

Figure 5.42 ^{1}H NMR spectrum (400 MHz, THF d_8, 298 K) of complex (S)-**1**.

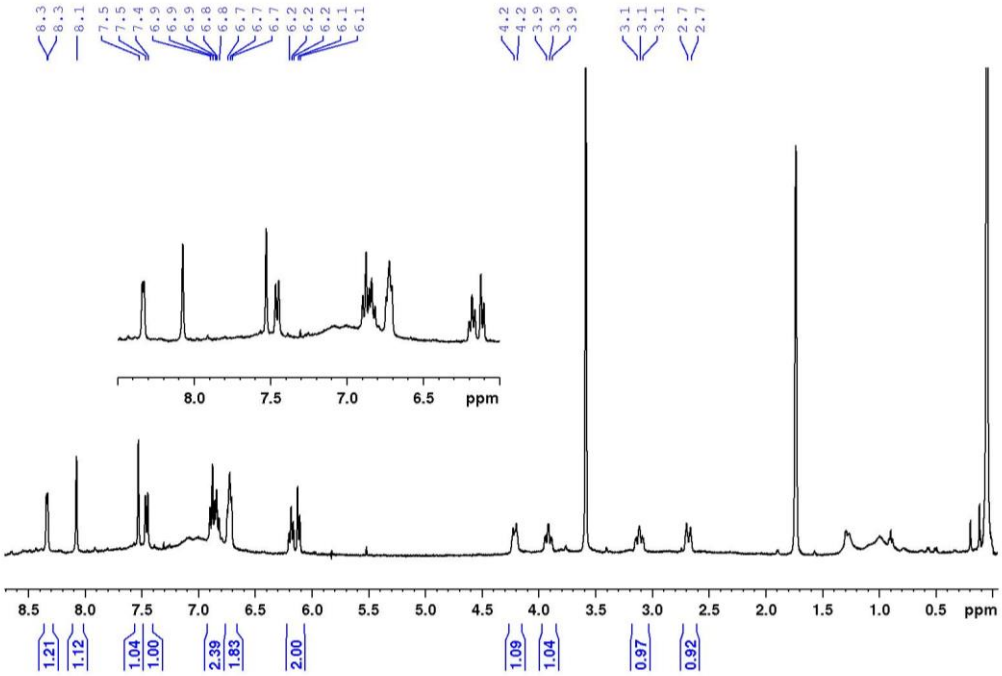

Figure 5.43 ^{1}H NMR spectrum (400 MHz, THF d_8, 298 K) of complex (S)-**1** + 2 equiv. iPrOH.

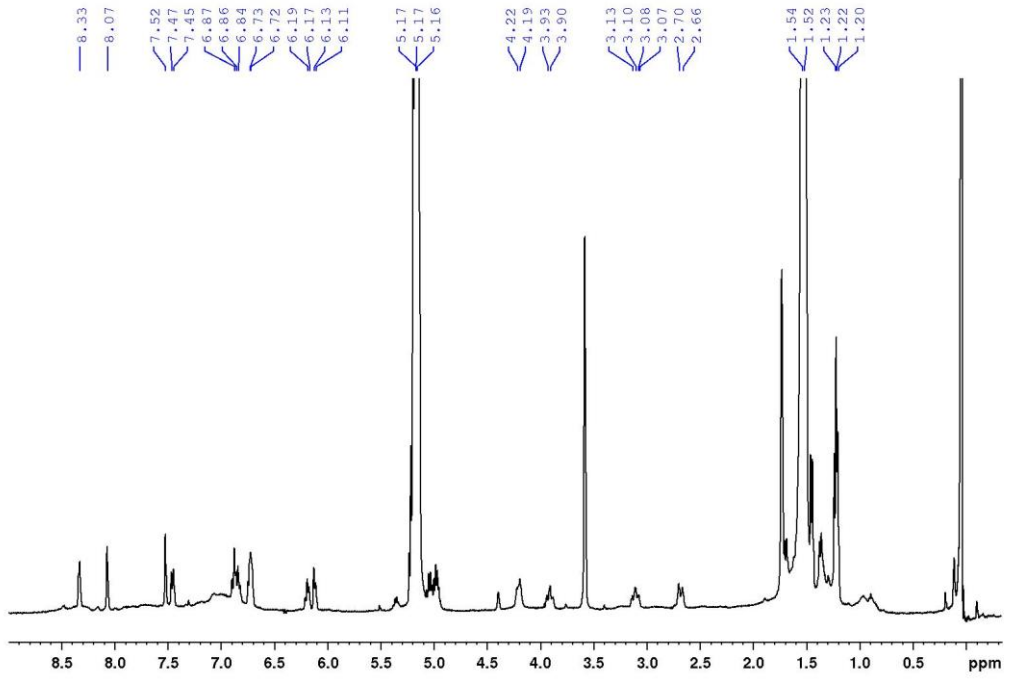

Figure 5.44 ^{1}H NMR spectrum (400 MHz, THF d_8, 298 K) of complex (S)-**1** + 2 equiv. iPrOH + 20 equiv. di L-LA.

Synthesis of mononuclear complex (S)-1a

In a glove box, ligand (S)-LH_2 (0.094 g, 0.170 mmol) was dissolved in benzene (4 ml). Zinc diethyl $ZnEt_2$ (0.021 g, 0.170 mmol) was dissolved in benzene (5 ml) and was slowly added to the solution of the ligand. The solution was allowed to stir for 2 h. The solvent was removed under vacuum. The desired product is an orange powder. Yield 89 %

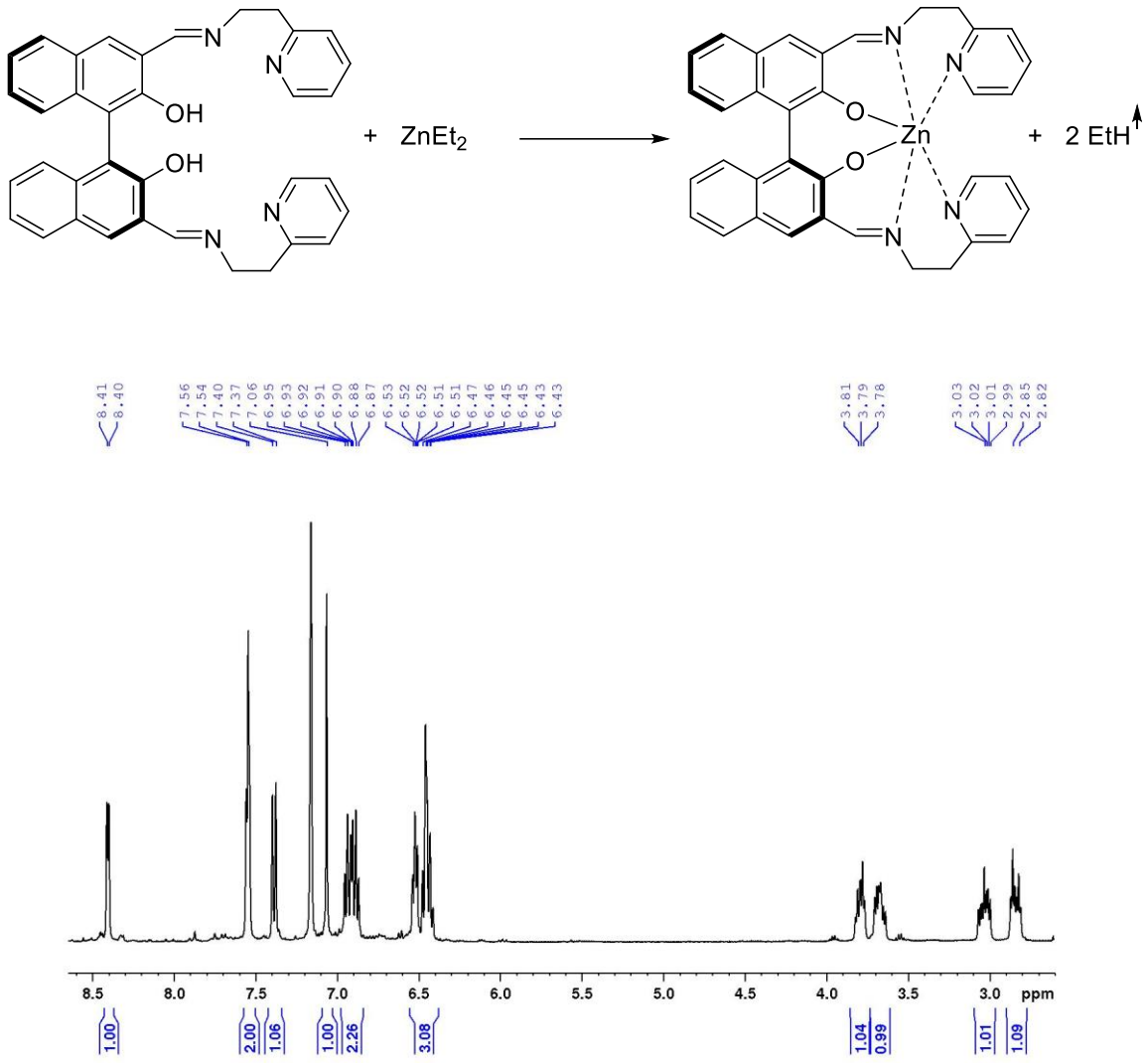

Figure 5.45 ^{1}H NMR spectrum (400 MHz, C_6D_6, 298 K) of complex (S)-**1a**.

^{1}H NMR (400 MHz, C_6D_6, 298 K): δ 8.40 (d, J = 4.6 Hz, 2H), 7.54 (m, 4H), 7.38 (d, J = 8.4 Hz, 2H), 7.06 (s, 2H, CH=N), 6.91 (m, 4H), 6.51 (m, 2H), 6.46 (m, 4H), 3.78 (m, 2H, CH_2), 3.68 (m, 2H, CH_2), 3.00 (m, 2H, CH_2), 2.82 (m, 2H, CH_2).

References

[1] Gregory, G. L., Lopez-Vidal, E. M., Buchard, A. Polymers from sugars: cyclic monomer synthesis, ring-opening polymerisation, material properties and applications. *Chemical Communications* **53**, 2198–2217 (2017).

[2] Zhu, Y., Romain, C. & Williams, C. K. Sustainable polymers from renewable resources. *Nature* **540**, 354–362 (2016).

[3] Platel, R. H., Hodgson, L. M., Williams, C. K. Biocompatible initiators for lactide polymerization. *Polymer Reviews* **48**, 11–63 (2008).

[4] Kong, W. L., Wang, Z. X. Dinuclear magnesium, zinc and aluminum complexes supported by bis(iminopyrrolide) ligands: Synthesis, structures, and catalysis toward the ring-opening polymerization of ε-caprolactone and rac-lactide. *Dalton Transactions* **43**, 9126–9135 (2014).

[5] [a]Kremer, A. B., Mehrkhodavandi, P. Dinuclear catalysts for the ring opening polymerization of lactide. Coordination *Chemistry Reviews* **380**, 35–57 (2019).
[b]Matsunaga, S., Shibasaki, M. Recent advances in cooperative bimetallic asymmetric catalysis: Dinuclear Schiff base complexes. *Chemical Communications* **50**, 1044–1057 (2014).

[6] Mitić, N., Smith, S. J., Neves, A., Guddat, L. W., Gahan, L. R., Schenk, G. The catalytic mechanisms of binuclear metallohydrolases. *Chemical Reviews* **106**, 3338–3363 (2006).

[7] [a]Knight, P. D., White, A. J. P., Williams, C. K. Dinuclear zinc complexes using pentadentate phenolate ligands. *Inorganic Chemistry* **47**, 11711–11719 (2008).
[b]Williams, C. K., Brooks, N. R., Hillmyer, M. A., Tolman, W. B. Metalloenzyme inspired dizinc catalyst for the polymerization of lactide. *Chemical Communications* **2**, 2132–2133 (2002).

[8] Soobrattee, S., Zhai, X., Nyamayaro, K., Diaz, C., Kelley, P., Ebrahimi, T., Mehrkhodavandi, P. Dinucleating Amino-Phenolate Platform for Zinc Catalysts: Impact on Lactide Polymerization. *Inorganic Chemistry* **59**, 5546–5557 (2020).

[9] [a]Honrado, M., Otero, A., Fernández-Baeza, J., Sánchez-Barba, L. F., Garcés, A., Lara-Sánchez, A., Rodríguez, A. M. Stereoselective ROP of rac-lactide mediated by enantiopure NNO-scorpionate zinc initiators. *Organometallics* **33**, 1859–1866 (2014).
[b]Otero, A., Fernández-Baeza, J., Sánchez-Barba, L. F., Sobrino, S., Garcés, A., Lara-Sánchez, A., Rodríguez, A. M. Mono- and binuclear chiral N,N,O-scorpionate zinc alkyls as efficient initiators for the ROP of: Rac - lactide. *Dalton Transactions* **46**, 15107–15117 (2017).

[10] Thevenon, A., Romain, C., Bennington, M. S., White, A. J. P., Davidson, H. J., Brooker, S., Williams, C. K. Dizinc Lactide Polymerization Catalysts: Hyperactivity by Control of Ligand Conformation and Metallic Cooperativity. *Angewandte Chemie* **55**, 8680–8685 (2016).

[11] [a]Schäfer, P. M., Fuchs, M., Ohligschläger, A., Rittinghaus, R., McKeown, P., Akin, E., Schmidt, M., Hoffmann, A., Liauw, M. A., Jones, M. D., Herres-Pawlis, S. Highly Active N,O Zinc Guanidine Catalysts for the Ring-Opening Polymerization of Lactide. *ChemSusChem* **10**, 3547–3556 (2017).
[b] McKeown, P., McCormick, S. N., Mahon, M. F., Jones, M. D. Highly active Mg(II) and Zn(II) complexes for the ring opening polymerisation of lactide. *Polymer Chemistry* **9**, 5339–5347 (2018).
[c]Hermann, A., Hill, S., Metz, A., Heck, J., Hoffmann, A., Hartmann, L., Herres-Pawlis, S. Next Generation of Zinc Bisguanidine Polymerization Catalysts towards Highly Crystalline, Biodegradable Polyesters. *Angewandte Chemie* **59**, 21778–21784 (2020).
[d]D'Auria, I., Ferrara, V., Tedesco, C., Kretschmer, W., Kempe, R., Pellecchia, C. Guanidinate Zn(II) Complexes as Efficient Catalysts for Lactide Homo- And Copolymerization under Industrially Relevant Conditions. *ACS Applied Polymer Materials* **3**, 4035–4043 (2021).

[e]D'Alterio, M. C., D'Auria, I., Gaeta, L., Tedesco, C., Brenna, S., Pellecchia, C. Are Well Performing Catalysts for the Ring Opening Polymerization of l -Lactide under Mild Laboratory Conditions Suitable for the Industrial Process? the Case of New Highly Active Zn(II) Catalysts. *Macromolecules* **55**, 5115–5122 (2022).

[12] Munusamy, S., Kulathu Iyer, S. A chiral (S)-BINOL based fluorescent sensor for the recognition of Fe(III) and cascade discrimination of α-amino acids. *Tetrahedron Asymmetry* **27**, 492–497 (2016).

[13] Jena, H. S. Diastereoselective self-assembly of heterochiral Zn(II) complexes of racemic Schiff bases in a chiral self-discriminating process: effect of non-covalent interactions on solid state structural self-assembly. *RSC Advances **4***, 3028-3044 (2014).

[14] Sarazin, Y., Wright, J. A., Harding, D. A. J., Martin, E., Woodman, T. J., Hughes, D. L., Bochmann, M. Synthesis and structures of new binuclear zinc alkyl, aryl and aryloxo complexes. *Journal Organometallic Chemistry **693***, 1494-1501 (2008).

[15] Price, W. S. Pulsed-field gradient nuclear magnetic resonance as a tool for studying translational diffusion: Part 1. Basic theory *Concepts in Magnetic Resonance* **9**, 299-336 (1998).

[16] [a]Macchioni, A., Ciancaleoni, G., Zuccaccia, C., Zuccaccia, D. Determining accurate molecular sizes in solution through NMR diffusion spectroscopy. *Chemical Society of Chemistry* **37**, 479–489 (2008).
[b] Neufeld, R., Stalke, D. Accurate molecular weight determination of small molecules via DOSY-NMR by using external calibration curves with normalized diffusion coefficients Chemical Science **6**, 3354-3364 (2015).
[c] Voorter, P.-J., McKay, A., Dai, J., Paravagna, O., Cameron, N. R., Junkers, T. Solvent-Independent Molecular Weight Determination of Polymers Based on a Truly Universal Calibration. Angewandte Chemie International Edition **61** ,e202114536 (2022).

[17] [a]Mazzeo, M., Tramontano, R., Lamberti, M., Pilone, A., Milione, S., Pellecchia, C. Rare earth complexes of phenoxy-thioether ligands: synthesis and reactivity in the ring opening polymerization of cyclic esters. *Dalton Transactions* **42**, 9338-9351 (2013).
[b]Pilone, A., Lamberti, M., Mazzeo, M., Milione, S., Pellecchia, C. Ring-opening polymerization of cyclic esters by phenoxy-thioether complexes derived from biocompatible metals. *Dalton Transactions* **42**, 13036-13047 (2013).
[c]Chen, H. C., Chen, S. H. Diffusion of Crown Ethers In Alcohols. *The Journal of Physical Chemistry* **88**, 5118–5121 (1984).

[18] Chamberlain B. M., Cheng M., Moore D. R., Ovitt T. M., Lobkovsky E. B., Coates G. W. Polymerization of Lactide with Zinc and Magnesium β-Diiminate Complexes: Stereocontrol and Mechanism. *Journal of the American Chemical Society* **123**, 3229-3238 (2001).

[19] Boulmaaz, S., Hubert-Pfalzgraf, L. G. The Quest for Mixed-Metal Alkoxides Based on Zinc: Synthesis and Characterization of Zinc-Tantalum Oxoisopropoxides. *Journal of Sol-Gel Science and Technology* **2**, 11-15 (1994).

CHAPTER 6

Zirconium tris(phenolate) amino complexes for the polymerization of lactide

During my PhD, I carried out a visiting research period at the School of Chemistry of Tel Aviv University under the supervision of Prof. Moshe Kol.

6.1 Introduction

As reported in *Introduction*, the chirality of lactic acid gives rise to three stereoisomers of lactide: L-(S, S) lactide, D-(R, R) lactide or *meso*-(S, R) lactide (**Figure 6.1**). The chemical and physical properties of PLA depend on its stereoregularity, which is the result of the chirality of the monomer and the stereoselectivity of the catalyst employed for the ROP.[1] Of all forms of PLA, the one commercially used to be isotactic PLA, and in particular the poly (L-lactic acid) (PLLA) derived from the natural enantiomer L-LA.

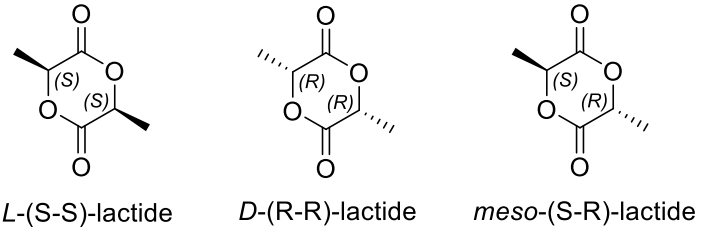

Figure 6.1 Stereoisomers of lactide

Generally, L-LA is produced industrially through a two-step process in which L-lactic acid is condensed into an oligomer at a high temperature which subsequently and then undergoes a catalytic depolymerization.[1b] During this process there may be epimerization reactions leading to the formation of stereoisomers, in particular of *meso*-lactide up to 5-10 % depending on the process used.[2] $Sn(Oct)_2$ shows low discrimination between the different lactide stereoisomers and, therefore, the PLLA obtained is essentially a stereo-random copolymer in which the stereo-errors are randomly distributed along the chain.[3] It is estimated that for every 1 % of *meso*-LA present in the L-LA flow there is a loss of about 5 °C in the melting temperature (T_m) of the polymer, up to the loss of crystallinity with 10-12 % of *meso*-LA.[4] Therefore, to produce crystalline PLLA it would be necessary to either introduce an additional *meso*-LA removal step, e.g. vacuum distillation, or developing alternative methods for L-LA production in which the *meso*-LA contamination is reduced to a minimum. Both methods are quite expensive, adding to the final price of the polymer. A desirable solution would be the use of a stereoselective catalyst for the *meso*-LA/L-LA mixture able of producing stereo-gradient copolymers that show improved crystallinity compared to stereo-random copolymers.

In recent years, several reports showing active catalysts in the ROP of lactide have been published. Most of these reports concerned solution polymerizations, typically performed at room temperature or at 70-80 °C.[5] Nevertheless, in order to be a valid alternative to $Sn(Oct)_2$, currently used industrially, a catalyst should satisfy the following requirements: high thermo-stability, non-toxic, be very active in the production of high molecular weight PLLA, show a high stereo-control in solvent-free conditions and at T_m of the polymer (180 °C).[6]

Titanium complexes with tris(phenolate) amino ligands were synthesized for the first time by Kol et al. in the 2001. They were mononuclear complexes, having a slightly distorted trigonal bipyramidal geometry.[7]

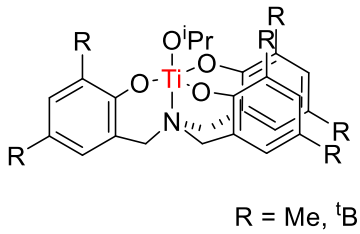

Figure 6.2 Kol complexes.

In 2008, Davidson et al. developed similar complexes with group 4 metals bearing a ligand with bulky *ortho-tert*-butylphenolate groups.[8] (**Figure 6.2**) The single crystal X-ray structures revealed pentacoordinate monomeric complexes in which the ligand scaffold adopted a helix-like C_3 symmetrical arrangement around the metal center. They were used for the polymerization of *rac*-LA in industrially relevant conditions (solvent

free at 130 °C). The Zr-based complex was the most active reaching a 78 % PLA conversion after 6 min. Interestingly, the rapid conversion was accompanied by a high degree of stereocontrol furnishing a highly heterotactic polymer with P_r (probability of heterotactic enchainment) = 0.96. No complex, until then, had been able to combine high activity and stereoselectivity under solvent-free conditions. The Hf complex was less active, with 95 % of lactide conversion after 30 min and reduced stereo-control (P_r = 0.88). The dramatic result was discovered for the Ti complex, which in addition to being the least active, the analysis of the microstructure of the polymer had revealed an atactic PLA (P_r = 0.50).

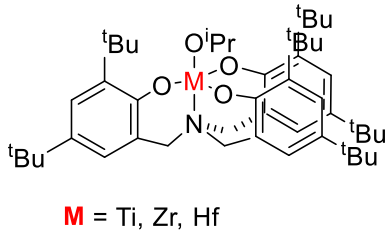

Figure 6.2 Davidson **L$^{tert\text{-}butyl}$M(O^{i}Pr)** complexes.

In 2022, Kol et al. reported new Zr complex **L^{mesityl}Zr(O^{i}Pr)(HO^{i}Pr)** with the tris(phenolate) amino ligand family that contained bulky aryl groups (*ortho*-mesityl-substituents) (**Figure 6.3**).[9] From the NMR study it was observed that the complex had an average C_3 symmetry, with a bound isopropanol molecule, whose position changes fast on the NMR timescale with the isopropoxide group on the metal. This was the earliest example of a Zr mononuclear complex that featured a tris(phenolate) amino ligand along with two monodentate ligands completing an octahedral geometry. The authors proposed that the octahedral geometry of **L^{mesityl}Zr(O^{i}Pr)(HO^{i}Pr)** may relate with the structure of the propagating ROP catalytic species, in which the position *trans* at the neutral amine donor would be occupied by the polymeric group and the position *trans* to one of the anionic phenolate oxygens by the carbonyl-oxygen of an incoming lactide monomer.

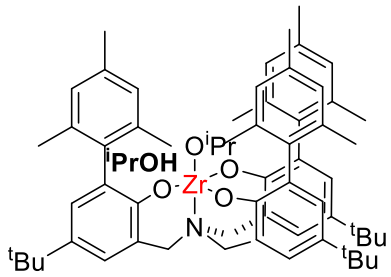

Figure 6.3 Kol **L^{mesityl}Zr(O^{i}Pr)(HO^{i}Pr)** complex.

The **L^{mesityl}Zr(O^{i}Pr)(HO^{i}Pr)** complex was used in the ROP polymerization of lactide under industrially relevant conditions. Unpurified L-LA was converted to PLLA, outperforming other complexes of the same ligand family and $Sn(Oct)_2$. Indeed, about 10 g of L-LA had been polymerized almost completely after 100 min using **L^{mesityl}Zr(O^{i}Pr)(HO^{i}Pr)** and benzyl alcohol (BnOH) in the molar ratio of [**Zr**/BnOH /LLA] of 1:107:107000. The molecular weight of the obtained polymer was very high (61.5 KDa), even if lower than the theoretically calculated value based on the number of equiv. of used BnOH.

Surprisingly, **L^{mesityl}Zr(O^{i}Pr)(HO^{i}Pr)** was stereoselective under industrially relevant conditions too. Indeed, the polymerization of pure *meso*-LA at 180 °C in a ratio of **Zr**/BnOH/*meso*-LA of 1:10:10000 had resulted in a 95 % conversion of the monomer after 5 min with high degree of syndiotacticity P_s (probability of syndiotactic enchainment) = 0.76, obviously lower than that obtained at room temperature (P_s = 0.93). With $Sn(Oct)_2$ the monomer conversion of 70 % was observed and the polymer was almost atactic (P_s = 0.58).

In the presence of a 10:90 mixture of *meso*-LA/L-LA, the **L^{mesityl}Zr(O^{i}Pr)(HO^{i}Pr)** complex was selective towards one of the two stereoisomers of the lactide even under polymer melting conditions.[10] Indeed, after 10 min and at a conversion of 76 % of the total monomer, the unreacted lactide was up of > 99 % of the L isomer,

meaning that the *meso*-LA was completely consumed. The analogous polymerization reaction with $Sn(Oct)_2$ had resulted in a very similar conversion of 74 %. However, the remaining monomer comprised both *meso*-LA and L-LA, in a similar proportion to the original. The different behavior of the two catalysts was reflected in the properties of the polymer. The stereo-gradient copolymer obtained with **$L^{mesityl}Zr(O^iPr)(HO^iPr)$** exhibited greater crystallinity, manifested as lower solubility and higher melting temperatures and enthalpies, compared to the essentially stereo-random copolymer obtained with $Sn(Oct)_2$.

The authors hypothesized that the extraordinary performances observed could be the result of specific interactions between the aromatic substituents on the phenoxy groups with the growing polymer and the incoming monomer and / or the formation of a stable, but not sterically hindered mononuclear complex at high temperature. During the six months that I spent in Kol's research group, as will be illustrated through this *Chapter*, new Zr-based complexes have been synthesized with tris(phenolate) amino ligands which have different substituents in the *ortho* position to the phenoxy group. The position of methyl groups on the mesityl aromatic ring was initially evaluated using a durene group. The cumyl group was subsequently introduced, in which the aromatic ring is not directly bound to the phenoxy group and other hybrid ligands with different stoichiometry between cumyl and mesityl groups were synthesized. All synthesized complexes were used for the polymerization of the *rac*-LA and *meso*-LA.

6.2 Results and discussion

6.2.1 Synthesis and characterization

The symmetric ligand $L^{durene}H_3$, bearing *ortho*-durene/*para-tert*-butyl was obtained by Mannich's reaction of *ortho*-durene phenol with hexamethylenetetramine (HMTA). While, the *ortho*-durene phenol was obtained from the reaction of 2-bromo-4-tert-butyl phenol and the Grignard reagent 2,3,5,6-tetramethylmagnesium bromide, catalyzed by *para*-toluene sulfonic acid $Pd(OAc)_2$. The NMR spectra and experimental details were collected in the Experimetal Part (**Figures 6.10-6.13**).

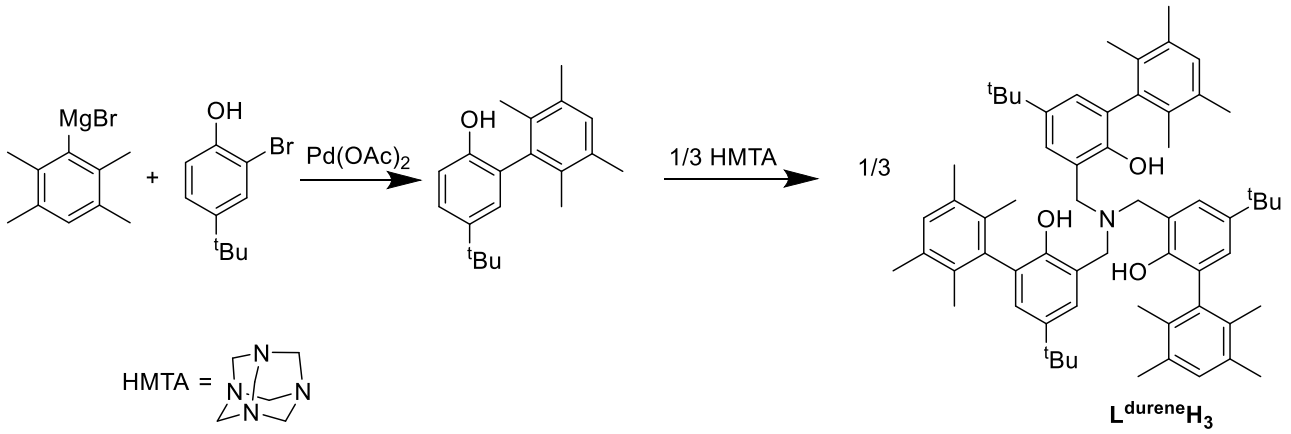

Scheme 6.1 Synthesis of $L^{durene}H_3$

The symmetric ligand $L^{cumyl}H_3$ bearing *ortho*-cumyl/*para-tert*-butyl substituents was synthesized for the first time in this work. The corresponding phenol was obtained by reaction between 4-*tert*-butyl phenol and α-methyl styrene, catalyzed by $Pd(OAc)_2$. The product, purified by a chromatographic column, was reacted with HMTA and the produced ***A*** was reduced in ***B*** with hydrochloric acid (HCl). The latter was employed in a reaction with the *ortho*-cumyl/*para-tert*-butyl (bromomethyl)phenol, obtaining the ligand $L^{cumyl}H_3$, purified by column chromatography. The asymmetric ligand $L^{cumyl\text{-}mesityl}H_3$ was obtained with the same procedure, using

the *ortho*-mesityl/*para-tert*-butyl (bromomethyl)phenol. The NMR spectra and experimental details were collected in the Experimetal Part (**Figures 6.14-6.20**).

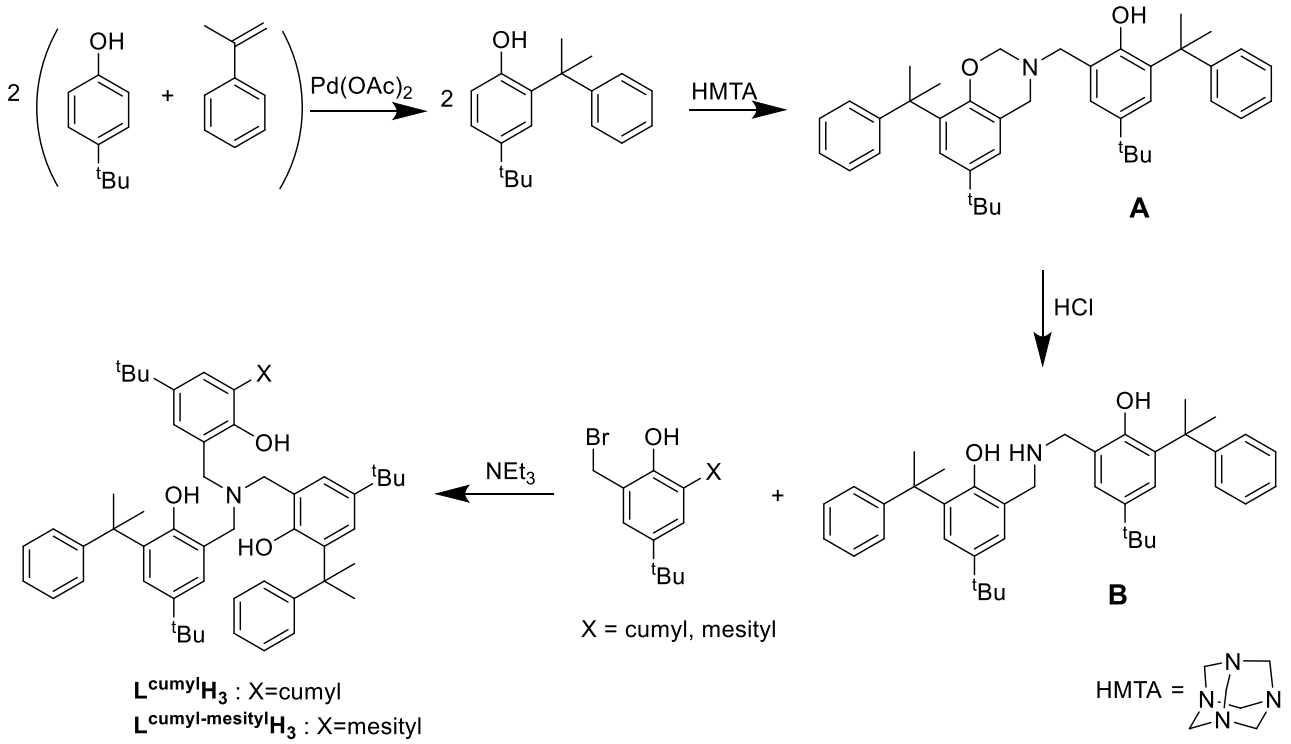

Scheme 6.2 Synthesis of $L^{cumyl}H_3$ and $L^{cumyl\text{-}mesityl}H_3$

Finally, another asymmetric ligand $L^{mesityl\text{-}cumyl}H_3$ was obtained with a different procedure. *Ortho*-mesityl (bromomethyl)phenol (***E***) was obtained by reaction of the corresponding phenol with HBr in acetic acid. *Ortho*-mesityl phenol was synthesized by reaction of 2-bromo-4-*tert*-butyl phenol and the Grignard's reagent 2-mesitylmagnesium bromide, catalyzed by $Pd(OAc)_2$. The primary amine (***F***), on the other hand, was obtained by the Staudinger reaction of the azide (***D***). The condensation reaction between 2 equiv. of (bromomethyl)phenol (***E)*** and (aminomethyl)phenol (***F***) led to the synthesis the $L^{mesityl\text{-}cumyl}H_3$ ligand, which was purified by column chromatography. The NMR spectra and experimental details were collected in the Experimetal Part (**Figures 6.21-6.24**).

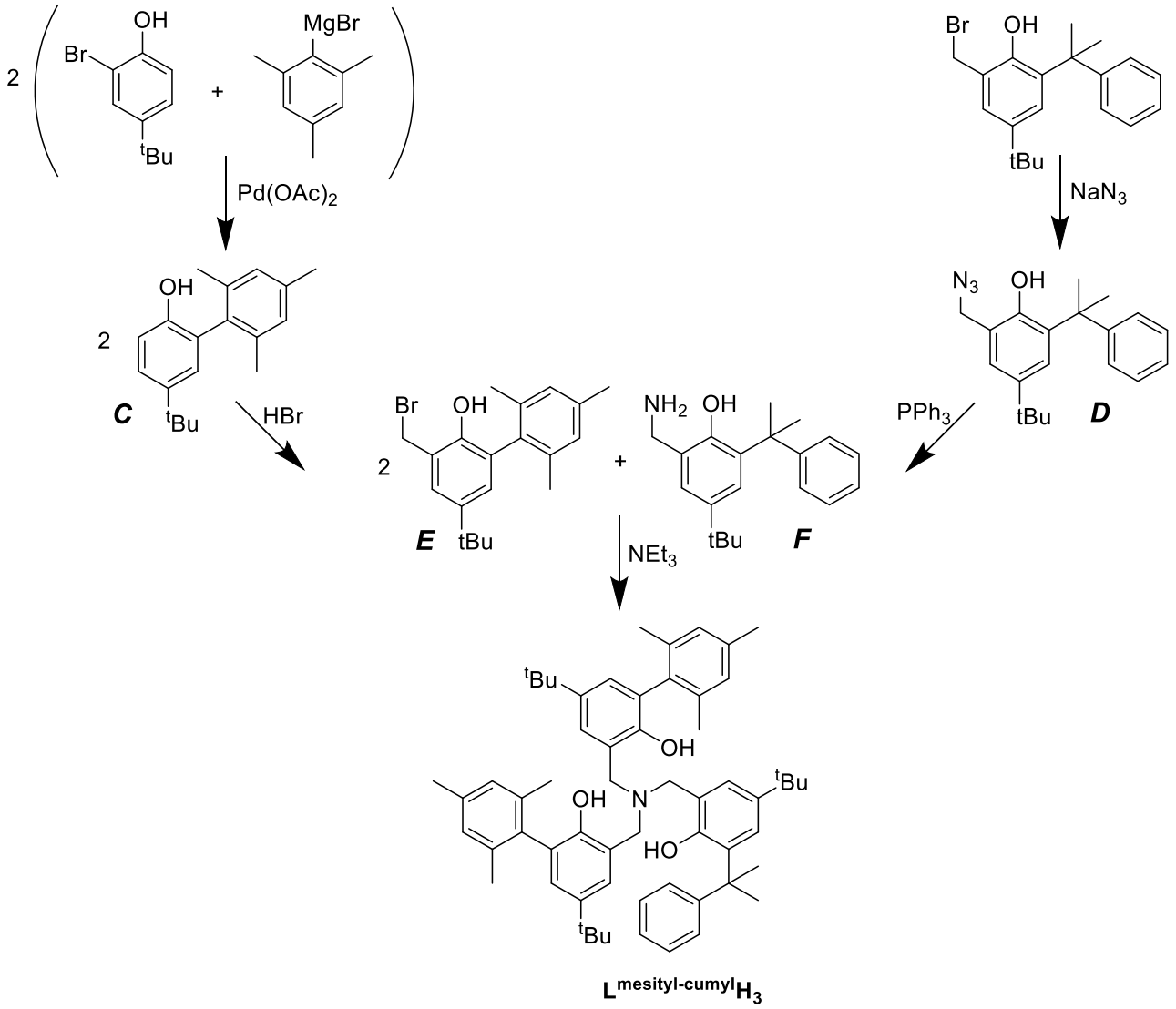

Scheme 6.3 Synthesis of $L^{mesityl\text{-}cumyl}H_3$

All the complexes were synthesized by direct reaction between the ligands and $Zr(O^iPr)_4(HO^iPr)$ in toluene at room temperature. After 2 h, the volatile fraction was removed by vacuum, and the white solid was characterized by ^1H and ^{13}C NMR spectroscopy.

For the **$L^{durene}Zr(O^iPr)(HO^iPr)$** complex (**Scheme 6.4**), the ^1H NMR spectrum is very simple as just the peaks of a phenoxy portion are observed, consistent with a C3 symmetry of the complex (**Figure 6.4**). The integration of the doublet at $\delta = 0.62$ ppm corresponding to the methyl protons of the isopropyl group suggests that two groups are present. This is consistent with a hexacoordinate mononuclear complex in which the metal is coordinated with an isopropoxide group that quickly exchanges with isopropanol. With the ^1H NMR analysis at low temperature, the two separate doublets are observed, highlighting the presence of two groups. The methylene protons resonate as a single broad peak around $\delta = 3.60$ ppm at room temperature, that resolves into 6 signals at low temperature (**Figure 6.25**). Similar observations had previously been rationalized with the **$L^{mesityl}Zr(O^iPr)(HO^iPr)$** complex.

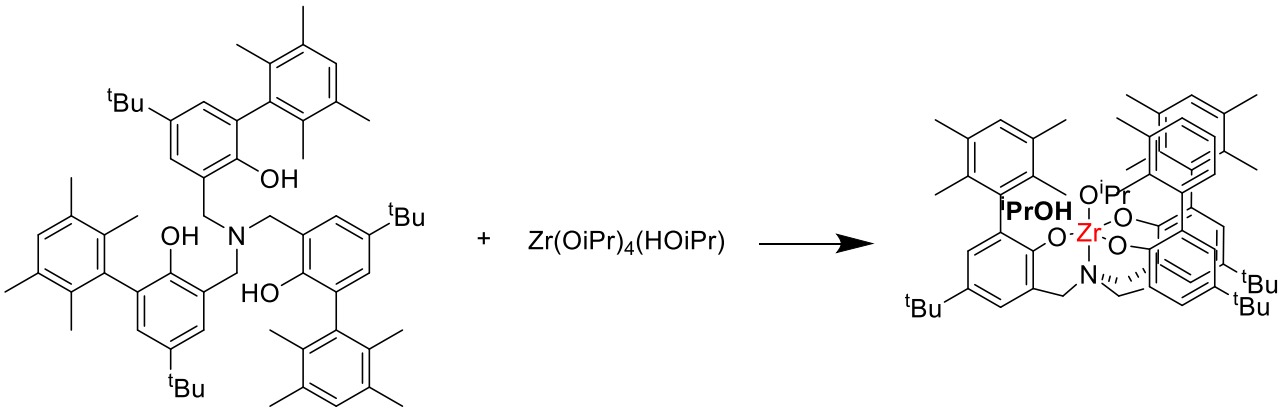

Scheme 6.4 Synthesis of **L^{durene}Zr(O^{i}Pr)(HO^{i}Pr)** complex.

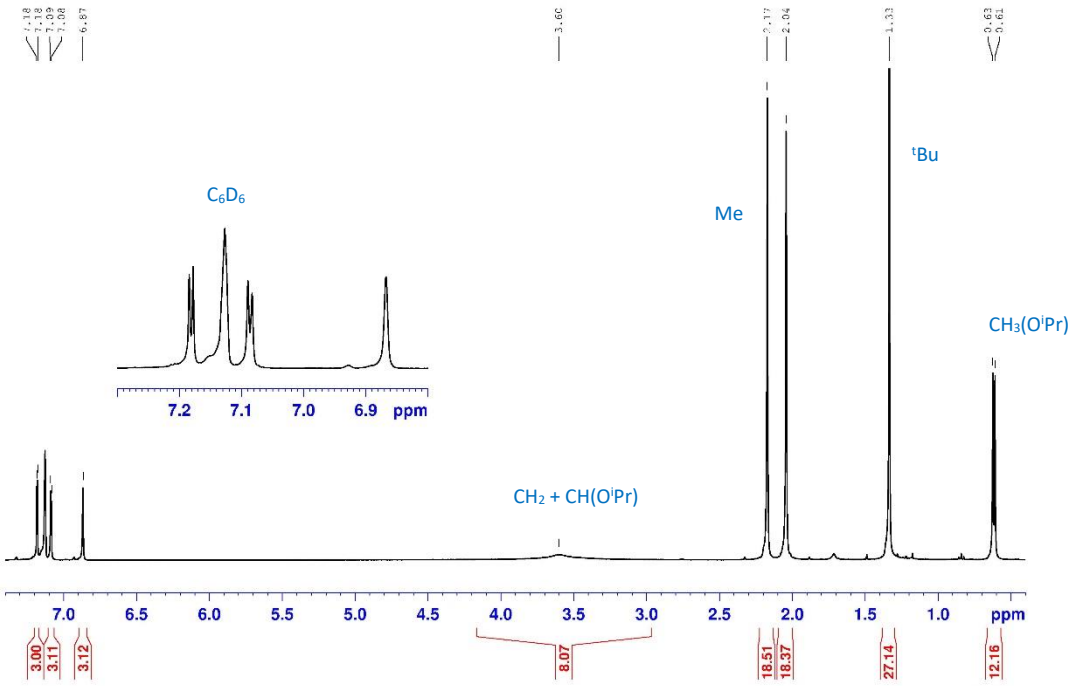

Figure 6.4 ^{1}H NMR spectrum (400 MHz, C_6D_6, 298 K) of **L^{durene}Zr(O^{i}Pr)(HO^{i}Pr)** complex.

The ^{1}H NMR spectrum of the **L^{cumyl}Zr(O^{i}Pr)** (**Scheme 6.5**) reveals a fluxional structure with a C_3v symmetry (**Figure 6.5**). The signals related to the three arms of the tris(phenolate) amino ligand are equal and only one set of peaks is observed. The methylene protons of the ligand are diastereotopic, indeed, in the ^{1}H NMR spectrum two broad peaks are observed at δ = 2.62 and 3.64 ppm in benzene d_6. Similarly, also for the methyl protons of the cumyle group which passed from a broad peak at 25 °C, to separate into two peaks at -50 °C in toluene d_8 (**Figure 6.27**). The tris(phenolate) amino ligand and the signals relating to the bound isopropoxide are in a 1: 1 ratio to each other. These observations are consistent with a pentacoordinate mononuclear complex, different from that observed for the **L^{durene}Zr(O^{i}Pr)(HO^{i}Pr)** complex.

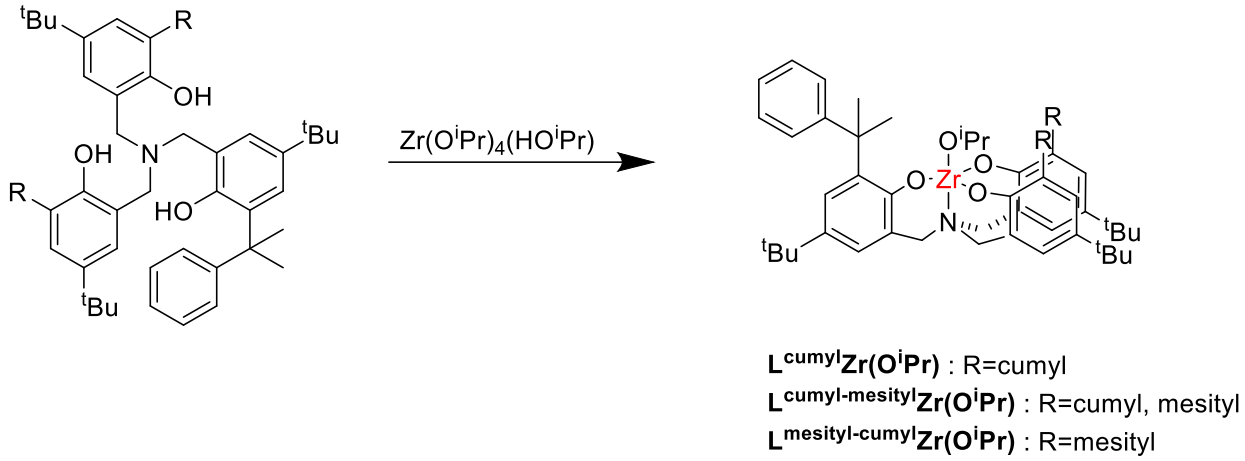

Scheme 6.5 Synthesis of cumyl complexes.

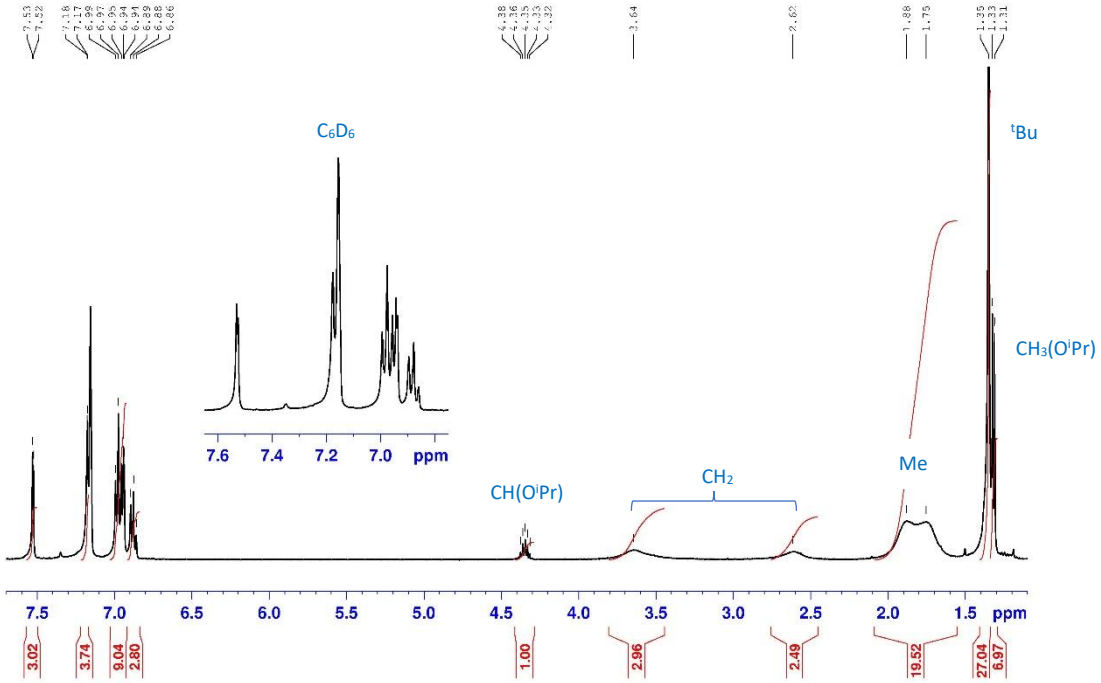

Figure 6.5 ^{1}H NMR spectrum (400 MHz, C_6D_6, 298 K) of **L^{cumyl}Zr(O^{i}Pr)** complex.

From ^{1}H NMR analysis, the **L$^{mesityl\text{-}cumyl}$Zr(OiPr)** (**Scheme 6.4**) presents the *ortho*-mesityl phenoxide arm (**Figure 6.31**) related signals which integrate twice with respect to the *ortho*-cumyl phenoxide arm. Indeed, the *tert*-butyl groups of the two different sections resonate at different chemical shift values (δ = 1.27 ppm for *ortho*-mesityl and δ = 1.39 ppm for *ortho*-cumyl). The methylene protons resonate as a single broad peak at δ = 3.5 ppm. When the complex is dissolved in toluene d_8 at low temperature, the peak dissolves in 6 doublets with different chemical shifts in the range δ = 2.5 - 4.5 ppm (**Figure 6.32**). The formation of pentacoordinate mononuclear complex is assumed, which has a single isopropoxide molecule coordinated to the metal, as observed for **L^{cumyl}Zr(O^{i}Pr)**. Probably the large steric hindrance of the cumyl group does not allow the molecule of free isopropanol to coordinate to the metal.

A similar situation was also observed with the **L$^{cumyl\text{-}mesityl}$Zr(OiPr)** complex (**Scheme 6.4**). The only difference is the signal ratio between the phenoxy *ortho*-cumyl moiety and the *ortho*-mesityl moiety (**Figure 6.33**). The spectrum has numerous impurities that have not been removed after subsequent pentane washes for this reason. The complex was not used for the lactide polymerization tests.

6.2.2 Polymerization studies

All the complexes synthesized in this work were used in the polymerization of purified *rac*- and *meso*-lactides, and selected results are reported in **Table 6.1**.

Table 6.1
Polymerization Data of lactide.

Entry[a]	cat	lactide (eq)	time	T (°C)	Solvent	Conv (%)	P	M_{nGPC}[d] (KDa)	Đ[d]	M_{nth}[e] (KDa)
1	L^{durene}Zr(O^{i}Pr)(HO^{i}Pr)	*meso*LA (1000)	15 min	25	CH_2Cl_2 (2mL)	99	P_s 0.95	11.8	1.07	14.3
2	L^{durene}Zr(O^{i}Pr)(HO^{i}Pr)	*rac*LA (1000)	10 min	25	CH_2Cl_2 (2mL)	98	P_r 0.93	8.55	1.20	14.1
3	L^{cumyl}Zr(O^{i}Pr)	*rac*LA (1000)	30 h	25	CH_2Cl_2 (2mL)	0	-	-	-	-
4[b]	L^{cumyl}Zr(O^{i}Pr)	*rac*LA (100)	48 h	25	toluene (1mL)	18	P_r 0.84	-	-	2.6
5[c]	L^{cumyl}Zr(O^{i}Pr)	*rac*LA (300)	6 min	130	-	10	P_r 0.75	9.56	1.07	4.30
6	L$^{mesityl\text{-}cumyl}$Zr(O^{i}Pr)	*meso*LA (1000)	15 min	25	CH_2Cl_2 (2mL)	46	P_s 0.88	7.54	1.06	6.63
7	L$^{mesityl\text{-}cumyl}$Zr(O^{i}Pr)	*rac*LA (1000)	15 min 1 h	25	CH_2Cl_2 (2mL)	41 86	P_r 0.94 P_r 0.94			

[a]Polymerizations were carried out by using 5 µmol of catalyst in 2 mL of CH_2Cl_2, with 10 equiv. of BnOH and 1000 eq. of LA, at 25 °C. [b]The reaction was carried out with 100 equiv. of *rac*-LA in 1 mL of toluene, at 25 °C. [c]Solvent-free condition with 300 eq. of *rac*-LA, at 130 °C. [d]Experimental Mn and Đ values of the polymers were determined by gel-permeation chromatography (GPC) in THF relative to polystyrene standards and multiplied by a correction factor of 0.58. [e]Calculated according to the monomer conversion: M_{nth} (KDa) = 144.14 $gmol^{-1}$ × ([LA]/[ROH]) × conversion of LA.

Initially, the polymerizations were carried out with a high amount of monomer (1000 equiv.) in a dichlorometane solution at 25 °C and using 10 equiv. of BnOH as a chain transfer agent for controlling the molecular weights. The **L^{durene}Zr(O^{i}Pr)(HO^{i}Pr)** complex appears to be very active, quantitatively polymerizing *meso*-LA and *rac*-LA in 15 and 10 min respectively, showing in both cases a high stereo-control (Entries 1-2, **Table 6.1**). Similar results were found with the **L^{mesityl}Zr(O^{i}Pr)(HO^{i}Pr)** complex which converted all *meso*-LA (P_s = 0.93) and 83 % *rac*-LA (P_r = 0.99) after 5 min. These results highlight how the presence of *ortho*-aryl substituents in the tris(phenolate) amino ligand guarantees extraordinary performance both in terms of activity and stereo-control. While the position of the methyl groups in the aromatic ring does not involve a substantial modification of the catalyst performance.

Therefore, we wanted to synthesize a new Zr complex in which the aryl substituents were not directly bound to the phenoxy groups of the ligand, introducing the cumyle group. The **L^{cumyl}Zr(O^{i}Pr)** complex has a different geometry than the **L^{mesityl}Zr(O^{i}Pr)(HO^{i}Pr)** and **L^{durene}Zr(O^{i}Pr)(HO^{i}Pr)** complexes, as discussed in the *Synthesis and Characterization* section. Under the same conditions used previously, the **L^{cumyl}Zr(O^{i}Pr)** complex is not able to polymerize *rac*-LA even after prolonged times (entry 3, **Table 6.1**). So, we reduced the equiv. of lactide and after 48 h in toluene we had the conversion of only 18 equiv. of *rac*-LA (entry 4, **Table 6.1**). The activity is also lower than that of pentacoordinate **L$^{tert\text{-}butyl}$Zr(O^{i}Pr)** complex for which, under the same conditions, the conversion of 50 equiv. of *rac*-LA and greater stereo-control was observed (P_r = 0.98). Even at high temperatures (130 °C) and solvent-free conditions, the reactivity of **L^{cumyl}Zr(O^{i}Pr)** complex was very slow, almost 8 times slower than the **L$^{tert\text{-}butyl}$Zr(O^{i}Pr)**, in addition the polymer obtained had a low degree

of heterotacticity (entry 5, **Table 6.1**). Thus comparing two catalysts with the same geometry (**L$^{tert\text{-}butyl}$Zr(O^{i}Pr)** vs **L^{cumyl}Zr(O^{i}Pr)**), the presence of the aromatic ring worsens the activities drastically.

The results obtained push towards the hypothesis that the extraordinary performances of the **L^{mesityl}Zr(O^{i}Pr)(HO^{i}Pr)** and **L^{durene}Zr(O^{i}Pr)(HO^{i}Pr)** complexes do not depend only on the presence of the aromatic ring in the ligand scaffold, but also on its position: it is necessary that it is in the *ortho* position of phenoxy group. Only in these cases is the octahedral geometry at the metal center is observed, ensuring the presence of a coordinating pocket able of hosting the growing chain and the incoming monomer.

Finally, the **L$^{mesityl\text{-}durene}$Zr(O^{i}Pr)** complex was synthesized, in which the asymmetric ligand has two portions with mesityl group and one with cumyl group. The activities and stereo-control appear to be almost an average between the **L^{mesityl}Zr(O^{i}Pr)(HO^{i}Pr)** and **L^{cumyl}Zr(O^{i}Pr)** complexes. Indeed, after 15 min we observe a conversion higher than 40 % with both *rac*-LA and *meso*-LA and high stero-control.

The molecular weights of the polymers obtained with the synthesized complexes agree with the theoretically calculated values and narrow molecular weight distributions with dispersity (Đ) values close to 1 are observed.

6.3 Conclusion

Based on the excellent performances observed in the literature with the **L^{mesityl}Zr(O^{i}Pr)(HO^{i}Pr)** complex, we decided to modify the tris(phenolate) amino ligand in order to better understand the reasons of the high efficient and stereoselectivity. Indeed, in this *Chapter*, new zirconium complexes supported by tris(phenol) amino ligands with different *orto*-substituents have been synthesized and used as catalysts for the ROP of lactide. The substitution of the *ortho*-mesityl group with *ortho*-durene group and therefore the synthesis of the hexacoordinate complex **L^{durene}Zr(O^{i}Pr)(HO^{i}Pr)** has preserved the high activity and stero-control, obtaining polymers with a high degree of heterotacticity (using *rac*-LA) and syndiotacticity (using *meso*-LA). The performances have collapsed with the pentacoordinate complexes **L^{cumyl}Zr(O^{i}Pr)** and **L$^{mesityl\text{-}cumyl}$Zr(O^{i}Pr)** demonstrating that not just the presence of the aryl group is an important factor in the reaction, but it is essential that it is directly bound to the phenoxy group. This generates an octahedral geometry in which the coordinating pocket is suitable for hosting both the labile isopropoxide group and another isopropanol molecule. By translating this situation during the polymerization reaction, we could imagine that both the growing chain and the incoming monomer are coordinated at the metal center. This reasonably results in the excellent performance observed for the **L^{mesityl}Zr(O^{i}Pr)(HO^{i}Pr)** and **L^{durene}Zr(O^{i}Pr)(HO^{i}Pr)** complexes in the ROP of lactides.

6.4 Experimental part

Materials and methods

Moisture and air-sensitive materials were manipulated under nitrogen using Schlenk techniques or an MBraun Labmaster glovebox. Toluene and methanol were refluxed over Na and distilled under nitrogen. Tetrahydrofuran (THF) was refluxed over Na and benzophenone and distilled under nitrogen. Monomers (Sigma-Aldrich) were purified before use.

$CDCl_3$, C_7D_8 and C_6D_6 were purchased from Eurisotop and used as received. All other reagents and solvents were purchased from Aldrich and used without further purification.

Instruments and measurements

NMR spectra of polymers were performed at room temperature on Bruker Avance 300, 400 or 600 spectrometers (^1H: 300.13, 400.13, 600.13 MHz; ^{13}C: 75.47, 100.62, 150.92 MHz, respectively). The resonances are reported in ppm (δ) and the coupling constants in Hz (J) and are referenced to the residual solvent peak at δ = 7.16 ppm for C_6D_6 and δ = 7.27 for $CDCl_3$. Spectra recording was performed using Bruker-TopSpin v2.1 software. Data processing was performed using TopSpin v2.1 or MestReNova v6.0.2 software.

The average molecular masses and the molecular weight dispersities (Đ) of the obtained polylactide samples were determined by GPC in THF as the mobile phase at a flow rate of 1 mL min^{-1}. The utilized GPCmax VE-2001 from Viscotek was a combination of an HPLC pump, two Malvern Viscotek T columns (porous styrene divinylbenzene copolymer) with a maximum pore size of 500 and 5000 a, a refractive index detector (VE-3580), and a viscometer (Viscotek 270 Dual Detector). Polystyrene standards were used for calibration. The evaluation of the molar masses was carried out with a universal method or with a conventional method in combination with multiplying a factor of 0.58 for PLA.

Synthesis of ligand $L^{durene}H_3$

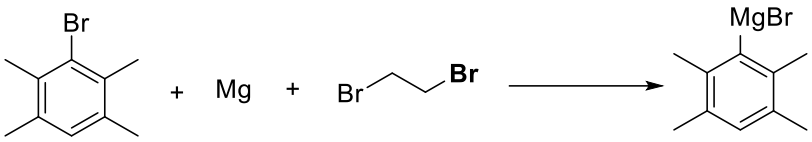

A dry 250mL Sclenk flask equipped with a magnetic stir bar was flushed with nitrogen. The flask was charged with Mg turnings (35.2 mmol, 850 mg), and it was heated for 15 min. THF dry (40 mL) was added, followed by adding of 1,2-dibromoethane (0.202 mmol, 38 mg). The mixture was allowed to stir for 20 min at room temperature.
2,3,5,6-tetramethyl bromobenzene (23.5 mmol, 5.0 g) was dissolved in 10 ml of THF and was added to the flask. The cup was changed with the condenser and the mixture was heated to reflux temperature for 5 h.

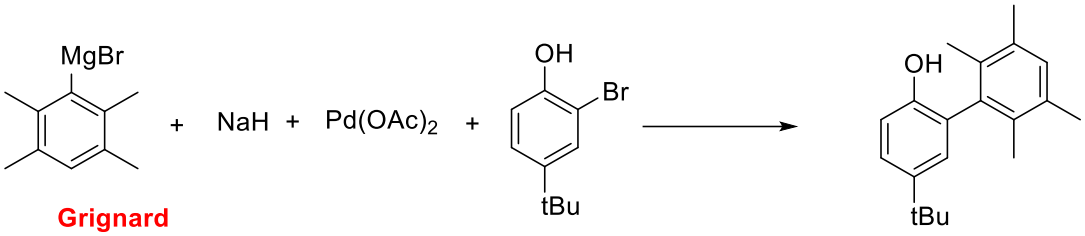

A 150 mL pressure flask equipped with a magnetic stir bar was charged with NaH (19.1 mmol, 762 mg), and THF to 0 °C. 2-bromo-4-tertbutyl phenol (14.7 mmol, 3.36 g) was added dropwise to the mixture, allowed stirring to room temperature for 10 min. $Pd(OAc)_2$ (0.660 mmol, 148 mg) was added, followed by Grignard solution, previously prepared, and the resulting mixture was heated to 70 °C overnight.

After cooling to 0 °C, HCl (50 mL, 2 M) was carefully added to the mixture. It was filtered through celite, and the resulting phases were separated. The aqueous phase was extracted 3 times with Et_2O. The combined organic layers were washed with brine, dried with Na_2SO_4, filtered and the solvent evaporated.

The clean product was obtained by crystallization in hexane (**Figure 6.6**). Yield 70 %

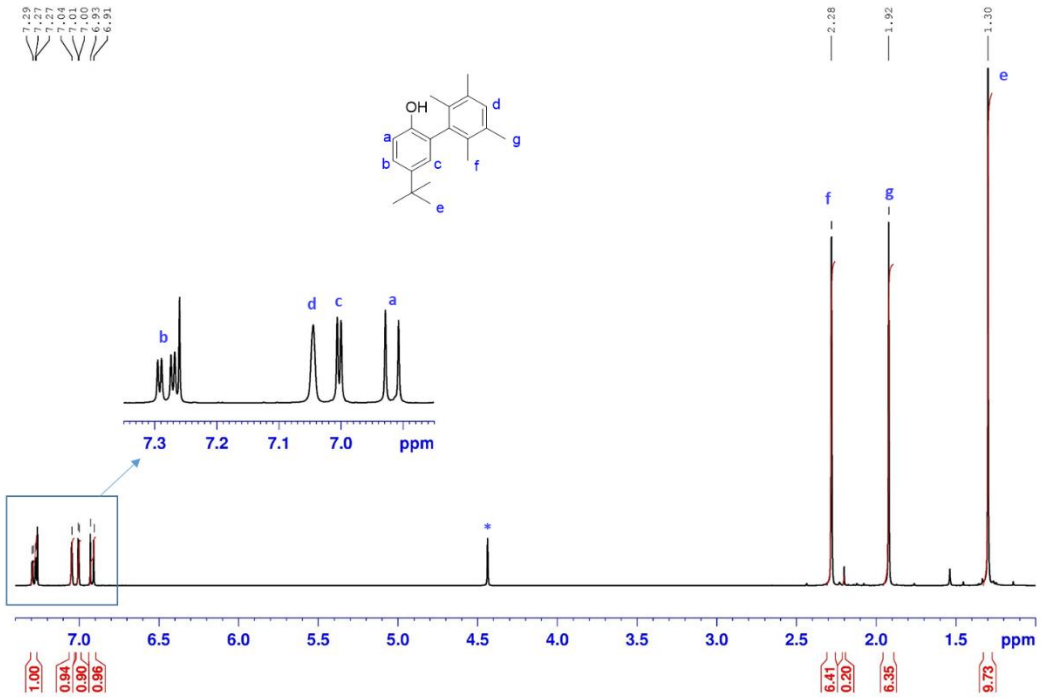

Figure 6.6 ^{1}H NMR spectrum (400 MHz, $CDCl_3$, 298 K) of *ortho*-durene/*para*-*tert*-butyl phenol.

^{1}H NMR (400 MHz, $CDCl_3$, 298 K): δ 7.28 (dd, J_1 = 8.0 Hz, J_2 = 1.2 Hz, 1H, Hb), 7.04 (s, 1H, Hd), 7.01 (d, J = 1.2 Hz, 1H, Hc), 6.92 (d, J = 8.0 Hz, 1H, Ha), 2.28 (s, 6H, Hf), 1.92 (s, 6H, Hg), 1.30 (s, 9H, He).

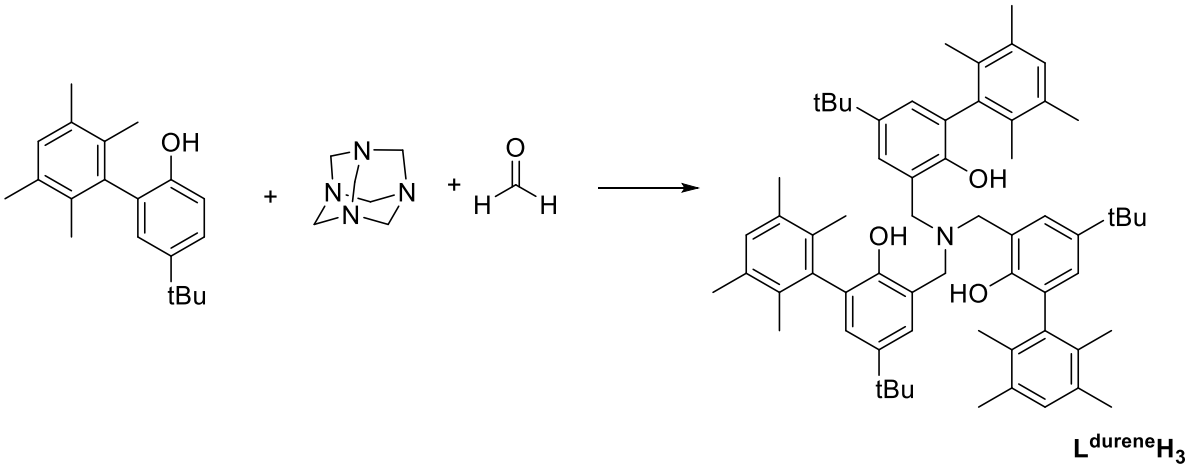

A mixture of *ortho*-durene/*para*-*tert*-butyl phenol (5.35 mmol, 1.51 g), hexamethylenetetramine *HMTA* (0.438 mmol, 61.4 mg), and formaldehyde (15 drops) was heated at 130 °C for 48 h.
The reaction mixture was cooled to 25 °C, and MeOH (20 mL) was added to the yellow slurry. The solution was sonicated until a pale white solid evolved from the solution. The solid was filtered and washed with MeOH (**Figures 6.7-6.9**). Yield 39 %

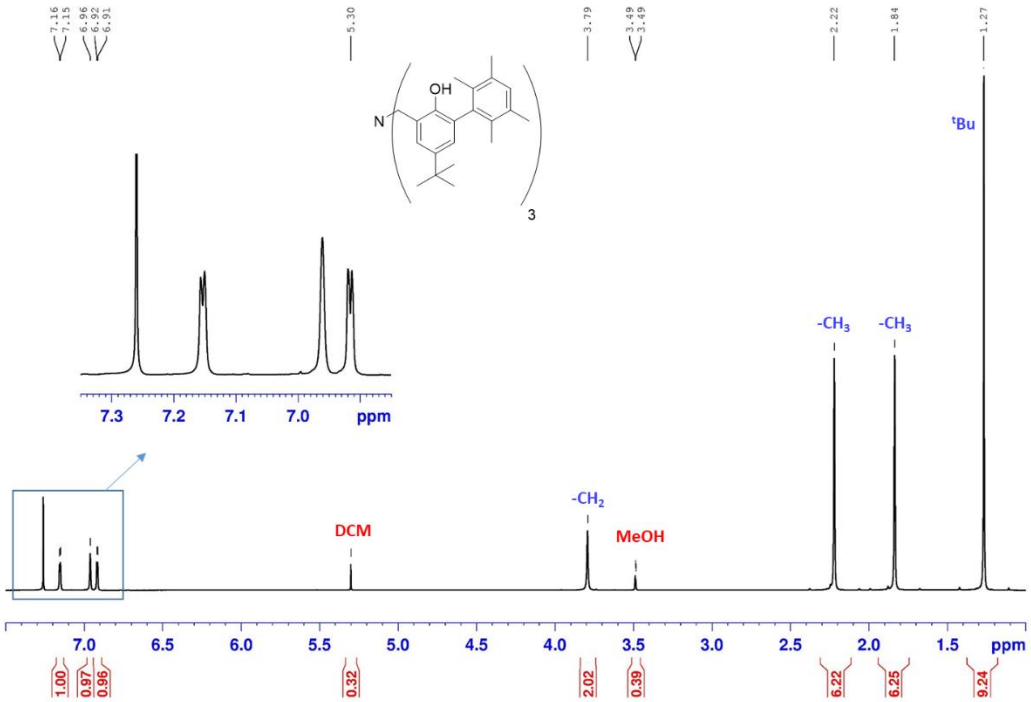

Figure 6.7 ^{1}H NMR spectrum (400 MHz, $CDCl_3$, 298 K) of $L^{durene}H_3$.

^{1}H NMR (400 MHz, $CDCl_3$, 298 K): δ 7.16 (d, J = 1.2 Hz, 3H, ArH), 6.96 (s, 3H, ArH), 6.92 (d, J = 1.2 Hz, 3H, ArH), 3.79 (s, 6H, -NCH_2), 2.22 (s, 18H, -CH_3), 1.84 (s, 18H, -CH_3), 1.27 (s, 27H, -^{t}Bu).

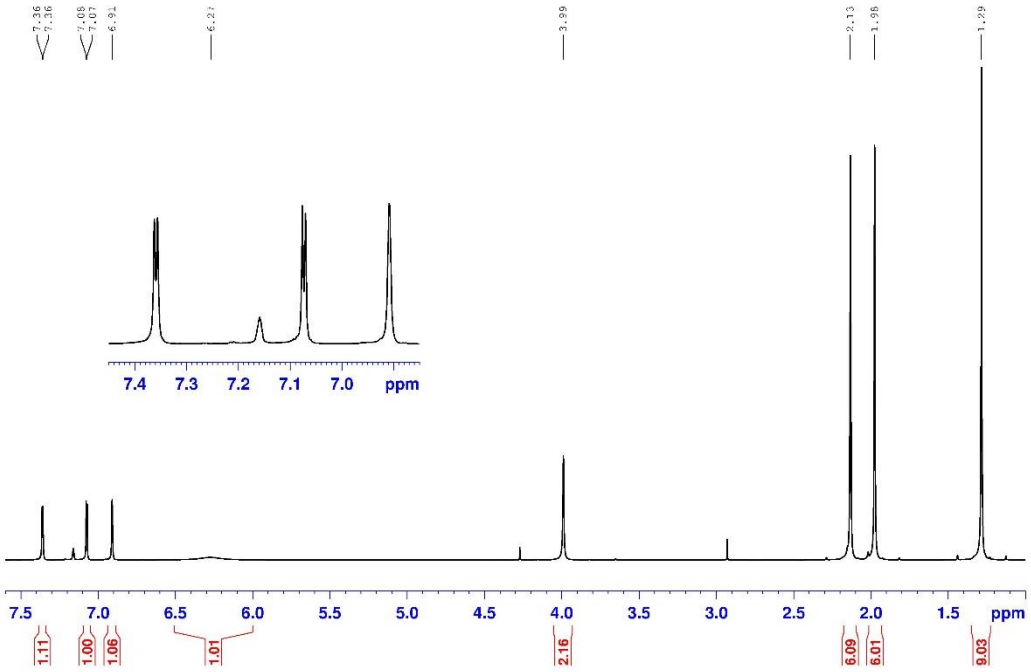

Figure 6.8 ^{1}H NMR spectrum (400 MHz, C_6D_6, 298 K) of $L^{durene}H_3$.

^{1}H NMR (400 MHz, C_6D_6, 298 K): δ 7.36 (d, J= 1.5 Hz, 3H, ArH), 7.08 (d, J = 1.2 Hz, 3H, ArH), 6.91 (s, 3H, ArH), 6.27 (b, 3H, -OH), 3.99 (s, 6H, -NCH_2), 2.13 (s, 18H, -CH_3), 1.98 (s, 18H, -CH_3), 1.29 (s, 27H, -^{t}Bu).

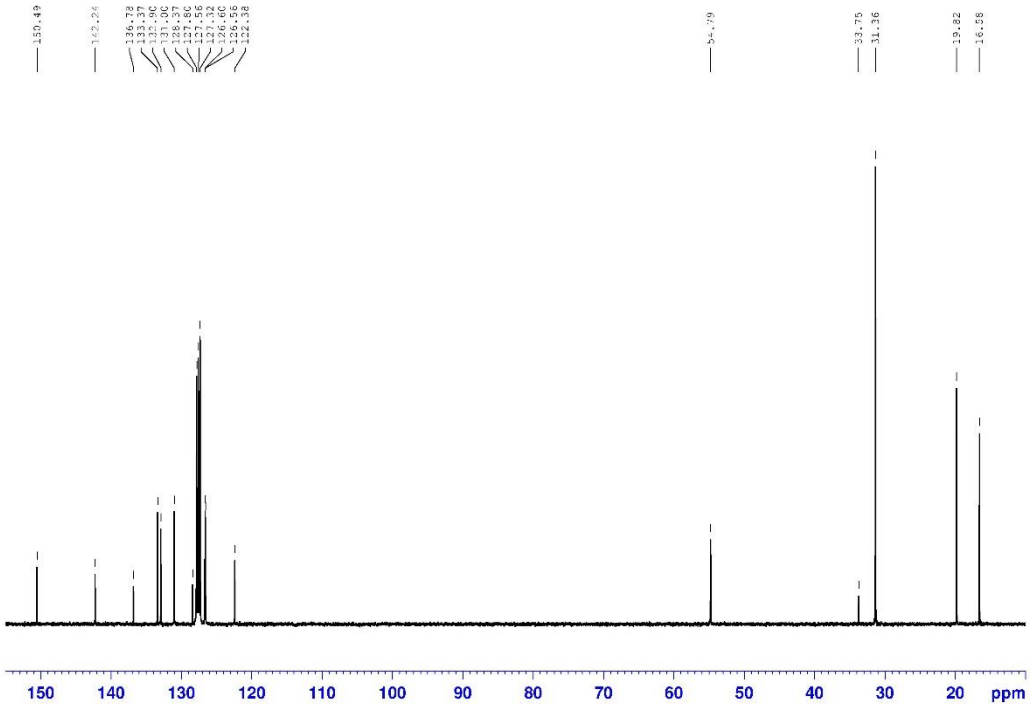

Figure 6.9 ^{13}C NMR spectrum (100 MHz, C_6D_6, 298 K) of $L^{durene}H_3$.

^{13}C NMR (100 MHz, C_6D_6, 298 K): δ 150.5, 142.2, 136.8, 133.4, 132.9, 131.0, 128.4, 127.8, 127.6, 127.3, 126.6, 126.5, 122.4, 54.8, 33.8, 31.4, 19.8, 16.6.

Synthesis of ligand $L^{cumyl}H_3$

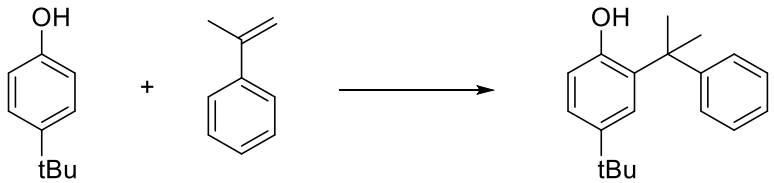

para-Toluenesulfonic acid (0.651 mmol, 122 mg) was added to 4-tert-butyl phenol (71.6 mmol, 10.7 g) kept in an ice bath, under stirring. To the mixture, α-methyl styrene (190 mmol, 25 mL) was added dropwise. The system was allowed to reach room temperature, then was heated at 80 °C for 4 h. The crude product was purified by vacuum column chromatography over alumina eluted with 10 % ethyl acetate in hexane to yield the desired product as a colorless oil (**Figure 6.10**). Yield 40 %

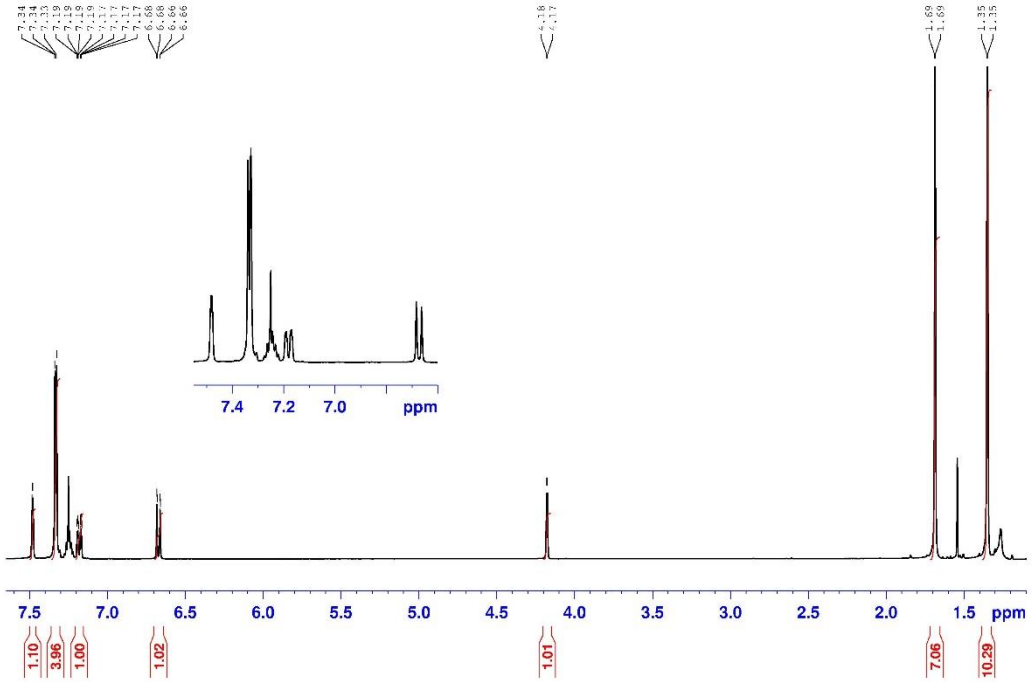

Figure 6.10 ^{1}H NMR spectrum (400 MHz, $CDCl_3$, 298 K) of *ortho*-cumyl/*para-tert*-butyl phenol.

^{1}H NMR (400 MHz, $CDCl_3$, 298 K): δ 7.44 (d, J = 1.1 Hz, 1H, ArH), 7.33 (d, J = 6.8 Hz, 4H, ArH), 7.19 (m, 1H, ArH), 7.17 (d, J = 7.9 Hz, 1H, ArH), 6.67 (d, J = 8.0 Hz, 1H, ArH), 1.69 (s, 6H, -CH_3), 1.35 (s, 9H, -^{t}Bu).

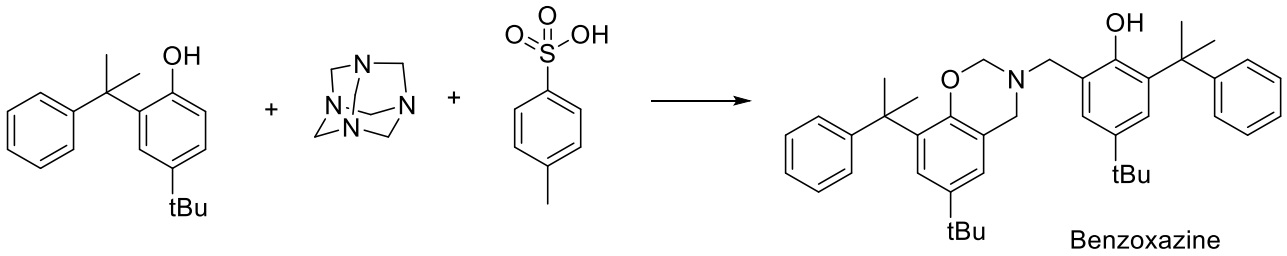

A mixture of *ortho*-cumyl/*para-tert*-butyl phenol (3.76 mmol, 1.01 g), HMTA (0.836 mmol, 117 mg), and para-toluene sulfonic acid (0.0167 mmol, 3 mg) was heated at 110 °C for 22 h.

The reaction mixture was cooled to 25 °C, and MeOH (20 mL) was added to the yellow slurry. The solution was sonicated until a pale white solid evolved from the solution. The solid was filtered and washed with cold MeOH (**Figure 6.11**) Yield 73 %

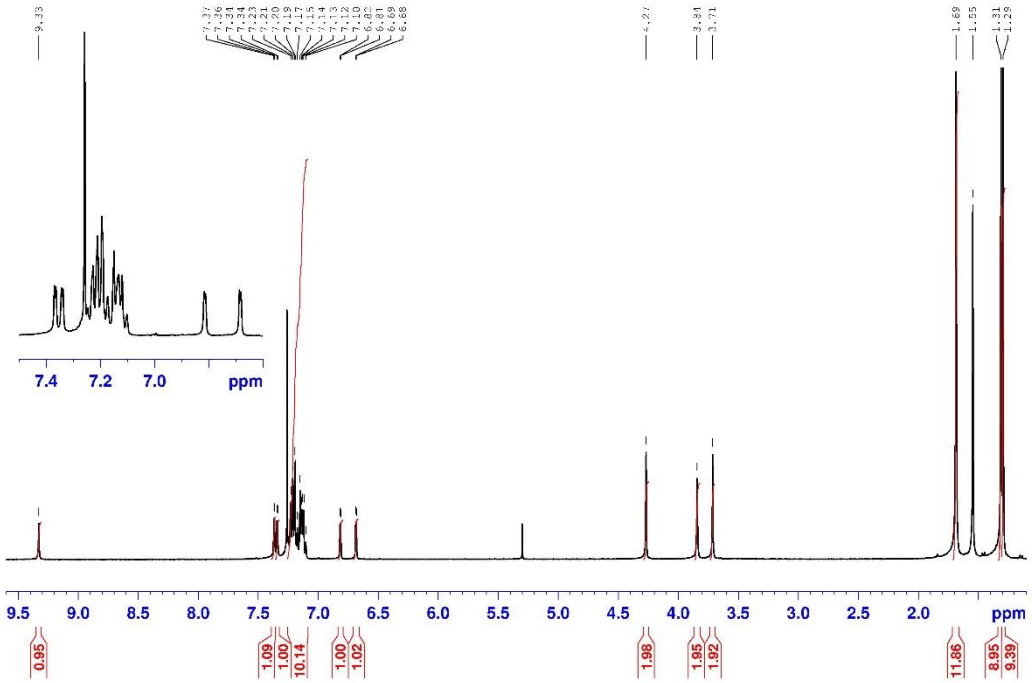

Figure 6.11 ^{1}H NMR spectrum (400 MHz, $CDCl_3$, 298 K) of *benzoxazine*.

^{1}H NMR (400 MHz, $CDCl_3$, 298 K): δ 9.33 (s, 1H, -OH), 7.35 (d, J = 8.2 Hz, 1H, ArH), 7.15 (m, 11H, ArH), 6.82 (d, J = 1.2 Hz, 1H, ArH), 6.68 (d, J = 1.3 Hz, 1H, ArH), 4.27 (s, 2H, -NCH_2), 3.84 (s, 2H, -NCH_2), 3.71 (s, 2H, -NCH_2), 1.69 (s, 12H, -CH_3), 1.31 (s, 9H, -^{t}Bu), 1.29 (s, 9H, -^{t}Bu).

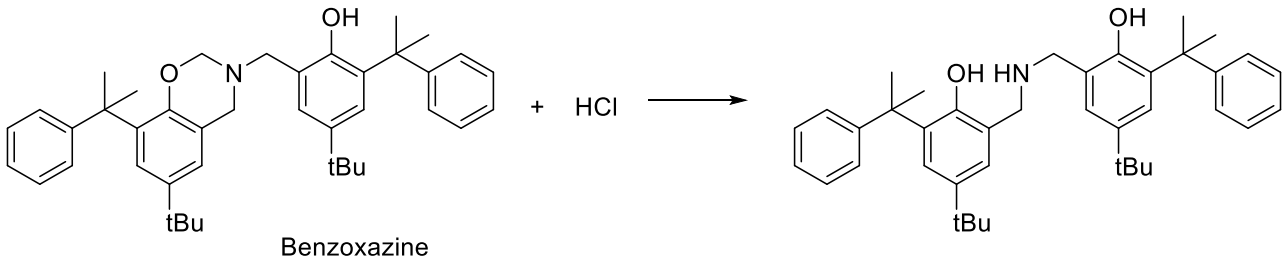

Benzoxazine, previously synthesized, (2.21 mmol, 968 mg) was dissolved in ethylene glycol (60 mL) and hydrochloric acid (30 mL) and heated overnight at 130 °C. After cooling to room temperature, the hydrochloride salt of the desired product was collected by filtration, washed with water, and dried under vacuum. The resulting solid was slowly added to a stirred mixture of aqueous KOH (1.8 M, 50 mL) and diethyl ether (100 mL). The organic layer was separated, dried over Na_2SO_4, and the solvent was removed under vacuum to give a brown powder (**Figure 6.12**). Yield 65 %

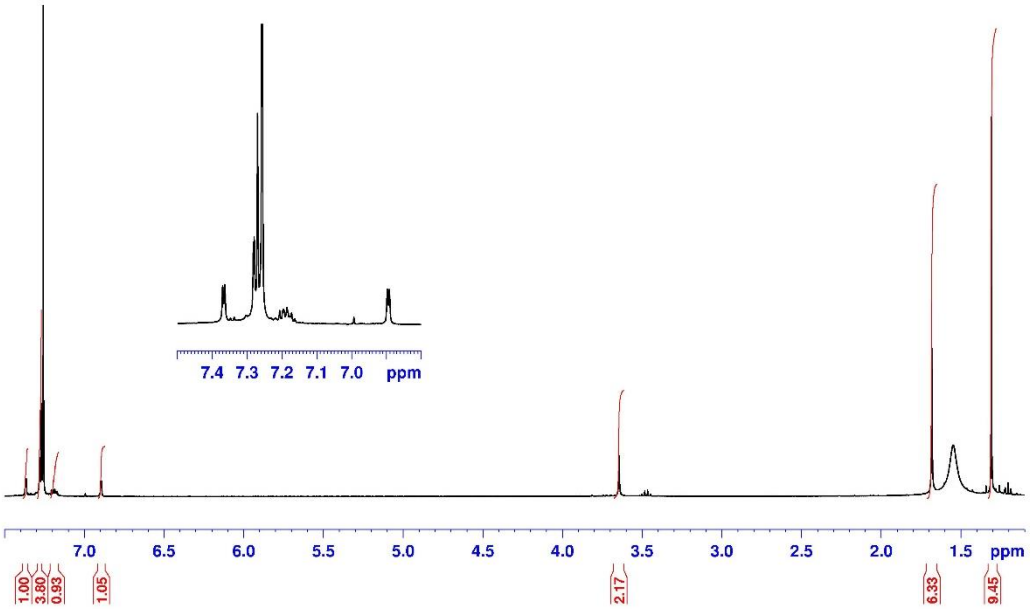

Figure 6.12 ^{1}H NMR spectrum (400 MHz, $CDCl_3$, 298 K) of *reduced benzoxazine*.

^{1}H NMR (400 MHz, $CDCl_3$, 298 K): δ 7.78 (d, J = 1.5 Hz, 2H, ArH), 7.28 (m, 8H, ArH), 7.19 (m, 2H, ArH), 6.98 (d, J = 1.5 Hz, 2H, ArH), 3.68 (s, 4H, -NCH_2), 1.69 (s, 12H, -CH_3), 1.29 (s, 18H, -^{t}Bu).

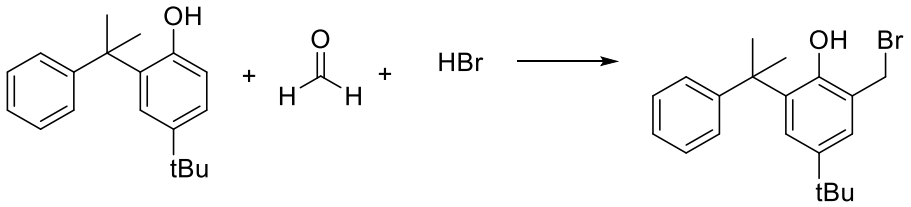

Ortho-cumyl/*para*-*tert*-butyl phenol (2.61 mmol, 700 mg) was dissolved in acetic acid (6 mL). Paraformaldehyde (3.91 mmol, 117 mg) was added to the yellow solution, and it was left to stir to room temperature for 2 h. After that, the HBr 33 % solution (9.13 mmol, 1.6 mL) was added and left to stir for another 30 min. The solvent was removed for evaporation and the yellow oil was obtained (**Figure 6.13**). Yield 92 %

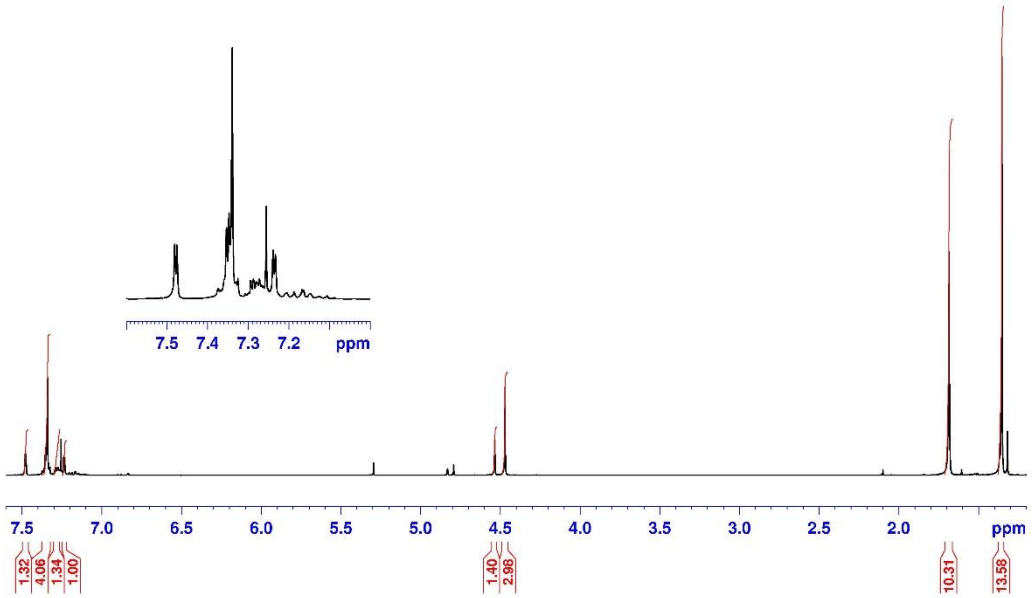

Figure 6.13 ^{1}H NMR spectrum (400 MHz, $CDCl_3$, 298 K) of *ortho-cumyl(bromomethyl)phenol*.

^{1}H NMR (400 MHz, $CDCl_3$, 298 K): δ 7.48 (d, J = 1.7 Hz, 1H, ArH), 7.35 (m, 4H, ArH), 7.28 (m, 1H, ArH), 7.23 (d, J = 1.5 Hz, 1H, ArH), 4.54 (s, 1H, -OH), 4.45 (s, 2H, -NCH_2), 1.69 (s, 6H, -CH_3), 1.29 (s, 9H, -^{t}Bu).

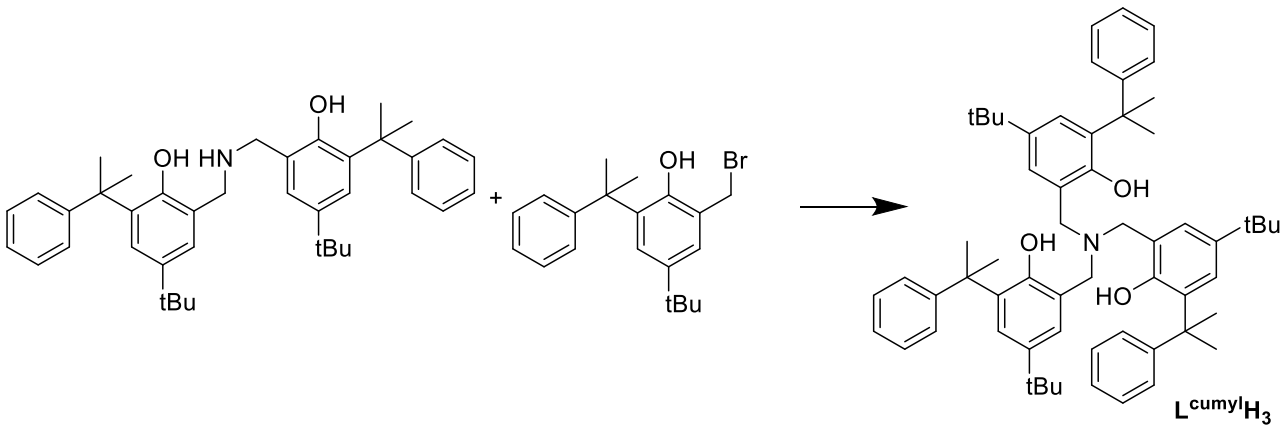

Reduced benzoxazine (1.01 mmol, 586 mg) was dissolved in 1 mL of THF and NEt_3 (5.08 mmol, 0.7 mL) was added to the solution. The mixture was allowed to stir for a few min. *Ortho-cumyl(bromomethyl)phenol* (1.52 mmol, 550 mg) was dissolved in 2 mL of THF and was added to the other solution. Precipitation was observed after 5 min.

After 2 h, the suspension was filtrated, and the solvent was evaporated. The crude product was purified by vacuum column chromatography over silica eluting with DCM in hexane and washed with MeOH to yield the desired product as a white-brown powder (**Figures 6.14-6.16**).

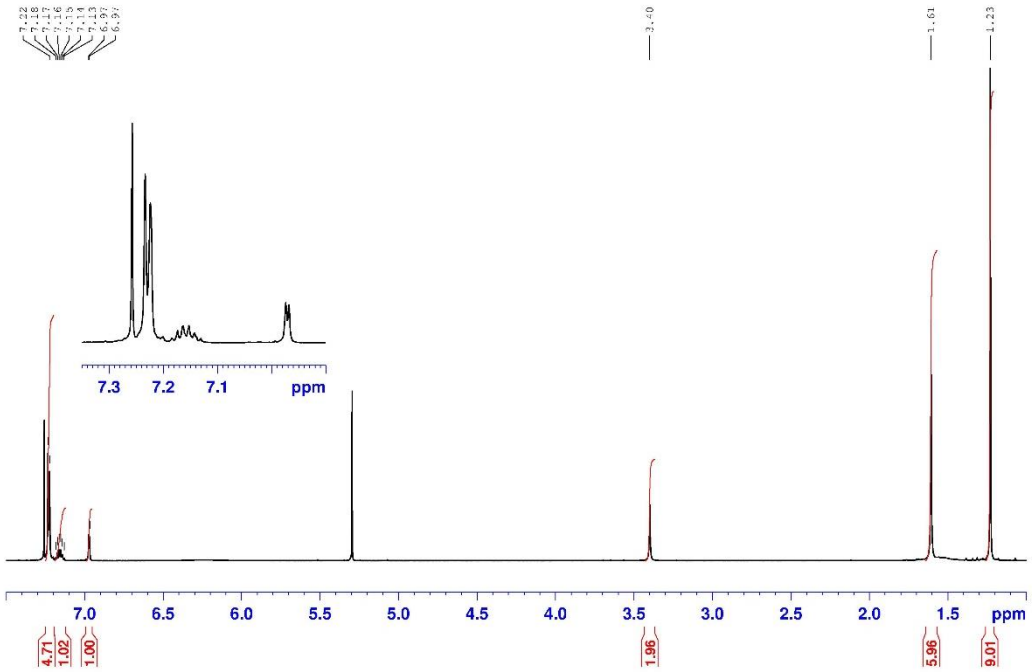

Figure 6.14 ^{1}H NMR spectrum (400 MHz, $CDCl_3$, 298 K) of $L^{cumyl}H_3$.

^{1}H NMR (400 MHz, $CDCl_3$, 298 K): δ 7.22 (m, 15H, ArH), 7.15 (m, 3H, ArH), 6.97 (d, J = 1.3 Hz, 3H, ArH), 3.40 (s, 6H, -NCH_2), 1.61 (s, 18H, -CH_3), 1.23 (s, 27H, -^{t}Bu).

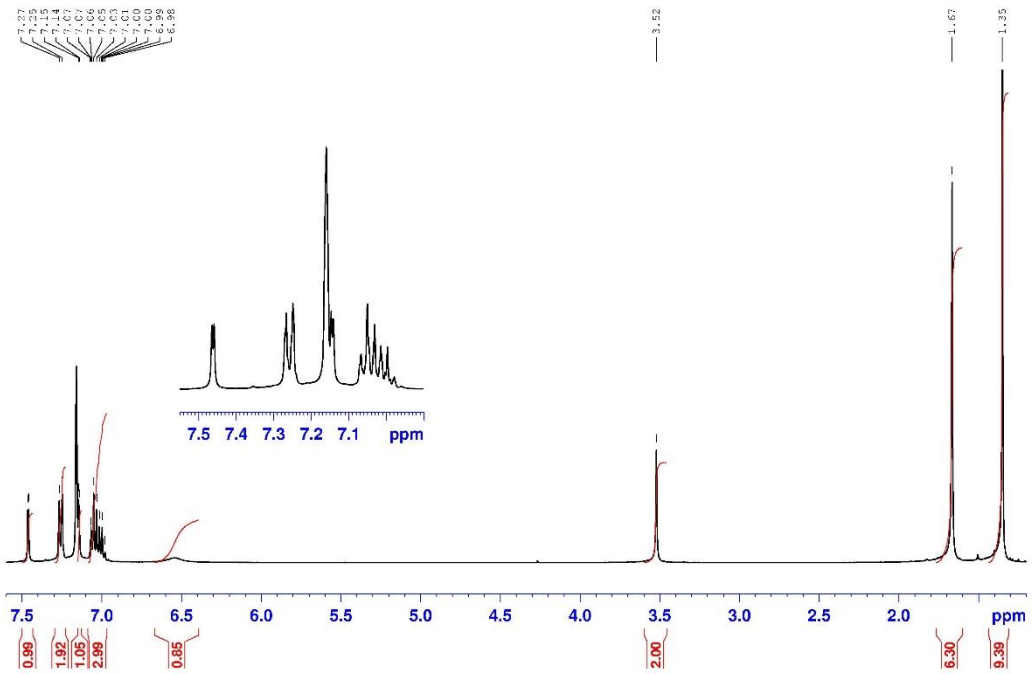

Figure 6.15 ^{1}H NMR spectrum (400 MHz, C_6D_6, 298 K) of $L^{cumyl}H_3$.

^{1}H NMR (400 MHz, C_6D_6, 298 K): δ 7.47 (d, J = 1.2 Hz, 3H, ArH), 7.26 (d, J = 8.4 Hz, 6H, ArH), 7.15 (m, 3H, ArH), 7.00 (m, 9H, ArH), 6.58 (b, 3H, -OH), 3.52 (s, 6H, -NCH_2), 1.67 (s, 18H, -CH_3), 1.35 (s, 27H, -^{t}Bu).

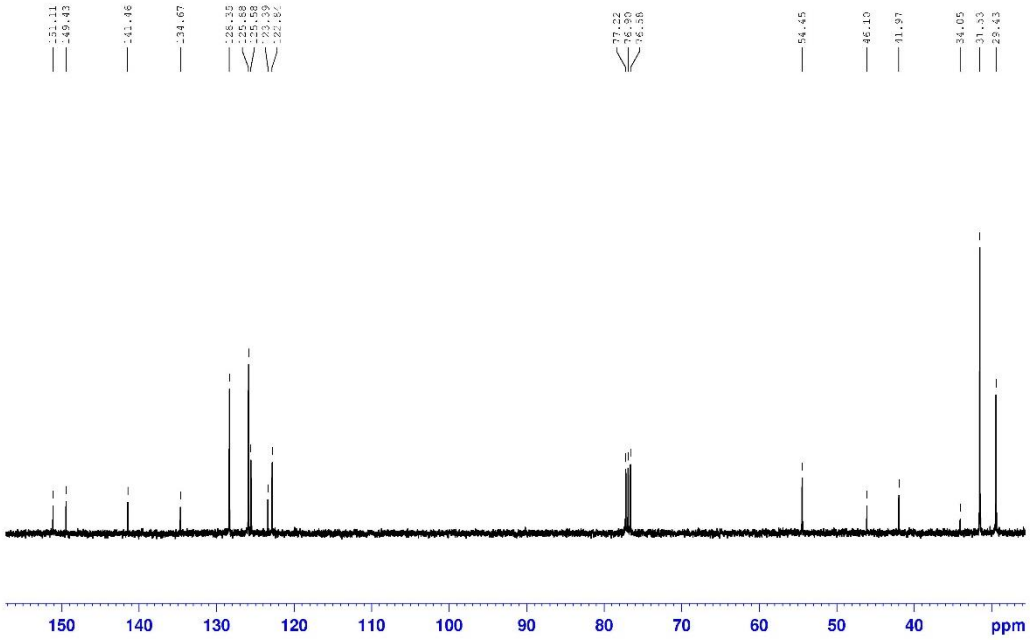

Figure 6.16 ^{13}H NMR spectrum (100 MHz, $CDCl_3$, 298 K) of $L^{cumyl}H_3$.

^{13}C NMR (100 MHz, $CDCl_3$, 298 K): δ 151.1, 149.4, 141.5, 134.7, 128.3, 125.6, 123.4, 122.8, 54.4, 46.1, 42.0, 34.0, 31.5, 29.4.

Synthesis of ligand $L^{cumyl\text{-}mesityl}H_3$

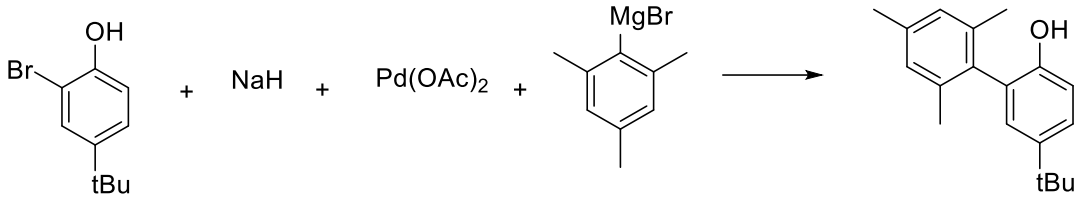

2-bromo-4-tertbutyl phenol (25.0 mmol, 5.73 g) was added dropwise to a mixture of NaH (32.5 mmol, 1.3 g) and THF dry (40 mL) at 0 °C, followed by stirring at room temperature for 10 min. $Pd(OAc)_2$ (1.12 mmol, 252 mg) was added, followed by 2-mesitylmagnesium bromide solution 1 M in THF (40.0 mmol, 36 mL) and the resulting mixture was heated to 70 °C overnight. Upon cooling to 0 °C, HCl (50 mL, 2 M) was carefully added. The mixture was filtered through celite. The resulting phases were separateded and the aqueous solution was extracted with Et_2O for 3 times. The combined organic layers were collected, washed with brine, dried with Na_2SO_4, filtered and concentrated under reduced pressure. The crude product was purified by vacuum column chromatography over silica eluted with 5 % ethyl acetate in hexane (**Figure 6.17**). Yield 67 %

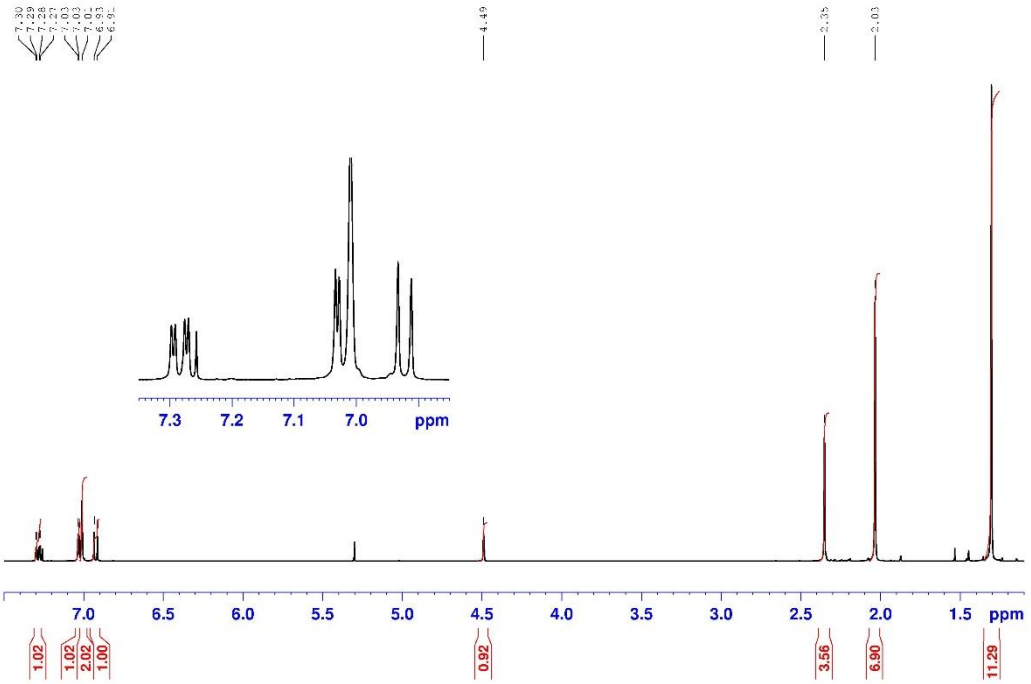

Figure 6.17 ^{1}H NMR spectrum (400 MHz, $CDCl_3$, 298 K) of *ortho-mesityl/para-tert-butyl phenol.*

^{1}H NMR (400 MHz, $CDCl_3$, 298 K): δ 7.28 (dd, J_1 = 8.2 Hz, J_2 = 1.3 Hz, 1H, ArH), 7.03 (m, 3H, ArH), 6.93 (d, J = 8.0 Hz, 1H, ArH), 4.49 (s, 1H, -OH), 2.35 (s, 3H, -CH_3), 2.03 (s, 6H, -CH_3), 1.29 (s, 9H, -^{t}Bu).

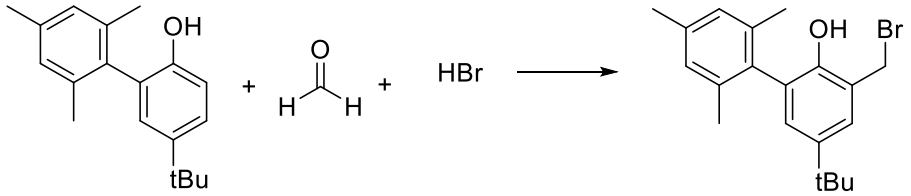

Ortho-mesityl/para-tert-butyl phenol (0.386 mmol, 104 mg) was dissolved in acetic acid (3 mL). Paraformaldehyde (0.579 mmol, 17.4 mg) was added to the yellow solution, and it was left to stir to room temperature for 2 h. After that, the HBr 33 % solution (1.35 mmol, 0.2 mL) was added and left to stir for another 30 min. The solvent was removed for evaporation and the yellow oil was obtained (**Figure 6.18**). Yield 87 %

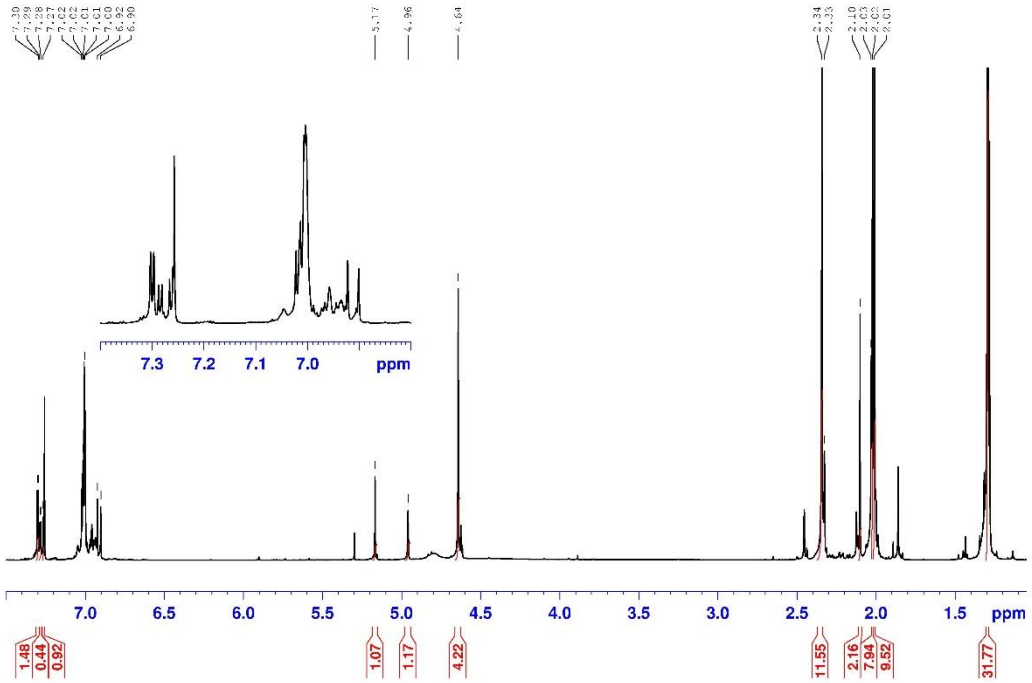

Figure 6.18 ^{1}H NMR spectrum (400 MHz, $CDCl_3$, 298 K) of *ortho-mesityl(bromomethyl)phenol*.

^{1}H NMR (400 MHz, $CDCl_3$, 298 K): δ 7.28 (m, 2H, ArH), 7.02 (m, 1H, ArH), 6.90 (m, 1H, ArH), 5.17 (s, 1H, -NCH_2), 4.96 (s, 1H, -NCH_2), 2.33 (s, 3H, -CH_3), 2.03 (s, 6H, -CH_3), 1.32 (s, 9H, -^{t}Bu).

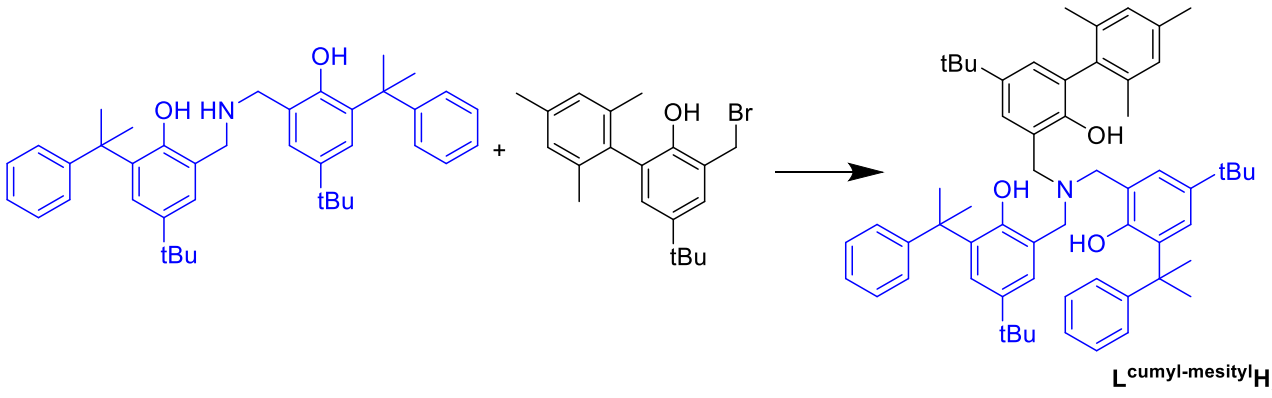

Reduced benzoxazine, previously synthesized, (25.6 mmol, 148 mg) was dissolved in 1 mL of THF and NEt_3 (1.28 mmol, 0.18 mL) was added to the solution. The mixture was allowed to stir for a few min. *Ortho-mesityl(bromomethyl)phenol* was dissolved in 2 mL of THF and was added to the other solution. Precipitation was observed after 5 min.

After 2 h, the suspension was filtrated, and the solvent was evaporated. The crude product was purified by vacuum column chromatography over silica eluting with ethyl acetate in hexane (**Figures 6.19-6.20**).

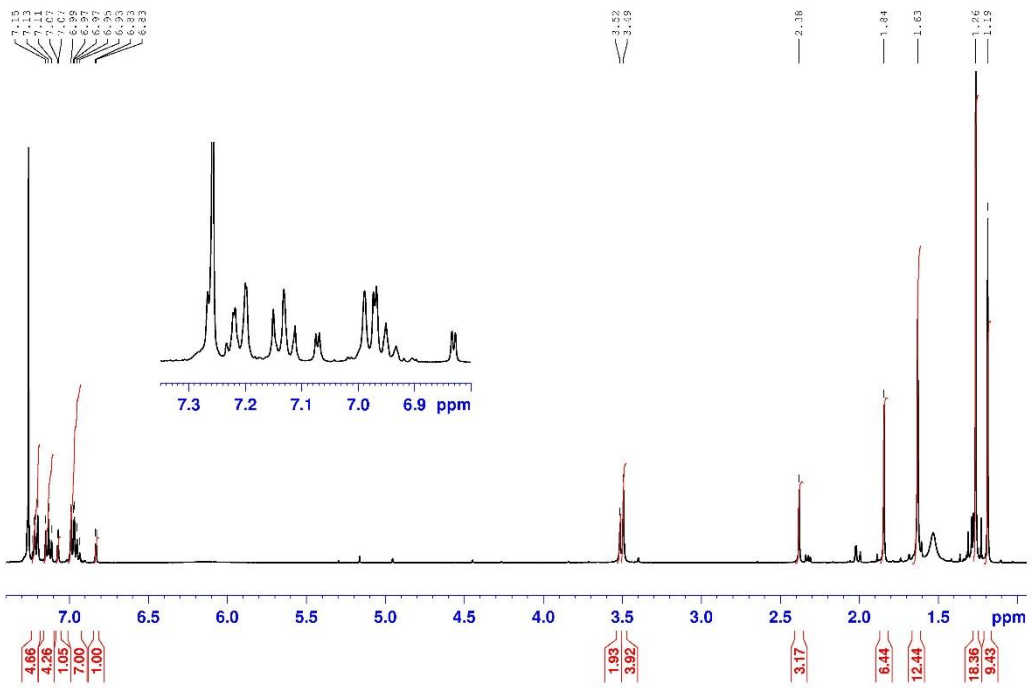

Figure 6.19 ^{1}H NMR spectrum (400 MHz, $CDCl_3$, 298 K) of $L^{cumyl\text{-}mesityl}H_3$.

^{1}H NMR (400 MHz, $CDCl_3$, 298 K): δ 7.23 (m, 5H, ArH), 7.14 (m, 4H, ArH), 7.07 (d, J = 1.2 Hz, 1H, ArH), 6.97 (m, 7H, ArH), 3.52 (s, 2H, -NCH_2), 3.49 (s, 4H, -NCH_2), 2.38 (s, 3H, -CH_3), 1.84 (s, 6H, -CH_3), 1.63 (s, 12H, -CH_3), 1.26 (s, 18H, -^{t}Bu), 1.19 (s, 9H, -^{t}Bu).

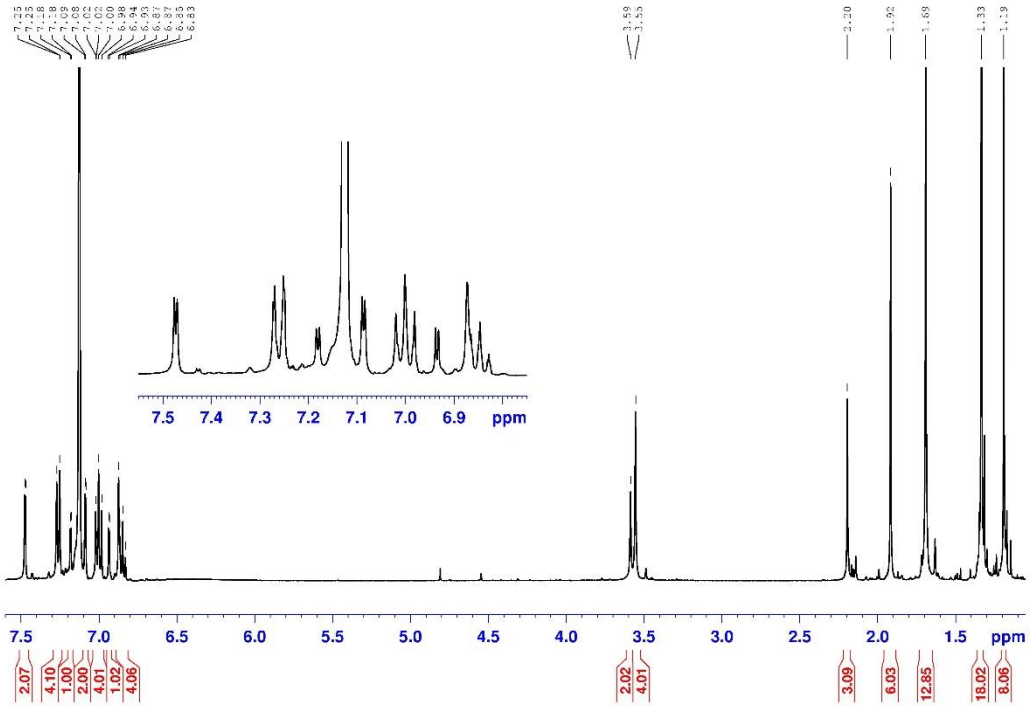

Figure 6.20 ^{1}H NMR spectrum (400 MHz, C_6D_6, 298 K) of $L^{cumyl\text{-}mesityl}H_3$.

^{1}H NMR (400 MHz, C_6D_6, 298 K): δ 7.47 (d, J = 1.2 Hz, 2H, ArH), 7.26 (d, J = 7.8 Hz, 4H, ArH), 7.18 (d, J = 1.2 Hz, 1H, ArH), 7.08 (d, J = 1.3 Hz, 2H, ArH), 7.0 (t, J = 6.4 Hz, 4H, ArH), 6.93 (d, J = 1.2 Hz, 1H, ArH), 6.85 (m, 5H, ArH), 3.59 (s, 2H, -NCH_2), 3.55 (s, 4H, -NCH_2), 2.20 (s, 3H, -CH_3), 1.92 (s, 6H, -CH_3), 1.69 (s, 12H, -CH_3), 1.33 (s, 18H, -^{t}Bu), 1.19 (s, 9H, -^{t}Bu).

Synthesis of ligand $L^{mesityl\text{-}cumyl}H_3$

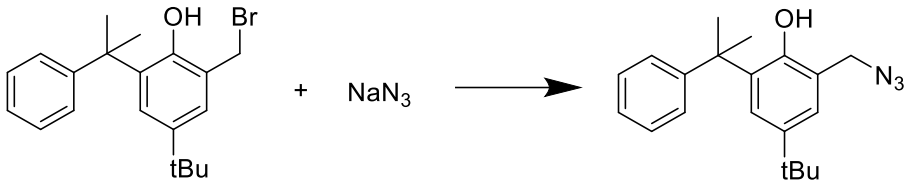

To a solution of *ortho-cumyl(bromomethyl)phenol* (2.77 mmol, 1.08 g) in a mixture of H_2O (2 mL) and CH_3CN (6 mL) was added NaN_3 (4.15 mmol, 290 mg) at 0 °C. The mixture was stirred at room temperature for 3 h. After addition of 50 mL of EtOAc, the organic phase was washed twice with brine (30 mL), dried over Na_2SO_4 and the solvent evaporated. The crude product was purified by pressure column chromatography over silica eluting with 1 % ethyl acetate in hexane to yield the desired product as a white powder (**Figure 6.21**). Yield 73 %

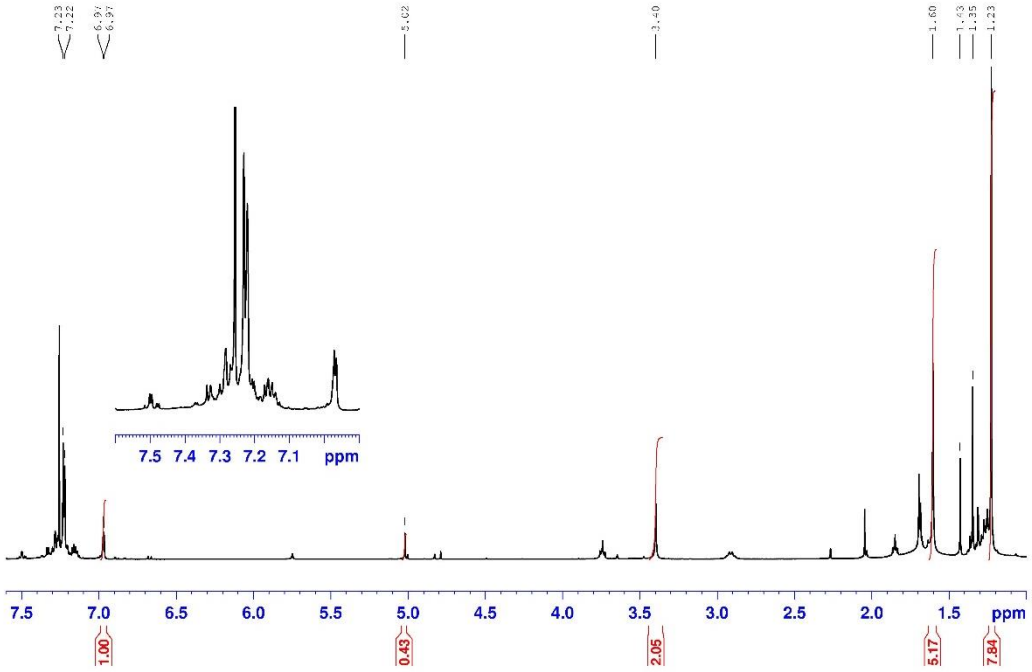

Figure 6.21 ^{1}H NMR spectrum (400 MHz, $CDCl_3$, 298 K) of *ortho-cumyl(azidemethyl)phenol*.

^{1}H NMR (400 MHz, $CDCl_3$, 298 K): δ 7.32 (m, 5H, ArH), 7.23 (m, 1H, ArH), 6.97 (d, J = 1.3 Hz, 1H, ArH), 3.40 (s, 2H, -CH_2), 1.60 (s, 6H, -CH_3), 1.23 (s, 9H, -^{t}Bu).

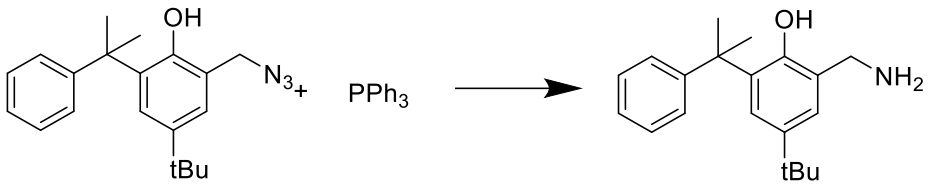

To a solution of *ortho-cumyl(azidemethyl)phenol* (2.01 mmol, 651 mg) in a mixture of H_2O (3 mL) and THF (62 mL) was added triphenyl phosphite PPh_3 (2.01 mmol, 528 mg). The reaction mixture was stirred at room remperature overnight. After addition of 50 mL of EtOAc, 50 ml of H_2O and 30 mL of brine, the organic phase was separated and dried over Na_2SO_4. The solvent was evaporated. The crude product was purified by pressure column chromatography over silica eluting with 50 % ethyl acetate in hexane to yield the desired product as a white powder (**Figure 6.22**). Yield 64 %

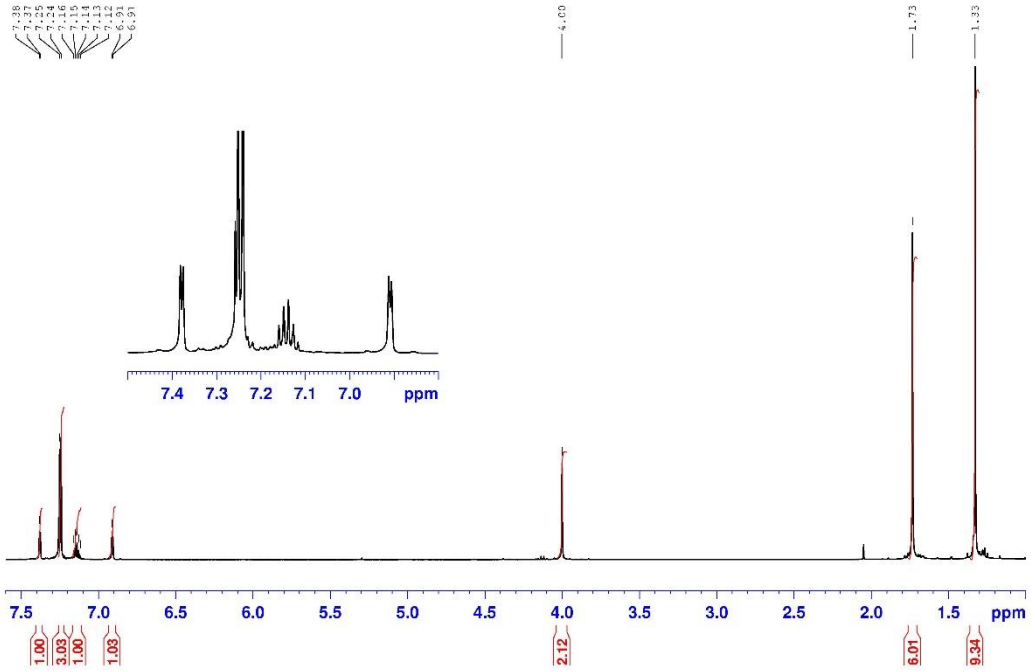

Figure 6.22 ^1H NMR spectrum (400 MHz, $CDCl_3$, 298 K) of *ortho-cumyl(aminomethyl)phenol*.

^1H NMR (400 MHz, $CDCl_3$, 298 K): δ 7.38 (d, J = 1.3 Hz, 1H, ArH), 7.27 (m, 3H, ArH), 7.13 (m, 1H, ArH), 6.91 (d, J = 1.3 Hz, 1H, ArH), 4.00 (s, 2H, -CH_2), 1.73 (s, 6H, -CH_3), 1.33 (s, 9H, -^{t}Bu).

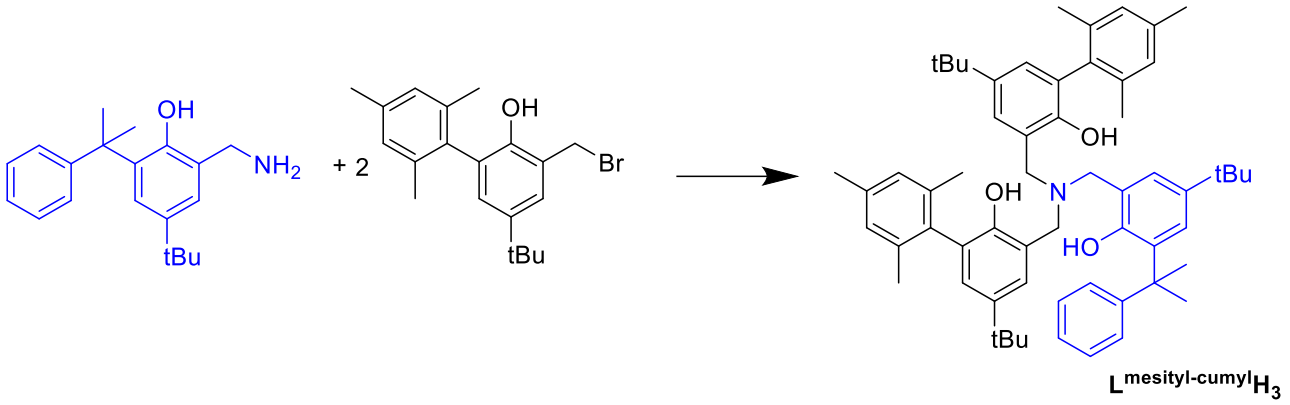

Ortho-cumyl(aminomethyl)phenol (1.28 mmol, 380 mg) was dissolved in 1 mL of THF and NEt_3 (12.8 mmol, 1.7 mL) was added to the solution. The mixture was allowed to stir for a few min. *Ortho-mesityl(bromomethyl)phenol* (3.83 mmol, 1.33 g) was dissolved in 2 mL of THF and was added to the solution. Precipitation was observed after 5 min. After 7 h, the suspension was filtrated, and the solvent was evaporated. The crude product was washed with hexane and the soluble fraction was purified by pressure column chromatography over silica eluting with 1 % ethyl acetate in hexane to yield the desired product as a yellow powder (**Figure 6.23-6.24**). Yield 20 %

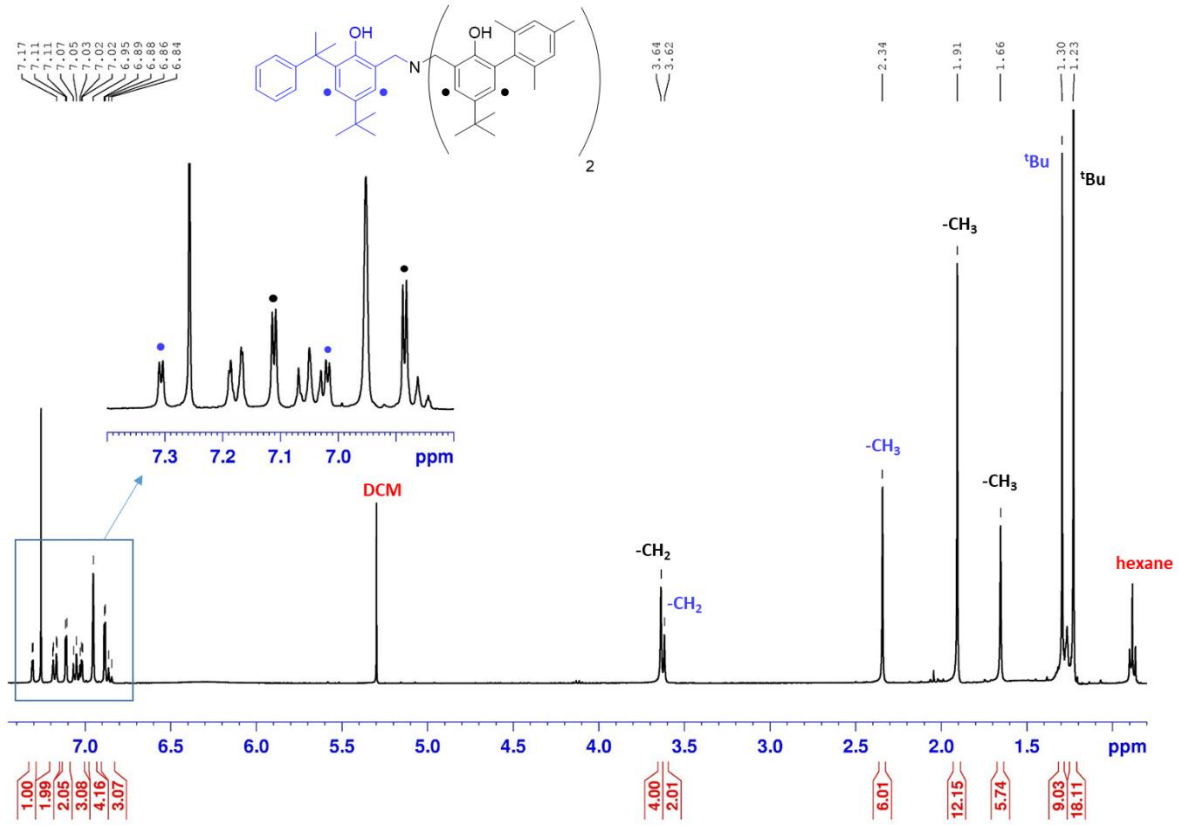

Figure 6.23 ^{1}H NMR spectrum (400 MHz, $CDCl_3$, 298 K) of $L^{mesityl\text{-}cumyl}H_3$.

^{1}H NMR (400 MHz, $CDCl_3$, 298 K): δ 7.31 (d, J = 1.3 Hz, 1H, ArH), 7.17 (d, J = 7.8 Hz, 2H, ArH), 7.11 (d, J = 1.2 Hz, 2H, ArH), 7.08 (t, J = 7.5 Hz, 2H, ArH), 7.03 (d, J = 1.3 Hz, 1H, ArH), 6.95 (s, 4H, ArH), 6.88 (d, J = 1.3 Hz, 2H, ArH), 6.84 (m, 1H, ArH), 3.64 (s, 4H, -NCH_2), 3.62 (s, 2H, -NCH_2), 2.34 (s, 6H, -CH_3), 1.91 (s, 12H, -CH_3), 1.66 (s, 6H, -CH_3), 1.30 (s, 9H, -^{t}Bu), 1.23 (s, 18H, -^{t}Bu).

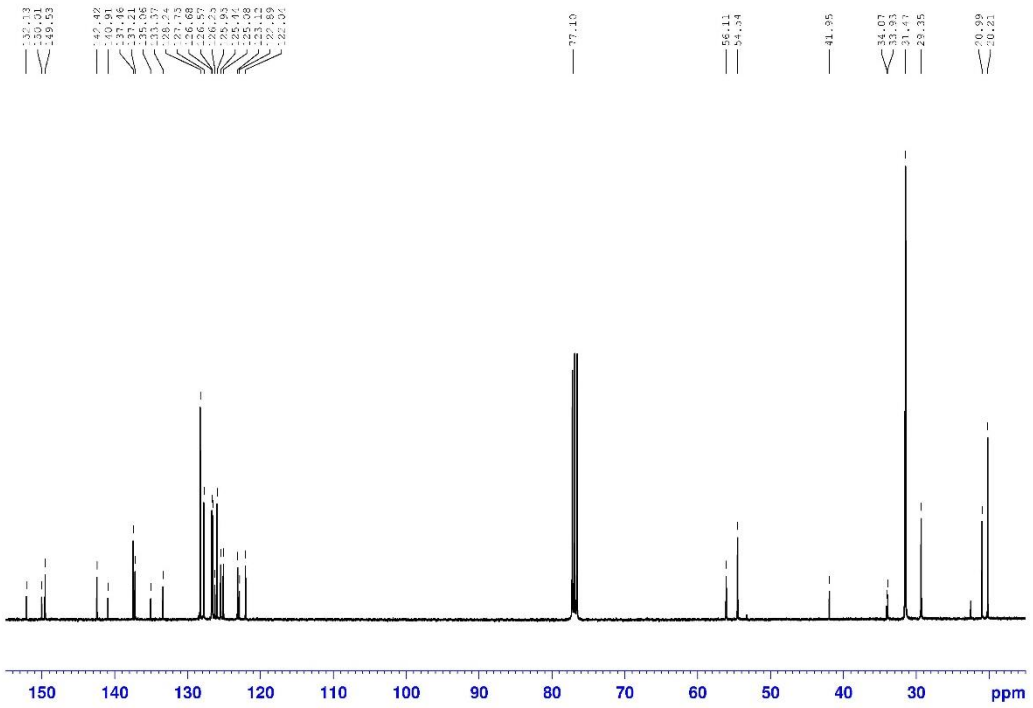

Figure 6.24 ^{13}C NMR spectrum (100MHz, $CDCl_3$, 298K) of $L^{mesityl\text{-}cumyl}H_3$.

^{13}C NMR (100 MHz, $CDCl_3$, 298 K): δ 152.1, 150.0, 149.5, 142.4, 140.9, 137.5, 137.2, 135.0, 133.4, 128.2, 127.8, 126.7, 126.6, 126.2, 126.0, 125.4, 125.1, 123.1, 122.9, 122.0, 56.1, 54.5, 42.0, 34.0, 31.5, 29.3, 21.0, 20.2.

Synthesis of $L^{durene}Zr(O^iPr)(HO^iPr)$ complex

In a glove box, zirconium (IV) isopropoxy isopropanol (0.241 mmol, 93.5 mg) was dissolved in toluene (5 mL). The ligand $L^{durene}H_3$ (0.241 mmol, 217 mg) was dissolved in toluene (6 mL) and was slowly added to the solution of the zirconium complex. After 2 h, the solvent was removed under vacuum and the residue was washed with cold pentane and dried under vacuum. Yield 85 %

^{1}H NMR (400 MHz, C_6D_6, 298 K): δ 7.18 (d, J= 1.7 Hz, 3H, ArH), 7.08 (d, J = 1.7 Hz, 3H, ArH), 6.87 (s, 3H, ArH), 3.60 (b, 7H, -NCH_2 + -O$\underline{CH}(CH_3)_2$), 2.17 (s, 18H, -CH_3), 2.04 (s, 18H, -CH_3), 1.33 (s, 27H, -^{t}Bu), 0.62 (d, J = 7.4 Hz, 6H, -OCH($\underline{CH_3}$)$_2$).

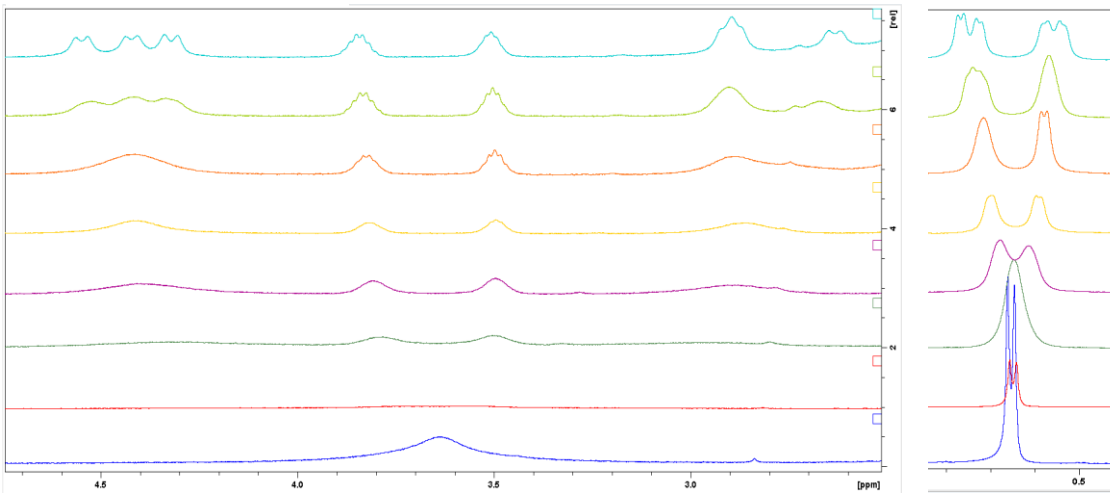

Figure 6.25 ^{1}H NMR spectra of the methylene region of **$L^{durene}Zr(O^iPr)(HO^iPr)$** complex in toluene-$d_8$, 400MHz. From the bottom to top: 25 °C, 10 °C, 0 °C, -10 °C, -20 °C, -30 °C, -40 °C, -50 °C.

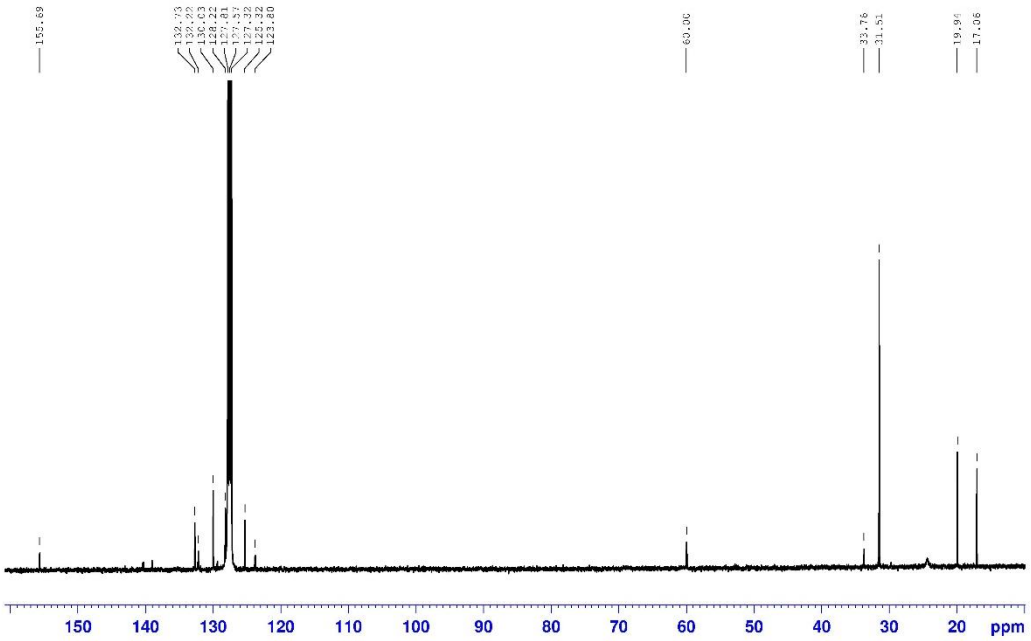

Figure 6.26 ^{13}C NMR spectrum (100MHz, C_6D_6, 298K) of **$L^{durene}Zr(OiPr)(HOiPr)$**.

^{13}C NMR (100 MHz, C_6D_6, 298 K): δ 155.7, 132.7, 132.2, 130.0, 128.2, 127.8, 127.3, 125.3, 123.8, 60.0, 33.8, 31.5, 19.9, 17.1.

Synthesis of $L^{cumyl}Zr(O^iPr)$ complex

In a glove box, zirconium (IV) isopropoxy isopropanol (0.107 mmol, 40 mg) was dissolved in toluene (1 mL). The $L^{cumyl}H_3$ (0.107 mmol, 92 mg) was dissolved in toluene (1 mL) and was slowly added to the solution of the zirconium complex. After 2 h, the solvent was removed under vacuum and the residue was washed with cold pentane (3×1 mL) and dried under vacuum to yield the desired complex as a white solid (**Figure 6.27-6.30**). Yield 77%

^{1}H NMR (400 MHz, C_6D_6, 298 K): δ 7.53 (d, J = 1.1 Hz, 3H, ArH), 7.18 (m, 6H, ArH), 6.96 (m, 9H, ArH), 6.88 (m, 3H, ArH), 4.35 (sept, 1H, -OCH$(CH_3)_2$), 3.64 (b, 3H, -NCH_2), 2.62 (b, 3H, -NCH_2), 1.80 (b, 18H, -CH_3), 1.35 (s, 27H, -^{t}Bu), 1.32 (d, J = 7.1 Hz, 6H, -OCH(CH_3)$_2$).

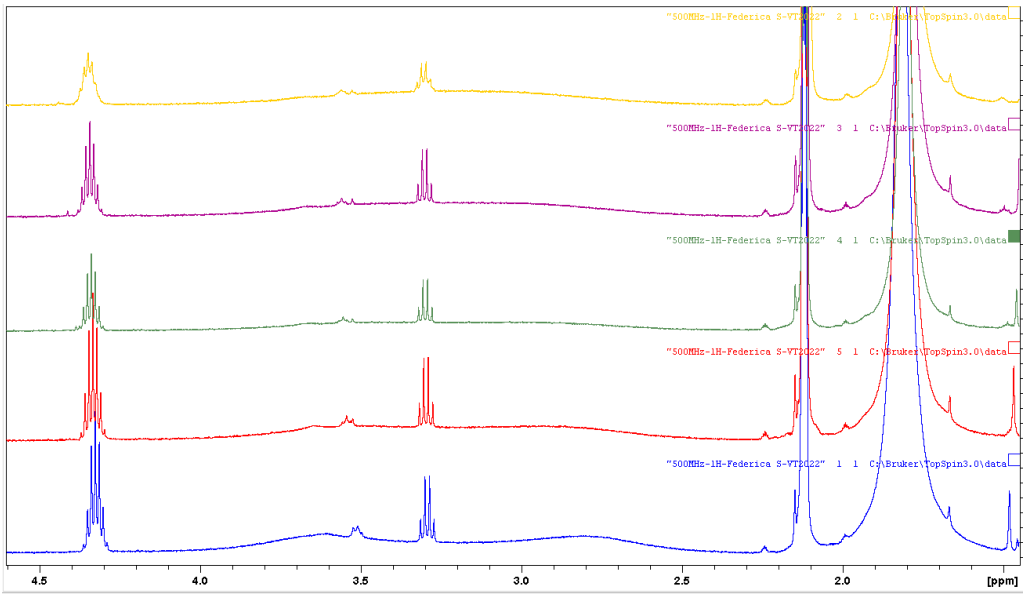

Figure 6.28 VT ^{1}H NMR spectra of the methylene region of **$L^{cumyl}Zr(OiPr)$** complex in toluene-d_8, 500 MHz. From the bottom to top: 25 °C, 40 °C, 50 °C, 60 °C, 70 °C.

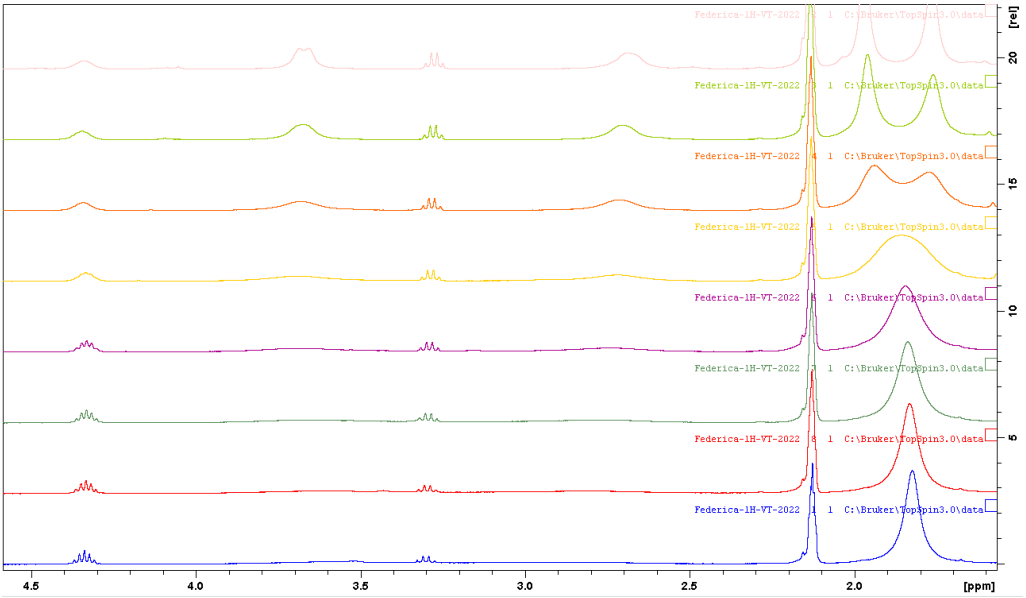

Figure 6.29 VT ^{1}H NMR spectra of the methylene region of **$L^{cumyl}Zr(OiPr)$** complex in toluene-d_8, 400 MHz. From the bottom to top: 25 °C, 10 °C, 0 °C, -10 °C, -20 °C, -30 °C, -40 °C, -50 °C.

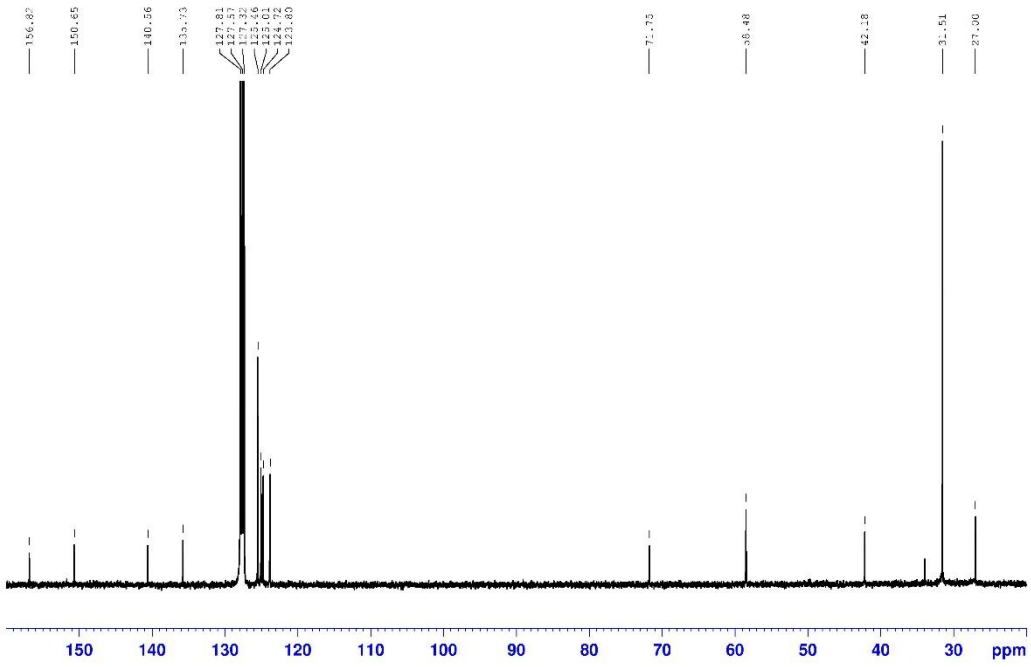

Figure 6.30 ^{1}H NMR spectrum (400 MHz, C_6D_6, 298 K) of **L^{cumyl}Zr(OiPr)**.

^{13}C NMR (100 MHz, C_6D_6, 298 K): δ 156.8, 150.6, 140.6, 135.7, 125.5, 125.0, 124.7, 123.8, 71.8, 58.5, 42.2, 31.5, 27.0.

Synthesis of $L^{mesityl\text{-}cumyl}Zr(O^iPr)$ complex

In a glove box, zirconium (IV) isopropoxy isopropanol (0.0555 mmol, 21.5 mg) was dissolved in toluene (1 mL). The $L^{mesityl\text{-}cumyl}H_3$ (0.0555 mmol, 47.7 mg) was dissolved in toluene (1 mL) and was slowly added to the solution of the zirconium complex. After 2 h, the solvent was removed under vacuum and the residue was washed with pentane and dried under vacuum (**Figure 6.31-6.32**).

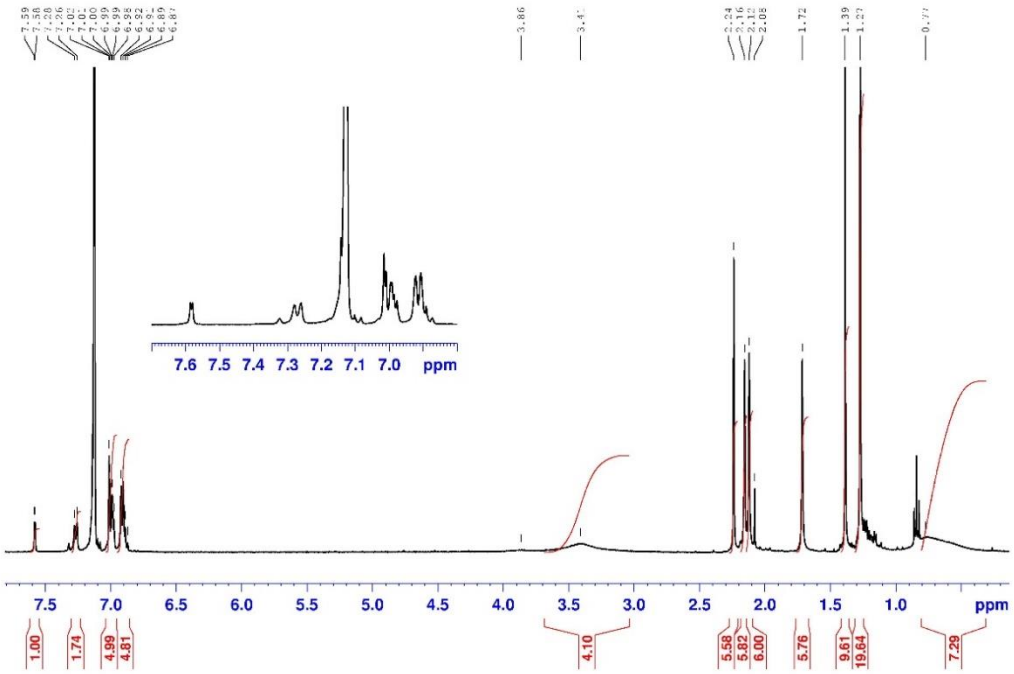

Figure 6.31 ^{1}H NMR spectrum (400 MHz, C_6D_6, 298 K) of **$L^{mesityl\text{-}cumyl}Zr(OiPr)$**.

^{1}H NMR (400 MHz, C_6D_6, 298 K): δ 7.58 (d, J = 1.1 Hz, 1H, ArH), 7.26 (d, J = 7.6 Hz, 2H, ArH), 7.16 (m, 2H, ArH), 6.99 (m, 5H, ArH), 6.89 (m, 5H, ArH), 3.64 (m, 7H, -O<u>C</u>H$(CH_3)_2$ + -NCH_2), 2.24 (s, 6H, -CH_3), 2.12 (s, 6H, -CH_3), 2.08 (s, 6H, -CH_3), 1.72 (s, 6H, -CH_3), 1.39 (s, 9H, -^{t}Bu), 1.27 (s, 18H, -^{t}Bu), 0.77 (m, 6H, -OCH(<u>CH_3</u>)$_2$).

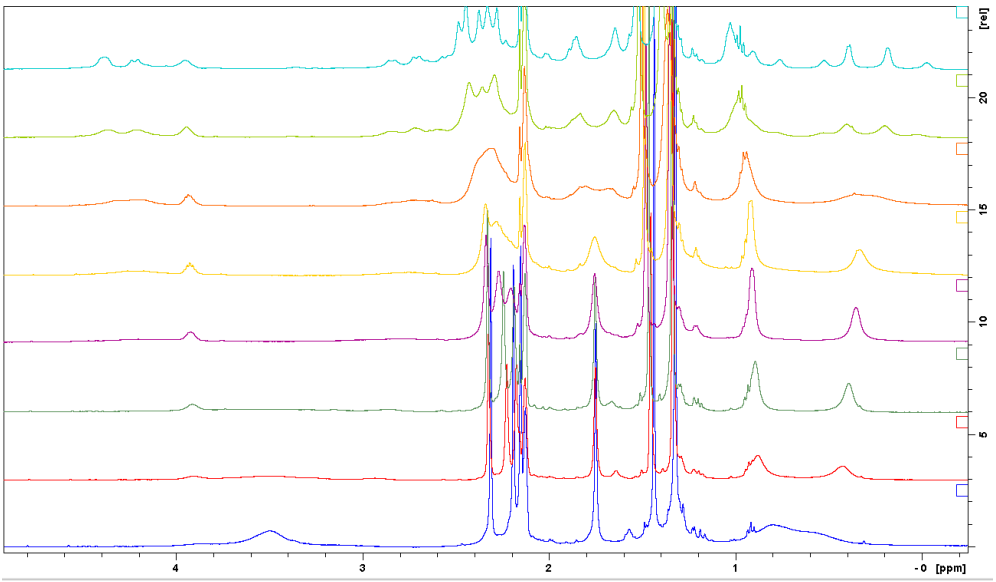

Figure 6.32 ^{1}H NMR spectra of the methylene region of **$L^{mesityl\text{-}cumyl}Zr(OiPr)$** in toluene-$d_8$, 400 MHz. From the bottom to top: 25 °C, 10 °C, 0 °C, -10 °C, -20 °C, -30 °C, -40 °C, -50 °C.

Synthesis of $L^{cumyl\text{-}mesityl}Zr(O^iPr)$ complex

In a glove box, zirconium (IV) isopropoxy isopropanol (0.0116 mmol, 4.8 mg) was dissolved in toluene (1 mL). The $L^{cumyl\text{-}mesityl}H_3$ (0.0116 mmol, 10 mg) was dissolved in toluene (1 mL) and was slowly added to the solution of the zirconium complex. After 2 h, the solvent was removed under vacuum and the residue was washed with pentane and dried under vacuum (**Figure 6.33**).

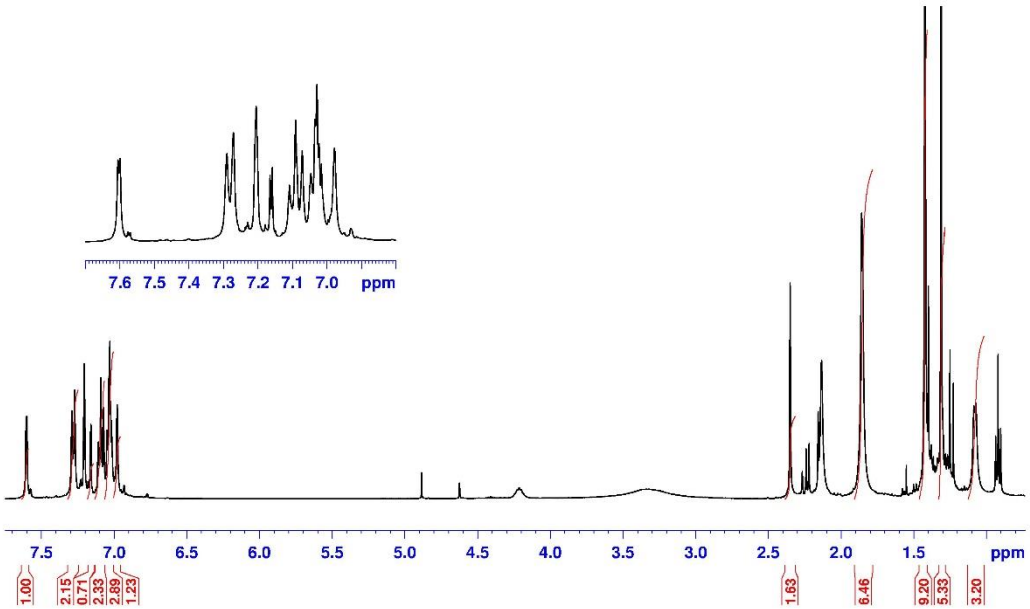

Figure 6.33 ^1H NMR spectrum (400 MHz, C_6D_6, 298 K) of **$L^{cumyl\text{-}mesityl}Zr(OiPr)$**.

References

[1] [a]Thomas, C. M. Stereocontrolled ring-opening polymerization of cyclic esters: Synthesis of new polyester microstructures. *Chemical Society Reviews* **39**, 165–173 (2010).
[b]VanWouwe, P., Dusselier, M., Vanleeuw, E., Sels, B. Lactide Synthesis and Chirality Control for Polylactic acid Production. *ChemSusChem* **9**, 907–921 (2016).

[2] Dusselier, M., van Wouwe, P., Dewaele, A., Jacobs, P. A., Sels, B. F. Shape-selective zeolite catalysis for bioplastics production. *Science* **349**, 78–80 (2015).

[3] Auras, R., Harte, B., Selke, S. An overview of polylactides as packaging materials. *Macromolecular Bioscience* **4**, 835–864 (2004).

[4] Saeidlou, S., Huneault, M. A., Li, H., Park, C. B. Poly(lactic acid) crystallization. *Progress in Polymer Science* **37**, 1657–1677 (2012).

[5] [a]Santoro, O., Zhang, X., Redshaw, C. Synthesis of biodegradable polymers: A review on the use of schiff-base metal complexes as catalysts for the ring opening polymerization (ROP) of cyclic esters. *Catalysts* **10**, 1–49 (2020).
[b]Roy, S. S., Sarkar, S., Chakraborty, D. Macrocycles in dual role: ancillary ligands in metal complexes and organocatalysts for the ring-opening polymerization of lactide. Journal of Inclusion Phenomena and Macrocyclic *Chemistry* **100**, 1-36 (2021).

[6] [a]McKeown, P., McCormick, S. N., Mahon, M. F. & Jones, M. D. Highly active Mg(II) and Zn(II) complexes for the ring opening polymerisation of lactide. *Polymer Chemistry* **9**, 5339–5347 (2018).
[b]D'Alterio, M. C., D'Auria, I., Gaeta, L., Tedesco, C., Brenna. S., Pellecchia, C. Are Well Performing Catalysts for the Ring Opening Polymerization of l -Lactide under Mild Laboratory Conditions Suitable for the Industrial Process? the Case of New Highly Active Zn(II) Catalysts. *Macromolecules* **55**, 5115–5122 (2022).

[7] Kol, M., Shamis, M., Goldberg, I., Goldschmidt, Z., Alfi, S., Hayut-Salant, E. Titanium(IV) complexes of trianionic amine triphenolate ligands. *Inorganic Chemistry* **4**, 177-179 (2001)

[8] Chmura, A. J., Davidson, M. G., Frankis, C. J., Jones, M. D., Lunn, M. D. Highly active and stereoselective zirconium and hafnium alkoxide initiators for solvent-free ring-opening polymerization of rac-lactide. *Chemical Communications* **11**, 1293–1295 (2008).

[9] Hador, R., Shuster, M., Lipstman, S., Kol, M. Fast-Tracking the l -Lactide Polymerization Activity of Group 4 Metal Complexes of Amine Tris(phenolate) Ligands. *ACS Catalysis* **12**, 4872–4879 (2022).

[10] Hador, R., Shuster, M., Venditto, V., Kol, M. Stereogradient Poly(Lactic Acid) from meso-Lactide/L-Lactide Mixtures. *Angewandte Chemie* **61**, 2-7 (2022).

Concluding Remarks

In recent decades, the use of plastics has become a very sensitive issue, all over the world. Most of the synthetic polymers come from non-renewable raw resources and are not biodegradable; therefore, they persist in the environment even for several years. Currently, about 70% of all produced plastics follow a linear economy and it is estimated that by 2050, approximately 12 000 Mt of plastic waste will be massively landfilled or released into the environment, with dramatic consequences for all natural ecosystems.[1]

Different approaches have to try to contain these problems, such as the chemical recycling of traditional plastics[2] and/or the introduction of new bio-based polymers for which an effective waste management strategy is designed from the outset, coherently with a vision of circular economy for plastics.[3]

Among the sustainable polymers, polylactide (PLA) is the most promising material because it is obtained from annually renewable resources and combines good mechanical properties and biodegradability.[4] Although these characteristics define it as a green material, there are still some criticisms related to its life cycle.

Currently, PLA is industrially produced using a highly toxic tin catalyst. Thus, the development of efficient, easily synthesized, low-cost and not toxic catalysts is of crucial importance.[5]

About the end-of-life options, PLA waste is currently collected for composting, although high temperature and moisture content are required. Since the recovery of lactic acid from PLA waste is more energetically favorable than its production from biomass, chemical recycling is highly desirable. The degradation by alcoholysis produces alkyl lactates as final products that are chemical platforms to obtain the monomer lactide or can be used as green solvents in agriculture and pharmaceuticals.

My Ph.D. project focused on planning the design of the catalytic species in terms of structure of the ancillary ligand, nature of the metal center and coordination geometry to promote the synthesis and chemical degradation of PLA. New zinc and magnesium complexes supported by pyridyl phenoxy-imine based-ligand have been synthesized (**Figure 7.1**).

In lactide polymerization, high activity and efficient control have been observed for Zn-based complexes even under industrially relevant conditions (technical grade monomer, solvent-free conditions, and high temperature). Mechanistic studies on the Zn active species have demonstrated the formation of active species with defined identities, while the Mg-based complexes are involved in different equilibria which generate a mixture of active species in the polymerization medium resulting in an uncontrolled process.

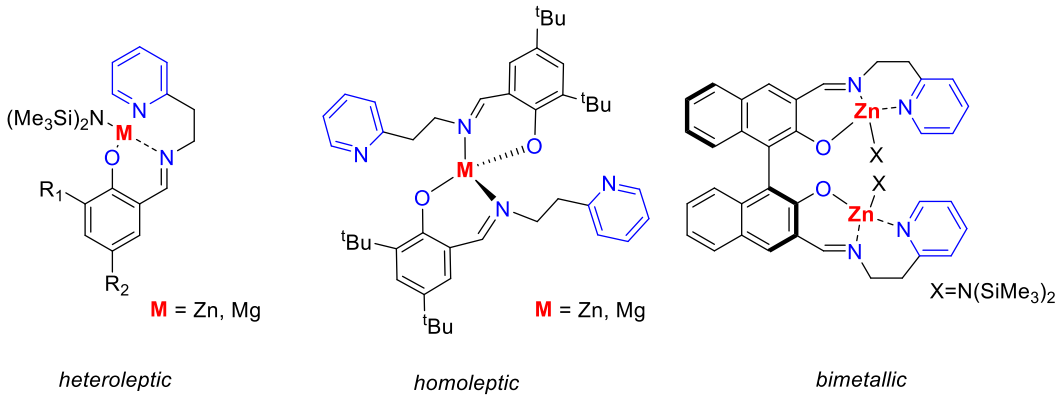

Figure 7.1 Zn and Mg complexes supported by pyridyl phenoxy-imine based-ligand synthesized in this thesis.

The family of Zn heteroleptic complexes showed the highest activities, classifying among the most efficient catalysts reported in literature and comparable to the industrial tin catalyst. Complexes with *para*-electron donor groups on the phenoxy moiety showed higher activities, on the other hand the *ortho*- and *para*-bulk substituents or electron withdrawing groups made the reaction slower.

When a binaphthyl backbone was introduced between two pyridyl phenoxy-imine moieties, the resulting hexacoordinate ligands possess coordinative pockets that allowed the formation of bimetallic zinc complexes. These catalytic systems, in addition to being highly active in the polymerization of the lactide, show good polymerization control, indeed transesterification reactions are absent during polymerization reactions. On the other hand, when the monomer is no longer present in the reaction mixture, we observe intermolecular transesterifications at room temperature. Differently, at higher temperature, the bimetallic catalyst completely switches to intramolecular transesterifications, allowing the complete conversion of the monomer into low molecular weight cyclic polymers.

To evaluate the ability of the described zinc complexes to fulfill the principles of circular economy, same of them were tested in the degradation reaction of PLA. The Zn heteroleptic complexes showed the highest activities, with the substituents on the phenoxy moiety slightly influencing the activity of the complexes. Electron-donor groups or hydrogen atoms increased the activities, which decreased with bulky or electro-withdrawing groups. Interestingly, different mechanisms were highlighted under different degradation conditions. In THF solution, the degradation occurred through a two-step process in which the random scission of the polymer chains led to the formation of oligomers which are progressively converted into alkyl lactate, while under solvent-free conditions the degradation occurred through a progressive erosion of the chain end with the direct formation of alkyl lactate.

Simple and commercially available compounds, such as amides of several non-toxic metals, have been subsequently explored in PLA degradation reactions. In the presence of methanol or ethanol at room temperature, the Mg amide showed the highest activity followed by the Zn and Y amides, while the amides of group 4 metals were scarcely efficient. In the ethanolysis of PLA at higher temperature, Zn amide preserved the high activities, Mg and Y observed significant decrease, while group 4 metals exceed expectations. The study of these metal amides has also been extended to the chemical degradation of PET, a commercially widespread polymer. At high temperatures, Zr amide proved to be the best catalyst showing high activity combined with good selectivity towards bis(2-hydroxyethyl) terephthalate (BHET).

Kol's research group of Tel Aviv University, where I carried out a visiting research period, synthesized a new Zr hexacoordinate complex supported by amino tris(phenolate) ligand with mesityl moieties[6], which showed the highest activity ever recorded for metal complexes in lactide polymerization under industrial conditions. In this context, my work has focused on the synthesis of new Zr complexes with different *ortho*-substituents in the phenoxy moieties (**Figure 7.2**) and the study of their behavior in the polymerization of *meso*- and *rac*-LA. The substitution of the *ortho*-mesityl group with the *ortho*-durene group and therefore the synthesis of the hexacoordinated complex has preserved its high activity and stereocontrol, obtaining polymers with a high degree of heterotacticity (using *rac*-LA) and sindiotacticity (using *meso*-LA). Performance plummeted with the pentacoordinate complexes with cumyl groups demonstrating that not just the presence of the aryl group is an important factor in the reaction, but it is essential that it is directly bound to the phenoxy group.

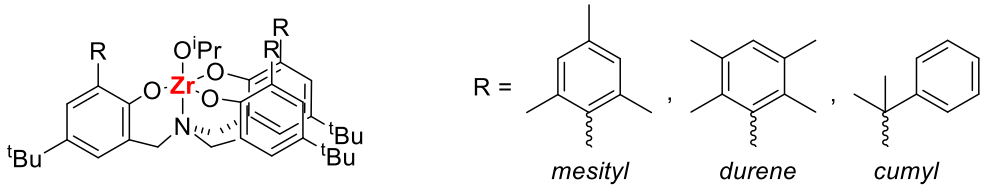

Figure 7.2 Zr complexes supported by amino tris(phenolate) ligand synthesized in this work.

References

[1] Geyer, R., Jambeck, J. R., Law, K. L. Production, use, and fate of all plastics ever made. *Science Advances* **3**, e1700782 (2017).

[2] Coates, G. W., Getzler, Y. D. Y. L. Chemical recycling to monomer for an ideal, circular polymer economy. *Nature Reviews Materials* **5**, 501–516 (2020).

[3] Kaur, G., Uisan, K., Ong, K. L., Ki Lin, C. S. Recent Trends in Green and Sustainable Chemistry & Waste Valorisation: Rethinking Plastics in a circular economy. *Current Opinion in Green and Sustainable Chemistry* **9**, 30–39 (2018).

[4] Farah, S., Anderson, D. G., Langer, R. Physical and mechanical properties of PLA, and their functions in widespread applications — A comprehensive review. *Advanced Drug Delivery Reviews* **107**, 367–392 (2016).

[5] Balla, E., Daniilidis, V., Karlioti, G., Kalamas, T., Stefanidou, M., Bikiaris, N. D., Vlachopoulos, A., Koumentakou, I., Bikiaris, D. N. Poly(lactic acid): A versatile biobased polymer for the future with multifunctional properties-from monomer synthesis, polymerization techniques and molecular weight increase to PLA applications. *Polymers* **13**, 1822-1872 (2021).

[6] [a]Hador, R., Shuster, M., Venditto, V., Kol, M. Stereogradient Poly(Lactic Acid) from meso-Lactide/L-Lactide Mixtures. *Angewandte Chemie* **61**, 2-7 (2022).
[b]Hador, R., Shuster, M., Lipstman, S., Kol, M. Fast-Tracking the L -Lactide Polymerization Activity of Group 4 Metal Complexes of Amine Tris(phenolate) Ligands. *ACS Catalysis* **12**, 4872–4879 (2022).